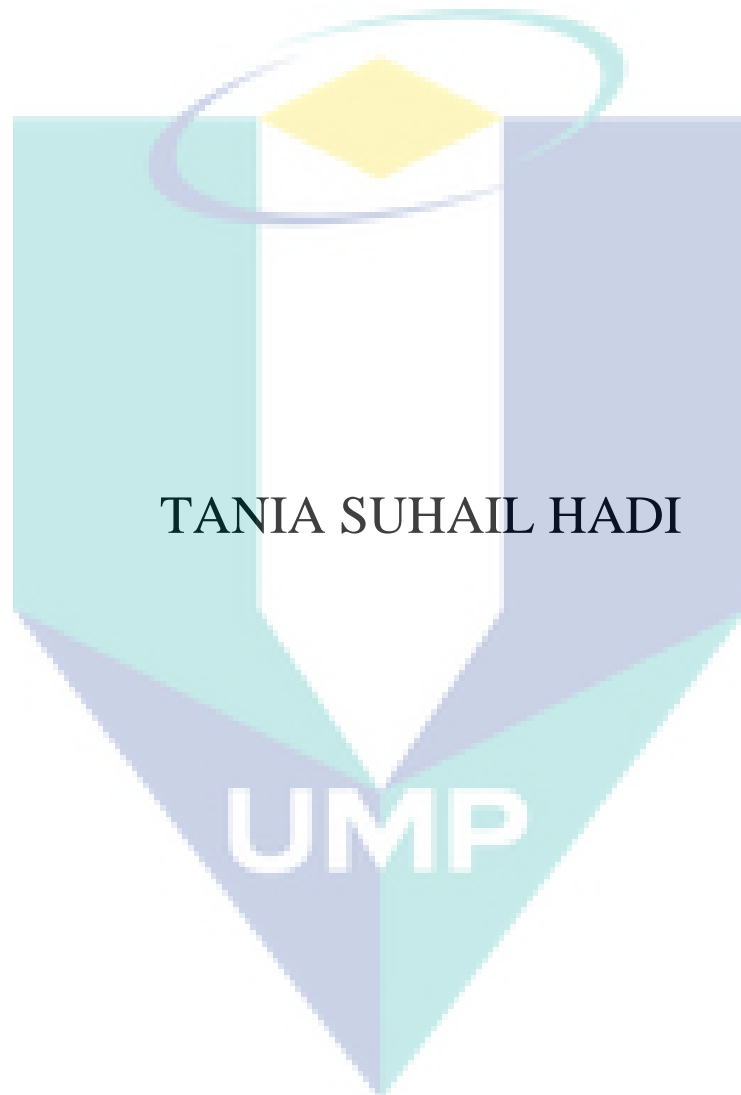
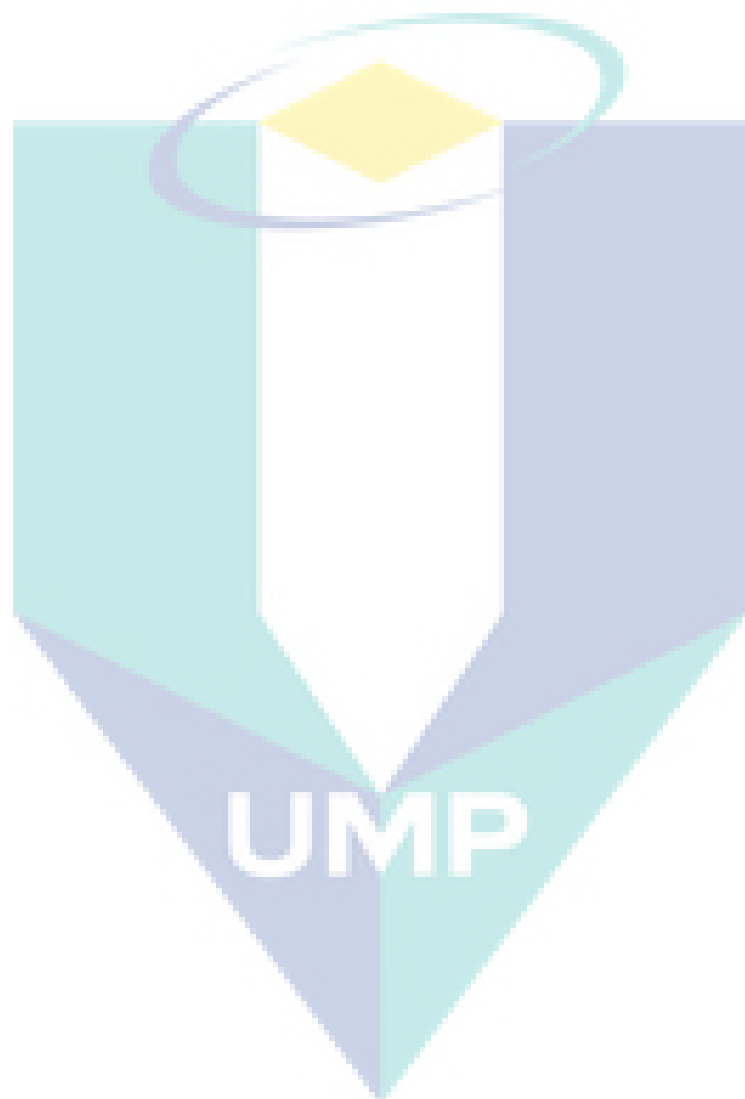


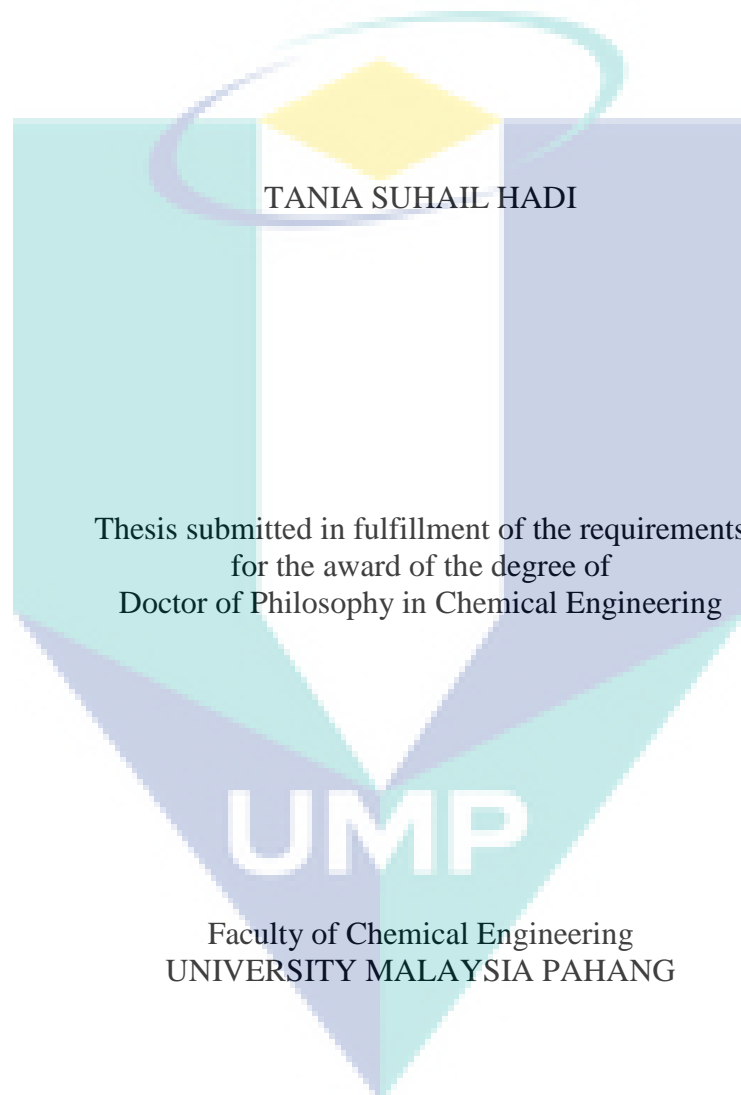
**SUSPENDED SOLIDS AS DRAG REDUCTION
AGENTS FOR LIQUID FLOW IN A PIPELINE**



**DOCTOR OF PHILOSOPHY IN CHEMICAL
ENGINEERING
UNIVERSITI MALAYSIA PAHAG**



SUSPENDED SOLIDS AS DRAG REDUCTION AGENTS FOR LIQUID FLOW IN
A PIPELINE



JUNE 2011

SUPERVISOR'S DECLARATION

I/We* hereby declare that I/we* have checked this thesis and in my/our* opinion, this thesis/project* is adequate in terms of scope and quality for the award of the degree of Doctor of Philosophy in Chemical Engineering.

SIGNATURE

NAME OF SUPERVISOR: ASSOCIATE PROFESSOR DR. HAYDER A. ABDUL BARI

POSITION: ASSOCIATE PROFESSOR

DATE: 28 JUNE 2011

SIGNATURE

NAME OF CO-SUPERVISOR: DATO' PROFESSOR DR. ROSLI BIN MOHD YUNUS

POSITION: PROFESSOR

DATE: 28 JUNE 2011



UMP

* Delete if unnecessary

STUDENT'S DECLARATION

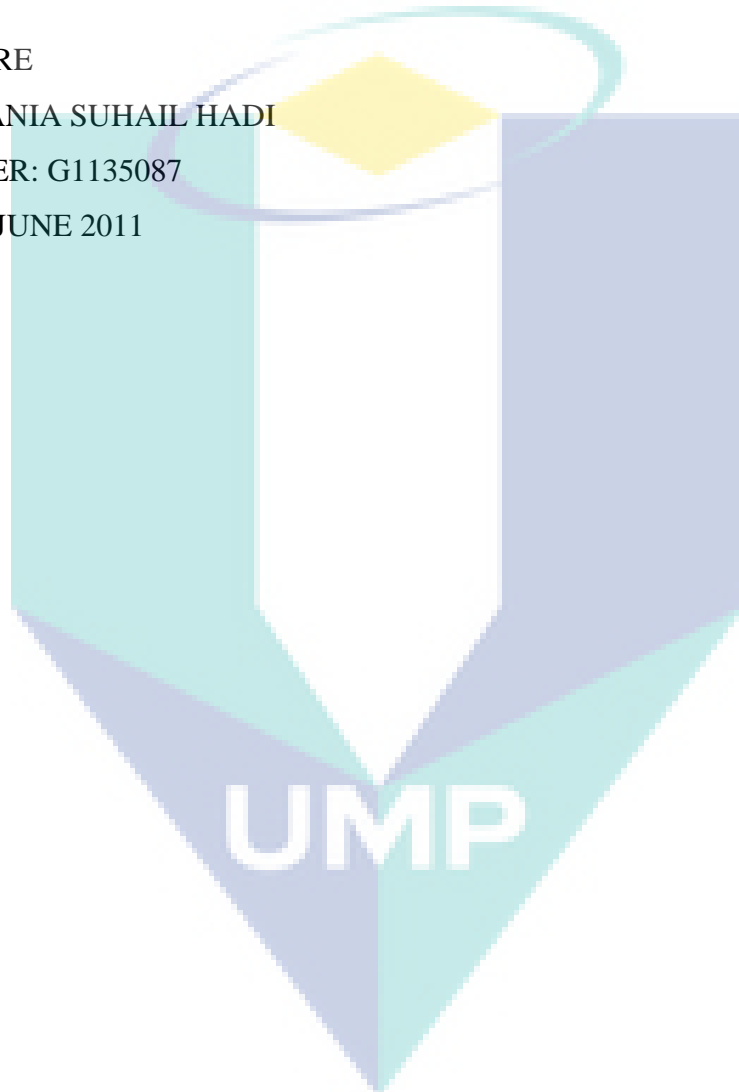
I hereby declare that the work in this thesis/~~project~~* is my own except for quotations and summaries which have been dully acknowledged. The thesis/~~project~~* has not been accepted for any degree and is not concurrently submitted for award of other degree.

SIGNATURE

NAME: TANIA SUHAIL HADI

ID NUMBER: G1135087

DATE: 28 JUNE 2011



*Delete if unnecessary

ACKNOWLEDGEMENTS

I am grateful and would like to express my sincere gratitude to my supervisor Associate Professor Dr. Hayder A. Abdul Bari for his germinal ideas, invaluable guidance, continuous encouragement and constant support in making this research possible. He has always impressed me with his outstanding professional conduct, his strong conviction for science, and his belief that a PhD program is only a start for a life-long learning experience. I appreciate his constant support from the first day I applied to graduate program to these concluding moments. I am truly grateful for his progressive vision about my training in science, his tolerance of my naïve mistakes, and his commitment to my future career. I also would like to express very special thanks to my co-supervisor professor Dr. Rosli Bin Mohd. Yunus for his suggestions and co-operation throughout the study. I also sincerely thanks for the time spend proofreading and correcting my many mistakes.

My sincere thanks go to all my labmates and members of the staff of the Chemical Engineering Department, UMP, who helped me in many ways and made my stay at UMP pleasant and unforgettable. Many special thanks go to member engine research group for their excellent co-operation, inspirations and supports during this study.

I acknowledge my sincere indebtedness and gratitude to my parents for their love, dream and sacrifice throughout my life. I acknowledge the sincerity to my husband for his sacrifice, patience, and understanding that were inevitable to make this work possible. I cannot find the appropriate words that could properly describe my appreciation for his devotion, support and faith in my ability to attain my goals. Special thanks should be given to my committee members. I would like to acknowledge their comments and suggestions, which was crucial for the successful completion of this study.

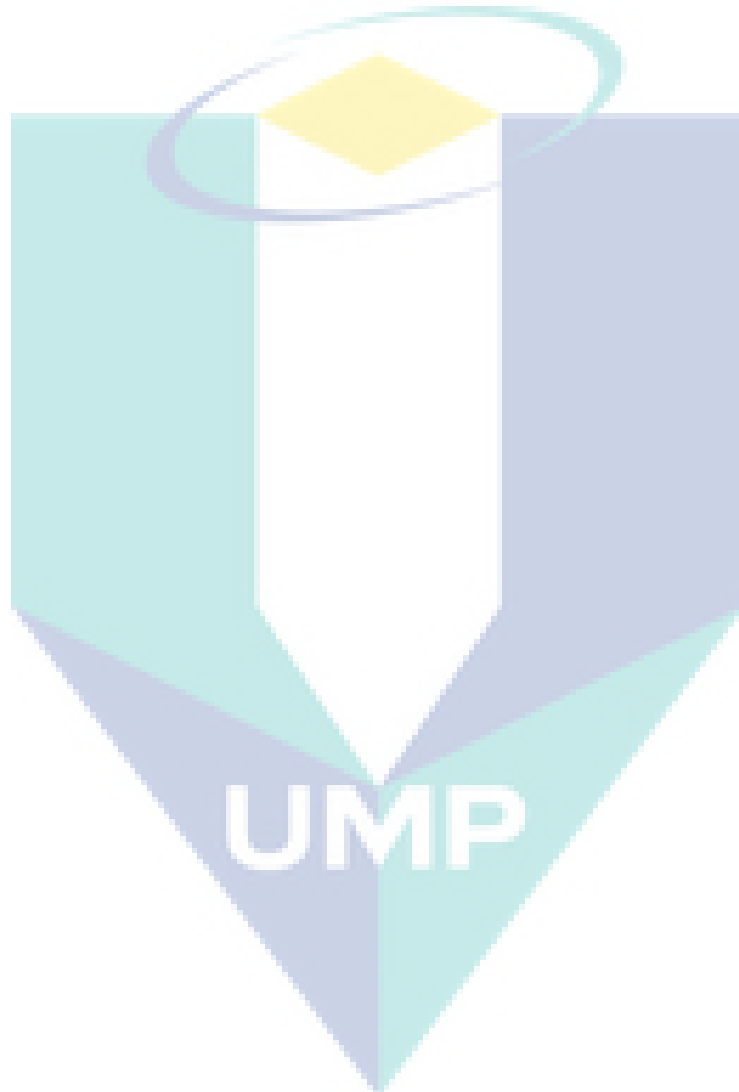
The logo of Universiti Malaysia Perlis (UMP) is a large, stylized letter 'U' composed of four overlapping triangles in shades of teal and light blue. The letters 'UMP' are printed in white, bold, sans-serif font across the center of the 'U' shape.

UMP

ABSTRACT

One of the major problems faced by the modern industrial applications is the power consumption and the limited power sources in the world. One of the most power consuming sectors in the industry is the liquid transportation through strategic pipelines for hundreds and thousands of miles. It is considered one of the most power dissipation industrial applications due to the turbulent mode these liquids are transported with. This is why; supporting pumping stations are assembled and located along the transportation pipeline to regain the pumping power lost during transportation. During the past century, many solutions for this problem were introduced. One of these solutions is the introduction of minute quantities of long chained polymeric additives that have the ability to interfere within the turbulent media formed inside the pipelines and reduce the power losses. The solubility and shear degradation of these polymers during transportation added more problems to the major problem to be solved. A more effective solution is needed. In the present investigation, three types of suspended solid materials, which are sand, aluminum and coal powders, are investigated as drag reducing agents to overcome the solubility problems that any new material finding to be recognized as drag reducing agent. Also, two types of commercially available zwitterionic surfactants ((3-(Decyldimethyl-ammonio) propanesulfonate inner salt) and (3-(N-N Dimethylpalmityl-ammonio) propanesulfonate) are investigated their efficiency in improving the suspended solid drag reducing abilities. An experimental closed loop liquid recirculation rig was built to carry out the experimental work. The rig consists of tanks, pumps, three pipes with three different diameters 0.0125, 0.0254 and 0.0381 m I.D. Each pipe was divided into four testing sections with 0.5 m length for each one. The flow rate of the transported water was measured using ultrasonic flow meter and the pressure drop measurement for each section was made using differential manometer. The powders were added within three different concentrations 100,300 and 500 ppm while the surfactants were added to the suspension solutions within three different concentrations 10, 20 and 30 ppm. The variables investigated in the present work were; the pipe diameter effect, the testing section length, the suspended solid type, the suspended solid concentrations, the suspended solid particle size two sizes were investigated 45 and 71 μm , the surfactant type, the surfactant concentrations and the solution flow rates. Using the suspended solids as drag reducing agents, the experimental results showed that, the powders can act as a powerful drag reducing agents and the Percentage of Drag Reduction (%Dr) increases by increasing the solution flow rate represented by the dimensionless form of Reynolds Number (Re). The %Dr was found to be higher for smaller pipe diameters and the testing section length didn't show a noticeable effect on the powder performance as drag reducing agent. Maximum %Dr up to 38, 45 and 38% were observed for the sand, aluminum and coal powders respectively. The %Dr was found to increase by increasing the suspended solid concentrations inside the pipe. The values of the %Dr were higher for the larger particles size (71 μm). Generally, the aluminum powder showed the higher and more stable drag reduction performance compared with the other two powders investigated due to the powder density effect. The addition of the surfactants to the suspended solid solution improved its drag reduction performance up to 78% in certain cases. The drag reduction performance was found to increase by increasing the surfactant concentrations

reaching certain maximum values up to (67, 67 and 69)% for DAPI and (64.5, 65.5 and 69.8)% for the NNAP added aluminum, coal and sand powders respectively. A numerical model (correlation) is derived and introduced as a mathematical representation for the experimental work. The final form was $f=a(\text{Re})^b$. Statistical analysis was applied for all the experimental data and compared with Virk's asymptote. All the results were close enough to that asymptote and one of the correlation passed Virk's asymptote with the form $f=0.798\text{Re}^{-0.746}$.



ABSTRAK

Salah satu masalah utama yang dihadapi oleh industri di zaman moden ini ialah penggunaan tenaga dan kekangan sumber tenaga di dunia. Salah satu sektor utama industri yang menggunakan tenaga yang tinggi ialah di dalam pengangkutan cecair melalui paip yang boleh menjangkau beribu batu panjangnya. Pengangkutan cecair melalui aliran paip adalah penyumbang utama kehilangan tenaga di dalam aplikasi industri disebabkan kehadiran aliran turbulen di dalam paip. Untuk mengatasi kejatuhan tekanan yang menggerakkan aliran cecair di dalam paip, stesen pam telah ditempatkan pada jarak tertentu di sepanjang paip untuk memastikan aliran cecair tidak tergendala dan berupaya sampai ke destinasi akhir. Sejak abad yang lalu, beberapa kaedah telah diperkenalkan untuk menyelesaikan masalah kejatuhan tekanan ini. Salah satu kaedah yang digunakan ialah dengan menambah satu kuantiti kecil penambah polimer berantai panjang yang berkeupayaan menyekat atau merosakkan pembentukan aliran turbulen di dalam paip dan mengurangkan kehilangan tenaga di dalam paip. Walaubagaimanapun, masalah keterlarutan dan kejatuhan daya ricih bahan polimer semasa pengangkutan cecair di dalam paip telah menambah masalah lain kepada masalah besar yang sedia ada yang perlu diselesaikan. Satu kaedah penyelesaian yang lebih berkesan adalah diperlukan. Dalam penyelidikan ini, tiga jenis pepejal terampai iaitu pepejal halus pasir, aluminium dan arang batu dikaji keberkesannya sebagai ejen pengurang heretan bagi menyelesaikan masalah keterlarutan yang dihadapi semasa penggunaan penambah polimer sebagai ejen pengurang heretan pada masa ini. Dua jenis surfaktan Zwitterionic komersial, ((3-(Decyldimethyl-ammonio) garam dalaman propanesulfonate, dan (3-(N-N Dimethylpalmityl-ammonio) propanesulfonate) juga dikaji keberkesannya di dalam meningkatkan keupayaan pepejal terampai sebagai ejen pengurang heretan. Satu radas ujikaji kitaran tertutup cecair dibina untuk menjalankan kajian ini. Radas tersebut terdiri dari dua tangki, dua pam dan tiga paip berlainan diameter (0.0125, 0.0254 dan 0.0381 m diameter dalaman). Setiap paip dibahagikan kepada empat bahagian dengan panjang 0.5 m setiap satu. Kadar alir cecair yang diangkut diukur menggunakan meter pengukur ultrasonik sementara kejatuhan tekanan di setiap bahagian diukur menggunakan manometer pembezaan. Tiga kepekatan pepejal halus atau debu telah dikaji di dalam penyelidikan ini iaitu 100, 300 dan 500 ppm sementara tiga kepekatan surfaktan diselidik iaitu 10, 20 dan 30 ppm. Beberapa parameter dikaji dalam penyelidikan ini, termasuk kesan diameter paip, kesan kepanjangan paip, jenis pepejal terampai, kepekatan pepejal terampai, diameter pepejal terampai (45 dan 71 μm), jenis surfaktan, kepekatan surfaktan dan kadar alir cecair di dalam paip. Menggunakan pepejal terampai sebagai ejen pengurang heretan, hasil kajian menunjukkan pepejal halus atau debu tersebut dapat bertindak sebagai suatu ejen pengurang heretan yang amat berkuasa dan peratus pengurangan heretan (%Dr) meningkat dengan peningkatan kadar alir cecair di dalam paip, ditunjukkan oleh Nombor Reynold (Re) Tak Berdimensi. Peratus pengurangan heretan (%Dr) di dapati lebih tinggi bagi paip berdiameter kecil dan kepanjangan paip tidak menunjukkan sebarang kesan yang signifikan terhadap kebolehan debu sebagai ejen pengurang heretan. %Dr maksima sehingga 38, 45 dan 38% dicapai di dalam penggunaan pasir, aluminium dan arang batu sebagai ejen pengurang heretan di dalam kajian ini. %Dr didapati meningkat dengan peningkatan kepekatan pepejal di dalam paip. %Dr di dapati lebih tinggi bagi pepejal bersaiz besar (71 μm) berbanding pepejal bersaiz kecil (45 μm). Secara amnya, pepejal aluminium

menunjukkan kebolehan yang lebih tinggi dan lebih stabil sebagai ejen pengurang heretan berbanding pasir dan arang batu kerana ketumpatannya yang lebih tinggi. Penambahan surfaktan ke dalam pepejal terampai telah meningkatkan %Dr sehingga 78% di dalam beberapa kes. %Dr didapati meningkat dengan peningkatan kepekatan surfaktan sehingga mencecah nilai maksima 67, 67 dan 69% bagi DAPI dan masing-masing 64.5, 65.5 dan 69.8% bagi sistem aluminium, arang batu dan pasir yang ditambah NNAP. Suatu model berangka (korelasi) diterbitkan dan digunakan sebagai gambaran matematik bagi kajian ini. Bentuk akhir model ini adalah $f=a(Re)^b$. Analisa statistik telah digunakan bagi kesemua data ujikaji dan telah dibandingkan dengan asimtot Virk. Kesemua keputusan menunjukkan nilai yang cukup hampir dengan asimtot tersebut dan salah satu korelasi menunjukkan nilai yang melebihi asimtot Virk iaitu dalam bentuk $f = 0.798 Re^{-0.746}$.

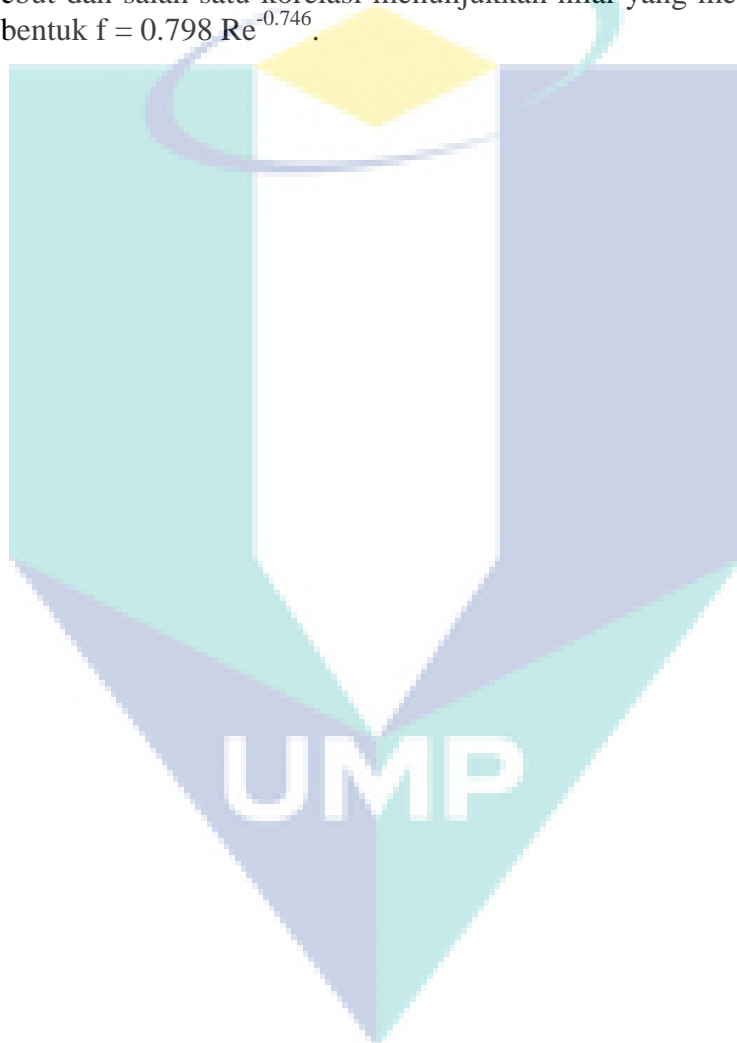


TABLE OF CONTENTS

SUPERVISOR'S DECLARATION	ii
STUDENT'S DECLARATION	iii
ACKNOWLEDGEMENTS	iv
ABSTRACT	v
ABSTRAK	vii
TABLE OF CONTENTS	ix
LIST OF TABLES	xiii
LIST OF FIGURES	xiv
LIST OF SYMBOLS	xxi
LIST OF ABBREVIATIONS	xxiii
LIST OF APPENDIXES	xxiv
CHAPTER 1 INTRODUCTION	
1.1 Backgrounds	1
1.2 Problem Statement	3
1.3 Objectives	4
1.4 Scopes of the Study	4
1.5 Research Contributions	5
1.6 Thesis Organizations	6

CHAPTER 2 LITERATURE REVIEW

2.1	Introduction	7
2.2	Turbulence	8
2.3	Energy Loss in Pipelines	14
2.4	Viscoelasticity	16
2.5	Drag Reduction	17
2.6	Drag Reducing Agent	18
2.6.1	Polymers	18
2.6.2	Fiber Suspensions	20
2.6.3	Surfactants	24
2.7	Drag Reduction Mechanisms	35
2.8	Commercial Application	39

CHAPTER 3 EXPERIMENTAL WORK

3.1	Introduction	41
3.2	Materials Used	41
3.2.1	Drag Reducing Agents (powders)	41
(i)	Aluminum Powder	42
(ii)	Sand Powder	42
(iii)	Coal Powder	43
3.2.2	Drag Reducing Agents (surfactants)	43
(i)	3-(N-N, Dimeethylpalmityl- ammino) propanesulfonate	44
(ii)	3-(Decyldimethyle-Ammino) Propanesulfonate Inner Salt	45

3.3	Experimental work	46
	Sieve Analysis	46
3.3.1	Flow System Description	47
	(i) Experimental Rig	48
	(ii) Portable Minisonic P Flow Meter	54
	(iii) Baumer Bellows Differential Pressure Gage	55
3.3.2	Solution Preparation	55
3.3.3	Experimental Work	56
3.4	Experimental Calculations	60
3.4.1	Percentage Drag Reduction	60
3.4.2	Velocity and Reynolds Number	60
3.4.3	Fraction Factor	60
CHAPTER 4	RESULTS AND DISCUSSIONS	
4.1	Liquid Recirculation System Verification	63
4.2	Suspended Solid Particles as Drag Reducing Agents	67
4.2.1	Effect of Reynolds Number (Re)	67
4.2.2	Effect of Additive Concentration	75
4.2.3	Effect of Pipe Diameter	81
4.2.4	Effect of Pipe Testing Section Length	87
4.2.5	Effect of Particle Size on the %Dr	92
4.2.6	Effect of Particle Type on the %Dr	98
4.3	Effect of Surfactant Addition on the %Dr	101
4.3.1	Effect of (DAPI) and (NNAP) additive on the %Dr-Re Relation	102

4.3.2	Effect of (DAPI) and (NNAP) additive on the %Dr for the suspended particles performance	111
4.4	Numerical Model (Correlations)	125
4.5	Mechanism	134

CHAPTER 5 CONCLUSIONS AND RECOMMENDATIONS

5.1	Conclusions	137
5.2	Recommendations	139
	References	141
	Appendices	149-214



UMP

LIST OF TABLES

Table No.	Title	Page
2.1	The advantage and disadvantage for the DRA's	35
3.1	Specification of Aluminum powder investigated	42
3.2	Specification of Sand powder investigated	42
3.3	Specification of Coal powder investigated	43
3.4	Properties of 3-(N-N,Dimethylpalmityl-ammino) propanesulfonate	44
3.5	Properties of 3-(Decyldimethyle-ammonio) propanesulfonate	46
3.6	Experimental flow system symbols description	50
4.1	Values of the correlations coefficients for each system investigated	128

The logo of UMP (Universiti Malaysia Perlis) is a large, downward-pointing arrow shape. It is composed of four colored triangular sections: a light blue section on the top left, a light purple section on the top right, a teal section on the bottom left, and a light blue section on the bottom right. The letters 'UMP' are written in white, bold, sans-serif font across the center of the arrow.

UMP

LIST OF FIGURES

Figure No.	Title	Page
2.1	Flow issuing at constant speed from a pipe: (a) high viscosity, low-Reynolds-number, laminar flow; (b) low-viscosity, high-Reynolds-number, and turbulent flow	9
2.2	Formation of a turbulent puff in pipe flow: (a) and (b) near the entrance; (c) somewhat downstream; (d) far downstream	10
2.3	(a) Laminar flow shear stress caused by random motion of molecules. (b) Turbulent flow as a result of random three dimensional eddies	12
2.4	Random Velocity Fluctuation at a point in turbulent flow	13
2.5	Velocity distribution in laminar and turbulent flows in pipelines	14
2.6	Schematic diagram of surfactant molecules	25
2.7	Structure of Triton X-100	26
2.8	A portion of soap micelle interface with the polar	29
2.9	Micelle structures	29
2.10	Concentration and diameter effect for Aluminum dioctoate in toluene	30
2.11	Effect of pipe diameter on drag reduction for 0.5% Brij96 Na ₂ SO ₄ at 45.7 °C in aqueous media flow	32
3.1	Structure of 3-(N-N,Dimethylpalmityl-ammino) propanesulfonate	44
3.2	Structure of 3-(Decyldimethyle-ammonio) propanesulfonate	45
3.3	Fritsch Sieve Analysis system	47
3.4	Schematic diagram of the experimental flow system	49
3.5	Schematic of test section	51
3.6	Experimental rig located in UMP laboratory	52
3.7	The main Pump (model CPM-158 with maximum load equal to (6.5 m ³ /hr))	52
3.8	The main pump circulation tank	53

3.9	The differential pressure manometer	53
3.10	Portable Minisonic P flow meter	54
3.11	Flow diagram of the experimental work with the investigated powders	58
3.12	Flow diagram of the experimental work with the investigated surfactant-suspended solid solution	59
4.1	Experimental friction factor versus Reynolds number for water flow in 0.0125 m pipe diameter and different pipe lengths	65
4.2	Experimental friction factor versus Reynolds number for water flow in 0.0254 m pipe diameter and different pipe lengths	66
4.3	Experimental friction factor versus Reynolds number for water flow in 0.0381 m pipe diameter and different pipe lengths	66
4.4	Effect of Re on the %Dr for sand particles ($D_p = 45 \mu\text{m}$) suspended in water and flowing in 0.0125 m I.D. and 0.5 m pipe	69
4.5	Effect of Re on the %Dr for sand particles ($D_p = 45 \mu\text{m}$) suspended in water and flowing in 0.0254 m I.D. and 0.5 m pipe	69
4.6	Effect of Re on the %Dr for Aluminum particles ($D_p = 71 \mu\text{m}$) suspended in water and flowing in 0.0381 m I.D. and 0.5 m pipe	70
4.7	Effect of Re on the %Dr for Aluminum particles ($D_p = 71 \mu\text{m}$) suspended in water and flowing in 0.0125 m I.D. and 0.5 m pipe	71
4.8	Effect of Re on the %Dr for Aluminum particles ($D_p = 71 \mu\text{m}$) suspended in water and flowing in 0.01254 m I.D. and 1.0 m pipe	71
4.9	Effect of Re on the %Dr for Aluminum particles ($D_p = 71 \mu\text{m}$) suspended in water and flowing in 0.0125 m I.D. and 2.0 m pipe	72
4.10	Effect of Re on the %Dr for Coal particles ($D_p = 45\mu\text{m}$) suspended in water and flowing in 0.0125 m I.D. and 0.5 m pipe	73
4.11	Effect of Re on the %Dr for Coal particles ($D_p = 45\mu\text{m}$) suspended in water and flowing in 0.0125 m I.D. and 1.5 m pipe	73
4.12	Effect of Re on the %Dr for Coal particles ($D_p = 45\mu\text{m}$) suspended in water and flowing in 0.0125 m I.D. and 2 m pipe	74

4.13	Effect of addition concentration on the %Dr for sand particles ($D_p = 45 \mu\text{m}$) suspended in water and flowing in 0.0125 m I.D. and 1.0 m pipe	77
4.14	Effect of addition concentration on the %Dr for sand particles ($D_p = 71 \mu\text{m}$) suspended in water and flowing in 0.0125 m I.D. and 1.0 m pipe	77
4.15	Effect of addition concentration on the %Dr for Aluminum particles ($D_p = 71 \mu\text{m}$) suspended in water and flowing in 0.0125 m I.D. and 1.0 m pipe	78
4.16	Effect of addition concentration on the %Dr for Aluminum particles ($D_p = 71 \mu\text{m}$) suspended in water and flowing in 0.0381 m I.D. and 1.0 m pipe	79
4.17	Effect of addition concentration on the %Dr for Coal particles ($D_p = 45 \mu\text{m}$) suspended in water and flowing in 0.0125 m I.D. and 1.0 m pipe	80
4.18	Effect of addition concentration on the %Dr for Coal particles ($D_p = 45 \mu\text{m}$) suspended in water and flowing in 0.0254 m I.D. and 1.0 m pipe	80
4.19	Effect of pipe diameter on the %Dr for 500 ppm concentration of sand particles suspended in water flowing with particle size of $45 \mu\text{m}$ and pipe length of 1 m	82
4.20	Effect of pipe diameter on the %Dr for 500 ppm concentration of sand particles suspended in water flowing with particle size of $71 \mu\text{m}$ and pipe length of 1 m	82
4.21	Effect of pipe diameter on the %Dr for 100 ppm concentration of aluminum particles suspended in water flowing with particle size of $71 \mu\text{m}$ and pipe length of 1 m	85
4.22	Effect of pipe diameter on the %Dr for 500 ppm concentration of aluminum particles suspended in water flowing with particle size of $71 \mu\text{m}$ and pipe length of 0.5 m	85
4.23	Effect of pipe diameter on the %Dr for 500 ppm concentration of coal particles suspended in water flowing with particle size of $45 \mu\text{m}$ and pipe length of 2.0 m	86
4.24	Effect of testing section length on the %Dr for 300 ppm concentration of sand particles suspended in water flowing with particle size of $45 \mu\text{m}$ and pipe diameter of 0.0125 m I.D	88

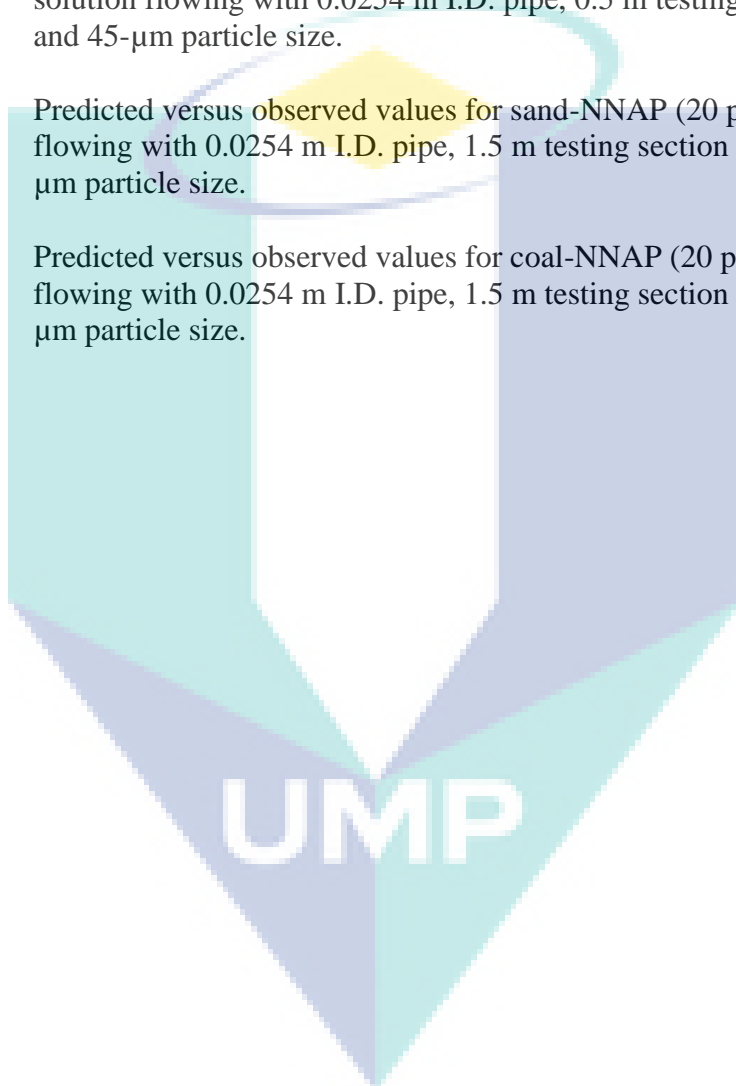
4.25	Effect of testing section length on the %Dr for 500 ppm concentration of sand particles suspended in water flowing with particle size of 45 μm and pipe diameter of 0.0125 m I.D.	89
4.26	Effect of testing section length on the %Dr for 100 ppm concentration of aluminum particles suspended in water flowing with particle size of 71 μm and pipe diameter of 0.0381 m I.D.	90
4.27	Effect of testing section length on the %Dr for 300 ppm concentration of aluminum particles suspended in water flowing with particle size of 71 μm and pipe diameter of 0.0125 m I.D	90
4.28	Effect of testing section length on the %Dr for 100 ppm concentration of coal particles suspended in water flowing with particle size of 71 μm and pipe diameter of 0.0254 m I.D.	91
4.29	Effect of testing section length on the %Dr for 500 ppm concentration of coal particles suspended in water flowing with particle size of 71 μm and pipe diameter of 0.0381 m I.D.	91
4.30	Effect of particle size on the %Dr for 300 ppm concentration of sand particles suspended in water flowing with and pipe diameter of 0.0381 m I.D and pipe length of 1 m.	93
4.31	Effect of particle size on the %Dr for 500 ppm concentration of sand particles suspended in water flowing with and pipe diameter of 0.0381 m I.D and pipe length of 1.0 m	94
4.32	Effect of particle size on the %Dr for 500 ppm concentration of sand particles suspended in water flowing with and pipe diameter of 0.0381 m I.D and pipe length of 2.0 m	95
4.33	Effect of particle size on the %Dr for 300 ppm concentration of aluminum particles suspended in water flowing with and pipe diameter of 0.0125 m I.D and pipe length of 0.5 m	96
4.34	Effect of particle size on the %Dr for 100 ppm concentration of aluminum particles suspended in water flowing with and pipe diameter of 0.0254 m I.D and pipe length of 1.5 m	97
4.35	Effect of particle size on the %Dr for 300 ppm concentration of coal particles suspended in water flowing with and pipe diameter of 0.0125 m I.D and pipe length of 0.5 m	97
4.36	Effect of particle type on the %Dr for 500 ppm concentration of sand, coal and aluminum particles suspended in water flowing with particle size of 71- μm , pipe diameter of 0.0254 m I.D and pipe length of 2.0 m	99

4.37	Effect of particle type on the %Dr for 300 ppm concentration of sand, coal and aluminum particles suspended in water flowing with particle size of 71- μm , pipe diameter of 0.0125 m I.D and pipe length of 1.0 m	100
4.38	Effect of particle type on the %Dr for 500 ppm concentration of sand, coal and aluminum particles suspended in water flowing with particle size of 42- μm , pipe diameter of 0.0125 m I.D and pipe length of 1.0 m	100
4.39	Effect of DAPI surfactant additive on the %Dr for water flowing through 0.0125 m I.D. pipe and 1 m pipe length	103
4.40	Effect of NNAP surfactant additive on the %Dr for water flowing through 0.0125 m I.D. pipe and 1 m pipe length	103
4.41	Effect of NNAP surfactant additive on the %Dr for water flowing through 0.0254 m I.D. pipe and 1 m pipe length	104
4.42	Effect of 10 ppm of DAPI surfactant additive on the Re-%Dr relation for aluminum particles ($D_p = 45 \mu\text{m}$) suspended in water and flowing in 0.0254 m I.D. and 1.0 m pipe length	105
4.43	Effect of 10 ppm of DAPI surfactant additive on the Re-%Dr relation for Aluminum particles ($D_p = 45 \mu\text{m}$) suspended in water and flowing in 0.0381 m I.D and 1.0 m pipe length	106
4.44	Effect of 10 ppm of DAPI surfactant additive on the Re-%Dr relation for Sand particles ($D_p = 45 \mu\text{m}$) suspended in water and flowing in 0.0125 m I.D. and 2.0 m pipe length	107
4.45	Effect of 10 ppm of DAPI surfactant additive on the Re-%Dr relation for Sand particles ($D_p = 45 \mu\text{m}$) suspended in water and flowing in 0.0254 m I.D. and 2.0 m pipe length	107
4.46	Effect of 20 ppm of NNAP surfactant additive on the Re-%Dr relation for Coal particles ($D_p = 45 \mu\text{m}$) suspended in water and flowing in 0.0125 m I.D. and 0.5 m pipe length	108
4.47	Effect of 20 ppm of NNAP surfactant additive on the Re-%Dr relation for Coal particles ($D_p = 71 \mu\text{m}$) suspended in water and flowing in 0.0125 m I.D. and 0.5 m pipe length	109
4.48	Effect of 30 ppm of NNAP surfactant additive on the Re-%Dr relation for Aluminum particles ($D_p = 71 \mu\text{m}$) suspended in water and flowing in 0.0125 m I.D. and 2.0 m pipe length	110

4.49	Effect of DAPI surfactant additive on the Sand particles ($D_p = 45 \mu\text{m}$ and 500 ppm additive concentration) performance as DRA for suspension in water and flowing in 0.0125 m I.D. and 0.5 m pipe length	112
4.50	Effect of DAPI surfactant additive on the Sand particles ($D_p = 45 \mu\text{m}$ and 300 ppm additive concentration) performance as DRA for suspension in water and flowing in 0.0125 m I.D. and 0.5 m pipe length	112
4.51	Effect of NNAP surfactant additive on the Sand particles ($D_p = 45 \mu\text{m}$ and 100 ppm additive concentration) performance as DRA for suspension in water and flowing in 0.0125 m I.D. and 0.5 m pipe length	113
4.52	Effect of NNAP surfactant additive on the Aluminum particles ($D_p = 45 \mu\text{m}$ and 500 ppm additive concentration) performance as DRA for suspension in water and flowing in 0.0254 m I.D. and 0.5 m pipe length	114
4.53	Effect of NNAP surfactant additive on the Aluminum particles ($D_p = 45 \mu\text{m}$ and 500 ppm addition concentration) performance as DRA for suspension in water and flowing in 0.0254 m I.D. and 1.0 m pipe length	115
4.54	Effect of NNAP surfactant additive on the Aluminum particles ($D_p = 45 \mu\text{m}$ and 500 ppm addition concentration) performance as DRA for suspension in water and flowing in 0.0254 m I.D. and 1.5 m pipe length	115
4.55	Effect of NNAP surfactant additive on the Aluminum particles ($D_p = 45 \mu\text{m}$ and 500 ppm addition concentration) performance as DRA for suspension in water and flowing in 0.0254 m I.D. and 2.0 m pipe length	116
4.56	Effect of DAPI surfactant additive on the Coal particles ($D_p = 71 \mu\text{m}$ and 100 ppm additive concentration) performance as DRA for suspension in water and flowing in 0.0125 m I.D. and 0.5 m pipe length	117
4.57	Effect of DAPI surfactant and Aluminum powder with particle size of 71- μm on the %Dr for water flowing through 0.0125 m I.D pipe and for 1 m pipe length	118
4.58	Effect of DAPI surfactant and Coal powder with particle size of 71- μm on the %Dr for water flowing through 0.0125 m I.D pipe and for 1 m pipe length	119

4.59	Effect of NNAP surfactant and Sand powder with particle size of 45- μm on the %Dr for water flowing through 0.0254 m I.D pipe and for 1 m pipe length	119
4.60	Effect of adding 20 ppm of DAPI and NNAP on the performance of the Aluminum powder ($D_p = 45 \mu\text{m}$) suspended in water and flowing in 0.0254 m I.D. and 1.5 m pipe length	121
4.61	Effect of adding 10 ppm of DAPI and NNAP on the performance of the Sand powder ($D_p = 71 \mu\text{m}$) suspended in water and flowing in 0.0125 m I.D. and 1.0 m pipe length	122
4.62	Effect of adding 20 ppm of DAPI and NNAP on the performance of the Aluminum powder ($D_p = 45 \mu\text{m}$) suspended in water and flowing in 0.0254 m I.D. and 2.0 m pipe length	123
4.63	Effect of adding 30 ppm of DAPI and NNAP on the performance of the Aluminum powder ($D_p = 71 \mu\text{m}$) suspended in water and flowing in 0.0125 m I.D. and 0.5 m pipe length	123
4.64	Effect of adding 20 ppm of DAPI and NNAP on the performance of the Coal powder ($D_p = 45 \mu\text{m}$) suspended in water and flowing in 0.0254 m I.D. and 1.0 m pipe length	124
4.65	Effect of adding 20 ppm of DAPI and NNAP on the performance of the Coal powder ($D_p = 45 \mu\text{m}$) suspended in water and flowing in 0.0125 m I.D. and 1.0 m pipe length	124
4.66	Friction factor versus Reynolds number correlations comparison with Virk correlation	129
4.67	Predicted versus observed values for aluminum-surfactant free solution flowing with 0.0254 m I.D. pipe, 1.0 m testing section length and 71- μm particle size	130
4.68	Predicted versus observed values for aluminum-surfactant free solution flowing with 0.0125 m I.D. pipe, 0.5 m testing section length and 45- μm particle size	130
4.69	Predicted versus observed values for sand-surfactant free solution flowing with 0.0254 m I.D. pipe, 1.0 m testing section length and 45- μm particle size.	131
4.70	Predicted versus observed values for coal-surfactant free solution flowing with 0.0125 m I.D. pipe, 2.0 m testing section length and 71- μm particle size.	131

4.71	Predicted versus observed values for aluminum-NNAP (10 ppm) solution flowing with 0.0381 m I.D. pipe, 0.5 m testing section length and 45- μ m particle size	132
4.72	predicted versus observed values for aluminum-NNAP (10 ppm) solution flowing with 0.0254 m I.D. pipe, 2.0 m testing section length and 71- μ m particle size	132
4.73	Predicted versus observed values for aluminum-DAPI (20 ppm) solution flowing with 0.0254 m I.D. pipe, 0.5 m testing section length and 45- μ m particle size.	133
4.74	Predicted versus observed values for sand-NNAP (20 ppm) solution flowing with 0.0254 m I.D. pipe, 1.5 m testing section length and 45- μ m particle size.	133
4.75	Predicted versus observed values for coal-NNAP (20 ppm) solution flowing with 0.0254 m I.D. pipe, 1.5 m testing section length and 45- μ m particle size.	134



LIST OF SYMBOLS

A	Area of surface fluid in pipe
C_f	Fanning friction factor
C	Concentration
I.D.	Inner diameter of pipe
F1	Ultrasonic Flow meter
f	Fanning friction factor
L	Pipe length
M_n	Number-average molecular weight
M_w	Molecular weight
n	Molecular number
$^\circ$	Inclination degree
ppm	Part per million
ρ	Density of fluid solution
ΔP	Pressure drop
ΔP_a	Pressure drop after addition
ΔP_b	Pressure drop before addition
μ	Absolute solution viscosity
v	Velocity
V_{avg}	Average velocity of fluid
ν	Kinematics viscosity
Q	Flow rate
R	Pipe radius
wt	Weight

r Radius at measuring position
 τ_w Wall shear stress

TS1 }
 TS2 }
 TS3 } Testing sections
 TS4 }

V1 Pump valve

V2 Bypass valve

V3,V6 0.0127m Pipe valve

V4,V7 0.0254m Pipe valve

V5,V8 0.0381m Pipe valve

P9,P10 Circulation pipe

V9,V10 Circulation valve

P11 Draining pipe of tank 1

P12 Draining pipe of tank 2

V11 Draining valve of tank 1

V12 Draining valve of tank 2

P1 Main pipe

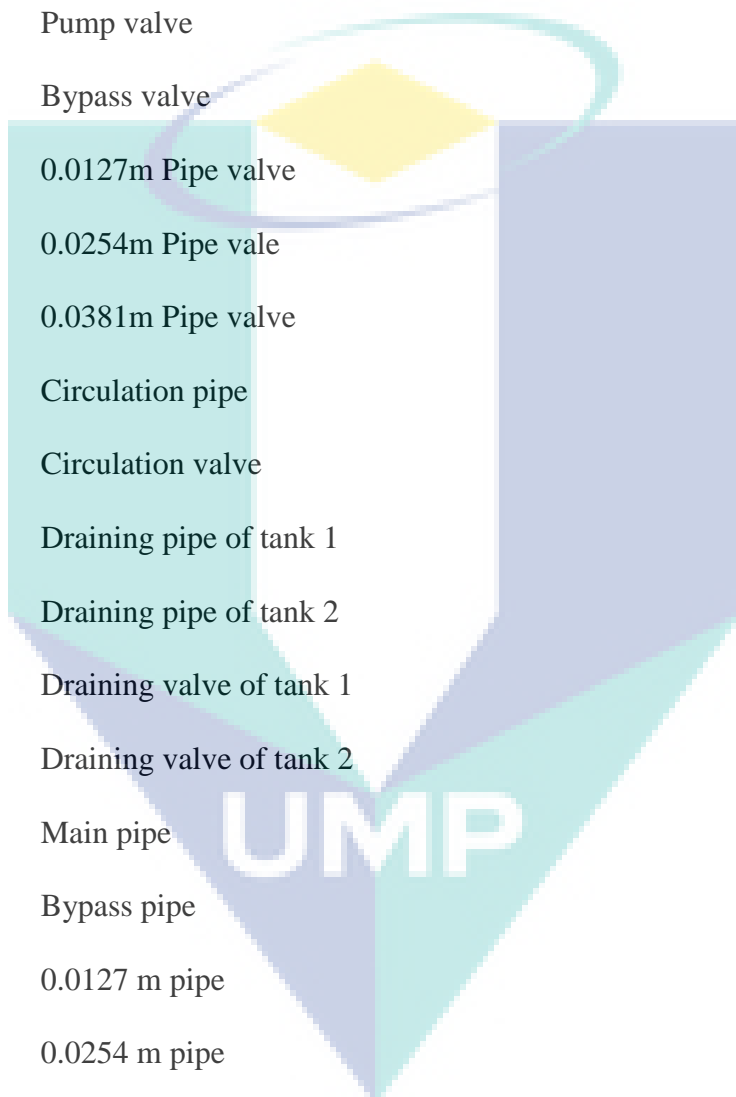
P2 Bypass pipe

P3 0.0127 m pipe

P4 0.0254 m pipe

P5 0.0381 m pipe

F1 Ultrasonic flow meter

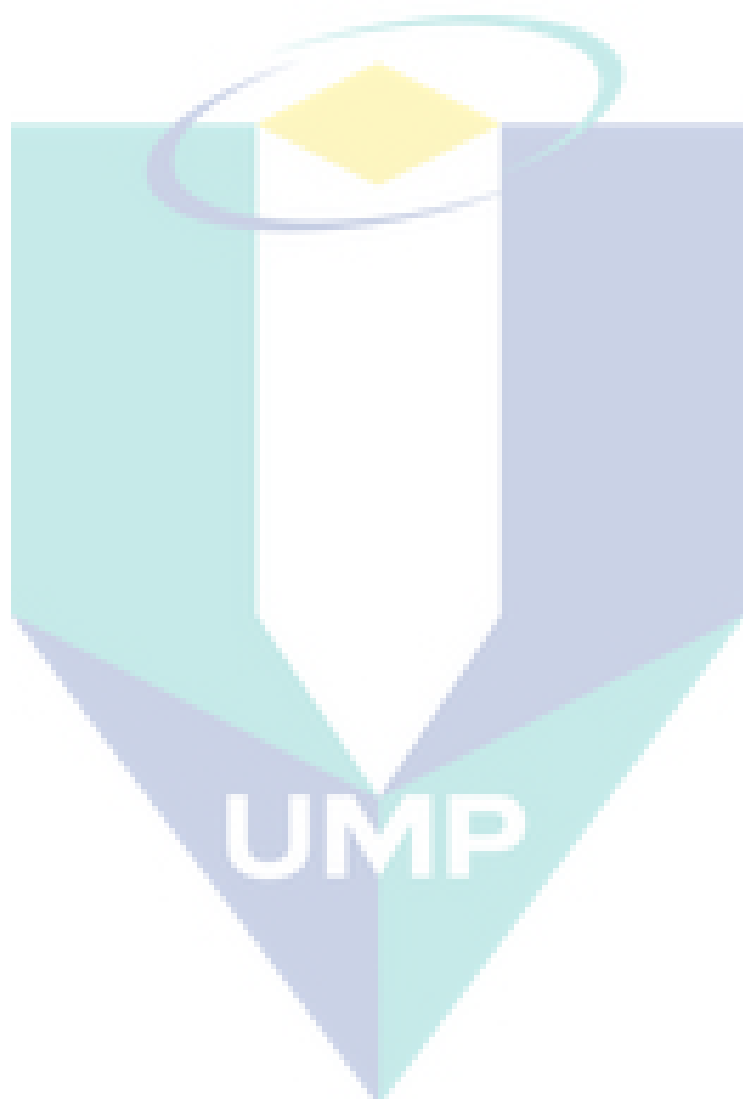


LIST OF ABBREVIATIONS

DR	Drag Reduction
DRA	Drag Reducing Agent
ASTM	American Society for Testing and Materials
CMC	Critical Micelle Concentration
CTAB	Cetyl Trimethyl Ammonium Chloride
CTAC	Cethyl Trimethyl Ammonium Chloride
TTAS	Tallow Trimethyl Ammonium Salicylate
ETAS	Erucyl Trimethyl Ammonium Salicylate
NaSal	Sodium Salicylate
SAOB	Stearyl Amine Oxide + Betaine
DAPI	3-(Decyldimethyl-Ammonio) Propanesulfonate Inner Salt)
NNAP	(3-(N-N,Dimethylpalmityl-Ammonio) Propanesulfonate)



UMP



List of Appendixes

Appendix	Title	Page
A1	Experimental Data For Coal Powder ($D_p = 45$, $D=0.0127$ m, $L=0.5$ m)	149
A2	Experimental Data For Coal Powder ($D_p = 45$, $D=0.0127$ m, $L=1$ m)	150
A3	Experimental Data For Coal Powder ($D_p = 45$, $D=0.0127$ m, $L=1.5$ m)	151
A4	Experimental Data For Coal Powder ($D_p = 45$, $D=0.0127$ m, $L=2$ m)	152
A5	Experimental Data For Coal Powder ($D_p = 71$, $D=0.0127$ m, $L=0.5$ m)	153
A6	Experimental Data For Coal Powder ($D_p = 71$, $D=0.0127$ m, $L=1$ m)	154
A7	Experimental Data For Coal Powder ($D_p = 71$, $D=0.0127$ m, $L=1.5$ m)	155
A8	Experimental Data For Coal Powder ($D_p = 71$, $D=0.0127$ m, $L=2$ m)	156
A9	Experimental Data For Coal Powder (NNAP 20 ppm, $D_p = 45$, $D=0.0254$ m, $L=0.5$ m)	157
A10	Experimental Data For Coal Powder (NNAP 20 ppm, $D_p = 45$, $D=0.0254$ m, $L=1$ m)	158
A11	Experimental Data For Coal Powder (NNAP 20 ppm, $D_p = 45$, $D=0.0254$ m, $L=1.5$ m)	159
A12	Experimental Data For Coal Powder (NNAP 20 ppm, $D_p = 45$, $D=0.0254$ m, $L=2$ m)	160
A13	Experimental Data For Coal Powder (DAPI 30 ppm, $D_p = 71$, $D=0.0127$ m, $L=0.5$ m)	161
A14	Experimental Data For Coal Powder (DAPI 30 ppm, $D_p = 71$, $D=0.0127$ m, $L=1$ m)	162
A15	Experimental Data For Coal Powder (DAPI 30 ppm, $D_p = 71$, $D=0.0127$ m, $L=1.5$ m)	163
A16	Experimental Data For Coal Powder (DAPI 30 ppm, $D_p = 71$, $D=0.0127$ m, $L=2$ m)	164
B1	Experimental Data For Aluminum Powder ($D_p = 71$, $D=0.0127$ m, $L=0.5$ m)	165

B2	Experimental Data For Aluminum Powder ($D_p = 71$, $D = 0.0127$ m, $L = 1.0$ m)	166
B3	Experimental Data For Aluminum Powder ($D_p = 71$, $D = 0.0127$ m, $L = 1.5$ m)	167
B4	Experimental Data For Aluminum Powder ($D_p = 71$, $D = 0.0127$ m, $L = 2.0$ m)	168
B5	Experimental Data For Aluminum Powder ($D_p = 71$, $D = 0.0381$ m, $L = 0.5$ m)	169
B6	Experimental Data For Aluminum Powder ($D_p = 71$, $D = 0.0127$ m, $L = 1.0$ m)	170
B7	Experimental Data For Aluminum Powder ($D_p = 71$, $D = 0.0127$ m, $L = 1.5$ m)	171
B8	Experimental Data For Aluminum Powder ($D_p = 71$, $D = 0.0127$ m, $L = 2.0$ m)	172
B9	Experimental Data For Aluminum Powder + 10 ppm of NNAP ($D_p = 45$, $D = 0.0127$ m, $L = 0.5$ m)	173
B10	Experimental Data For Aluminum Powder + 10 ppm of NNAP ($D_p = 45$, $D = 0.0127$ m, $L = 1.0$ m)	174
B11	Experimental Data For Aluminum Powder + 10 ppm of NNAP ($D_p = 45$, $D = 0.0127$ m, $L = 1.5$ m)	175
B12	Experimental Data For Aluminum Powder + 10 ppm of NNAP ($D_p = 45$, $D = 0.0127$ m, $L = 2.0$ m)	176
B13	Experimental Data For Aluminum Powder + 30 ppm of NNAP ($D_p = 45$, $D = 0.0127$ m, $L = 0.5$ m)	177
B14	Experimental Data For Aluminum Powder + 30 ppm of NNAP ($D_p = 45$, $D = 0.0127$ m, $L = 1.0$ m)	178
B15	Experimental Data For Aluminum Powder + 30 ppm of NNAP ($D_p = 45$, $D = 0.0127$ m, $L = 1.5$ m)	179
B16	Experimental Data For Aluminum Powder + 30 ppm of NNAP ($D_p = 45$, $D = 0.0127$ m, $L = 2.0$ m)	180
B17	Experimental Data For Aluminum Powder + 10 ppm of NNAP ($D_p = 71$, $D = 0.0381$ m, $L = 0.5$ m)	181

B18	Experimental Data For Aluminum Powder + 10 ppm of NNAP ($D_p = 71$, $D=0.0381$ m, $L=1.0$ m)	182
B19	Experimental Data For Aluminum Powder + 10 ppm of NNAP ($D_p = 71$, $D=0.0381$ m, $L=1.5$ m)	183
B20	Experimental Data For Aluminum Powder + 10 ppm of NNAP ($D_p = 71$, $D=0.0381$ m, $L=2.0$ m)	184
C1	Experimental Data For Sand Powder (NNAP 10 ppm , $D_p = 45$, $D=0.0254$ m, $L=0.5$ m)	185
C2	Experimental Data For Sand Powder (NNAP 10 ppm , $D_p = 45$, $D=0.0254$ m, $L=1.0$ m)	186
C3	Experimental Data For Sand Powder (NNAP 10 ppm , $D_p = 45$, $D=0.0254$ m, $L=1.5$ m)	187
C4	Experimental Data For Sand Powder (NNAP 10 ppm , $D_p = 45$, $D=0.0254$ m, $L=2.0$ m)	188
C5	Experimental Data For Sand Powder (NNAP 20 ppm , $D_p = 45$, $D=0.0125$ m, $L=0.5$ m)	189
C6	Experimental Data For Sand Powder (NNAP 20 ppm , $D_p = 45$, $D=0.0125$ m, $L=1.0$ m)	190
C7	Experimental Data For Sand Powder (NNAP 20 ppm , $D_p = 45$, $D=0.0125$ m, $L=1.5$ m)	191
C8	Experimental Data For Sand Powder (NNAP 20 ppm , $D_p = 45$, $D=0.0125$ m, $L=2.0$ m)	192
C9	Experimental Data For Sand Powder (NNAP 30 ppm , $D_p = 45$, $D=0.0254$ m, $L=0.5$ m)	193
C10	Experimental Data For Sand Powder (NNAP 30 ppm , $D_p = 45$, $D=0.0254$ m, $L=1.0$ m)	194
C11	Experimental Data For Sand Powder (NNAP 30 ppm , $D_p = 45$, $D=0.0254$ m, $L=1.5$ m)	195
C12	Experimental Data For Sand Powder (NNAP 30 ppm , $D_p = 45$, $D=0.0254$ m, $L=2.0$ m)	196
C13	Experimental Data For Sand Powder (NNAP 10 ppm , $D_p = 71$, $D=0.0127$ m, $L=0.5$ m)	197

C14	Experimental Data For Sand Powder (NNAP 10 ppm ,Dp =71, D=0.0127 m, L=1.0 m)	198
C15	Experimental Data For Sand Powder (NNAP 10 ppm ,Dp =71, D=0.0127 m, L=1.5 m)	199
C16	Experimental Data For Sand Powder (NNAP 10 ppm ,Dp =71, D=0.0127 m, L=2.0 m)	200
C17	Experimental Data For Sand Powder (DAPI 10 ppm ,Dp =45, D=0.01257 m, L=0.5 m)	201
C18	Experimental Data For Sand Powder (DAPI 10 ppm ,Dp =45, D=0.01257 m, L=1.0 m)	202
C19	Experimental Data For Sand Powder (DAPI 10 ppm ,Dp =45, D=0.01257 m, L=1.5 m)	203
C20	Experimental Data For Sand Powder (DAPI 10 ppm ,Dp =45, D=0.01257 m, L=2.0 m)	204
D1	Correlation Equation Parameters Estimation Steps	205
D2	Correlation Equation Derivative	212
E	Sample Of Calculations	214

The logo for UMP (Universitas Muhammadiyah Purwokerto) is a large, downward-pointing arrow shape. It is composed of several overlapping geometric shapes in shades of teal, light blue, and yellow. The letters 'UMP' are printed in a bold, white, sans-serif font across the bottom of the arrow.

UMP

CHAPTER 1

INTRODUCTION

This chapter is a general preview of the current work, where the problem statement, the objective of the work and the scopes for this study are reviewed. A clear explanation presents for each of them in such a way easy for the readers to understand the main target of the present work.

1.1 BACKGROUNDS

Transporting liquids, especially crude oils, refinery products and water through pipelines always occur in turbulent mode through strategic pipelines. Massive amounts of the pumping power are lost during the transportation due to the power dissipation caused by the turbulent structures formed in the flow media. Due to the velocity difference between the laminar sub layer and the core of the turbulent flow system, eddies are formed.

Generally, eddies are the main structures causing the turbulence inside pipelines. It is believed that as the eddy continue within the main flow; the shape of the eddy will continue growing up with more swirling movement and shaping. Completing the eddy its shape means absorbing and redirecting more energy from the main flow toward the turbulence. And this will lead to the losses in the pumping power that can be sensed from the pressure drop across the piping system.

The introduction of minute quantities of certain chemical additives is proven to have the ability to improve the flow inside pipelines carrying liquids in turbulent flow regime. In some cases, it is necessary to increase the transported liquid flow rate in built pipelines to avoid any extra costs and time spend on building new pipelines to have the same flow improvement needed. The success of commercial application of drag reduction using chemical additives has been established in pipelines transporting crude oil or refinery products. In addition, this technique has been applied successfully in

many fields such as in sanitary engineering, hydro-transport of solids, medical application, fire fighting and irrigation. (Sellin and Ollis, 1980)

Surfactants, polymers and suspended solid were introduced successfully as drag reducing agents in many applications for raw water, crude oil and refinery products transportation through pipelines. Many companies like “CONOCO” and “TAPS” have established commercial applications of polymeric drag reducers for crude oil transportation (Conoco Philips, 2006). These commercial applications contributed significantly in improving the flow in strategic pipelines operating under severe conditions. The additives drag reduction ability at concentrations as low as parts per million (ppm) is attributed to the additive molecules and micelles present in the solution.

One of the major problems associated with the usage of these additives (especially polymers and surfactants), is the solubility of the additive in flowing media, the toxicity and the effect of the additive on the apparent physical properties of the liquid. This is why, there is a need to develop or discover a new drag reducing agent that can perform as an efficient drag reducing agent with various transported media (e.g. water and oil).

One of the very interesting results in the drag reduction science was the introduction of the suspended solids as drag reducing agent. As much as it helped to solve the solubility condition problem, it also added more questions and mystery to the real mechanism controlling the drag reduction systems.

Even though intensive researches have been done, a fully accepted theory behind the drag reduction does not exist. The reason for the difficulty is the nature of the problem; it is a combination of physics, chemistry, rheology and hydrodynamic. The chaotic media that the drag reducer works in (turbulent flow), where masses of liquid moves randomly through the pipe in a non-predictive manner, and the absence of a modern technique to establish a clear mapping of turbulence inside the pipe, made all the mechanisms that have been suggested highly speculative and all have been subjected to criticism. Nevertheless, the major categories of drag reduction mechanisms suggested

in the literatures were the adsorption mechanism, structure mechanism and viscous-elastic mechanisms. While, high percentages of drag reduction were established using fiber suspensions. This technique made the prediction of the drag reduction mechanism harder, because there is another phase presented during the turbulent flow and that minimized the idea of chemical additive dilution in transported fluid.

One of the important contributions of the present work is the introduction of Zwitterionic surfactant as performance enhancer for the proposed suspended solid drag reducing agent. This introduction show the effect of combining two different types of drag reducing agent on the drag reduction performance, which lead to a better understanding of the controlling mechanism and the optimum operating conditions, especially from the economic point of view.

1.2 PROBLEM STATEMENT

One of the solutions to the pumping power losses during the transportation of fluids through pipelines is by the addition of certain soluble chemicals to the main flow. These chemicals have the viscoelastic properties to interfere within the turbulent structures and suppress the degree of turbulence, which will lead to the improvement of flow inside pipelines.

It was a concrete condition for any chemical to be defined or introduced as drag reducing agent to be soluble in the transported media. That raises a new problem regarding the relation between the additive type and concentration on the apparent physical properties of the transported liquid and its quality. This is why the new commercial DRA's are very expensive and its usage is limited due to its solubility in the media and toxicity.

It is very important to introduce a new drag reducing agent that can improve the flow into the pipelines without changing any of the transported liquid apparent physical properties and to overcome the solubility problem. This drag reducing agent must have the ability to improve the flow inside the pipelines by the addition of very small concentrations that can be separate and removed later. A combination between the

effect of two types of additives “soluble and insoluble” may contribute significantly to the drag reduction operation and introduce new operating conditions that lead to decrease the amount and concentration of the chemical DRA within the same drag reduction efficiency.

1.3 OBJECTIVES

Different variables were investigated in the present work; this can be classified into two main categories depending on the type of additives. The first category is the suspended solid and surfactants variables that include the apparent properties of the suspended solids such as the type, size, the surfactant type and the concentration. The other category included the closed loop liquid circulation system variables such as the pipelines geometry and the flow rate. The main objectives of the present work are:

1. To investigate the effects of adding different types, particle size and concentration of suspended solids in the turbulence levels to improve the flow inside pipes.
2. To investigate the effect of Zwitterionic surfactants additive on the suspended solid drag reduction performance. The surfactant variables investigated are:
 - a) The surfactant type
 - b) The surfactant concentration.
3. The effect of fluid Reynolds number (Re), pipe diameter (D_p) and testing section length (L) will be investigated for all the variables mentioned above.
4. To introduce a mathematical expression “empirical model correlation” for the experimental data using a statistical approach.

1.4 SCOPES OF THE STUDY

This research introduces three different types of suspended solid powders namely sand, aluminium and coal as insoluble drag reducing agents. An aqueous media used with turbulent mode through a pipeline to overcome the solubility condition for any material to be classified as drag reducing agent.

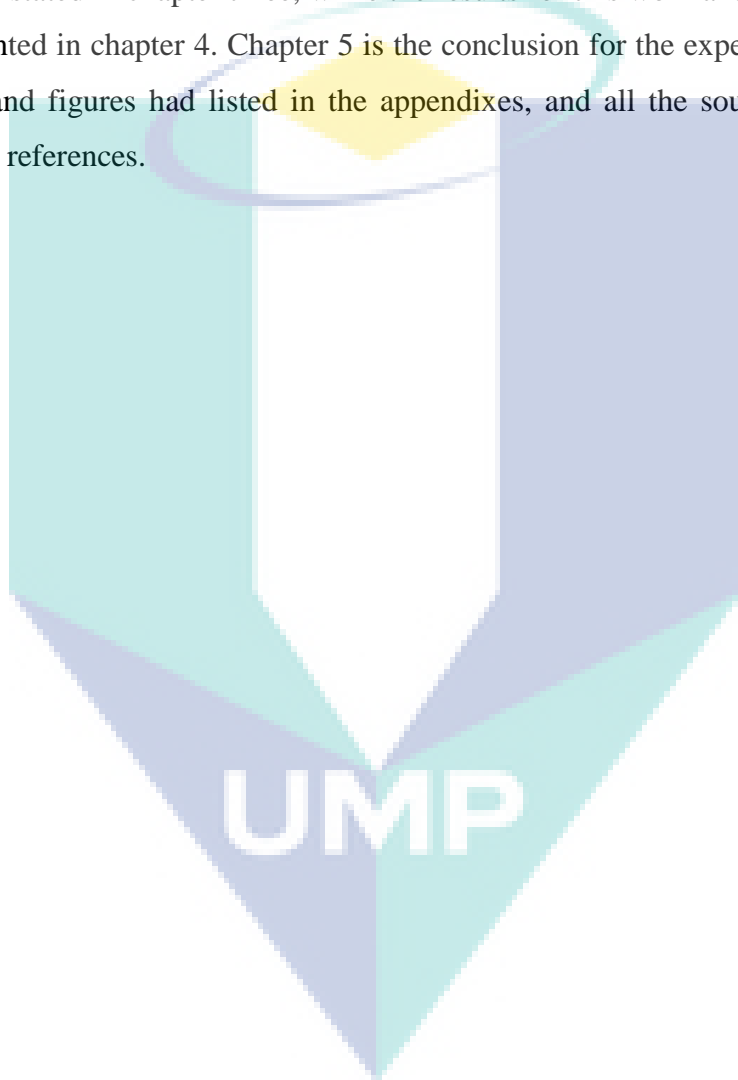
Also, this study present two types of Zwitterionic surfactants namely (3-(Decyldimethyl-ammonio) propanesulfonate inner salt) and (3-(N-N, Dimethylpalmityl-ammonio) propanesulfonate) as drag reduction performance improves for the suspended solids investigated. This will show its contribution in improving and optimizing the performance of the suspended solids as drag reducing agent. Finally, this study introduces a mathematical expression for the experimental data collected in the form of mathematical correlation(s).

1.5 RESEARCH CONTRIBUTIONS

The present work will introduce a very important concept of merging two types of drag reducing agents (suspended solids) and surfactants in the same flowing system. This will help significantly in understanding or approaching the real mechanism controlling the drag reduction phenomena. Aluminum powder will be used for the first time as a flow improver in pipelines in the present work. This will add another key in solving the drag reduction mechanism using suspended solids. The three different powders investigated (Coal, Aluminum and sand) will clear the idea regarding the effect of the suspended solid physical properties effect on the drag reduction performance due to the high differences in its densities. Furthermore, the two types of surfactants investigated are introduced for the first time as flow improvers in aqueous media flowing in turbulent flow.

1.6 THESIS ORGANIZATIONS

This thesis divided into five major chapters, which in turns divided into sections. The main parts, as in the sequence begin with chapter one, which is the introduction of this thesis. Chapter 2 is a review of past research efforts related to the drag reduction, surfactants, fiber suspensions and polymers. The experimental work with the related equations is stated in chapter three, while the results for this work and the discussion for it are presented in chapter 4. Chapter 5 is the conclusion for the experimental work. All the tables and figures had listed in the appendixes, and all the sources referred have listed in the references.



CHAPTER 2

LITERATURE REVIEW

2.1 INTRODUCTION

Drag can be defined as the drop in pressure per unit length when fluid flows in a pipe. While, drag reduction is the power recovering in the flow of fluid in the pipe by addition of a small amount of chemical additives to a solvent in turbulent flow in order to decrease the pressure drop (M. Fichman and G. Hetsroni, 2004). Since in a whole host of widely differing engineering devices, the operating power largely used in overcoming turbulent drag, the prospect of drastically reducing drag is an exciting one, implying possibilities of great commercial benefits.

Ordinary viscometry might fail to detect any significant difference between a drag reducing solution and the pure solvent, especially in the case of fluid motion. The stresses in the ordinary liquid are related to the velocity gradient by the three dimensional generalization of Newton's law of viscosity for simple shear flow. The shear stress is linearly proportional to the instantaneous velocity gradient for fluids in which the stresses obey such generalized relations called "Newtonian". However, in most complicated flows, the fluid may behave in a manner that is in part fluid like and in a part like an elastic solid. Such non-Newtonian behavior is termed viscoelasticity. From the above, it can be notice that the fluid motion (especially with turbulent flow), the type of chemical additives and its performance affect drag reduction as a phenomenon during operation.

In the present chapter, a brief introduction to the turbulent flow characteristics and the non-uniform movement of the liquid globes will be presented. Furthermore, types of drag reducing agents and brief description on the previous experimental work and results achieved by numerous authors are arranged chronologically.

2.2 TURBULENCE

Most examples of flow in nature and many in industry are turbulent. Turbulence is an instability phenomenon caused, in most cases, by the shearing of the fluid. Turbulent flow is characterized by rapid and chaotic fluctuations of all properties including the velocity and pressure. This chaotic motion is often described as being made up of 'eddies', but it is important to appreciate that eddies do not have a purely circular motion (Heywood, Karen J.,1993).

Turbulence is a fluctuating and chaotic state of fluid motion, which exists when non-linear inertial effects dominate over viscous effects. Apart from a rather qualitative insight into the dynamic, a complete theory of turbulence is still lacking because it is not possible until now to analyze in details the non-linearity that governs the turbulence flow. Turbulence mostly studied from a statistical point of view and accurately predicting the detailed evaluation of a turbulent, which is, in principle, impossible (White, 1999).

The first notification of the two flow systems (laminar and turbulent flow) observed in free surface flows. Figure 2.1 shows the liquid flow issuing from the open end of a tube. The low-Reynolds-number jet (Fig. 2.1 a) is smooth and laminar, with the fast center motion and slower wall flow forming different trajectories joined by a liquid sheet. The higher-Reynolds-number turbulent flow (Fig. 2.1 b) is unsteady and irregular but, when averaged over time, is steady and predictable (White, 1999).

The flow pattern and structure inside pipelines also observed experimenting with glass tube flow. Figure 2.2 shows a puff as photographed by Bandyopadhyay (1986). Near the entrance (Fig. 2.2 a and b), there are an irregular laminar-turbulent interface, and vortex roll-up is visible. Further downstream (Fig. 2.2 c) the puff becomes fully turbulent and very active, with helical motions visible. Far downstream (Fig. 2.2 d), the puff is cone-shaped and less active, with a fuzzy ill-defined interface, sometimes called the "re-laminarization" region.



Figure 2.1: Flow issuing at constant speed from a pipe: (a) high viscosity, low-Reynolds-number, laminar flow; (b) low-viscosity, high-Reynolds-number, and turbulent flow (White, 1999).

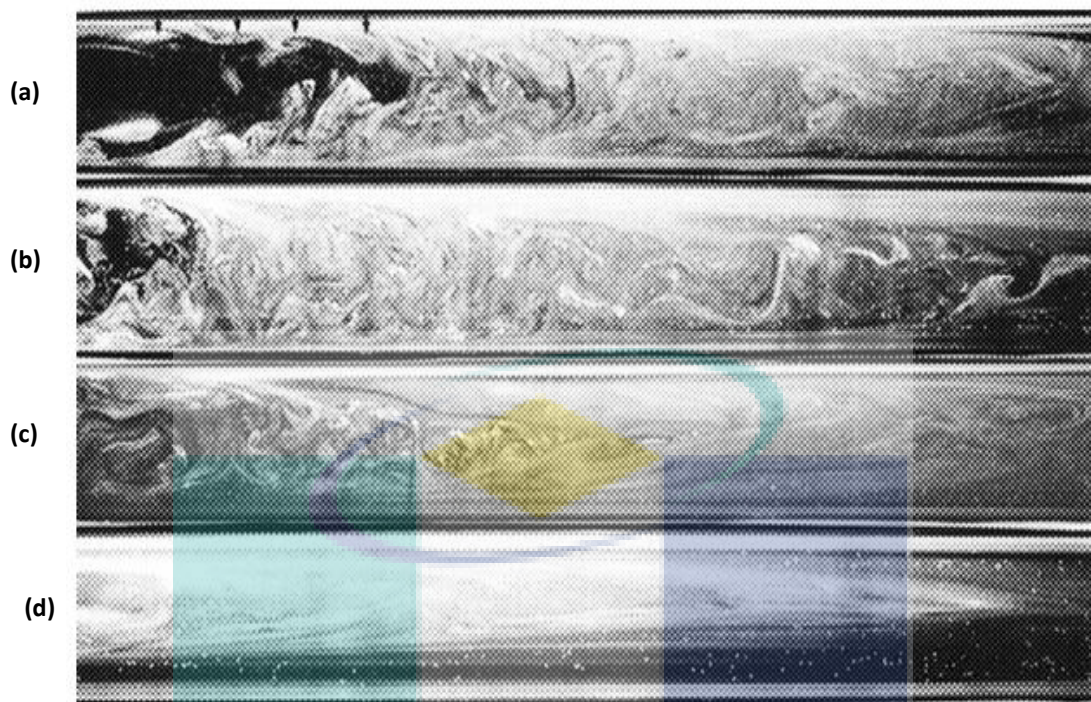


Figure 2.2: Formation of a turbulent puff in pipe flow: (a) and (b) near the entrance; (c) somewhat downstream; (d) far downstream (Bandyopadhyay 1986).

When turbulent flow occurs, eddies are generated due to the velocity differences between the fluid moving layers where the eddy flow direction differs from that of the general flow; the motion of the whole fluid is the net result of the movements of the eddies that compose it. Eddies can transfer much more energy and dissolved matter within the fluid in comparison to molecular diffusion in non-turbulent flow because eddies actually mix together large masses of fluid. Flow composed largely of eddies is called turbulent; eddies generally become more numerous as the fluid flow velocity increases. Energy is constantly transferred from large to small eddies until it is dissipated (Holland and Bragg, 1995)

The word ‘eddy’ is simply a convenient term to denote an identifiable group of fluid elements having a common motion, whether that motion is shearing, stretching or rotation. Eddies have a wide range of sizes: in a pipe flow, the largest eddies are comparable in size to the diameter of the pipe, while the size of the smallest eddies will be typically 1 per cent of the pipe diameters. The various sizes of eddy also have different characteristic speeds and lifetimes (Holland and Bragg, 1995).

It is known that, eddies form only when the flow around the obstacle reaches a critical velocity; they represent a flow of fluid into the space behind the obstacle, and this inflow begins only when the general flow is fast enough to produce a lowered pressure there. Eddies or vortices (whirlpools) so produced can also cause sound. Many sounds, both natural and manmade, occur in this way. The same thing can happen in pipe flows, where the wall resistance plays the roll in controlling the degree of turbulence and the shape of eddies formed (Holland and Bragg, 1995).

The large eddies are generated by the shearing of the mean (time averaged) flow and they produce smaller eddies which in turn generate yet smaller ones. Energy extracted from the mean flow in the generation of the large eddies is passed on to the successively smaller eddies. The smallest eddies are so small, and their velocity gradients therefore so large, that viscous stresses are dominant and viscosity destroys the smallest eddies, dissipating their kinetic energy by converting it into internal energy of the fluid. This process of passing energy from large to small eddies is known as the 'energy cascade' (Holland and Bragg, 1995).

It is known that every time vortex stretching occurs it generates a vortex stretching in the two orthogonal directions. In this way, energy is passed to smaller and smaller eddies. Equally importantly, with successively smaller eddies the turbulence becomes less oriented, that is it becomes more nearly isotropic. Turbulence is always three-dimensional, even if the mean flow is not (Holland and Bragg, 1995).

The properties of the turbulence are different at the two extremes of the scale of turbulence. The largest eddies; known as the macroscale turbulence, contain most of the turbulent kinetic energy. Their motion dominated by inertia and viscosity has a little direct effect on them. In contrast, at the microscale of turbulence, the smallest eddies are dominated by viscous stresses, indeed viscosity completely smoothes out the microscale turbulence (Holland and Bragg, 1995).

The Reynolds number of a flow gives a measure of the relative importance of inertia force and viscous force. In experiments on fluid systems, it is observed that at values below the so-called critical Reynolds number, the flow is smooth and adjacent layers of fluid slide past each other in orderly fashion. If the boundary

conditions do not change with time, the flow is steady. This regime called laminar flow as shown in figure 2.3 a. At values of Reynolds number above recruit, complicated series of events take place, which eventually leads to a radical change of the flow character. In the final state, the flow behavior is unstable and the velocity and all other flow properties vary in a random and chaotic way. This regime called turbulent flow, as shown in figure 2.3 b (White, 1999).

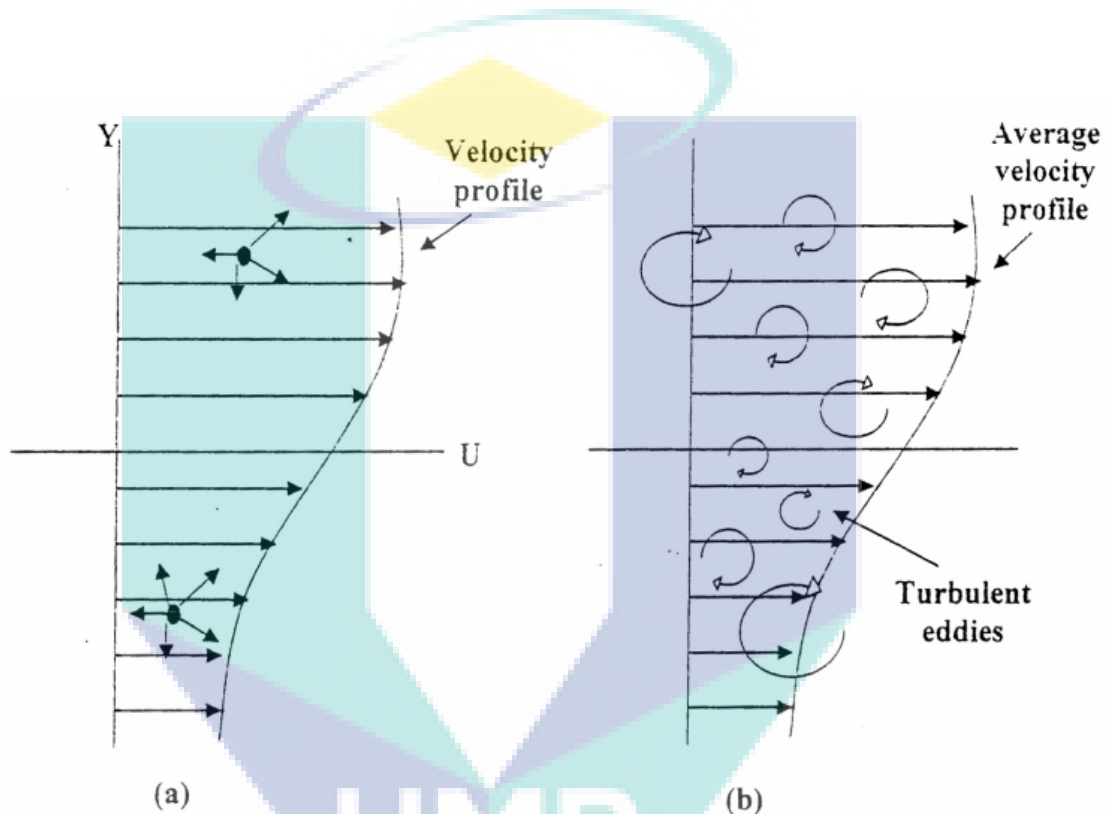


Figure 2.3: (a) Laminar flow shear stress caused by random motion of molecules. (b) Turbulent flow as a result of random three dimensional eddies (White, 1999).

The most essential feature of turbulent flow is the fact that at a given point, velocity and pressure are not constant with time but exhibit very irregular fluctuations of high frequency. These random velocity fluctuations at a point during turbulent flow are shown in figure 2.4 (Versteeg and Malalasekera, 1995).

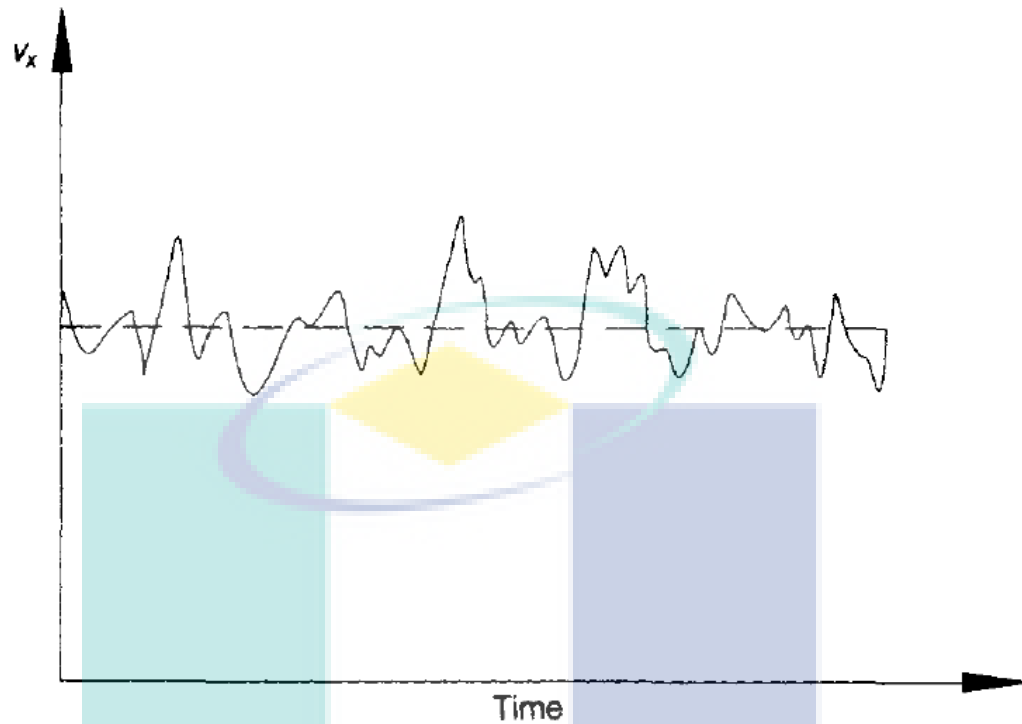


Figure 2.4: Random Velocity Fluctuation at a point in turbulent flow (Versteeg and Malalasekera, 1995).

The random nature of a turbulent flow precludes computation based on a complete description of the motion of all fluid particles. Instead the velocity in figure 2.4 can be decomposed into a steady mean velocity U with a fluctuating component $u'(t)$ superimposed on it: $U(t) = U + u'(t)$.

Even in flows where the mean velocities and pressure vary in only one or two space dimensions, turbulent fluctuation always have a three-dimensional special character. Furthermore, visualization of turbulent flows reveals rotational flow structure so-called turbulent eddies. These structures are ranged in size from a very small diameter (on the order of the size of the fluid particle) to fairly large diameters (on the order of the size of the flow geometry considered). This eddy structure greatly promotes mixing within the fluid, where bunches of fluid molecules (not merely individual molecules as in laminar flow) are randomly transported through the flow regime resulting in a relatively large (when compared with the laminar flow) shear force (Versteeg and Malalasekera, 1995).

Eddies are not isolated, small eddies exist inside large ones, and even smaller eddies exist inside small eddies. Smaller eddies are themselves stretched by somewhat larger eddies and more weakly by mean flow. In this way, the kinetic energy is handed from larger eddies to progressively smaller and smaller eddies in what is termed the energy cascade. The turbulence in a flow is self-sustaining. Once a flow becomes unstable and turbulence develops, it does not simply die out and repeat its self within the process (Hamilton, et. al. 1995).

By comparing the velocity distribution between the laminar and turbulent flows, a more uniform velocity distribution may be observed in turbulent flow. This is due to the nature of turbulent motion; the fluid with high kinetic energy carried by the transverse fluctuation towards the boundary, while the fluid moving at low kinetic energy near the boundary is carried away from the boundary into the region of high kinetic energy. Figure 2.5 shows the velocity distributions in laminar and turbulent flow through pipes (Dean, 1959).

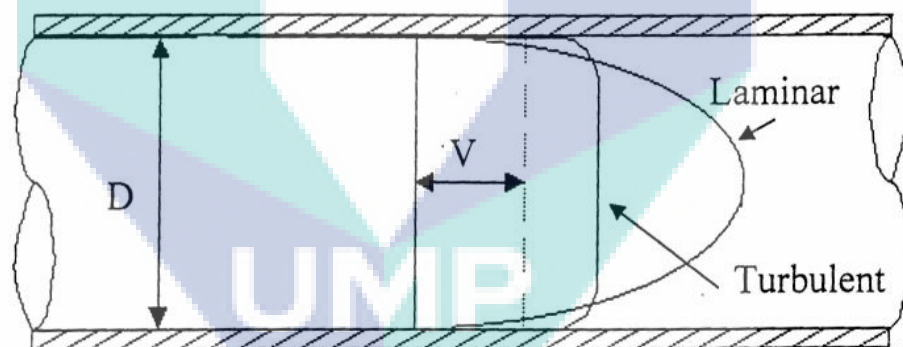


Figure 2.5: Velocity distribution in laminar and turbulent flows in pipelines (Dean, 1959).

2.3 ENERGY LOSS IN PIPELINES

The fluid flow through a pipe is required to overcome resistance due to friction offered by the pipe wall and fluid viscosity. As fluid flows along the pipe, part of its energy is dissipated in overcoming this resistance, with the result that the energy of fluid decreases continuously in the flow direction (Rashidi and Banerjee, 1990).

The measure of this energy loss or friction loss can be achieved by comparing the total energy at two points in the flow line, as a pressure gradient. Pressure gradient is usually expressed as the pressure difference relative to a selected horizontal datum divided by the distance between the two points, i.e. $(\Delta P/L)$ (Holland, 1973).

The friction loss can be expressed in terms of pressure drop per pipe length using energy balance equation for a circular horizontal pipe in a steady fluid flow, as follows: (Holland, 1973)

$$\tau_w = \frac{d(p_1 - p_2)}{4L} \quad (2.1)$$

The friction loss in pipe flow can also be expressed in dimensionless form of a friction factor (f):

$$f = \frac{2\tau_w}{\rho v^2} \quad (2.2)$$

Another expression for friction loss called fanning friction factor and it can be expressed as:

$$f = \frac{\Delta p \cdot d / 4L}{\rho \cdot v^2 / 2} \quad (2.3)$$

Break down of laminar flow usually commences at approximately $Re < 2000$, and transition to turbulent flow is usually completed by $Re > 4000$.

Blasius found that for values of Re up to 80,000 the friction factor could be expressed as follows (Bottural, 1999):

$$f = \frac{0.079}{Re^{0.25}} \quad (2.4)$$

Von-Karman suggested the logarithmic form for friction factor as (Hall and Osterhout, 1961):

$$1/f^{0.5} = 4\text{Log}(Re - f^{0.5} - 0.4) \quad (2.5)$$

Where:

- τ_w = friction loss (dimensionless)
- f = friction loss (dimensionless)
- p_1 =pressure at the first point (bar)
- p_2 =pressure at the second point (bar)
- Δp = pressure drop (bar)
- L =pipe length (m)
- d = pipe diameter (m)
- ρ = fluid density (kg/m^3)
- v = fluid velocity (m/s)
- Re =Reynold's number (dimensionless)

2.4 VISCOELASTICITY

One of the most important factors that made the drag-reducing additive to be functional is the viscoelasticity. The term viscoelastic came from the dual action of such additives that it is elastic material keeping the stress when it is under constant strain, and also it is a viscous material that dissipated the stress immediately after the strain action. In other words, when a stress is applied to any material, it will deform. The extent of deformation relative to the original dimension of the material defined as strain. If the deformation recovered on the removal of the stress, then the material is elastic. However, if the components of the material have been able to diffuse a sufficient distance during the experiment to relieve at least a part of the applied stress, then viscous flow will have occurred resulting in a permanent deformation (Billington and Tate, 1981).

The term “relaxation time” is one of the characteristics, especially in polymers, that give a close picture of the viscoelastic property of the additive. It is define as the

meantime needed to remove most of the stress when the drag reducing additives molecules are under a constant strain, reaching a new thermodynamic steady state of the solution (Cowie 1973).

2.5 DRAG REDUCTION

The drag reduction as a phenomenon dates back to the final years of World War II when Mysels (1954) led a team at Degwood Arsenal in studying the drag reducing characteristics of gasoline thickened with aluminum soaps.

It was a paper by Toms (1948), which gave the first clear scientific description of the effect that accordingly is often called “Toms’ phenomena”. Toms investigated the flow rate of various concentrations of poly (methyl methacrylate) in monochlorobenzene through tubes of two different diameters; he concluded the addition of this polymer would make the friction factor in turbulent flow through a pipe lower. Finally, the drag reduction was shown to increase by decreasing the pipe diameter.

A companion paper by Oldroyd (1948) suggested an interpretation of the effect based on the conception of a wall effect. Although it appears, that Oldroyd envisaged some modification of the condition of adherence of the fluid to the pipe wall. This idea based on the effective velocity of slip, which expected to be a function of wall shear stress, with the core of the flow behaving like an “ordinary” fluid in turbulent motion, is quite in accordance with current ideas. His experimental findings showed that the additive thickens the viscous sub-layer.

Lester (1985) published a series of articles on drag reduction reviewing the drag reducing agents, their fundamentals, applications and incidence as specified products and hardware. Later, the studies carried out by Vaseleski, and Metzener (1974), Hershy et. al., (1971) and Zakin (1983) in the past century were the leading investigations in establishing the first theoretical bases of drag reduction phenomena.

2.6 DRAG REDUCING AGENT

2.6.1 Polymers

Generally, a polymer is a macromolecule composed of repeating structural units typically connected by covalent chemical bonds. The study of polymer always been related with the degradation process. Degradation is a change in the properties such as tensile strength and shape. In 1949, Tom had unintentionally found that the polymers reduce the frictional drag in turbulent flow while conducting an experimental on mechanical degradation of polymer using simple pipes flow apparatus. The elasticity of polymer is the most important properties of polymer that make it to be used as drag reducing agent (Min and Choi, 2005).

Since in the early work of Toms (1948) polymers were one of the first chemical additives suggested to be used as drag reducing agents by many researchers. From the numerous experimental studies, it can be concluded that, in order to reduce turbulent drag, polymers should be very long chain structure with little branching, flexible and well diluted.

Virk et al. (1967) studied experimentally the drag reduction of distilled water solution with polyethylene oxide in turbulent pipe flow through 0.292 and 3.21 cm I.D. pipes. Onset of the drag reduction suggested occurring at a well-defined wall shear stress related to the random coiling effective diameter of the polymer. They also found that the maximum drag reduction possible is limited by an asymptote that is independent of polymer type and pipe diameter. They showed that the percent drag reduction increases by decreasing the pipe diameter. Flow structure measurements in a single polymer solution, 10 ppm of molecular weight 690,000 showed that the main flow follows as an effective slip mechanism.

Ram et al. (1967) studied the effects of some samples of poly-isobutylene on crude oil in a circulation loop system with high concentration (> 150 ppm). The results showed that there is a critical velocity, which depends on the type of the polymer and its molecular weight, where drag reduction starts above this velocity.

Hoyt (1972) investigated a wide variety of water-soluble polymers (poly(ethylene oxide), poly-acryl amide and guar gum) and showed that polyacrylamide was the most effective one as drag reducing agent with maximum %Dr of 30 % in concentrations as low as 3 ppm by weight. In these very low concentrations, the fluid has a viscosity that is independent of shear rate and not distinguishable from that of water. Thus, an apparent paradox became evident that a fluid was essentially the same as water in its values of density and viscosity could behave in a radically different way. They showed that, the polymers that could produce this effect were all of high or very high molecular weight and un-branched long chain structure. Finally, it was evident to their work that poly (ethylene oxide), poly-acryl amide and guar gum were effective drag reducers in aqueous media.

Warholc et al. (1999) injected Percol 727 into channel flow to study the effect of polymer on drag reduction in terms of Reynolds number and concentration, which the concentration of primary solution from 50 to 2000 ppm and the concentration at test section are from 0.25 to 50 ppm. It was found that the drag reduction decreases as the Re increases and increases as the concentration of solution increases. The maximum drag reduction obtained is 69 %. They found that the wall vortices that made up the turbulence flow were destroyed during the observation of this maximum drag reduction. They also suggested that the effectiveness of polymer as drag reducing agent is depended on aggregates, which these aggregates need to break up irreversibly.

Al-Sarkhi and Hanratty (2001) studied the effect of Percol 727 on drag reduction for annular gas-liquid flow in a horizontal pipe using two-way injection techniques, which were through downstream and through entrance of flow into the horizontal pipes. They found that the drag reduction increases as the solution concentration increases. The injection technique also affects the drag reduction which they found higher drag reduction when the injection done on downstream or directly to the annular flow. The maximum drag reduction obtained is 48 %. They suggested that the degradation of polymer related to values of drag reduction. They also suggested that degradation occurred in two ways, which is through the breakup of aggregates of polymer and through the mechanical break up of high molecular weight of polymer that made up the solution.

Mowla and Naderi (2006) used Polyalpha-olefin (Polyisobutylene) as drag reducing polymer to study the two-phase flow of crude oil and air in smooth and rough horizontal pipes surface. They found that the optimum concentration of polymer solution is 18 ppm. The drag reduction can be achieved up to 40 % in rough and 35 % in the smooth pipe for slug flow operated at 26423 Re. It is clearly shown that they obtained higher drag reduction in the rough pipe than in the smooth pipe. This phenomenon interpreted as an effect of turbulence fluctuation, which in rough surface the height of turbulence fluctuation is lower compares to smooth surface.

The study of drag reduction not only limited to the horizontal transporting system but also in inclined pipes. Al-Sarkhi et al. (2006) conducted an experiment on Magnafloc as drag reducing polymer on air-water annular flow in 7 m length of inclined pipe. The drag reduction achieved was up to 71 % in 1.28° of pipe inclination with 100 ppm of solution. They stated that the drag reduction in the pipe is due to the changes of flow pattern from annular to stratified flow. They also stated that the addition of polymer into pipes destroyed the turbulence disturbance wave. As a result, it promotes drag reduction in turbulent flow.

The study conducted by Al-Wahaibi et al. (2007) have a lot of similarity with Al-Sarkhi et al. (2006) which they used Magnafloc as drag reducing polymer except Al-Wahaibi using it to study the effect of polymer on water phase during the oil-water flow in horizontal pipes. They also studied the effect of polymeric solution to the flow pattern and drag reduction. The maximum drag reduction obtained is 50 % in 50 ppm of polymeric solution. This is interpreted due to the changes of velocity, which the velocity increases when the slug and annular flow changes to stratified flow in a presence of polymer.

2.6.2 Fiber Suspensions

Fiber suspensions had been recognized earlier than the polymer as drag reducing agent by a small circle of engineers working with paper pulps. This fiber suspension is well known as the cheapest raw material, could be from natural sources such as pulpwood, sand, and mechanically made such as alumina and expandable polystyrene. The effectiveness of these fiber suspensions depends on its properties such as its density

and concentrations. Drag reduction was found to be possible when the concentration is high for fiber-fiber interaction to occur, but below a critical concentration at which suspension viscosity dramatically increased.

The early observations of drag reduction used suspensions of natural products such as sediments as well as wood fiber, were motivated by the need to provide accurate hydraulic transport criteria. The attempts to establish the systematic effects of solid concentration, specific gravity and duct dimensions were report as unsuccessful, quite possibly because the suspended particles were not of uniform and reproducible dimensions and surface texture.

Lee (1974) and Peyser (1973) carried out a more progressive studies with well-defined synthetic fibers of rayon, nylon and asbestos to circumvent this difficulty. They showed that dilute suspensions of some fibrous solid particles may have very appreciable drag reduction effects.

Vaseleski and Metzner (1974) proposed an analysis of the velocity profile and pressure drop relationship for turbulent flow fiber suspension through smooth tubes. Their investigation was carried out experimentally over a range of flow rates, tube size, fiber concentrations, fiber geometry (aspect ratio) and fiber type (nylon, chrysotile asbestos). Surfactants in aqueous solution also used to disperse both fiber types. Their results showed an increase in the drag reduction with increasing the fiber concentration, and within an experimental accuracy, there were no clear effects of tube diameter. They concluded that the velocity profile in turbulent core predicted to be dramatically steeper in suspension than in Newtonian fluids, and that is due to the lowered rates of turbulent momentum transport.

Usually, the mechanisms of fiber suspension suggest that the drag reduction occurred in turbulent core and not near the wall. Fiber suspensions away from the wall will cause an increase in the effective viscosity in the turbulent core, damping turbulent fluctuations, while the viscosity in the viscous sub layer will be lowered. This mechanism, however, may not account for the large degree of drag reduction observed in some dilutes suspensions where the effective viscosity of the suspension is nearly the same as that of the carrier fluid alone (Luetzgen, 1991).

The available fiber suspension in the literature can be categorized into natural and mechanically made fibers. The term of mechanically made fiber is used to identify the modified properties of fiber for performance improvements. Barresi (1997) used glass spheres and plastic beads as mechanical made fiber suspension to study the interaction of turbulent flow with the suspended particle in a stirred tank, which related to drag reduction. He found that the solid modified the turbulence. The large change in turbulence found for high particle loading and the smaller but heavier particle. The large plastic bead showed no significant effect. Other types of fiber suspension has been used in the drag reduction studies such as polyethylene, glass beads, sand and polystyrene (Molerus and Heucke. 1999), Brownian rigid-rod particle (Manhart 2003) and the use of nonBrownian rigid cylindrical also was mentioned in (Shanliang et al. 2007) work.

Kerekes and Douglas (1982) observed drag reduction values as 50%. Drag reduction was found to be possible when the concentration was great enough for fiber-fiber interaction to occur, but below a critical concentration at which suspension viscosity dramatically increased. A critical parameter is the aspect ratio of the fiber, which must be greater than roughly 10-20 for drag reduction to be possible.

Seely (1968) found that turbulent velocity profiles in fibrous suspensions, when plotted in dimensionless turbulence coordinates, could be extrapolated to intersect at the point typically given as the end of the buffer layer in Newtonian fluids, although the profiles in the turbulent core had semi-logarithmic slopes lower than that of Newtonian fluids.

Inaba et al. (1995) study the behavior of pulp fiber as suspended solid on flow drag. They built up an experimental system consisted of a pump, water storage tank, flow resistance and heat transfer measurement test section and pipelines. The reduction of drag measured based on velocity profile in laminar and turbulent flow. They found that, the velocity profile of turbulent flow in a presence of fiber does not follow the values of 7th power velocity distribution law equation (u/U_m). When u stands for local velocity, and U_m stands for bulk mean velocity when plotted against the pipe central part (r/R), which r stands for radius at measuring position and R stands for pipe radius.

Radin, et. al. (1975) conducted an extensive study of drag reduction in suspensions of fibrous and no fibrous solids. Fibrous suspensions included chopped

nylon and rayon fibers, asbestos, cotton fibers and re-slashed newsprint. Non-fibrous solids included spherical, plate like, or needle-shaped rigid particles. No drag reduction obtained with non-fibrous particles. They noted that some claims, to the contrary, are due to incorrect definitions of drag reduction in which authors compared friction factors in suspensions to those in a fluid with a similar average density. If properly defined; however, drag reduction means a lower friction factor than would occur in the solvent alone at the same solvent flow rate.

Hayder (2006) built up closed liquid circulation system to investigate the effect of alumina and sand as suspended solid with drag reducing polymer named polyacrylamide on drag reduction. Generally, this system consists of the reservoir tank, pipes, valves, pump, flow meter and U-manometer. In the presence of 2000 ppm of polyacrylamide, the maximum drag reduction could achieve up to 53% and 40% in a solution with (2×10^3 ppm) concentration of sand powder.

The natural based fiber suspension such as paper pulp; Kraft hardwood pulp (Luetgen et al., 1991) and wood pulp (Kazi et al., 1999) become a considerable attention to study the drag reduction because of their harmless effect on environment and cheap in comparison to another drag reducing agent. Inaba et al. (2000) used paper pulp to study the effect of flow drag and heat transfer reduction for flowing water in a straight pipe. They found that there are flow drag reductions in a presence of pulp fiber at velocity equal to 2.44 m/s. The used of pulp fiber as fiber suspension was earlier mentioned in Moller's (1976) work.

Paul et.al (2009) presented a numerical model for predicting the flow and orientation state of semi dilute, rigid fiber suspensions in a tapered channel. They investigated the effect of the two-way flow/fiber coupling for low Reynolds number flow. The planar orientation distribution function is determined along streamlines of the flow and is coupled with the fluid momentum equations through a fourth-order orientation tensor. The coupling term accounts for the two-way interaction and momentum exchange between the fluid and fiber phases. The fibers are free to interact through long-range hydrodynamic fiber–fiber interactions, which are modeled using a rotary diffusion coefficient. Their numerical predictions were made for two different orientation states at the inlet to the contraction. Their results from these numerical

predictions show that the streamlines of the flow are altered and that velocity profiles change from Jeffery–Hamel, to something resembling a plug flow when the fiber phase is considered in the fluid momentum equations. This phenomenon was found when the suspension enters the channel either in a pre-aligned, or in a fully random orientation state. When the suspension enters the channel in an aligned orientation state, fiber orientation is shown to be only marginally changed when the two-way coupling is included. However, significant differences between coupled and uncoupled predictions of fiber orientation were found when the suspension enters the channel in a random orientation state. In this case, the suspension was shown to align much more quickly when the mutual coupling was accounted for and profiles of the orientation anisotropy were considerably different both qualitatively and quantitatively.

Nicole and Raimund (2010) considered the dynamics of long slender elastic fibers in turbulent flows, there exists a stochastic aerodynamic force concept for a general drag model based on a k turbulence description in literature. They generalized the concept and formulated an air drag model that is universally valid for all Reynolds number regimes and incident flow directions. The associated turbulent force overcomes the hitherto existing limitations and allows the simulation of all kind of fibers (flexible, stiff, light, and heavy) immersed in turbulent flows. Moreover, they hold a successful comparison of the numerical results with PIV-measurements that showed very convincing agreements in the industrial application of technical textile manufacturing.

2.6.3 Surfactants

Surface-active agents (Surfactants) are chemical compounds, when used in small quantities, modifies the surface properties of liquids or solids. A surface-active agent reduces surface tension in fluid or interfacial tension between two immiscible fluids. Surfactants are particularly useful in accomplishing the wetting or penetration of solids by liquids and serve in the manner as detergent, emulsifying or dispersing agents (Attwood and Florence, 1983).

All molecules that behave as a surfactant will have a structural group or groups that are lyophobic, solvent hate, and lyophilic, solvent loving. If the solvent is water,

then the chemical structural of the surfactant can be classified into two main portions as shown in figure 2.6, which are:

1. Hydrocarbon portion; that can be linear or branched. It interacts only very weakly with the water molecule in an aqueous environment. The strong interaction between the water molecules from dispersion forces and hydrogen bonding act cooperatively to squeeze the hydrocarbon out of the water, hence the chain is called hydrophobic. There are two main sources of supply for such materials that are cheap enough and available in sufficient quantity; biological sources such as agriculture and petroleum industry source.
2. Polar (ionic) portion, which usually called the head group that, is in the case of aqueous media, attracted to water, when it is called hydrophilic group. The hydrophilic group may vary widely due to the functionality of ionizing hydrofoils. These hydrofoils derived from a strongly acidic or basic character, which permits salt formation upon neutralization.

The balance between the hydrophilic and hydrophobic portions of the molecule, gives special properties for the surfactant, that the split personality of the surfactant which is composed of entirely different tendencies, make the surfactant to exhibit a unique behavior when it is in solvent.

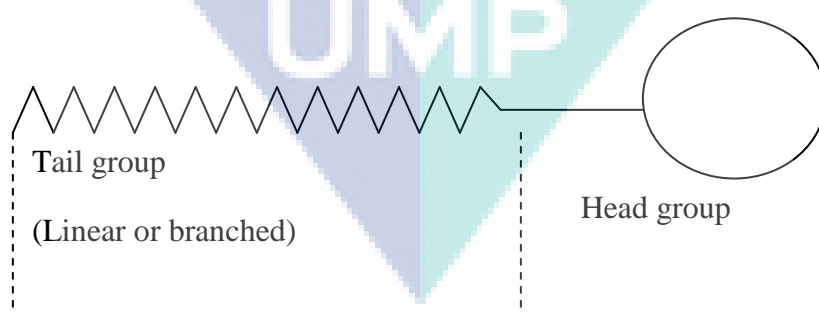


Figure 2-6: Schematic diagram of surfactant molecules.

The structures that are lyophobic and lyophilic change with the nature of the solvent, for instance, with a common surfactant such as Triton x-100.

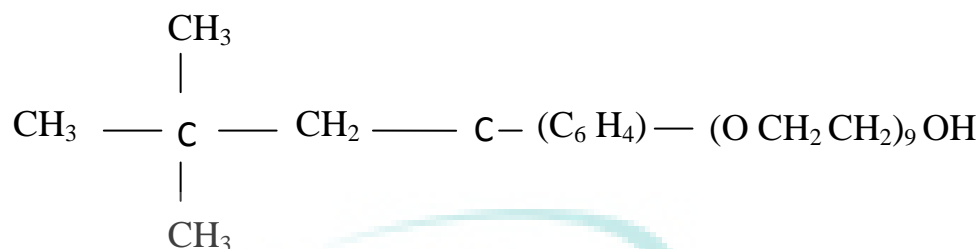


Figure 2-7: Structure of Triton x-100

If the solvent is very polar, the right hand part of the molecule is lyophilic, while the left-hand side is lyophobic.

In non-polar solvents, the roles would be reversed, making it more complex in silicon or fluorinated solvent, the whole molecule might be lyophobic and thus cease to be a surfactant. Not only that; but changes in the conditions of the system may also change the nature of the two structural groups. Thus, surface-active behavior for a given molecule is a function of the solvent and the conditions of the system (Mysels, et. al., 1954).

The reason for the surface-active nature of these molecules has to do with their impact on the solvent. The lyophobic structure “distors” the solvent phase, making it easier to bring the lyophobic structure to the surface and thus “remove” it from the solution.

By considering, strong acids (carboxylic acid) and weak acids (phenol), non-ionizing or non-ionic hydrophilic group has functionalities that are individually rather weak hydrofile but have additive effect. Therefore, increasing their number in a molecule increases the magnitude of their solublizing effect.

Surfactants can be classified in several ways, due to the multi-action or multi-effect of these materials. It can be classified according to their physical characteristics (water or oil solubility), or stability in harsh environments (Davidson and Milwidsky, 1972). Surfactant can be classified also as emulsifiers, foaming agent, and wetting agent.

The simplest way of classification and the most common one is that in which the primary types classified by the nature of the solubilizing functionality (lyophilic group).

Therefore, the major classification can be as followed: anionic, cationic, non-ionic and Zwitterionic surfactants.

Anionic surfactants in which, the surface-active portion of the molecule will bear a negative charge in solution. In anionic surfactants, the hydrophile comprises some highly electro-negative atoms, cation such as sodium. As determined by their hydrophilic groups, these can be classified into four main subgroups, which are:

1. Sulfate esters, which can be classified to fatty alcohol sulfate, sulfonated ethers, sulfonated fatty acid condensation products and sulfonated fats and oils.
2. Sulfonic acid salts, which can also classify to allyl-glyceryl ether sulfonates, lingo sulfonates, α -sulfo carboxylic acids, allyceryl sulfonates and aliphatic sulfonates.
3. Carboxylate soaps and detergents.
4. Phosphoric-acid esters.

Cationic surfactants produced as a mixture of homologous. Small variation in the chemical structure of the hydrophobic group of the surfactant can alter their surface-active properties. The source of the raw material in the manufacturing of such surfactant was the animal and vegetable fats. All of these materials could be considered to be derivative of two or three alkyl chains bonded directly or indirectly to a cationic nitrogen group. Cationic surfactants are very active in the biological field that it used as a microorganism inhibitor. In addition, it is very useful to be used as corrosion inhibitors and surface modifiers (Hiemenz and Rajagopalan, 1997).

Non-ionic surfactants are those, in which the surface-active portion of the molecule bears no charge (Sharma, 1995). An important group of non-ionic includes those where the hydrophile comprises a chain of ethoxy-groups and known as ethoxylates. Varying the number of ethoxy groups in the chain adjusts the amount of hydrophilic character in the chemical structure. The main subgroups of non-ionic surfactant are blocked copolymer non-ionic surfactant, which also can be classified to homogenous block non-ionic.

Zwitterionic surfactants might hold both the positive and negative charges in the surface-active portion of the molecule. The active charge of a Zwitterionic surfactant is dependent upon the pH of the system. The major subgroups of Zwitterionic surfactant are imidazoline derivatives (amine / carboxylic acid, quaternary ammonium / carboxylic acid, amine sulfonic acid and quaternary ammonium / sulfonic acid), surface-active betaines and sulfo-betaines and finally phosphatides and related zwitterionic surfactants (Hiemenz and Rajagopalan, 1997).

One of the most important properties of the surfactants is its capability to form aggregates called "Micelles". A micelle is an aggregate of surfactant molecules dispersed in a liquid colloid. A typical micelle in aqueous solution forms an aggregate with the hydrophilic regions in contact with surrounding solvent, sequestering the hydrophobic regions in the micelle centre as illustrated in figure 2.8 (Solomons and Fryhle, 2003). These processes had known as a micellization process. Micellization is therefore, an alternative mechanism to adsorption at the interfaces for removing hydrophobic groups from contact with the water, thereby reducing the free energy of the system.

The concentration of solution at which the micelle appears for the first time is known critical micelle concentration (CMC). The CMC depended on molecular structure and C atom in hydrophobic group. CMC halved by addition of methylene group (CH_2) to a straight chain hydrophobic group attached to a single terminal of hydrophilic. The CMC is higher in a present of C = double bonds in hydrophobic chains and C is isomers have higher CMC than the Trans isomer. Surfactant with either bulky (large) hydrophobic or hydrophilic group has larger CMC than not bulky group. As the hydrophilic move from terminal position to a more central position, the CMC increases and when the hydrophobic molecule increases, the CMC also decreases (Rosen, 2004).

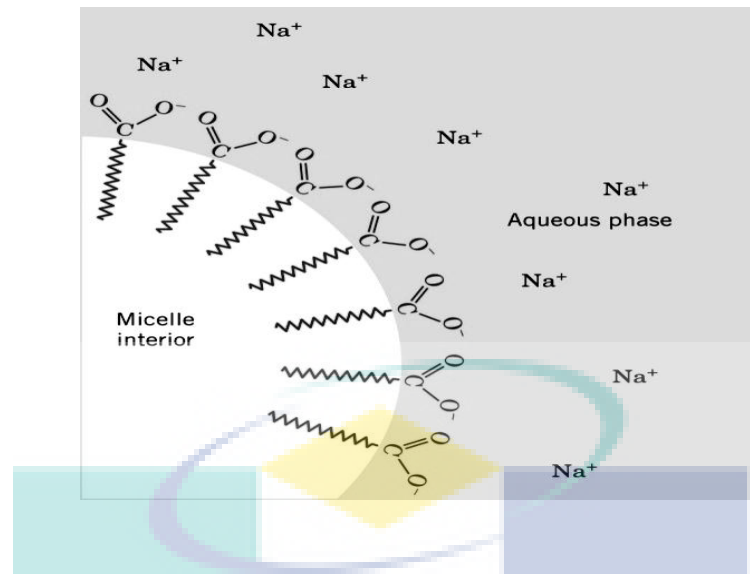


Figure 2.8: A portion of soap micelle interface with the polar dispersing medium

The micellization process depends on the balance between the factors promoting micellization and those opposing it. The major shapes of micelle appear in solvent are depending on its hydrophobic and hydrophilic carbon numbers. Usually, the major types of micelles appear to be relatively small, spherical structures, elongated cylindrical, rod like micelles with hemispherical ends, large and flat lamellar as shown in figure 2.9 (Rosen, 2004). Only threadlike, cylindrical, rod like and wormlike micelle can be use as drag reducer in turbulent flow.

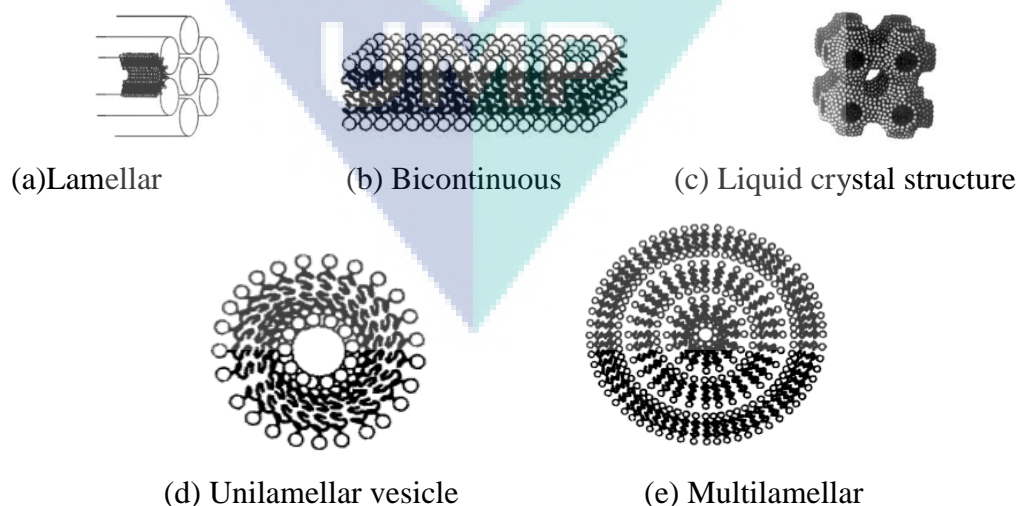


Figure 2.9: Micelle structures

White (1967) used a dilute solution of cetyl trimethyl ammonium chloride (CTAB) with 508 ppm in his experimental work on pipe flow. The drag reduction in large diameter pipes was greater than that of the smaller diameter, and it terminates at a limiting value of the flow of Reynolds number because of the degradation that occurred as results of oxidation after a period of several days.

Hershey et. al. (1971) used aluminum dioctoate in toluene as drag reducer. They showed that the method of preparing the disoap solution affects strongly the flow behavior. They found that the solution structure might temporarily break down by very high shear. They observed that the friction losses (friction factor) would be lower whenever the aluminum dioctoate concentration increases as shown in figure 2.10.

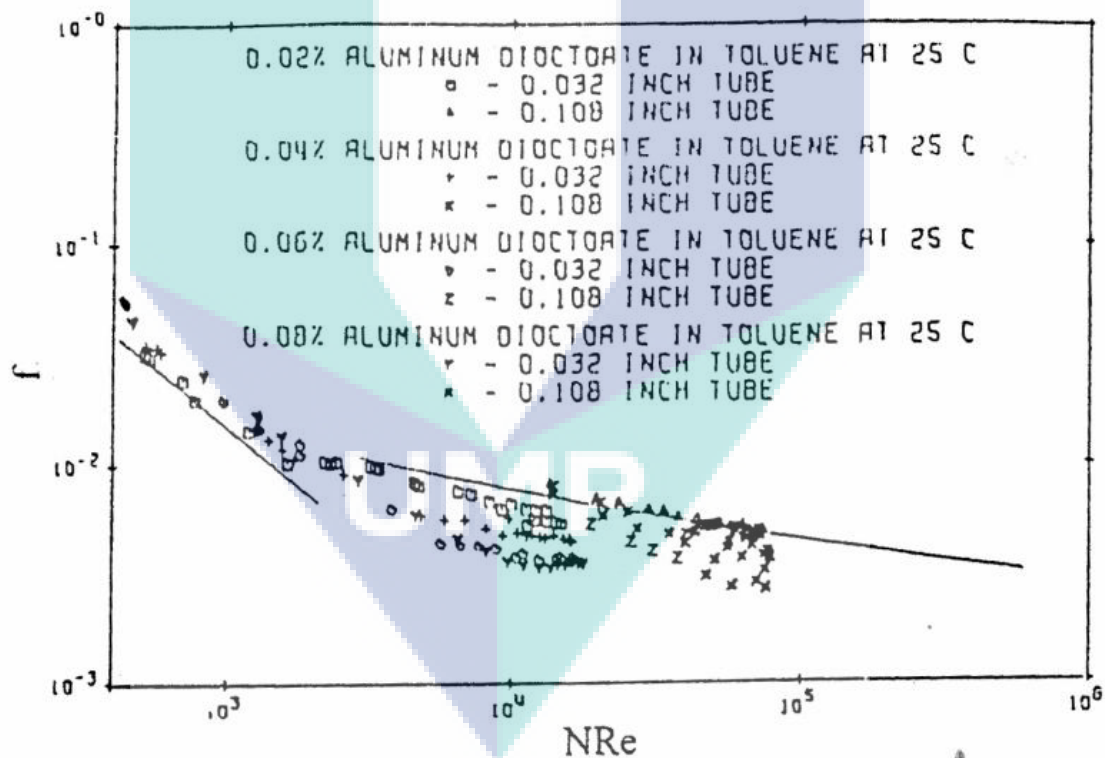


Figure 2.10: Concentration and diameter effect for Aluminum dioctoate in toluene (Hershey et. al., 1971).

Zakin (1983) studied the effect of surfactant structure, temperature, concentration and mechanical degradation on drag reduction. The investigation was carried out using a number of linear primary alcohol lethoxylate non-ionic surfactants in

aqueous solution. Most surfactants were effective as drag reducing additives. Among the large number of surfactants used, Brij96 ($C_{18}H_{35}-(OCH_2-CH_2)_{10}-OH$) was the most effective. The surfactants used were repairable, that is, after it is degraded mechanically, it recovers its drag reducing ability when it reaches a region of lower shear forces. Diameter effects on drag reduction are similar to those observed in solutions of high polymers (%Dr increases by decreasing pipe diameter).

Rose et. al. (1984) presented experimental work to measure the heat transfer coefficient and the drag reduction activity of aqueous solution of typical cationic surfactant (cetyl trimethyl ammonium chloride, CTAC, tallow trimethyl ammonium salicylate, TTAS and Erucyl trimethyl ammonium salicylate, ETAS) as a function of temperature. The surfactant had been shown to simultaneously lower the pipe flow friction and individual heat transfer coefficient from that of pure water. The surfactants have a critical temperature and Reynolds number above which the heat transfer coefficient and pipe flow friction return to that of the water as shown in figure 2.11. Finally, they concluded that non-uniform injection concentrations and bends substantially reduce the drag reducer's activity.

The logo for UMP (Université de Moncton) is a large, stylized letter 'V' shape. The top part of the 'V' is a light blue oval. The two sides of the 'V' are composed of overlapping triangles in shades of teal and light blue. At the bottom of the 'V', the letters 'UMP' are written in a bold, white, sans-serif font.

UMP

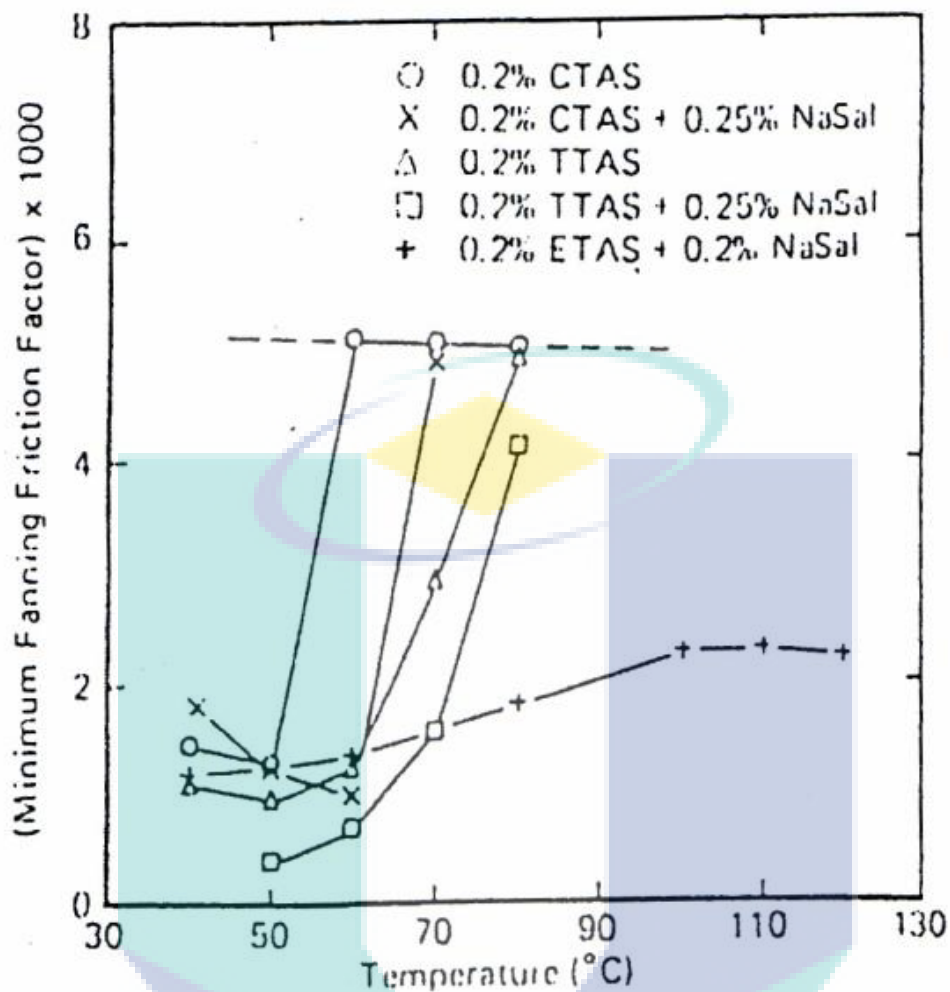


Figure 2.11: Effect of pipe diameter on drag reduction for 0.5% Brij96 Na_2SO_4 at 45.7°C in aqueous media flow (Rose et.al. 1984).

Lu et. al. (1998) carried out turbulent drag reduction using Arquad 16-50 with three isomeric counter ions, 2, 3 and 4-Cl-benzoate at $12.5\ \mu\text{m}$ to study the effect of chemical structure on drag reduction. The system was temperature-controlled to allow experiments to be run from (2 to 150) $^\circ\text{C}$. The purpose of using the temperature-controlled system is to study the most range that is effective on drag reduction. At temperature 30 to 50 $^\circ\text{C}$, the 3-Cl system capable of reduce drag up to 70 %. Beyond this temperature range, the drag reducing surfactant, lose their effectiveness. This method could be very useful to apply in the country with drastic temperature changes.

Kawaguchi et. al. (2002) studied the behavior of CTAC as drag reducing cationic (Lu et. al. 1998) surfactant in channel flow. At 40 ppm of CTAC solution, the maximum

drag reduction obtained is 60 %. They also study the effect of the addition of surfactant to friction factor and mean velocity profile. They found that the friction factor rises at Re equal to 51000 and the velocity gradient near the wall is lower than the flow of water without surfactants.

Myska and Mik (2004) studied the influence of solution age of CTAC mixed with NaSal on drag reduction. They found that the CTAC/NaSal solution with concentration 0.5 / 0.625 g/l can achieve up to 72 % of drag reduction. The study of CTAC as drag reducing agent also mentioned in work of Kang *et al.* (2001), Zhau *et al.*, (2006), Cho *et al.*, (2007), Ge *et al.*, (2008) and Li *et al.*, (2008).

Another drag reducing cationic surfactant that had used as investigating material in literature is oleyl bis (hydroxyethyl) methylammonium chloride and Oleyl tris (hydroxyethyl) methylammonium chloride. The maximum drag reduction was achieved of 5mM solution in water is 65 % for oleyl bis (hydroxyethyl) methylammonium chloride. In the range of temperature within 2 to 80 °C, the maximum drag reduction was achieved is 70% for oleyl tris (hydroxyethyl) methylammonium chloride (Zhang *et al.*, 2005).

Rozenblit *et al.* (2006) used alkyl polyglycosides in vertical upward air-water flow to study the flow pattern and the effect of heat transfer on drag reduction. They found that the gas bubbles in air-water mixture are smaller after the addition compared before the addition of surfactant. From their observation, the effect of surfactants on drag reduction depends on the flow regime, which its effect is more pronounced on bubble flow in comparison to annular flow, while the effect on slug flow is only weakly distinctive. At concentration 300 ppm of surfactant, the maximum drag reduction obtained is 19 % and 42 % for liquid superficial velocity of $USL = 0.5$ m/s and $USL = 0.1$ m/s, respectively. They also found that the addition of surfactant drastically reduced the heat transfer in the churn flow regime.

Cho *et al.* (2007) found that Stearyl amine oxide + betaine (SAOB) can achieve about 60 to 80 % drag reduction in solution concentration between 1000 and 2000 ppm at 70 °C. Another nonionic surfactants mentioned in literature is trioxyethylene

monododecyl ether and poly (oxyethylene) cholesteryl ether in Varade et. al. (2007) works and Triton-X in Cheng et. al.(2007) work.

Wilkins and Thomas (2007) found that the pressure drop is reduced by 25 to 40 % in a presence of 400 ppm of drag reducing anionic surfactant, sodium dodecyl sulfate (SDS). This material also mentioned in Cheng et. al. (2007), Varade et, al. (2007) and Duangprasert et. al. (2008) work.

Krope and Lucija (2010) suggested an application of specific surfactants in district heating and cooling systems that can give notable economical benefits due to a reduction in friction and heat transfer attributed to a formation of an additional viscous sublayer along the pipe walls, buffering the turbulence. A mathematical three-layer model of water velocity profile is composed for the calculation of drag reduction and flow-capacity increase. Their results showed that, at a properly chosen surfactant and concentration, the local drag can be reduced up to 80%. A computer simulation and optimization for a selected district heating network model with additive shows 4% saving in total costs because smaller pipes and weaker pumps are required.

Yunying et.al (2009) studied the effects of shear on three cationic drag-reducing surfactant solutions, each with very different nanostructures and rheological behaviors; Arquad 16-50/sodium salicylate (NaSal) with concentration of 5 m μ /5 m μ , has thread-like micelles, shear induced structure and large first normal stress (N1). Arquad S-50/NaSal with 5 m μ /12.5 m μ has branched micelles, no shear-induced structure and first normal stress is about zero and Arquad 16-50/sodium 3,4-dimethyl-benzoate with 5 m μ /5 m μ has vesicles and thread-like micelles, shear-induced structure and high first normal stress (N1) by small-angle neutron scattering (SANS). The differences in the rheological behavior and the SANS data of the solutions are explained by the different responses of the nanostructures to shear based on a two-step response to shear.

The less mentioned group of drag reducing surfactant in literature is Zwitterionic surfactant. Myska and Mik (2003) used DR-0205 and SPE 98330, which is drag reducing zwitterionic surfactant to study the degradation of surfactant solution by age and by a flow singularity in hydraulic loop. The highest drag reduction was obtained is

62 % at velocity 1.1 m/s in a presence of DR- 0205 and 71% at 2 m/s in a presence of SPE 98330.

Table 2.1 shows the advantage and disadvantage for the three additive drag reduction.

Table 2.1: The advantage and disadvantage for the DRA's

Suspended solids	Surfactant	Polymers
Not soluble in the flowing media (doesn't affect the apparent physical properties for the fluid)	Soluble in the flowing Media	Soluble in the flowing media
Reduce %Dr	Reduce %Dr	Reduce %Dr
Can found easily in the nature or mechanically maid(Cheap in price)	Expensive	Expensive
Can separate from the main flow	Cannot separate from the main flow	Cannot separate from the main flow
Cannot Degrade after long time flowing with the fluid	Degrade after long time flowing	Cannot degrade after long time flowing

2.7 DRAG REDUCTION MECHANISMS

One of the things that make the drag reduction as a science story such as a phenomena is its mechanisms. Li et. al. (1991) introduced an injection technique of surfactants to gas pipelines to reduce the drag in pipes. A gas flow loop of 0.25 in was used for the tests and was constructed to measure the flow rate and pressure drop across the length of the pipe before and after the drag reducer has injected. The injection technique is the most appropriate technique for drag reduction in gas phase. They defined that the structure of the polar group at one end bonds onto the side inner wall of pipeline. A non-polar group at the other side smoothes the gas-solid interface between the wall and flowing gas thereby, reducing gas turbulence at the side interface while conducting an experimental work on gas pipelines using drag-reducing surfactant, oxylated fatty acid amine.

Luetzgen et. al. (1991) believed that the addition of fiber suspension in turbulent flow changes the structure of turbulence in which this leads to drag reduction. A profound indication of an altered turbulence structure is the observation that increased turbulent dispersion and decreased momentum transfer can occur simultaneously when fibers have been added to a turbulent water flow. The presence of entangled fibers in a flow may force a redirection of turbulent bursts, which could alter the structure of turbulence. The resistance to elongation of fluid elements with fibers may also contribute to the changed turbulence structure.

Lu et. al. (1998) suggested that drag reduction by surfactant additive probably caused by suppression of turbulent eddies. Extensional motions dominate in the bursting and growth of these eddies. With the addition of surfactant drag reducers, apparent extensional viscosity is greatly increased, thus increasing the resistance of the fluid in eddies to extensional flow and suppressing eddy growth. They also suggested that not all drag reduction surfactant caused by viscoelastic, since they found drag reduction on non-viscoelastic drag reducing surfactants.

Inaba et. al. (1999) conducted an experiment on drag reduction of flow in the circular pipe. They found that there are changes of velocity profile near the wall because the pulp fibers unevenly dispersed in the pipe by the local velocity distribution. They concluded that the mechanism of drag reduction in a presence of pulp fiber occurred near the wall. Since, there is no clear explanation of a mechanism in their report; future work on fiber suspension could be very useful.

Dong et. al. (2003) strengthen the theory that the probability of the mechanism of drag reduction in a presence of fiber suspension is near the wall through their finding that the concentration results scaled by the fiber length show a linear region near the wall.

Kawaguchi et. al. (2002) studied the drag reducing channel flow with surfactant additives (CTAC) in closed loop fluid flow. They stated that the strong vortices fluctuation near the wall disappears and the vortex motions largely decrease near the wall after the addition of surfactant additive. One of the important events of turbulence

energy production and turbulent mixing is the instantaneous velocity distribution taken in water flow exhibits penetration from the low-speed fluid region into the high-speed region not found in drag-reducing flow under the same Reynolds number. This statement leads to the conclusion that they believe the drag reducing surfactant changes the structure of turbulent flow and the mechanism of drag reduction in a presence of surfactants additive probably also occurred near the wall.

Qi and Zakin (2002) believed that the mechanism of drag reduction in a presence of drag reducing cationic surfactants based on its capability to acts as “self-reparability” after mechanical degradation.

Myska and Mik (2003) studied the drag reduction phenomena in heating and cooling systems. They used such a large system to study the effectiveness of Zwitterionic surfactant named SPE 98330. The heating system consists of a gas furnace with water heater and blow-off tank. The water forced into the heater by a pump and warmed up water from the heater flows through a thermostatic valve into the system. The drag reducing agent solubilized and pressed into the system by a hand pump through a swing-check valve. One year later, Myska and Mik (2004) again study the behavior of drag reducing agent, which CTAC, Arquad SV-50, DR-0205 and SPE 98330 in terms of degradation by age in a simple built up system consisted of tanks, twin pumps, and transparent hose. They believe degradation behavior of surfactants is the key to understand the mechanism of drag reduction.

Zhang et. al. (2005) investigated the drag reduction and the behavior of two cationic surfactants named Ethoquad O/12 and Ethoquad O/13 in a closed flow loop. The test section was a stainless tube with a length of 1.22 m and an inner diameter of 6 mm. Flow rate was measured by a Rosemount 8100 magnetic flow meter. A Validyne pressure transducer measured the pressure drop. They studied the rheology of drag reducing surfactant and the effect of co-solvent on micelle formation in drag reducing surfactant solution. This investigation shows that the rheology properties and the micelle formation in drag reducing surfactant probably the key source to understand the mechanism of drag reduction in a presence of surfactants.

Zhou et. al. (2006) stated that the drag reduction in turbulent flow occurred because of the length of the rod-like micelles align themselves along the flow direction to suppress turbulent flow near the wall. As the concentration of surfactants increases, the length of micelle formed also increases. As a result, the skin friction between the flowing fluid and the solid boundary reduced. Therefore, a larger amount of energy from the flow is required to disrupt the super-order rod-like micelle structures.

Suksamranchit and Sirivat (2007) stated that the addition of salt affects the drag reduction in turbulent flow. They found that during the addition of salt, the critical micelle concentration decreased. These results support the theory of drag reduction occurred in turbulent flow because of the micelle formation. The theory that the formation of stable micelle increases drag reduction was support with the result of an experiment conducted by Varade et. al. (2007).

Cho et. al. (2007) suggested that there is a critical temperature limit on some surfactants additive. Beyond this critical temperature, the break-up of micelle structure decreases the drag reduction. This shows that they also agree that the formation of micelle is the source of drag reduction in turbulent flow. The result of their experiments also supported the results of an experiment conducted by Suksamranchit and Sirivat. (2007)

Ge et. al. (2008) stated that drag reduction effectiveness as shown by maximum percentage drag reduction strongly related to viscoelasticity of fluid in a presence of drag reducing surfactant.

Li et. al. (2008) observed that the near-wall vortex structures near the walls in the drag reducing surfactant solution flow changed gradually with the drag reduction level and the viscoelasticity of solution. This result has a good agreement with the proposed mechanisms in surfactants solution by Kawaguchi et. al. (2002) and Zhou et. al. (2006).

Most of the stated mechanisms agree that the micelle formation in surfactant solution damped the structure of turbulent flow and the mechanism likely occurred near

the wall. The same mechanism goes to fiber suspension in which the interaction of fibers in turbulent flow aligned with the eddies but the ability to return to its original position in turbulent flow disturbed the turbulent structure and this likely occurred near the wall. In order to understand the mechanisms behind the drag reduction, it is important to study on drag reducing agent concentration, rheology properties, the operation temperature and the fibers behavior that dispersed but insoluble in most of the solution.

2.8 COMMERCIAL APPLICATION

The development and application of DRA mostly related to gas, oil and petrochemical industry. The well-known and remarkable application of DRA is in transporting crude oil through Trans-Alaska pipelines. The gel-like drag reducing polymer injected in this pipeline and was successful to reduce the electricity consumption (Ragsdale, 2007).

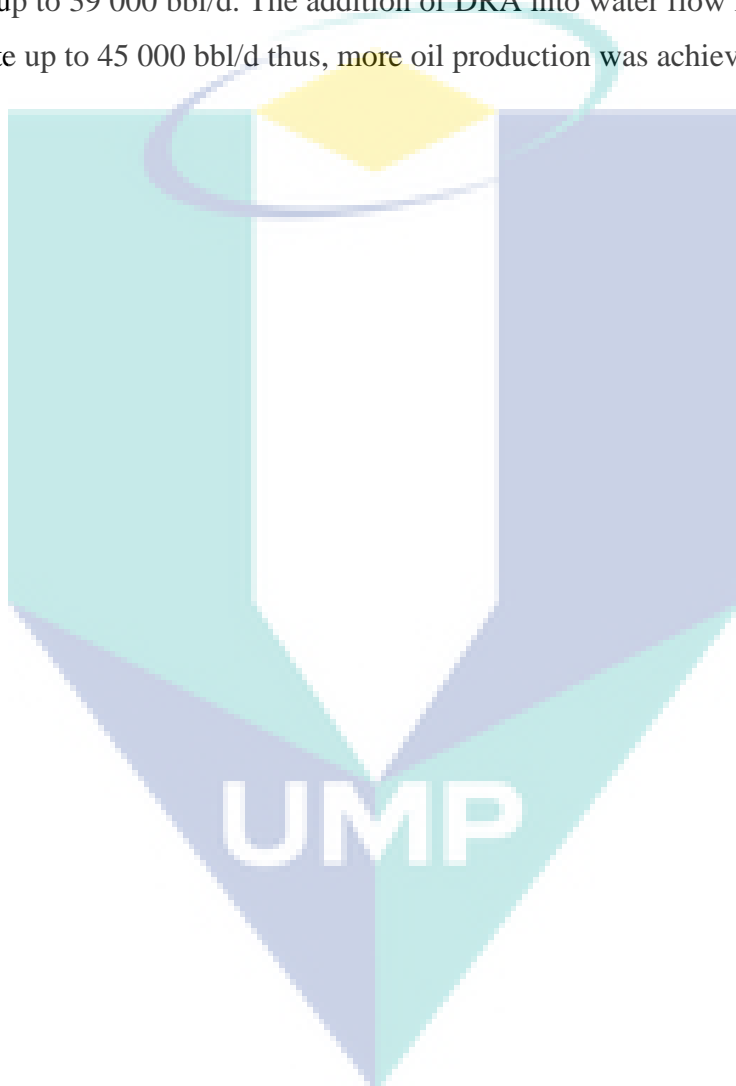
In 1977, discussions between Conoco and operators of the Trans-Alaska Pipeline System (TAPS), followed by an intensive research program led to the development of the CDR101 flow improver. In (1979), Alyeska pipeline service company initiated the first scale use of pipeline drag reducers (DRA's) in the 1.2 m diameter TAPS. The 1287-km long TAPS line designed for 12-pump station (PS) with a crude oil capacity of 2.0 million barrels per day (MBPD). TAPS start operation with only 8 pump stations with capacity of 1.0 MBPD. PS2 and PS7 were under construction. Sites were being prepared for PS5 and PS11. In an attempt to increase through put, DRA considered.

Application of DRA began at PS1 and PS6, when these pump stations become operational in 1980 and 1981; the mechanical capacity became 1.45 MBPD. The DRA applications then shifted to PS4 and PS10 to offset the absence of PS5 and PS11. Because of the ever-increasing advances in DRA technology from 1980 to the present time, it is remarkable that these pumping stations were never build. DRA's used instead.

The DRA also used to transport both raw and finished petroleum products, including, propane and refined products such as gasoline, diesel and jet fuel by ConocoPhillips Pipeline Company around the United States. Based on their study of one

pipeline segment forecast, the potential for \$300,000 in annual savings could be achieved if DRA applied (Conoco Philips 2006).

Nelson (2004) reported that the ChevronTexaco Galley reservoirs operated by Petrofac (UK) Ltd using the Northern Producer floating production facility used DRA to increase the flow rate of water injection in transporting the crude oil via pipeline to the Flotta Terminal. By injecting about 29 000 bbl/d of water could increase the oil production up to 39 000 bbl/d. The addition of DRA into water flow increased the water injection rate up to 45 000 bbl/d thus, more oil production was achieved.



CHAPTER 3

EXPERIMENTAL WORK

3.1 INTRODUCTION

Pipe diameter, powder type, solution flow rate, testing section length, surfactant type, particle size and additives concentrations were the variables investigated in the present work. One hundred and forty four sets of experimental work with 432 runs and 2592 data points carried out. Each run deals with one type of powder, one size of powder, one pipe diameter, one additive concentrations and six solution flow rates, as shown in appendix A. Aluminum, sand and coal were the three powder additives investigated and added to the tap water with three concentrations, which are (100,300 and 500) ppm respectively to water tank. Three pipes with three different internal diameters (0.0125, 0.0254 and 0.0381) m I.D. with four testing section lengths (0.5, 1.0, 1.5 and 2.0) m were investigated. Each one of the three powders handled with two-particle sizes (42 μ and 71 μ). Two Zwitterionic surfactants were used in the present investigation are (3-(Decyldimethyl-ammonio) propanesulfonate inner salt) and (3-(N,N-Dimethylpalmityl-ammonio) propanesulfonate) with (10,20 and 30) ppm as a concentration.

3.2 MATERIALS USED

Three types of powders and two types of surfactants are chosen in the present work to be introduced as drag reducing agents.

3.2.1 Drag Reducing Agents (Powders)

Three different types of powders investigated as drag reducing agents in the present work, which are:

(i) **Aluminum Powder**

The aluminum powder used in the experimental work, supplied by R&M chemicals, UK. The specifications of the powder are showing in table 3.1. The powder particle sizes analyzed and separated using sieve analysis technique. Two-particle sizes of powders introduced to investigate in the present works, which are (42 and 71 μm).

Table 3.1: Specification of Aluminum Powder Investigated

Specifications	Data
Density	Almost 2700 Kg/m ³
Metal Content	99.2% min
Burning Speed(s/5g)	30-100
Active Aluminum	75-80
Grease Content	1.0% max
Assay (Complexometric)	> 99.00%
Arsenic (As)	> 0.0005%
Heavy Metals (as pb)	> 0.03%
Standard	ISO9001
Iron (Fe)	> 0.5%
Fats	> 1.0%
$\mu = 26.98 \text{ g/mol}$	

(ii) **Sand Powder**

R&M chemicals, UK, supplied the Sand powder used in the experimental work, the specifications of the powder have described in table 3.2. The powder particle size analyzed and separated using sieve analysis technique. Two-particle sizes for powders introduced as the particle sizes to be investigate in the present work, which are (42 and 71 μm).

Table 3.2: Specification of Sand Powder Investigated.

Specifications	Percentage
Density	Almost 1700 Kg/m ³
Iron Oxide (Fe ₂ O ₃)	0.018%
Aluminum Oxide (Al ₂ O ₃)	0.150%
Calcium Oxide (CaO)	0.009%
Titanium Dioxide (TiO ₂)	0.015%

Table 3.2: Continued

Magnesium Oxide (MgO)	0.008%
Potassium Oxide (K ₂ O)	0.095%
Sodium Oxide (Na ₂ O)	0.005%
Silicon Dioxide (SiO ₂)	99.615%

(iii) Coal Powder

R&M chemicals, UK, supplied the Coal powder used in the experimental work; the specifications of the powder have described in table 3.3. The powder samples particle size analyzed and separated using sieve analysis technique. Two-particle size powders have introduced as the particle sizes are investigate in the present work; which are (42 and 71 μm).

Table 3.3: Specification of Coal Powder Investigated.

Specifications	Data
Density	Almost 1170 Kg/m ³
Soluble in water	0.2%
Soluble in HCL	1.0%
Soluble in C ₂ H ₅ OH	0.2%
Organic substance	Pass test
Decolorizing power	Pass test
Acidity	Pass test
Chloride (CL)	0.001%
Sulfide	Pass test
Sulphate	0.001%
Calcium (Ca)	0.05%
Copper (Cu)	0.002
Iron (Fe)	0.001%
Lead (Pb)	0.001%
Zinc (Zn)	0.001%

3.2.2 Drag Reducing Agents (Surfactants)

In the present work, two different types of Zwitterionic surfactants are investigated as drag reducing agents and drag reduction performance improvers for the flow in solid-liquid turbulent flow systems, which are (3-(Decyldimethyle-ammonio) propanesulfonate inner salt) and (3-(N-N,Dimethylpalmityl-ammino) propanesulfonate).

The molecular numbers for the two surfactants chosen were close (391 and 307). The reason behind using these two types is to study the effect of molecular structure on its drag reduction ability in two-phase flow systems.

i. 3-(N-N, Dimeethylpalmityl- ammino) propanesulfonat

3-(N,N,Dimethylpalmityl-ammino) propanesulfonate is a Zwitterionic surfactant with the properties shown in table 3.4. Commercially, these surfactants used for extraction of proteins for analysis by chromatography, mass spectroscopy, and electrophoretic methods. Figure 3.1 shows the chemical structure of the surfactant. This surfactant was purchase from sigma- Aldrich, and it holds the CAS number 2281-11-0. This surfactant also carries the scientific names (3(Hexadecyldimethylammonio) propanesulfonate), (3-(Palmityldimethylammonio) propanesulfonate), Palmityl sulfobetaine, and SB3-16.

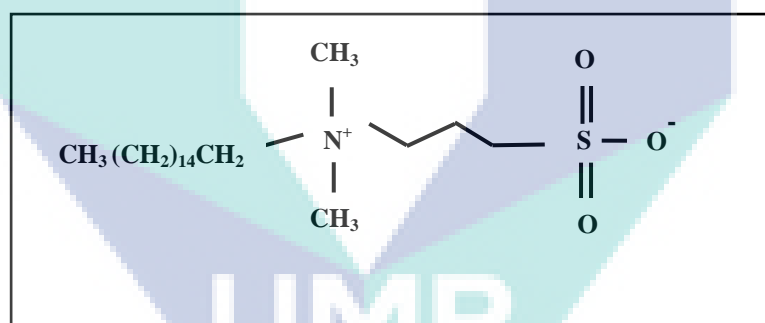


Figure 3.1: Structure of 3-(N,N,Dimethylpalmityl-ammino) propanesulfonate

Table 3.4: Properties of 3-(N,N,Dimethylpalmityl-ammino) propanesulfonate

Specifications	Data
CAS Number	2281-11-0
Linear Formula	CH ₃ (CH ₂) ₁₅ N ⁺ (CH ₃) ₂ CH ₂ CH ₂ CH ₂ SO ₃ ⁻
Molecular Weight	391.65
Beilstein Registry Number	4149854
Micellar Avg. mol. Wt.	60,700
CMC	0.01-0.06 mM(20-25°C)
XLogP3-AA	7.2
H-Bond Donor	0

Table 3.4: Continued

H-Bond Acceptor	3
Rotatable Bond Count	18
Exact Mass	391.312015
MonoIsotopic Mass	391.312015
Topological Polar Surface Area	75.2
Heavy Atom Count	26
Formal Charge	0
Complexity	389
Isotope Atom Count	
Defined Atom StereoCenter Count	0
Undefined Atom StereoCenter Count	0
Defined Bond StereoCenter Count	0
Undefined Bond StereoCenter Count	0
Covalently-Bonded Unit Count	1

ii. **3-(Decyldimethyle-Ammino) Propanesulfonate Inner Salt**

3-(Decyldimethyle-ammonio) Propanesulfonate inner salt is a Zwitterionic detergent used for protein solubilization. The appearance of this powder is white and its solubility will be a clear colorless solution at 100 mg plus 1 ml of water. The element analysis is (57.4-59.8%) carbon, and (4.3-4.7%) nitrogen. Figure 3.2 shows the chemical structure and Table 3.5 shows the properties of this surfactant, which was using as supplies.

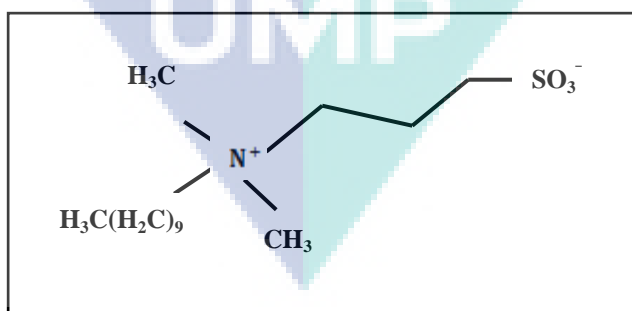


Figure 3.2: Structure of 3-(Decyldimethyle-ammonio) propanesulfonate

Table 3.5: Properties of 3-(Decyldimethyle-ammonio) propanesulfonate

Specifications	Data
Molecular weight (Mw)	307.49
Molecular formula	$\text{CH}_3(\text{CH}_2)_9\text{N}^+(\text{CH}_3)_2\text{CH}_2\text{CH}_2\text{CH}_2\text{SO}_3^-$
CAS Number	15163-36-7
CMC	25-40 mM(20-25) $^\circ\text{C}$
Aggregation Number	41
beilstein Registry Number	3967284
Micellar Avg. mol. Wt.	12,600
Beilstein Registry Number	3967284
Conductivity	<20 μ mho per cm at 24 $^\circ\text{C}$ (0.1 M aqueous solution)

3.3 EXPERIMENTAL WORK

Sieve Analysis

One of the main variables in the present investigation is the particle size. In order to separate the desired sizes for investigation, sieve analysis was applied. Vibratory sieve shaker ANALYSETTE 3 SPARTAN sieve analyzer (Fritsch, RoHS Germany) is used. This analyzer consists of six trays with particle sizes ranged from 280 μm to 36 μm as shown in figure 3.3.

The sieve analysis operation starts by arranging the sieves over the vibrator from the bigger to the smaller size, pouring the particle mix from the top side of the sieve column and starting vibration for 15-minute minimum to ensure the highest percentage of separation. The particles then are separated depending on the sieve size and the amount of solid particles on each sieve.



Figure 3.3: Fritsch Sieve Analysis system

3.3.1 Flow System Description

A closed loop liquid circulation system was used in the present work to test the drag reduction efficiency of the chosen additives. This system is shown in figures 3.4 to 3.7. The recirculation system consists mainly of two reservoir tanks to control the water temperature, two pumps, pipes, Portable Minisonic P flow meter and pressure gauges. The system has been designed and built to be at a maximum flexibility during the operation.

(i) Experimental Rig

The drag reduction experimental work was carried out in a closed loop liquid circulation system. This system was designed and constructed to provide flexibility and shortening the length of time required for the experimental work.

Figure 3.4 shows a schematic diagram for the design of the experimental rig. Moreover, figure 3.5 shows a schematic of testing section. The rig consists mainly of two storage tanks with maximum capacity 0.45 m^3 . Dimensions of the tank were 0.9 m in length, 0.9 m in width and 0.55 m in depth. The first tank (tank 1) is used as the main tank for delivering the solution to the testing sections through the pump, while tank 2 is used to store the circulated solution for certain period of time before returning it to the first main tank again. The purpose behind that is to control the temperature changes that might occur due to the high shearing rates supplied by the main pump to the liquid, which might change the circulated liquid temperature after certain time of continuous work.

Precision pump 1, model CPM-158 with maximum load equal to $6.5 \text{ m}^3/\text{hr}$ is used as the main solution circulation pump for the pressure drop testing section in the system. As shown in Figure 3.4, the pump and solution tank is connected with pipe 0.0381 m in diameter and 0.2 m in length.

As shown in figure 3.4, the main piping system starts by connecting the main tank to the main pump by 0.0381 m I.D pipe as the main delivering exit. The piping systems start from the main pump with 0.8 m vertical pipe with 0.0381 m I.D (P1) connected to a ball valve (V1) for safety reasons. Then the pipe goes horizontally for 0.4 m and separated into two parts, the first part (P2) will return to the main tank connected to a ball valve (V2) and act as a bypass pipe. This bypass pipe is used to control the flow entering to the testing sections.

The other part of the pipe is divided into three main sections (P3, P4 and P5). The three sections have three different pipe diameters (0.0125 m I.D. for P3, 0.0254 m I.D. for P4 and 0.0381 m I.D. for P5). Each section is connected to a ball valve in order to control the flow rate entering to the main pressure drop measurement sections.

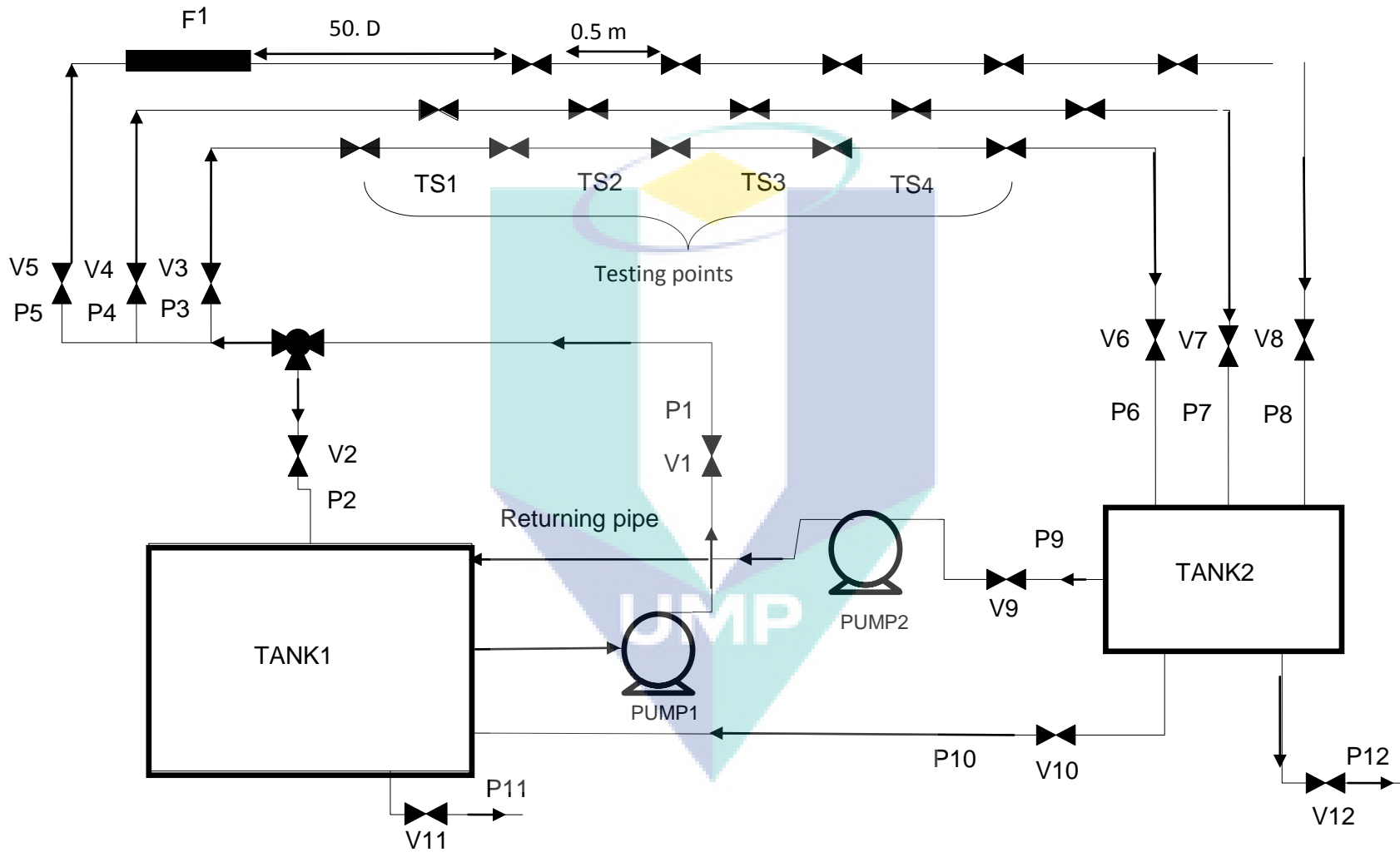


Figure 3.4: Schematic diagram of the experimental flow system.

Then the testing section rises for 0.5 m, 0.7 m and 0.9 m for the 3 pipe diameters respectively reaching the horizontal part where the pressure drop piping testing sections starts.

Before starting the sections for pressure drop measurement, certain length is left before the first pressure drop tab for each pipe. This horizontal part equals to 50-time diameters (50 D.) for each pipe, which equal to 0.7 m, 1.27 m and 2 m for P3, P4 and P5, respectively. This is to ensure fully developed turbulent flow before the testing section. The length of vertical P3, P4 and P5 before the horizontal part is 0.7 m, 0.8 m and 1.0 m, respectively.

The testing sections were divided into four parts (TS1, TS2, TS3 and TS4), with a distance of each part is equal to 0.5 m as shown in Figure 3.5. Each testing section has two pressure measurement tabs. Each tab is connected to a flexible tube for the pressure drop measurements by the differential pressure manometer.

After the test sections, all the pipes deliver the solution to the second tank (tank 2) which is connected to a small centrifugal pump that delivers the solution to the first tank for a complete liquid circulation system.

Each tank is connected from the bottom part to a draining pipe with 0.0125 m I.D. (P11 and P12). Each draining pipe is supported with ball valve (V11 and V12) to control the draining flow. After each experiment or run, the liquid inside the tank is drained through the draining pipe and fresh water is replaced instead.

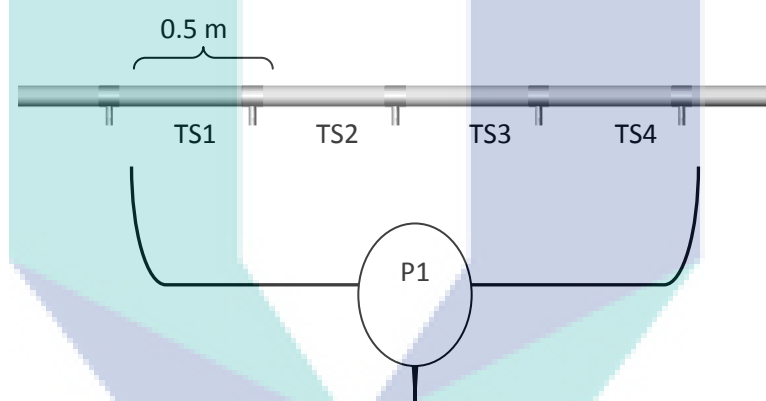
Table 3.6 shows the description of each term and symbols in figure 3.4 and 3.5. In general, the symbol of P is basically describes the pipe varied in diameter. In addition, the symbol of V is referred to the valve in each pipe and TS is the testing point in testing section.

Table 3.6: Experimental flow system symbols description.

Symbols	Description	Symbols	Description	Symbols	Description
P1	Main pipe	V4	0.0254 m pipe valve	V8	0.0381 m pipe valve
V1	Pump valve	P5	0.0381 m pipe	P9	Circulation pipe
P2	Bypass pipe	V5	0.0381 m pipe valve	V9	Circulation valve
V2	Bypass valve	P6	0.0127 m pipe	P10	Circulation pipe

Table 3.6: Continued

Symbols	Description	Symbols	Description	Symbols	Description
P3	0.0127 m pipe	V6	0.0127 m pipe valve	V10	Circulation valve
V3	0.0127 m pipe valve	P7	0.0254 m pipe	P11	Drainage pipe of tank 1
P4	0.0254 m pipe	V7	0.0254 m pipe valve	V11	Drainage valve of tank 1
TS1	Testing Section 1	V12	Drainage valve of tank 2	P12	Drainage pipe of tank 2
TS2	Testing Section 2	F1	Ultrasonic flow meter	TS3	Testing Section 3
				TS4	Testing Section 4

**Figure 3.5:** Schematic of testing section

Figures 3.6 to 3.9 shows the pictures of the experimental rig located at University Malaysia Pahang (UMP) Chemical Engineering laboratory and used in this experiment. From Figure 3.9, it is clearly shown the pressure gauges hanging on the beam. The black tank is the solution tank. This picture is taken during the circulation process of water without additive through the pipes.

Figure 3.7, shows a picture to the main Pump (model CPM-158 with maximum load equal to $6.5 \text{ m}^3/\text{hr}$) and the secondary pump, while figure 3.8 shows a picture to the main tank used (tank 1). Finally figure 3.9, shows one of the differential pressure manometers used.



Figure 3.6: Experimental rig located in UMP laboratory



Figure 3.7: The main pump (green) and secondary Pump (black) used in the experiment.



Figure 3.8: The main pump circulation tank.



Figure 3.9: The differential pressure manometer.

(ii) Portable Minisonic P Flow Meter

One of the main problems facing any experimental study regarding drag reduction is the disturbance that the liquid flow meters make in the main flow due to the way these flow meters are inserted inside the pipe. To overcome such problem, Portable Minisonic P flow meter product of Ultraflux Corporation was used to measure the flow rate of fluid in pipes. This flow meter can measure the flow rate using ultrasonic wave without any interference with the flow inside the pipe. The ultrasonic flow measurements were sensitive to small changes in flow rates low as 0.001 m/s. The system consists of a hand held control unit and two probes with support and cables as shown in figure 3.10. This flow meter can measure the flow rate using ultrasonic wave without any interference with the flow inside the pipe.

Several parameters were set on the flow meter before the experiments began such as the probe distance, which depends on the inner diameter of pipes. The probe distance for 0.0125 m pipe was 33 mm in W mode, for 0.0254 m was 27 mm in V mode and for 0.0381 m was 17 mm also in V mode. The operation mode either V or W is the measurement for the transit time for wave calculation.



Figure 3.10: Portable Minisonic P flow meter

(iii) **Baumer Bellows Differential Pressure Gage**

Baumer Bellows differential pressure gauges are used for the pressure drop measurements in the testing sections. Each gauge has two outlet stainless steel tubes to be connected to the flexible tubes from the testing tabs in the pipe sections. It is very important to make sure that these flexible tubes are empty from air to ensure accurate reading. The measurement mechanism of this gauge depends on two stainless steel bellows mounted on a force balance to enable direct reading of the actual differential pressure. It is important to mention that during the experimental work, mercury U-Manometer differential pressure measurement devices are used at certain experimental points. These devices are used in certain cases where the pressure drop reading is very low that the differential manometer cannot sense, or when the pressure drop exceeds the differential pressure manometer range.

3.3.2 Solutions Preparation

The re-circulated solutions investigated in the present work were prepared separately before each experiment for both powder solutions and surfactant-powder solutions.

For powder solutions, the desired amount of powder is prepared for certain concentration chosen for the experiment. For example: for 100-ppm addition concentration, 42 g of the investigated powder is prepared for 420 liters of water, mixed with water in a one-liter beaker, poured into the main tank, and mixed. By the end of this step, the solution is ready for circulation. The same step is repeated for the other concentrations (300 and 500 ppm) investigated. All the concentrations were in weight part per million (ppm) which the percentage of the additive weight to the total weight of the solution.

The other part of the experimental work involves the addition of the Zwitterionic surfactants chosen to the suspended solution re-circulated in the rig. In this case, the same suspended solid solutions with the same concentrations mentioned before will be prepared in the main. The surfactants are prepared in almost the same way the solid suspensions are, for example, to add 10 ppm of the surfactant, 4.2 g is weighted and mixed in one-liter beaker with water and poured into the main tank that contains the suspended solid solution.

The resulting mixture is circulated within the same operating conditions applied for the suspended solid solution before. This operation is repeated in each surfactant type, suspended solid type, suspended solid concentration and surfactant concentrations (10, 20 and 30 ppm).

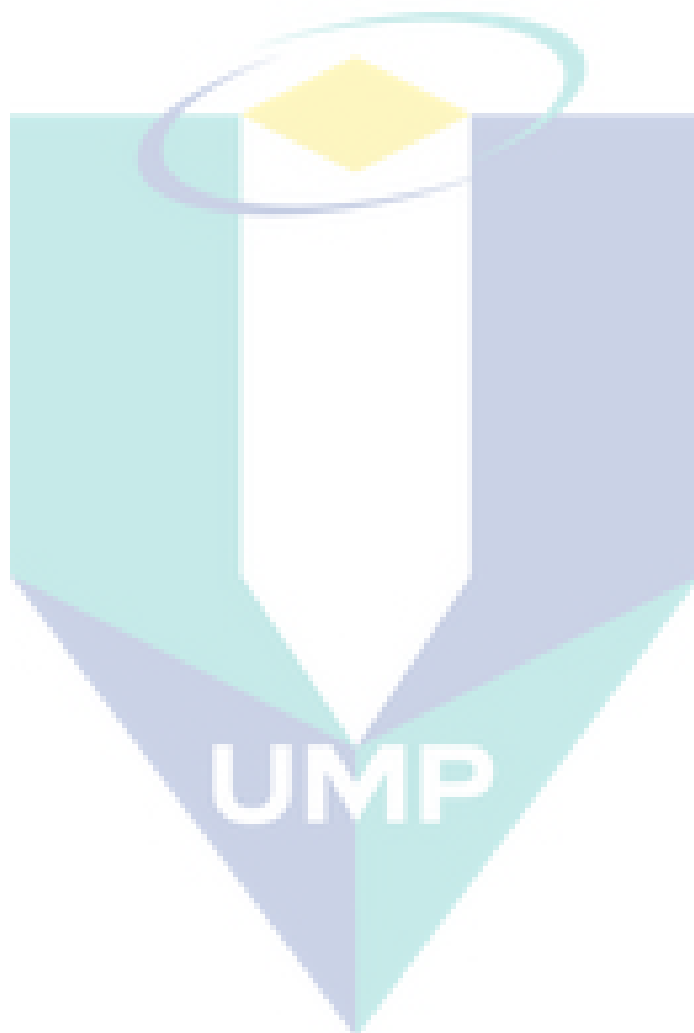
Continuous mixing in the main tank during the experimental work is very important to ensure the homogeneity of the solid-liquid solution entering to the main pump and delivered to the testing sections for the pressure drop measurements.

3.3.3 Experimental Work

All the experimental work was carried out in the closed loop experimental liquid recirculation rig described in the previous sections and shown in figures 3.4 to 3.9. The flow meter and pressure gauge were set up, and the circulation system was verified before the analysis began. In order to verify the circulation system, water without additive is first circulated through the circulation system by pump 1 and the flow rate was controlled using the bypass section (P2) with its control valve (V2) for each pipe. The system verification was conducted by comparing the friction factor of fluid in the experimental rig with friction factor obtained by using Blasius equation and Virk equation. The detailed results of the experimental verification are discussed in Chapter 4. The friction factor of flow in experimental work was measured through pressure drop analysis for each pipe.

After the preparation of the solution in the main tank, the operation starts by delivering the solution through the main pump into one of the testing sections. For example, the solution is delivered to the 0.0254 m I.D. pipe by closing V3 and V5 valves and opening V4. Then the solution flow rate is controlled and adjusted to certain value by adjusting V2 and V4 in the same time to have exact flow rate readings of the pure water. Pressure drop readings are taken for the chosen testing section investigated. Then new flow rate is adjusted in the same way to have the other pressure drop readings again and so on. Next, the other pipe diameter will be tested by closing the other two pipes valves and allowing the solution to flow within the selected pipe and the experimental steps will be repeated. This procedure is repeated for each pipe diameter, testing section and additive concentration. To ensure accuracy in the pressure drop and flow rates readings, each point

is repeated two to three times and the average readings are taken. Figures 3.11 and 3.12, shows the experimental workflow diagram for suspended solids particles and the surfactant-suspended solid solution respectively.



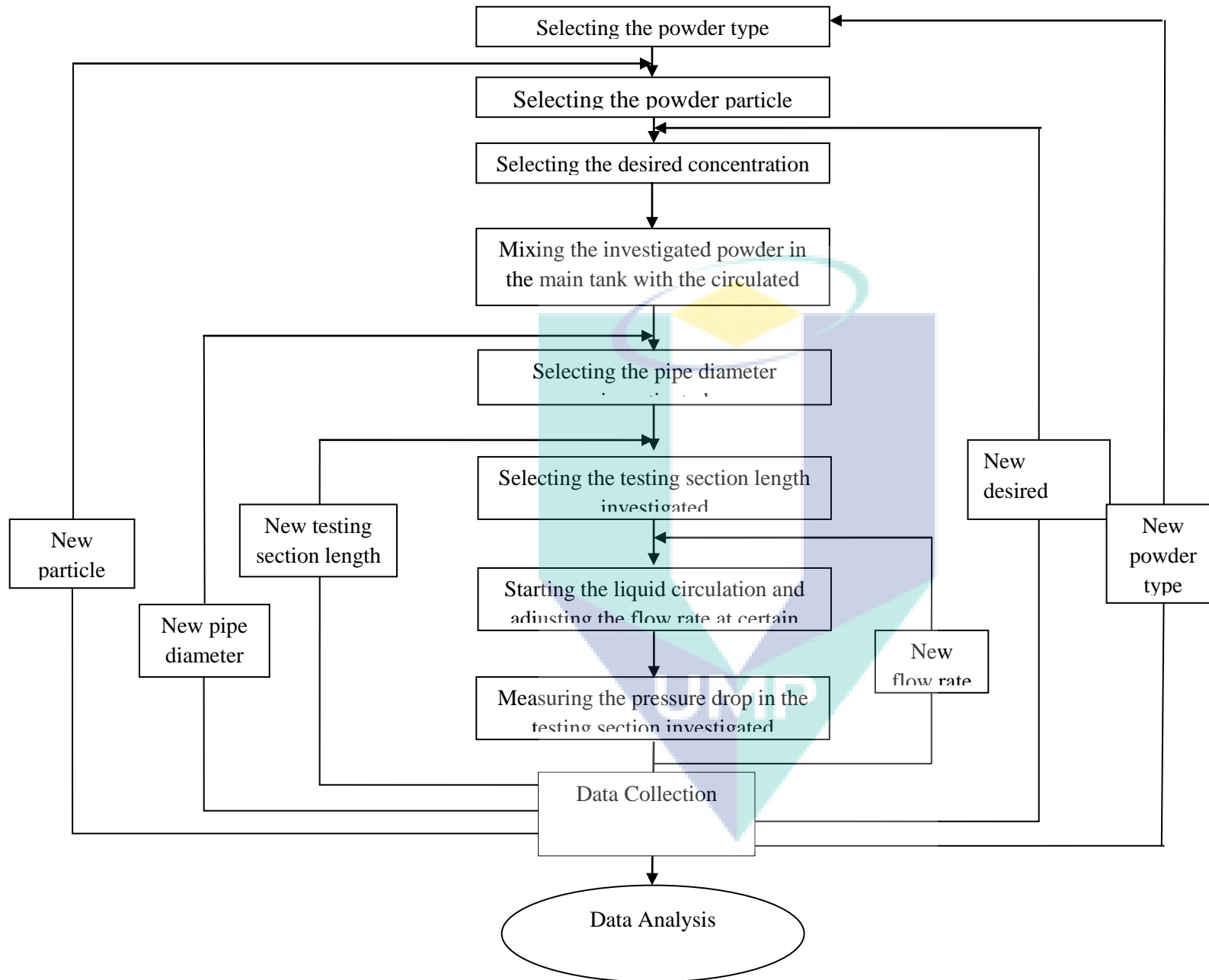


Figure 3.11: Flow diagram of the experimental work with the investigated powders

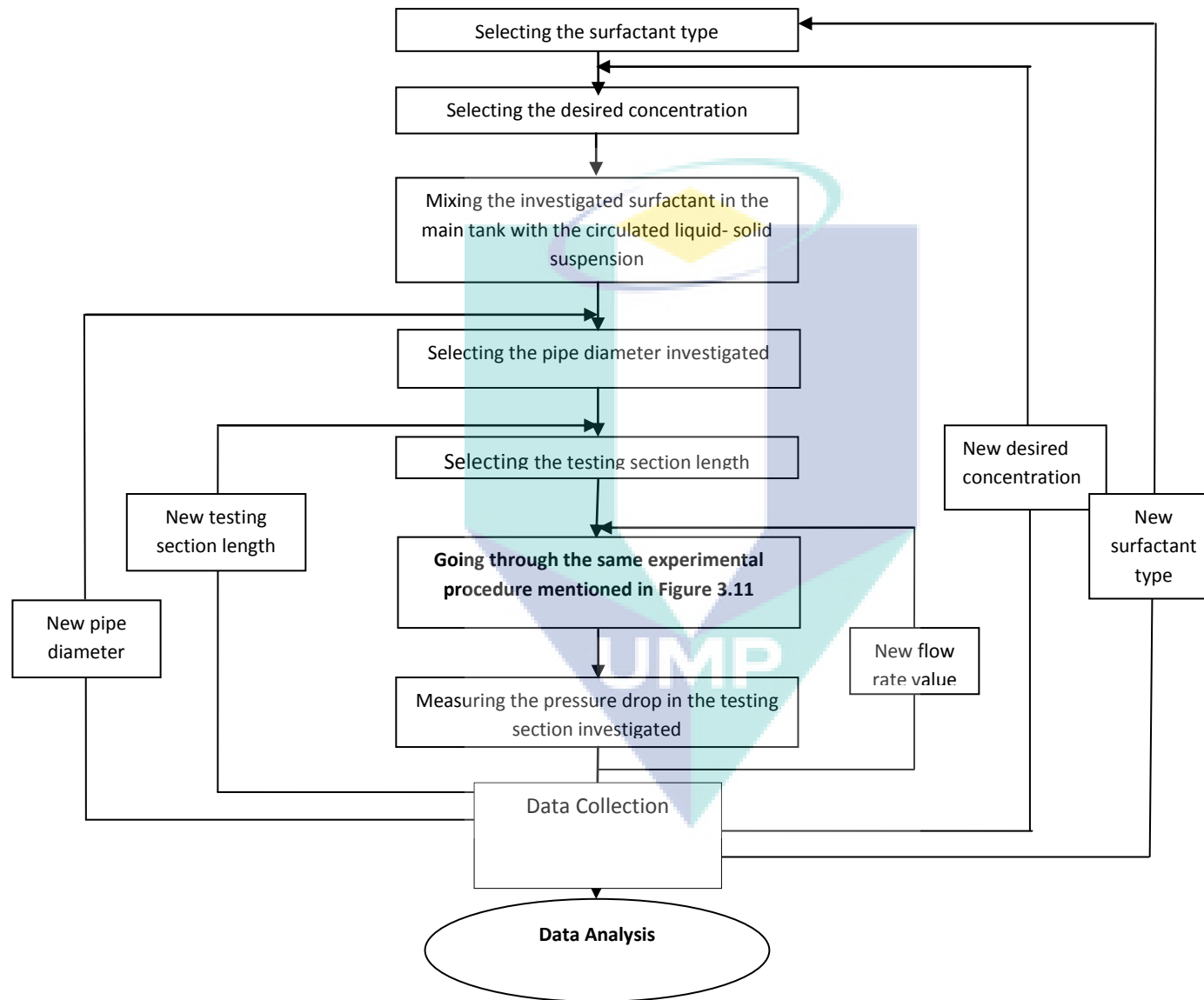


Figure 3.12: Flow diagram of the experimental work with the investigated surfactant- suspended solid solution

3.4 EXPERIMENTAL CALCULATIONS

3.4.1 Percentage Drag Reduction

Differential pressure drop readings through testing sections before and after adding the solid powder and the drag reducer is need to be used for the calculation of percentage drag reduction, %Dr as follows:

$$\%Dr = \frac{\Delta P_b - \Delta P_a}{\Delta P_b} \quad (3.1)$$

Where: %Dr = percentage drag reduction
 ΔP_b = pressure drop before drag reducer addition (bar)
 ΔP_a = pressure drop after drag reducer addition (bar)

3.4.2 Velocity and Reynolds Number

The velocity (v) and Reynolds Number (Re) were calculated using the flow rate readings (Q), density (ρ), velocity (μ) and pipe diameter (d), for each run as follows:

$$Re = \frac{\rho * d * v}{\mu} \quad (3.2)$$

Where: Re = Reynolds number (dimensionless)
 ρ = liquid density (kg/m^3)
 μ = liquid viscosity (cp)
 d = pipe diameter (m)

3.4.3 Friction Factor

Fanning friction factor calculated using the following equation:

$$f = \frac{(\Delta P * d / 4l)}{\rho * v^2 / 2} \quad (3.3)$$

Where: f =fanning friction factor (dimensionless)

ΔP =differential pressure (bar)

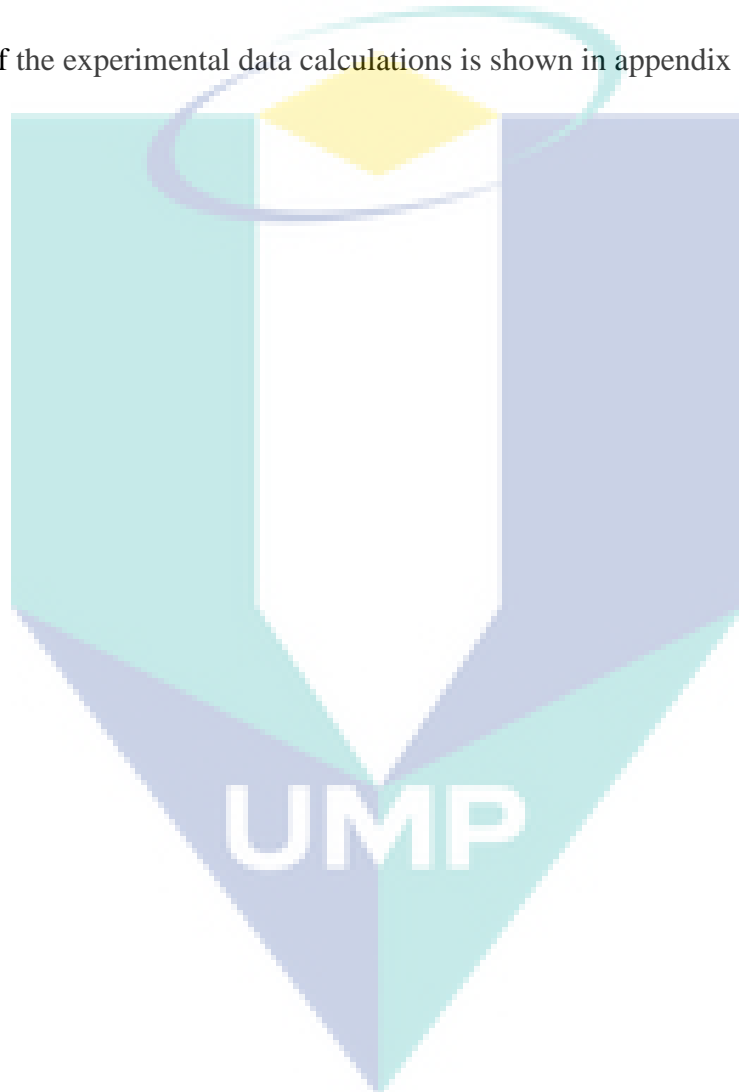
d =pipe diameter (m)

l =Pipe length (m)

ρ = liquid density (kg/m^3)

v = liquid velocity (m/s)

A sample of the experimental data calculations is shown in appendix E.



CHAPTER 4

RESULTS AND DISCUSSION

In this chapter, the influence of the drag reduction parameters investigated was shown and analyzed. The variables effect can be classified depending on the interaction of each variable with the other. The major variables investigated are:

1. The solution flow rate, which was represented by the dimensionless Reynolds number (Re).
2. The pipe diameter effect, where three pipe diameters were investigated (0.5, 1 and 1.5) inch.
3. Concentration of additives.
4. Zwitterionic surfactant types, where two Zwitterionic surfactants were chosen to be investigated in the present work namely: ((3-(Decyldimethyl-ammonio) propanesulfonate inner salt) and (3-(N-N,Dimethylpalmityl-ammonio) propanesulfonate)). The purpose behind choosing these surfactants is the close properties of these surfactants especially in the molecular weight and the high difference in the molecular structure.
5. Powder type. Three powder types were chosen to be investigated in the present works, namely aluminum powder, copper powder and coal powder.
6. Powder particle size. For each powder, two particle sizes were chosen to be investigated, (42 and 71) μm .

This chapter deliberated the effect of these variables on the flow behavior inside the investigated pipeline and the effect of combining their effect on the drag reduction performance.

4.1 LIQUID RECIRCULATION SYSTEM VERIFICATION

One of the important steps in the experimental work carried out in the present investigation is the verification of the variables obtained from the experimental rig for this work to ensure its workability and reliability in generating accurate data. In this work, the verification is achieved by comparing the friction factor data of the additive-free transported water with the standard mentioned in the literature, i.e. Blasius (1999), Hoyer, et al (1998) and Virk (1975). The data utilized in this comparison is collected from the experimental rig. The flow behavior of any liquid in a pipeline and its relation to the turbulence structures for different values of liquid flow rates, represented by Reynolds number Re , can be divided into four major regions:

- 1- Laminar flow region ($Re < 2300$), where a correlation was suggested by various researchers (Hoyer and Gyr, 1998, Cruz et al., 2004) as a representation to the flow mode in laminar flow system. The friction factor of laminar flow in pipe is defined as:

$$f = \frac{16}{Re} \quad (4.1)$$

- 2- Transition region ($Re = 2300$ to 3000), where the flow changes from laminar to turbulent flow with friction coefficient rises rapidly.
- 3- Turbulent region ($Re > 3000$), where the friction factor follows the correlation equation suggested by Blasius:

$$f = 0.0791 Re^{-0.25} \quad (4.2)$$

- 4- Virk asymptote region, which is suggested by Virk to represent the greatest possible fall in resistance in which the relation between friction factor (f) and Re does not depend on the nature of the additives or pipe diameter. The formula for Virk is:

$$f = 0.59Re^{-0.58} \quad (4.3)$$

The experimental friction factor values were calculated using Fanning friction factor definition, which was also adopted by the aforementioned correlations and asymptotes. The fanning friction factor can be defined as the ratio of the wall friction force (or the wall shear stress) to the inertial force inside the pipe (Yunus and Cimbala, 2006) as shown in following equation:

$$C_f = \frac{2\tau_w}{\rho v_{avg}^2} \quad (4.4)$$

The wall shear stress in a fully developed pipe flow was defined by (Perry et al. 1963). This equation relates the wall shear stress to the pressure drop during the turbulent flow inside pipelines. The equation can be represented as follows:

$$\tau_w = \frac{d\Delta P}{4l} \quad (4.5)$$

Where (d) is the pipe diameter, (ΔP) is the pressure drop in the pipe and (l) is the pipe length. The value of Re was universally used to distinguish the laminar and turbulent flow, where the relation of Re with the velocity and viscosity of fluid is defined as:

$$Re = \frac{\rho d v}{\mu} \quad (4.6)$$

Where: ρ = fluid density
 μ = kinematics viscosity of fluid
 v = fluid velocity

Figures 4.1 to 4.3 show the experimental friction factor comparison with the graphical representation of the standard correlations mentioned above. It is evident that the values of the experimental friction factor for all the samples selected in the three figures take place at/near Blasius asymptote. By comparing the experimental and theoretical friction factor values in the experimental rig, it can be noticed that the maximum error observed for the 0.0125 m I.D pipe is 1.8%, for the 0.0254 m I.D pipe is 0.8% and for the 0.0381 is 5.1%. This confirms the reliability of the rig to generate accurate data for all the investigated ranges. The data for these asymptotes are listed in appendices A, B and C.

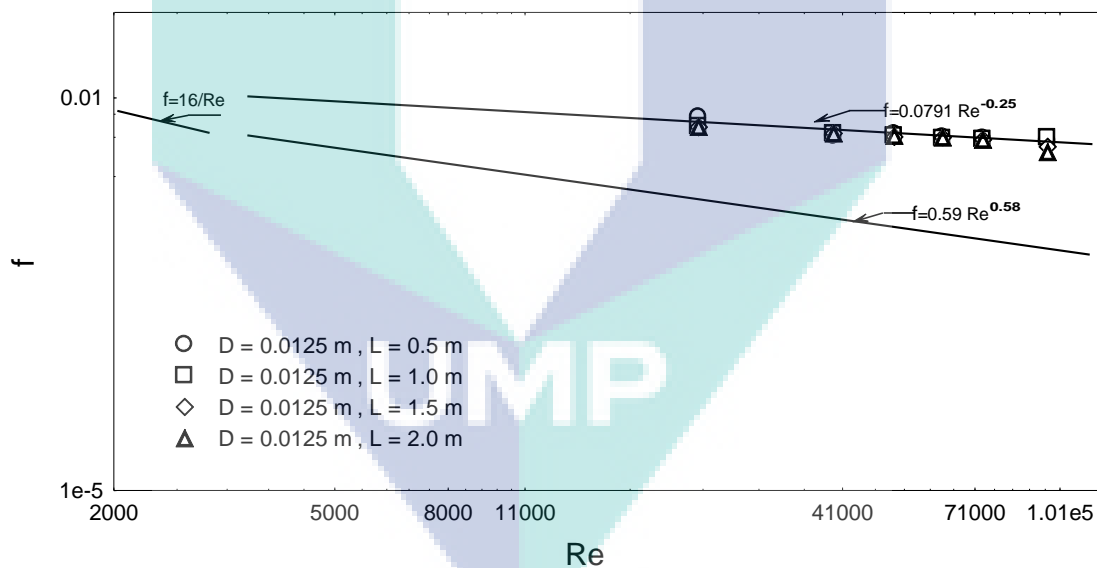


Figure 4.1: Experimental friction factor versus Reynolds number for water in 0.0125 m pipe diameter and different pipe lengths.

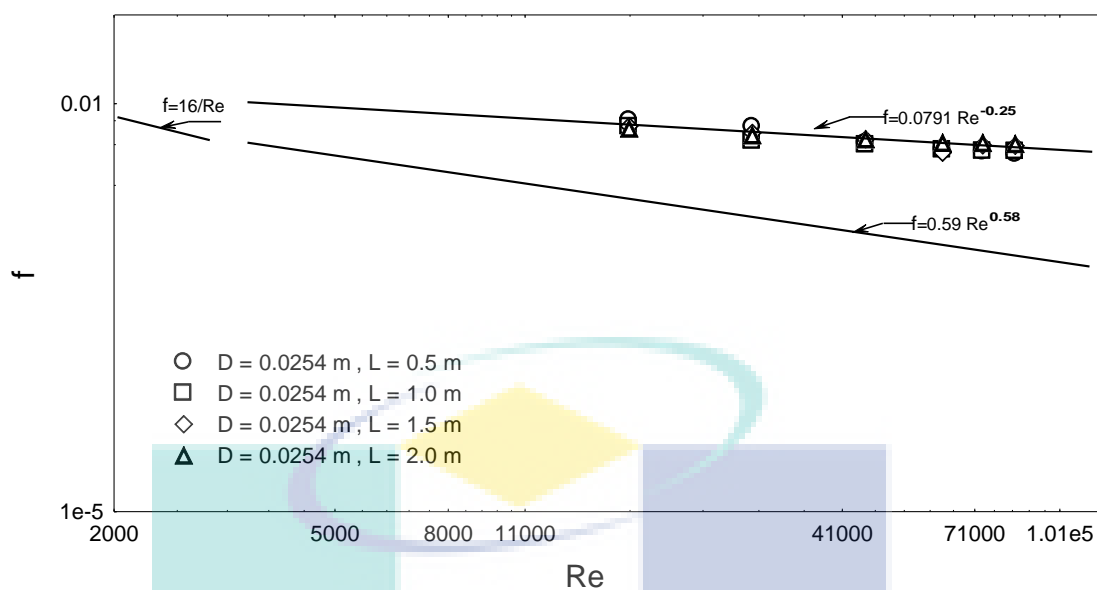


Figure 4.2: Experimental friction factor versus Reynolds number for water flow in 0.0254 m pipe diameter and different pipe lengths.

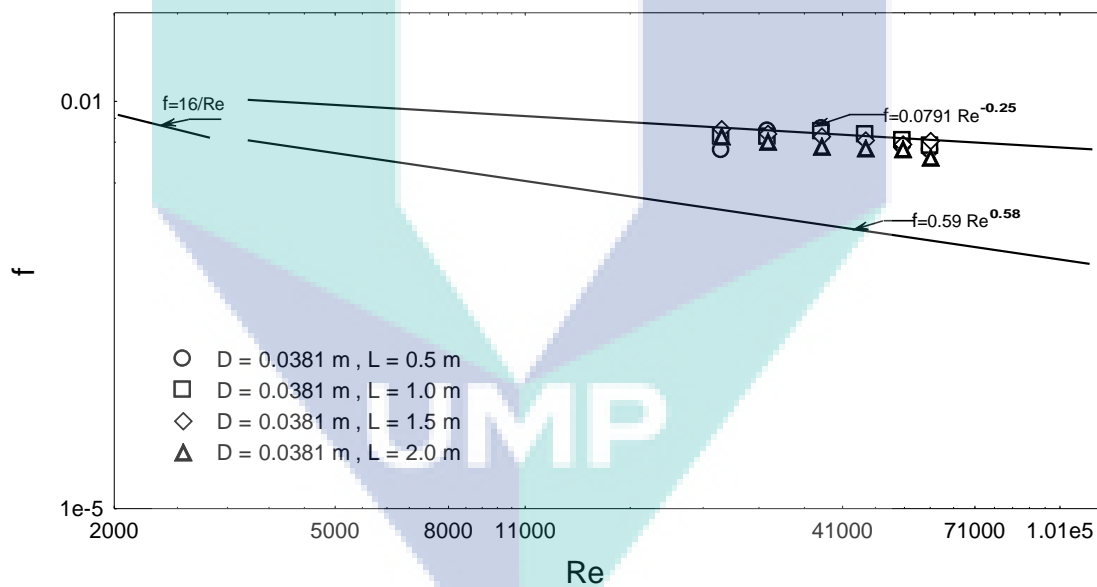


Figure 4.3: Experimental friction factor versus Reynolds number for water flow in 0.0381 m pipe diameter and different pipe lengths.

4.2 SUSPENDED SOLID PARTICLES AS DRAG REDUCING AGENTS

In this section, the performance of three solid particles as drag reducing agent and their effect in improving the flow and reducing the pumping power consumption were discussed.

4.2.1 Effect of Reynolds Number (Re)

In order to show the effect of the degree of turbulence represented by the dimensionless form of Reynolds number (Re) on the drag reduction, selected samples of the experimental data are shown in Figures 4.4 to 4.9. In addition, all the experimental data of the present investigation is tabulated in appendices A, B and C.

Figures 4.4 to 4.6 highlight the effect of the sand powder addition on the drag reduction performance for sand with a particle diameter of 45 μm . Figure 4.4 shows the effect of the sand powder addition in improving the flow of water inside 0.0125 m I.D and 0.5 m length pipe. Generally, it can be noticed that the percentage drag reduction %Dr increases by increasing the Re with different variables considered in the experimental work, such as the additive concentration and the pipe geometry. In most cases, the %Dr increases by increasing the Re, until reaching certain values where the %Dr increase is low and its value tends to be more stable. This can be seen clearly in figure 4.4 for each additive concentration (100 to 500 ppm). However, for the highest concentration (500 ppm), the value of the %Dr continues to increase at almost the same level by increasing the Re. The mechanism controlling the drag reduction performance will be discussed in section 4.5. Increasing the Re means increasing the degree of turbulence and degree of interaction between the additive and the turbulent structures formed inside the pipeline. That will enable more suspended solid particles to interfere within the turbulent median and suppress the eddies formed inside the pipe and improve the flow. Further increase in the Re will allow the degree of turbulence to overcome the effect particles drag reduction ability and the curves start to show stable or descending values of the %Dr.

Figure 4.5 shows another kind of behavior monitored and observed in the experimental work. This figure shows the effect of the sand powder addition in improving the flow of water inside 0.0254 m I.D and 0.5 m length pipe. It can be noticed that, the behavior is totally changed by changing the pipe diameter; the relation between the %Dr and Re is not as smooth as the one shown in figure 4.4. The 500 and 300 ppm curves continue to increase by increasing the Re, whereas the 100 ppm curve reaches its maximum at $Re = 61955$ with a value of 17.69 and then starts to decline reaching a value of 7.04 at $Re = 83808$. The behavior of the 100-ppm curve is justified in the coming paragraphs at the end of this section.

By further increase in the pipe diameter with the same operating conditions mentioned above, the behavior and relation between the %Dr and Re tend to be the same as described in figure 4.4. This can be noticed in figure 4.6, which shows the effect of the sand powder addition in improving the water flow inside 0.0381 m I.D and 0.5 m length pipe. In addition, it was observed that the %Dr increases by increasing Re and reaches a maximum of 4.99, 10.2 and 16.1 at $Re = 45058$, 45058 and 52568 respectively, then the %Dr starts to drop with any further increase in the Re. One of the important things to observe in figure 4.6 is the effect of the additive concentration on the location of the maximum %Dr in terms Re. The maximum %Dr for the 500 ppm is with $Re = 52568$, whereas the maximum %Dr for the 300 and 100 ppm is at $Re = 45058$. This increase in the value of the maximum %Dr highlights the relation between the degree of turbulence and the number of particles involved and interacted with the turbulent structures inside the main flow. Generally, increasing the additive concentration increases the number of particles involved in the drag reduction system. This leads to a new balancing effect between these two factors which increases the value of Re at which the maximum performance is delivered.

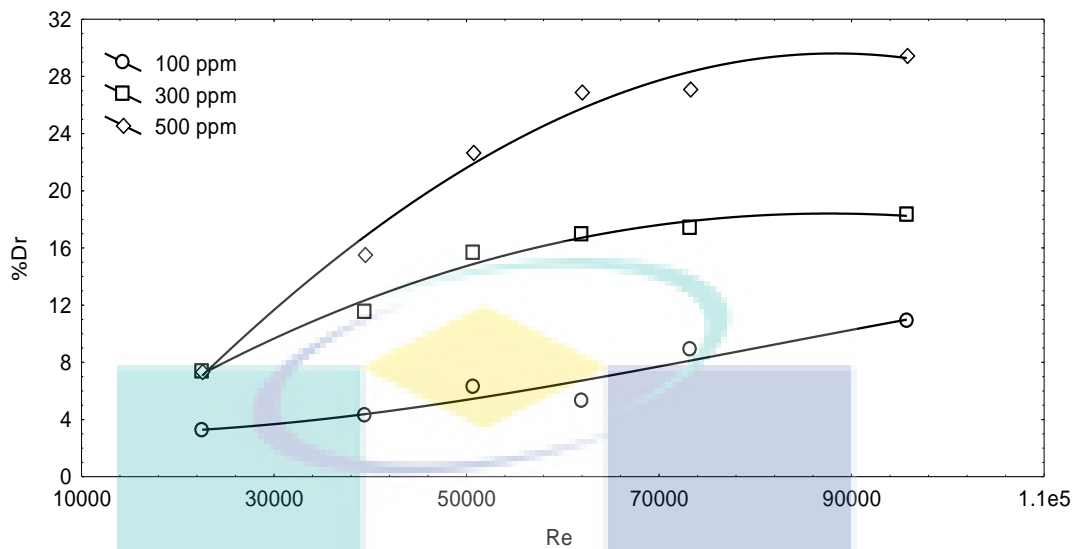


Figure 4.4: Effect of Re on the %Dr for Sand particles ($D_p = 45 \mu\text{m}$) suspended in water and flowing in 0.0125 m I.D. and 0.5 m pipe.

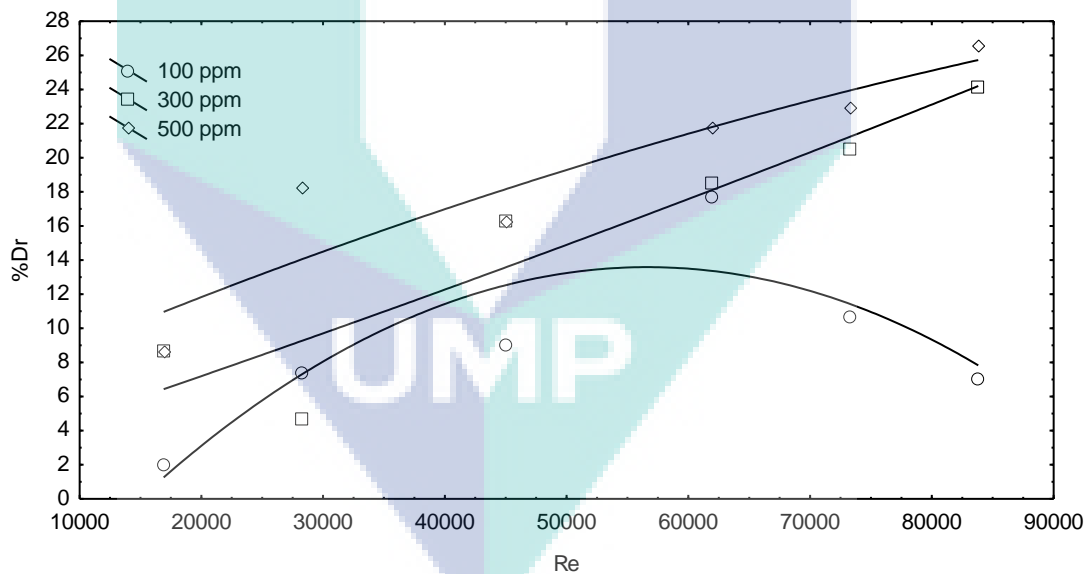


Figure 4.5: Effect of Re on the %Dr for Sand particles ($D_p = 45 \mu\text{m}$) suspended in water and flowing in 0.0254 m I.D. and 0.5 m pipe.

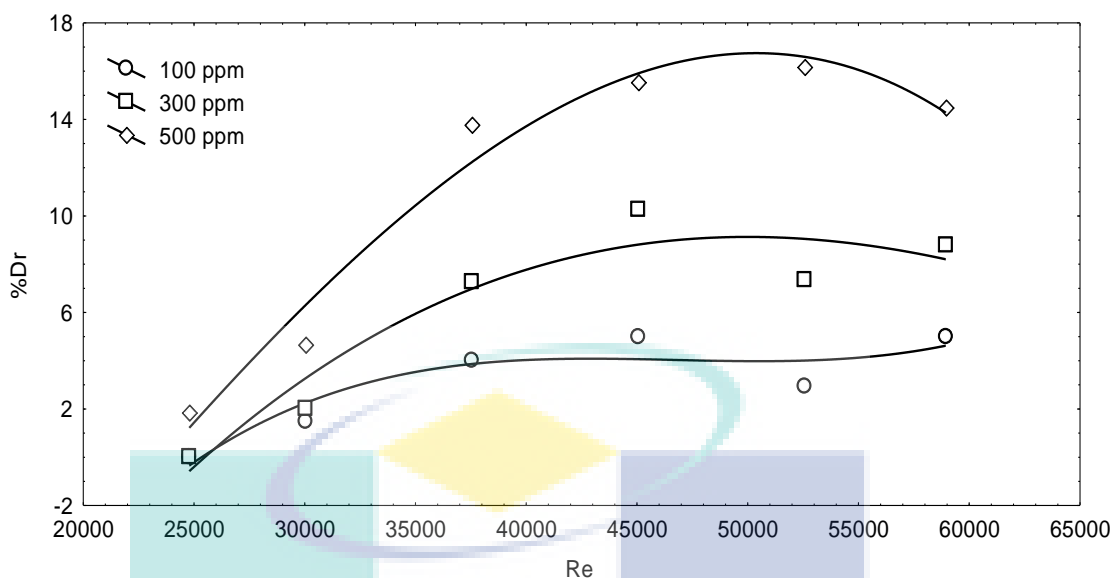


Figure 4.6: Effect of Re on the %Dr for Sand particles ($D_p = 45 \mu\text{m}$) suspended in water and flowing in 0.0381 m I.D. and 0.5 m pipe.

Figures 4.7 to 4.9, show selected samples of the experimental work using the aluminum powder as drag reducing agent with a particle diameter of $71 \mu\text{m}$ and different testing-section lengths. Figure 4.7 shows almost a typical performance from the aluminum powder in improving the flow, where %Dr increases by increasing the degree of turbulence inside the pipe (Re), reaching the maximum value of 34.08% at the optimum Re of 95749 with 500 ppm additive concentration for the water flowing in 0.0125 m I.D pipe and 0.5 m testing section length. On the other hand, it also can be noticed that, this value actually is one of the maximum values observed in the experiment. By simple observation for the curve behavior, an almost stable %Dr can be seen starting from $\text{Re} = 50690$ to $\text{Re} = 95749$ with %Dr ranged from 32.77 to 34.08 respectively. Hence, it can be recommended from the economical point of view that the optimum Re for the best %Dr depends on the stability that such solid drag reducing agent showed in a wide range of Re or degree of turbulence.

Figures 4.8 and 4.9, show effect of Re on the %Dr for Aluminum particles ($D_p = 71 \mu\text{m}$) suspended in water and flowing in 0.0125 m I.D and 1.0 and 2.0 m testing section lengths respectively. The general behavior still the same even by changing the testing section lengths where the three curves for the three additive concentrations

increases by increasing the value of Re, reaching the maximum %Dr of 26.22 at Re = 73220 for the 100 ppm curve in figure 4.8 and then drops down to 21.78 by a further increase in Re. For the other two curves (300 and 500 ppm addition concentration curves), in figure 4.8 %Dr showed more stable behavior after reaching the maximum value and the %Dr didn't change much, that, %Dr = 31.6 and 31.72 for Re = 73220 and 95749 respectively for the 300 ppm and 37.5 and 37.7 for Re = 73220 and 95749 respectively for the 500 ppm. Similar trend was observed in figure 4.9.

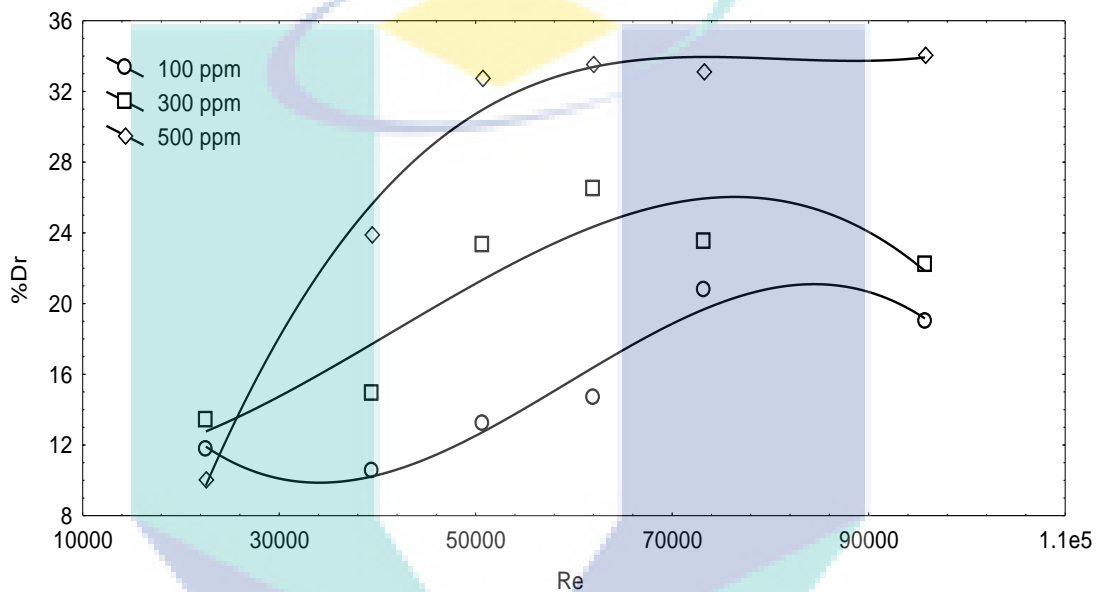


Figure 4.7: Effect of Re on the %Dr for Aluminum particles ($D_p = 71 \mu\text{m}$) suspended in water and flowing in 0.0125 m I.D and 0.5 m pipe.

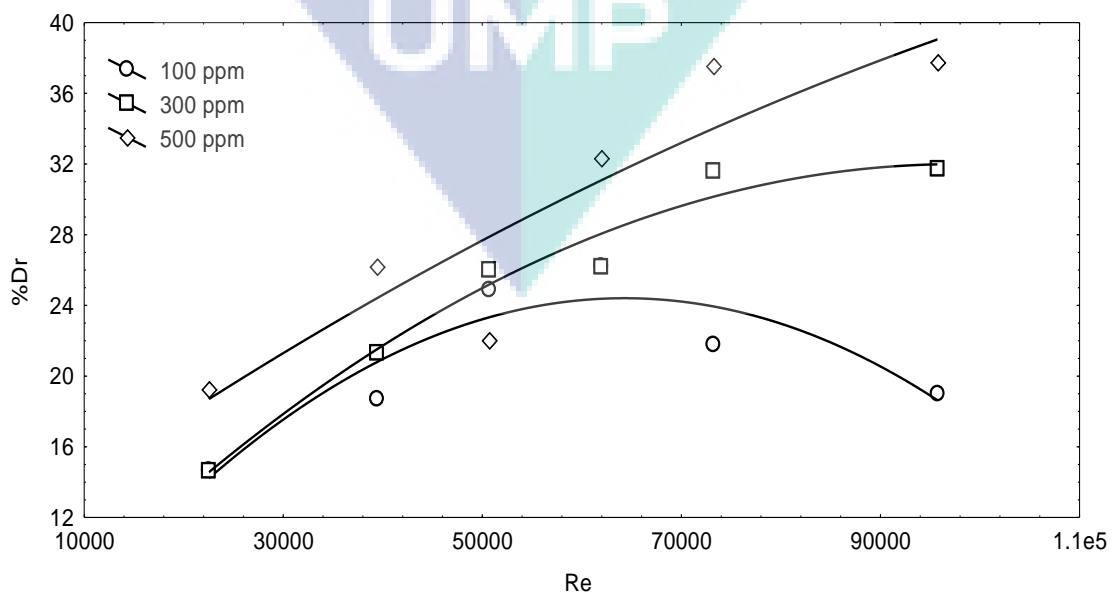


Figure 4.8: Effect of Re on the %Dr for Aluminum particles ($D_p = 71 \mu\text{m}$) suspended in water and flowing in 0.0125 m I.D and 1.0 m pipe.

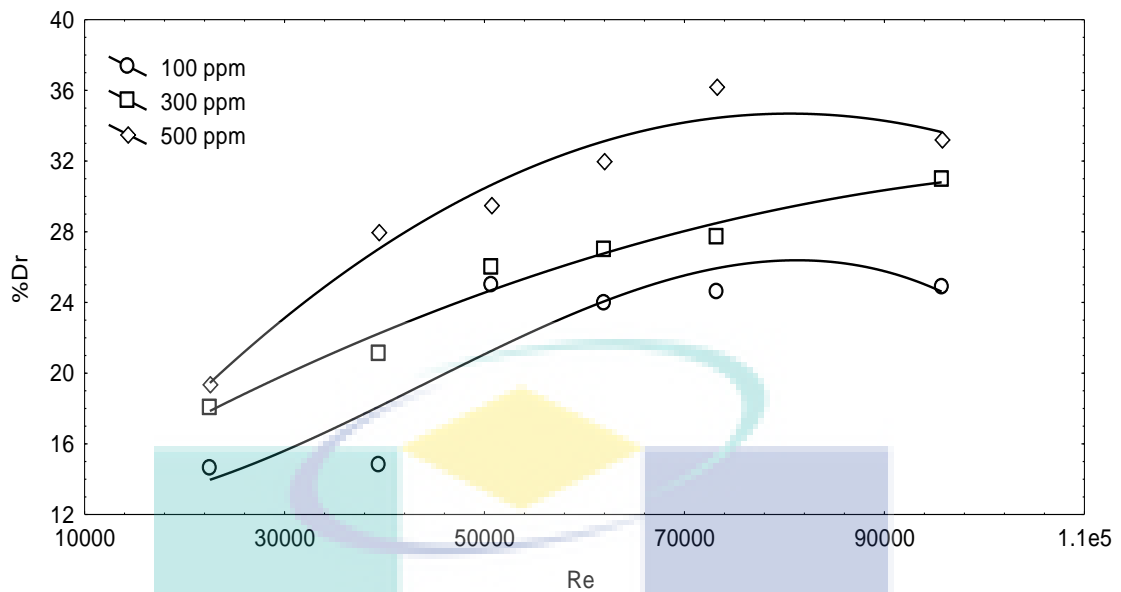


Figure 4.9: Effect of Re on the %Dr for Aluminum particles ($D_p = 71 \mu\text{m}$) suspended in water and flowing in 0.0125 m I.D and 2.0 m pipe.

Figures 4.10 to 4.12, show selected samples of the experimental data of drag reduction using coal suspended particles. Figure 4.10 shows typical and normal behavior of the %Dr versus Re where the %Dr increases by increasing the Re until reaching maximum value range of 30.4% to 32.8% within the Re range of 61967 to 95767 respectively. Within the same experimental conditions and by increasing the testing section length to 1.5 m, the behavior of the %Dr versus Re changed as shown in figure 4.11. Figure 4.11 shows that the maximum %Dr was achieved within a wider range of Re, where, maximum %Dr ranged from 29.4 to 31.9 was observed within the Re ranged between 50700 to 95767 with 500 ppm additive concentration. This behavior shows how complicated the relation between the system geometry, degree of turbulence, additive type and additive concentration on the drag reduction performance. It is most of the time unpredictable behavior, where all these factors affect the %Dr in the same time resulting in undefined optimum operating conditions. More details regarding the suggested explanation for the Re-%Dr behavior is shown in the next paragraph. Finally, figure 4.12, shows selected experimental results for the coal powder with $45 \mu\text{m}$ particle size, suspended in water and flowing in 0.0125 m I.D. and 2.0 m pipe. Despite the non-uniform behavior some of the points shows, the general behavior still the same as described in the previous sections with maximum %Dr of 34.99 at $\text{Re} = 73233$, 2 m testing section length and 500 ppm addition concentration.

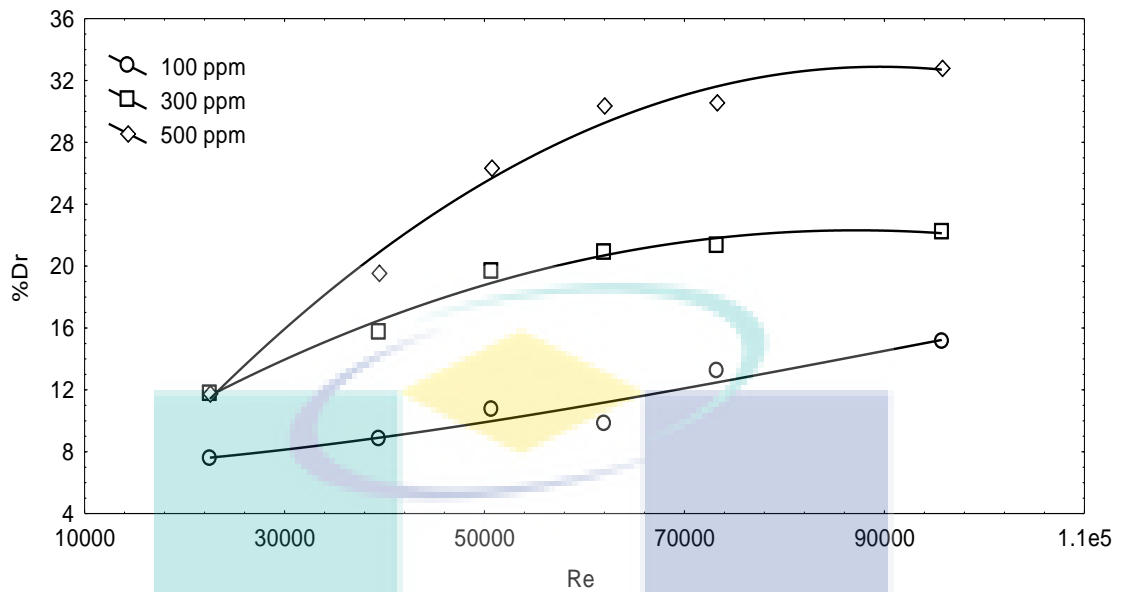


Figure 4.10: Effect of Re on the %Dr for Coal particles ($D_p = 45 \mu\text{m}$) suspended in water and flowing in 0.0125 m I.D. and 0.5 m pipe.

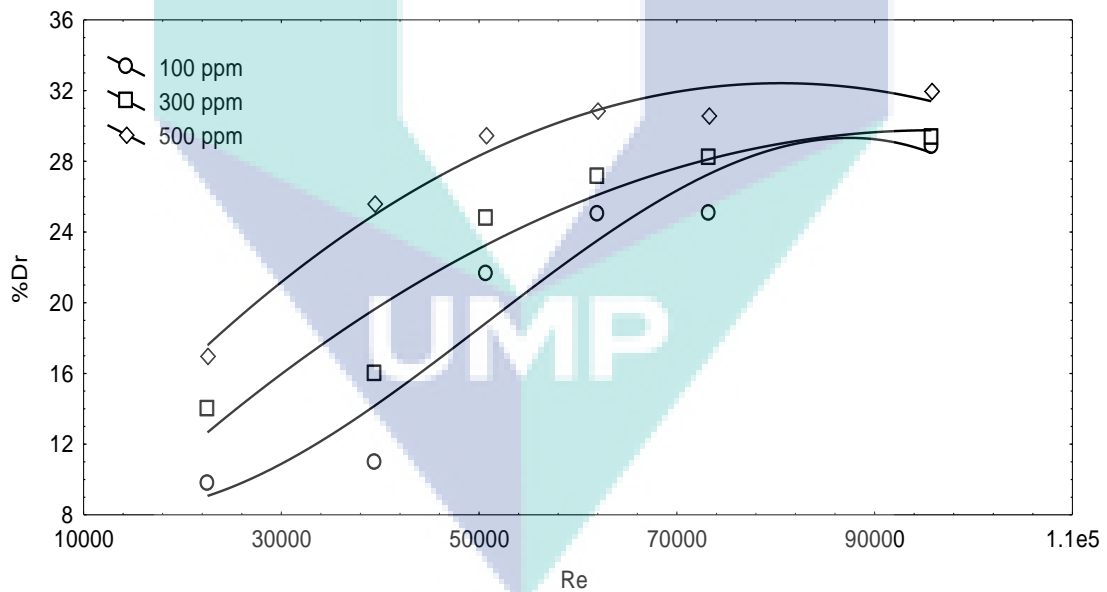


Figure 4.11: Effect of Re on the %Dr for Coal particles ($D_p = 45 \mu\text{m}$) suspended in water and flowing in 0.0125 m I.D. and 1.5 m pipe.

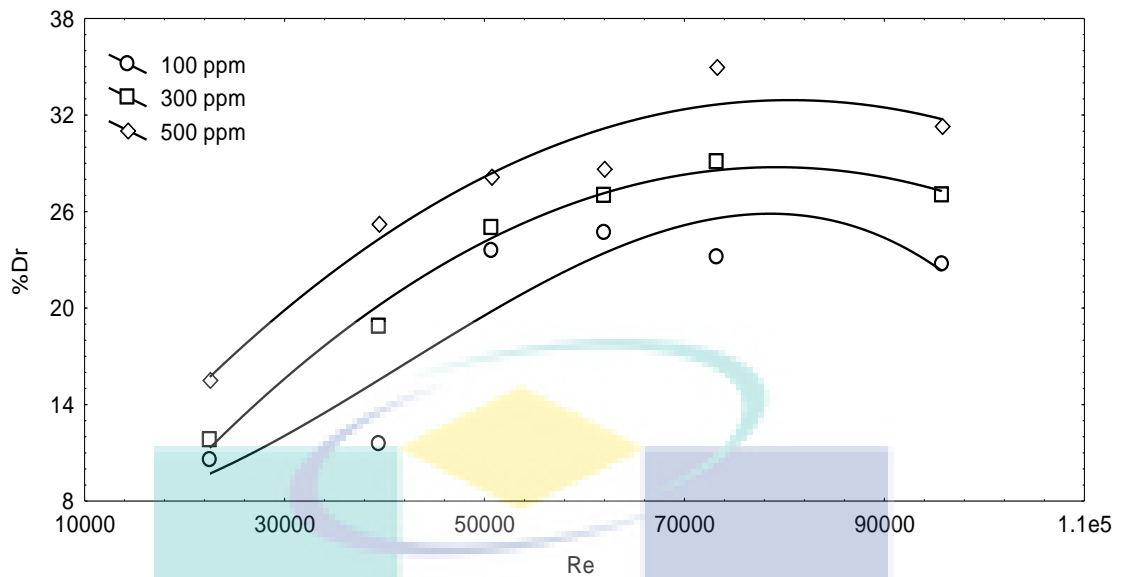


Figure 4.12: Effect of Re on the %Dr for Coal particles ($D_p = 45 \mu\text{m}$) suspended in water and flowing in 0.0125 m I.D. and 2.0 m pipe.

In general, all the selected samples showed almost typical general behavior that have been mentioned for all the types of the drag reducing agents, which are (polymers, surfactants and suspended solid) mentioned in the literatures. (Tom 1949, Warholic et al. 1999, Al-Sarkhi and Hanratty 2001, Al-Sarkhi et al. 2006, Barresi 1997, Molerus and Heucke 1999, Manhart 2003, Shanliang et al. 2007, Inaba et al. 2000, Hayder 2006, Lu et al. 1998, Kawaguchi et al. 2002, Myska and Mik 2004, Kang et al. 2001, Zhau et al. 2006, Cho et al. 2007, Ge et al. 2008, Li et al. 2008, Zhang et al., 2005, Rozenblit et al. 2006, Cho et al. 2007, Wilkens and Thomas 2007 and Myska and Mik 2003).

The effect of the degree of turbulence on the %Dr is very clear where the efficiency of the selected drag reducing agent started to increase by increasing the degree of turbulence (increasing Re) (which in another word means increasing the turbulence spectrum that is under the drag reducing agent effect). The experimental results indicated that the suspended solid particles started to be part of the turbulent structures inside the pipe flow systems, and that will enable the cracking of these turbulent structures inside the flow and prevented the eddies from forming within its complete shape and that led to the prevention of the pumping power absorption from the main flow. This prevention led to the flow improvement and prevented the dissipation of the pumping power in the turbulent structures inside the turbulent flow.

It is believed that, the penetration of these suspended solids in the eddy structure made it more difficult for the eddy to have the same normal shape. This is because of the high density and physical properties difference, which introduced new (but not permanent) rheological properties for the eddy viscosity and that led to the change in the eddy shape and size, resulted in the change in the turbulence flow structures and behavior.

After certain ranges of Re , maximum %Dr was achieved where maximum drag reducer performance can be observed. This maximum point(s) reflects the optimum solid-turbulence interaction point where the suspended solid give the maximum effect on the degree of turbulence inside the main flow. In certain cases during the experimental work, any further increase in the value of Re beyond the optimum (maximum %Dr) will result in a stable or descending value of the %Dr . This was due to the relation between the degree of turbulence and the concentration of the additive and its efficiency inside the flow and that is clearly seen in figure 4.6 where the maximum %Dr is reached in different Re depending on the concentration. In that figure it is obvious that the efficiency of the additives on suppressing eddies increases by increasing the concentration and the breakdown point start to be in higher values of Re when the concentration increases. Generally, by increasing the additive concentration, the number of solid particles involved in the drag reduction operation will be higher and that will lead to increase the value of Re “or the degree of turbulence” needed to overcome this increase in the number of particles involved with each eddy. It is important to know that, the effect of any parameter acting in the system and contributing in the drag reduction action is not independently performing.

4.2.2 Effect of additive concentration

The effect of additive concentration for the three types of the suspended solids investigated in the present work can be seen in figures 4.13 to 4.18. These figures represent selected samples from the experimental data results. The rest of the results can be seen in the experimental data tables in appendix (A1 to C20).

Figures 4.13 and 4.14, show the effect of additive concentration of the sand particles performance as drag reducing agent for the water media flowing in turbulent mode through the pipeline. Generally, the %Dr increases by increasing the suspended solid concentration, and that can be seen clearly in figure 4.13. Each curve represents the %Dr behavior with the increase in the additive concentrations (from 100 to 500 ppm) in an almost linear manner with some cases of non-linearity such as at $Re = 39426$ and $Re = 95749$ where the %Dr showed non-uniform behavior and the value of the %Dr decreases at 500 ppm. This non-uniform behavior was more pronounced in figure 4.14, for suspended sand particle system with D_p of $71 \mu\text{m}$ flowing in 0.0125 m I.D. and 1.0 m testing section length. All the curves interact with each other in a way that make the decision of the optimum operating conditions depending on the average behavior of the powder chosen. In the case of figure 4.13, the general behavior shows that the %Dr increases by increasing the additive concentration. Some of the points showed radical behavior during the experimental work where it increases with the increase of the additive concentration until a certain value where any further increase resulted in a decline in the %Dr.

For example, from figure 4.14 and at $Re = 95749$ it shows that, the value of the %Dr was 12.8 at 100 ppm, and that percentage increased to 29.6 at 300 ppm and showed a decline in the value of the %Dr down to 27.2% at 500 ppm. In this case, the behavior can be considered as an increase in the %Dr by increasing the additive concentration of the powder because the %Dr increased by 57% by increasing the concentration by 200 ppm (from 100 to 300 ppm), while the percentage of decrease in the %Dr was 8% when increasing the additive concentration from (300 to 500 ppm). While the rest of the experimental results represented in figure 4.14 didn't show linearity in their behavior and the %Dr increases by increasing the addition concentration reaching its maximum values at the 300 ppm addition concentration and then by any further increase in the concentration the %Dr became lower.

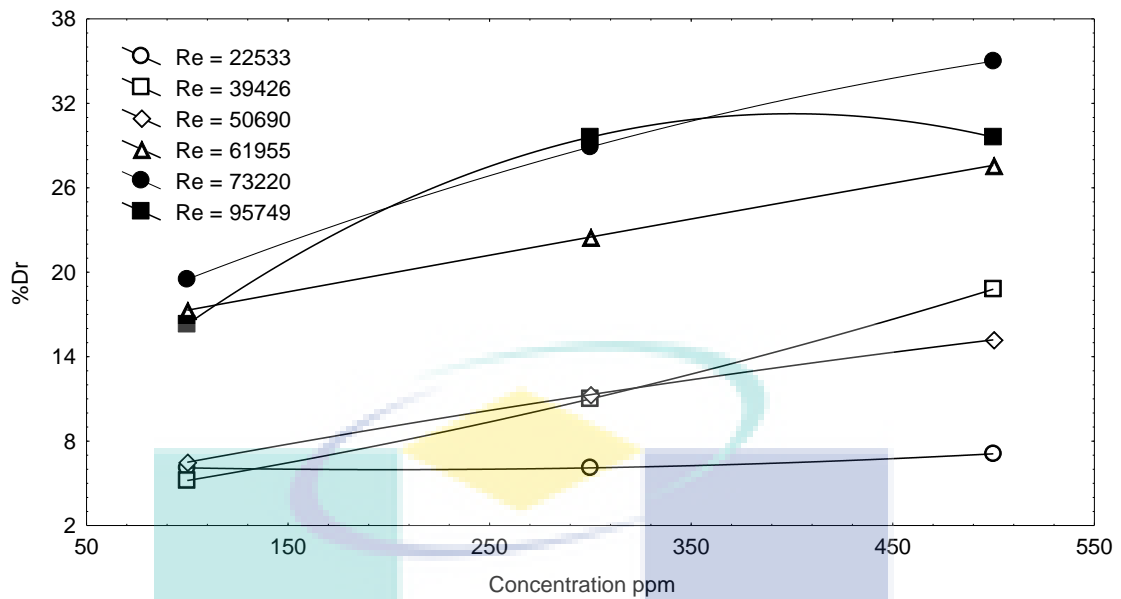


Figure 4.13: Effect of additive concentration on the %Dr for Sand particles ($D_p = 45 \mu\text{m}$) suspended in water and flowing in 0.0125 m I.D. and 1.0 m pipe.

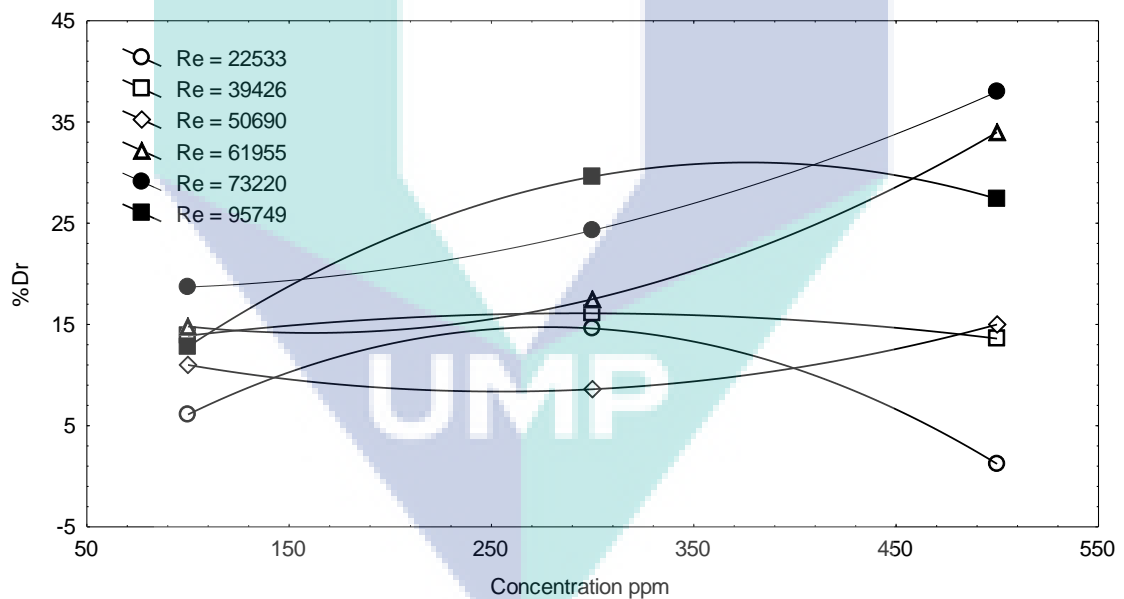


Figure 4.14: Effect of additive concentration on the %Dr for Sand particles ($D_p = 71 \mu\text{m}$) suspended in water and flowing in 0.0125 m I.D. and 1.0 m pipe.

Figures 4.15 and 4.16, shows the effect of the additive concentration of the aluminum powder on the %Dr for selected samples of the experimental data. Generally, it is clear that the %Dr increases by increasing the additive concentration with less intersected points compared with the sand case and more uniform behavior.

From figure 4.15, it can be noticed that the values of the %Dr for the $Re = 73220$ is higher than that with $Re = 83808$. That behavior also can be seen for some curves in the sand figures (4.13 and 4.14). That is a clear indication about the effect of the degree of turbulence and its effect on the drag reduction performance of the additive. Where for a non uniform flow media as in turbulent flow, some non uniform behavior for the additive concentration effect is expected but in general most of the experimental data point did show that the %Dr increases by increasing the addition concentration. These findings support highly what was mentioned in section 4.2.1 and shows how to choose the optimum operating conditions.

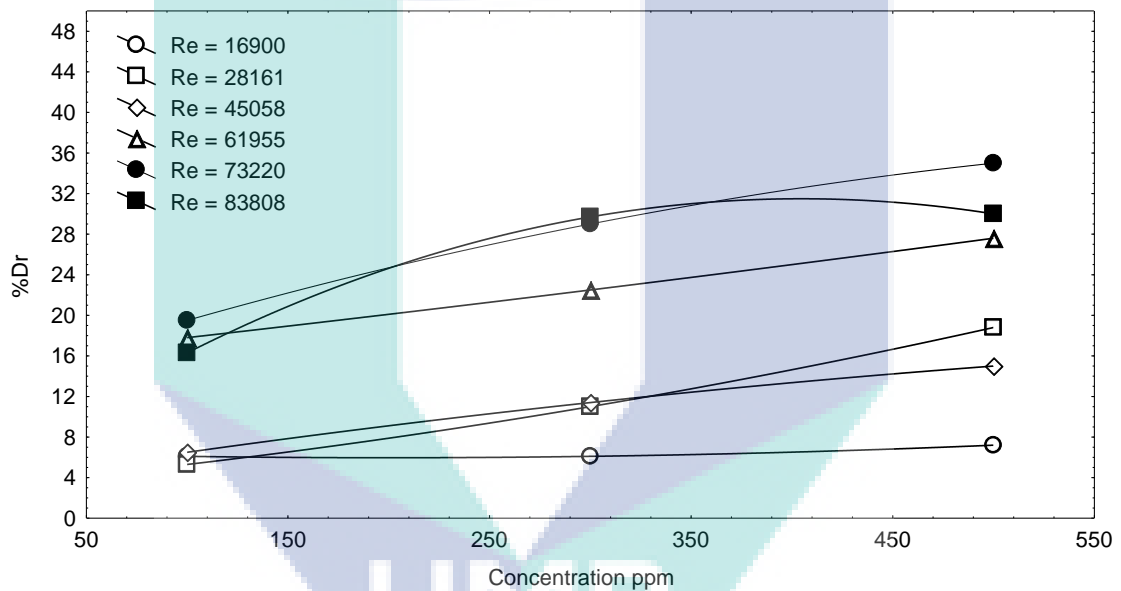


Figure 4.15: Effect of additive concentration on the %Dr for Aluminum particles ($D_p = 71 \mu\text{m}$) suspended in water and flowing in 0.0125 m I.D. and 1.0 m pipe.

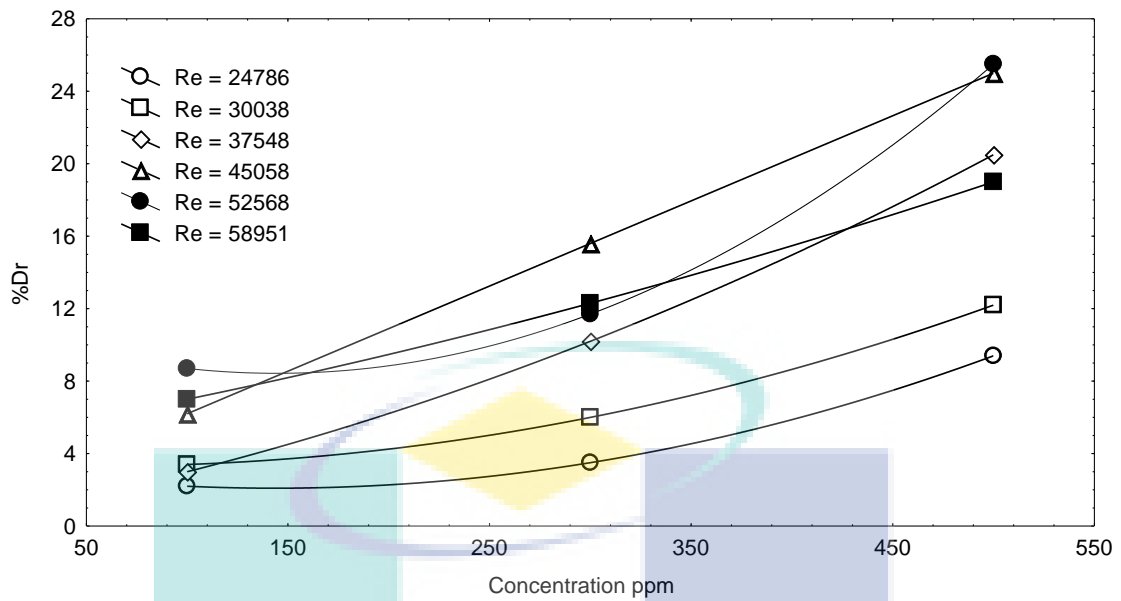


Figure 4.16: Effect of additive concentration on the %Dr for Aluminum particles ($D_p = 71 \mu\text{m}$) suspended in water and flowing in 0.0381 m I.D. and 1.0 m pipe.

Another representation for the additive concentration effect on the %Dr can be seen in figures 4.17 and 4.18 for selected samples of the experimental data for the coal powder added to the main flow. Figure 4.17 shows the effect of the additive concentration on the %Dr for coal particles ($D_p = 45 \mu\text{m}$) suspended in water and flowing in 0.0125 m I.D. and 1.0 m pipe, while figure 4.18 shows the same effect with the same conditions mentioned in figure 4.17 but with a different test pipe diameter. The general observation shows the same behavior observed with the sand and the aluminum powders where the %Dr increases by increasing the coal powder concentration. Almost the same intersections and instability can be seen in some curves representing the experimental work results. By comparing the results represented by the two figures. It can be concluded that by changing the pipe diameter the behavior of the %Dr against the additive concentration will change also. Where more intersection and random behavior can be seen in figure 4.18 when changing the pipe diameter from 0.0125 to 0.0254 m and that reflect the effect of the turbulence structure size (eddy size) and position on the drag reduction ability of the drag reducing agent which will be discussed in the coming sections.

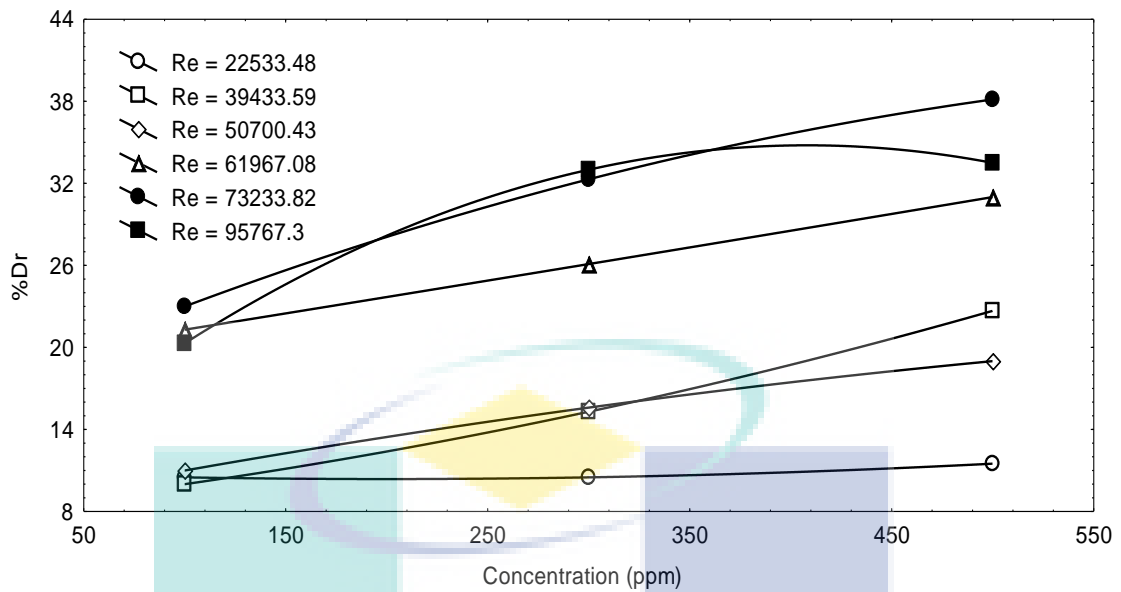


Figure 4.17: Effect of additive concentration on the %Dr for Coal particles ($D_p = 45 \mu\text{m}$) suspended in water and flowing in 0.0125 m I.D. and 1.0 m pipe.

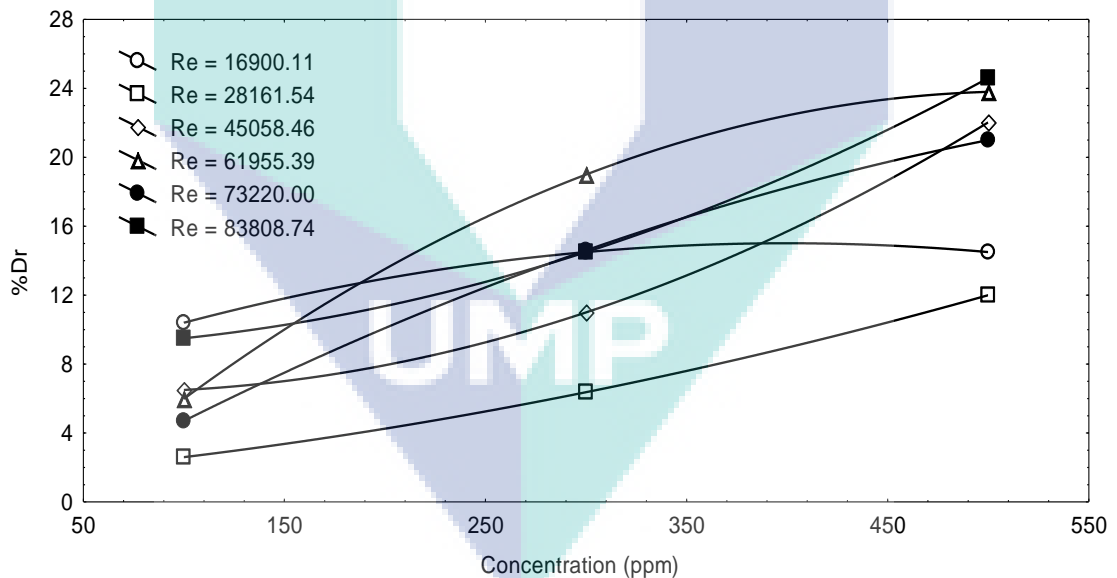


Figure 4.18: Effect of additive concentration on the %Dr for Coal particles ($D_p = 45 \mu\text{m}$) suspended in water and flowing in 0.0254 m I.D. and 1.0 m pipe.

Generally, the results showed that %Dr increases by increasing the powder concentration. This means increasing the number of powder particles involved in the drag reduction process. In another word, within certain Re, increasing the powder concentration means increasing the turbulence spectrum that is under the drag reducer effect. It is important to notice that, although %Dr increases by increasing the powder

concentration, but its behavior with Re at each concentration still the same as reported before (section 4.2.1).

Increasing the chemical additive concentration during the drag reduction process is limited. One of the important limitations of using drag reducer especially within commercial application is its effect on the apparent physical properties of the transported fluid. So, one of the advantages of using the powders investigated in the present work as drag reducing agents is to eliminate the possibility of changing the transported liquid through pipeline because all these powders are insoluble in the transported media and can be separated easily by simple physical operations.

The results of the present work concerning the effect of powder concentration on %Dr agrees well with a large number of the experimental results published by many workers. The result agrees with (Hayder et.al. 2008, Moghaddam and Staffan 2006, Ram et al. 1967, Tullis et al 1974). The results reported by (Kazi et al. 1999, Luetgen et al. 1991, Backtiyarov et al 1983 and Roberto 2002) somehow disagree with those established in the present investigation.

4.2.3 Effect of pipe diameter

Selected experimental data samples representing the effect of pipe diameter on the powders performance on the drag reduction operation are shown in figures 4.19 to 4.23. Due to the difference in the experimental flow rates achieved from the rig. This cause the change in the liquid capacity for different pipe diameters (which will result in changing the Re range that can be achieved during the experimental work), the comparison was held in the Re range shared by the three pipe diameters investigated (0.0125, 0.0254 and 0.0381 m ID). These Re ranges are shaded in the graphical representations in the figures.

Figures 4.19 and 4.20 show the effect of pipe diameter on the %Dr for 500 ppm concentration of sand particles suspended in water flowing with particle size of 45 and 71 μm respectively, and pipe length of 1 m. In both cases the %Dr increases by decreasing the pipe size but the performance of the drag reduction operation and the

effect of the pipe diameter is much clear with the second figure (4.20) compared with figure (4.19).

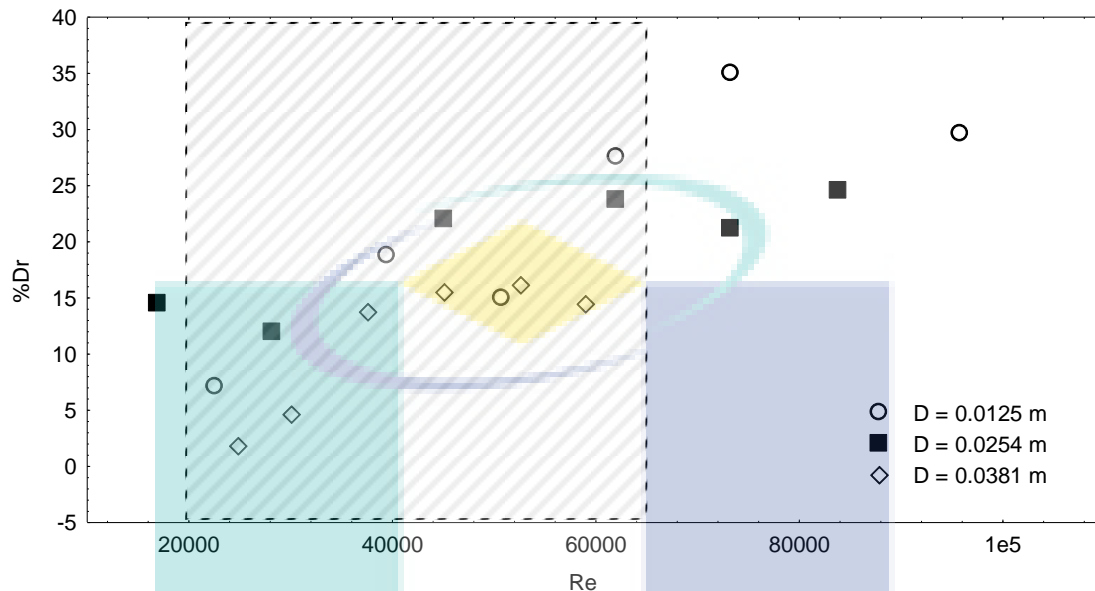


Figure 4.19: Effect of pipe diameter on the %Dr for 500 ppm concentration of Sand particles suspended in water flowing with particle size of 45 μm and pipe length of 1 m.

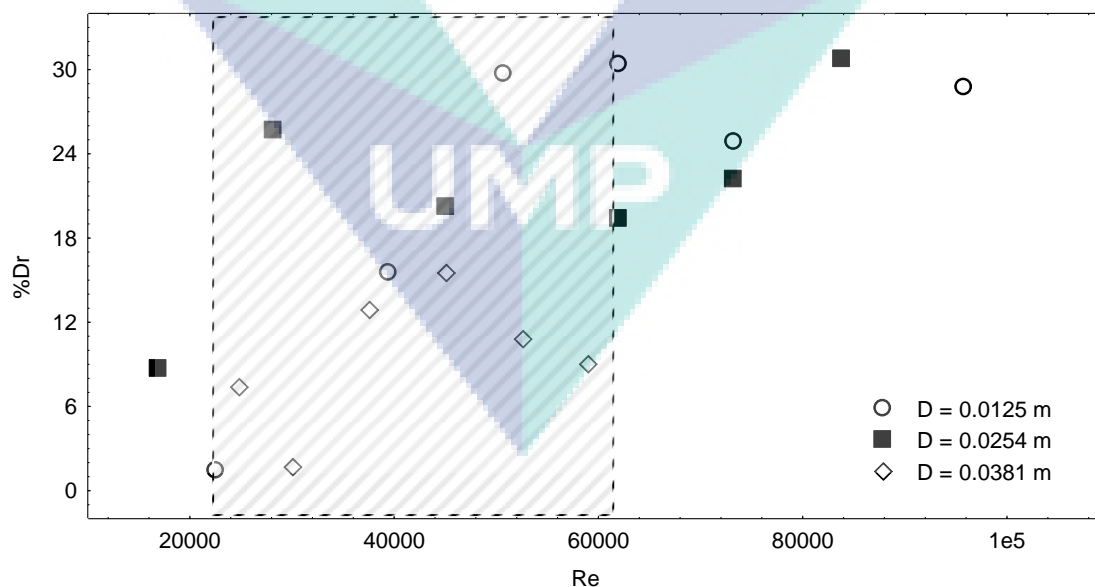


Figure 4.20: Effect of pipe diameter on the %Dr for 500 ppm concentration of Sand particles suspended in water flowing with particle size of 71 μm and pipe length of 1 m.

From figure 4.19, it can be noticed that the %Dr for the 0.0125 m I.D. pipe is higher than the other two diameter. This cannot be the conclusion from the figure because the differences in the %Dr value varies with the value of Re. That, in the Re range from 22000 to 48000 and especially when Re range around 40000, the value of the %Dr for all the pipe sizes are close to each other where the value of the %Dr 18 to 20 % . Further increase in the value of Re makes the difference in the value of the %Dr much clearly distinguish as it can be seen in the figure where the highest %Dr reached was 27.6% at $Re = 73233$ and 500 ppm for the 0.0125 m I.D. pipe.

Figure 4.20, shows the effect of pipe diameter on the %Dr for 500 ppm concentration of sand particles suspended in water flowing with particle size of $71 \mu\text{m}$ and pipe length of 1 m. The purpose behind choosing the experimental data for the following figure is to compare these results with the ones shown in figure 4.19 in order to show the effect of changing the particle size on the pipe diameter influence on the %Dr. Generally, the same performance can be seen which is close to that shown in figure 4.19 with maximum %Dr of 30.4% at $Re = 61967$ and the pipe diameter effect is clearer where the %Dr increases by decreasing the pipe diameter .

These two figures show the interaction between the effect of the pipe diameter and the particle size on the sand powder performance as drag reducing agent. It is very clear that the behavior is more clear and distinguished in figure 4.20 for the $71 \mu\text{m}$ particle size with less intersection in the point compared with figure 4.19. This fact influence the decision for the optimum operating conditions depending on the value of the %Dr and the pure performance in each pipe. By increasing the pipe diameter, the number of the eddies formed will be less, although the eddy will be larges, but due to the low liquid velocity compared with the smaller pipe diameters, the degree of turbulence will be lower and the number of eddies will be less. Increasing or decreasing the degree of turbulence controls the drag reduction effectiveness of the additive. Increasing the number of eddies will provide a better environment for the drag reducing agent to interfere within a more turbulent structure inside the main flow and that will enable suppressing larger numbers of small eddies that are formed in smaller pipe diameter pipes.

Figures 4.21 and 4.22, shows the effect of the pipe diameter on the %Dr for the aluminum powder flowing with different additive concentrations and pipe lengths. Generally, the two figures shows that the %Dr increases by decreasing the pipe diameter where 17% maximum drag reduction achieved for the 0.0125 m I.D. pipe compared with almost 5.0 and 6.0 % for the other two pipe diameters. As in the sand powder behavior, the %Dr values varied and intersected in the Re range 25000 to 50000 as shown in figure 4.21. For example, the values of the %Dr were 6.5 % to 5.2 % with 15% difference in the value for the 0.0125 to 0.0381 m I.D. pipe size range at the Re range around 30000 to 40000, but that difference increased up to 62% for higher Re ranges up to 60000. These results also highlights the interactive effect of the operation parameters for the drag reduction with each other and how distinctive the optimization or the optimum operation condition decision in the drag reduction science.

Figure 4.22 shows effect of pipe diameter on the %Dr for 100 ppm concentration of aluminum particles suspended in water flowing with particle size of 71 μm and pipe length of 0.5 m. In this figure, the effect of pipe diameter is totally changed. The highest values for the %Dr were in the 0.0254 m I.D. pipe while the 0.0381 m I.D. pipe still shows the poorest performance compared with the other two diameters. This figure added another factor controlling the pipe diameter effect on the %Dr which is the particle type (Aluminum). To be more precise, the figure highlights the effect of suspended solid physical properties on the drag reduction performance and its interaction with the other operating conditions controlling the system in the same time. By comparing the these results with the ones shown in figures 4.19 and 4.20 for the sand powder, it can be concluded that by increasing the suspended solid density, the relation between the %Dr and the pipe diameter will change. Actually, the balanced interaction between the operating conditions established within the sand powder will not be the same by changing the powder to aluminum and that will change the conclusion regarding the real pipe diameter effect.

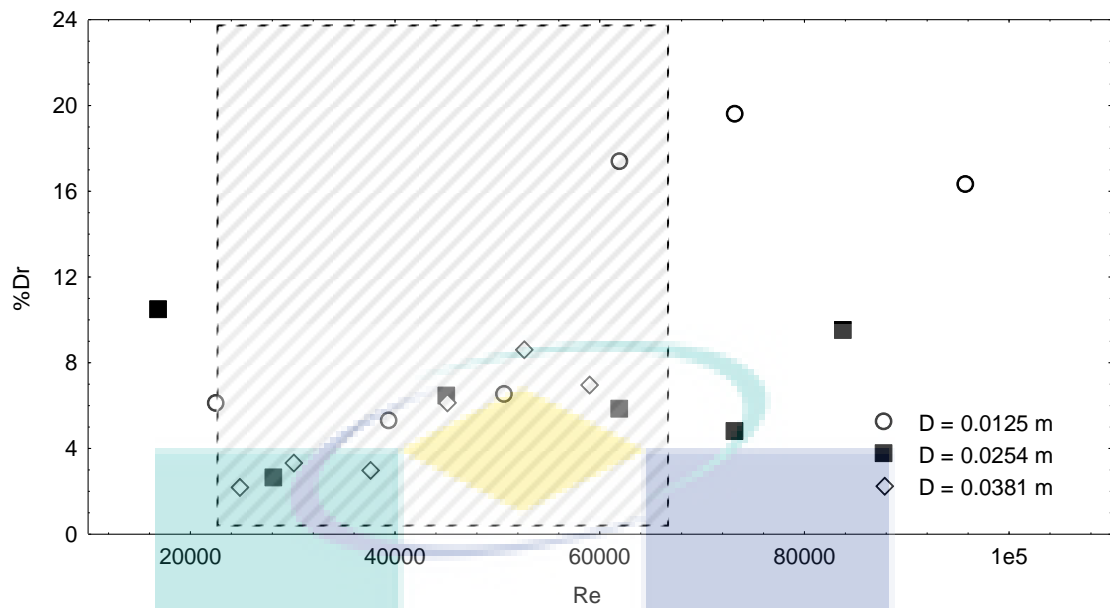


Figure 4.21: Effect of pipe diameter on the %Dr for 100 ppm concentration of Aluminum particles suspended in water flowing with particle size of 71 μm and pipe length of 1 m.

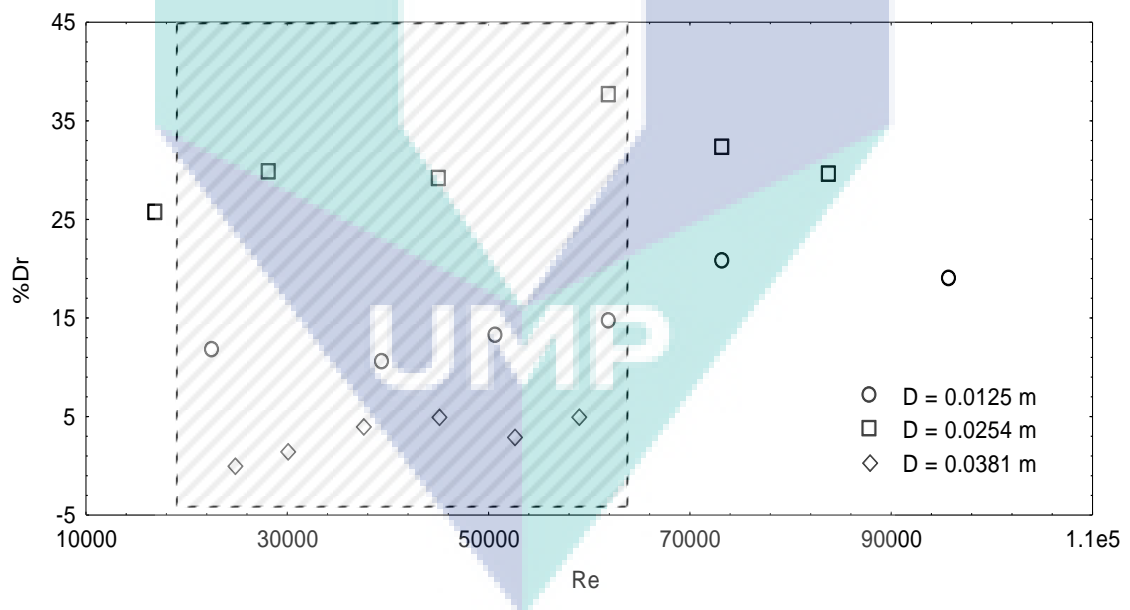


Figure 4.22: Effect of pipe diameter on the %Dr for 100 ppm concentration of Aluminum particles suspended in water flowing with particle size of 71 μm and pipe length of 0.5 m

Figure 4.23, shows a completely different behavior when testing the effect of pipe diameter on the %Dr for 500 ppm concentration of coal particles suspended in water flowing with particle size of 45 μm and pipe length of 2.0 m. The effect of pipe diameter was different where the %Dr values for the larger pipe size 0.0381 m I.D. showed the higher values compared with the other two sizes 0.0125 and 0.0254 m I.D. and that highlights again the importance of the interaction between the drag reduction operation parameters on the performance of the drag reducer. In this case, the effect of the pipe length is important because this behavior occurred with the maximum pipeline length investigated in the present work. This can lead us to the conclusion, that another parameter is taking the role, which is the turbulent structures shapes and sizes (eddy size and shape), that changes by changing the testing section length and which will be discussed in the pipe length effect section. Also it is worth to notice that the other two curves for the 0.0125 and 0.0254 m I.D. continue to show the same conclusions mentioned before where the %Dr increases by decreasing the pipe size.

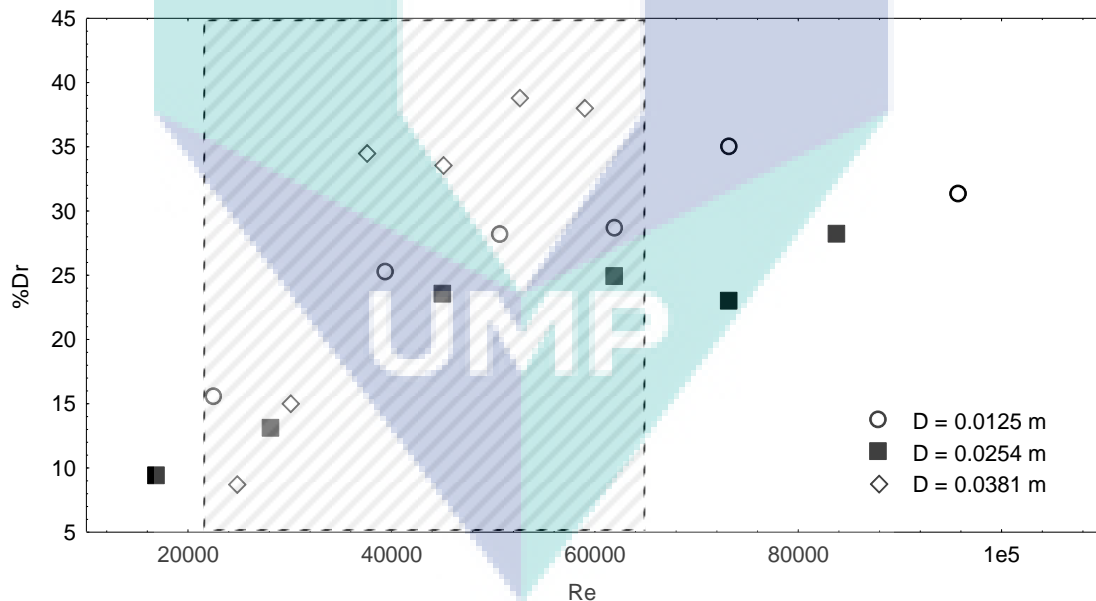


Figure 4.23: Effect of pipe diameter on the %Dr for 500 ppm concentration of Coal particles suspended in water flowing with particle size of 45 μm and pipe length of 2.0 m.

As a general conclusion, the 0.0125 m I.D. showed the most stable performance compared with the other two diameter, although it didn't consistently showed the highest performance, but in most of the experimental data collected (see appendix A1 to

C20), the 0.0125 m I.D. pipe was more consistent (stable in shape and performance). This is why a conclusion can be made that within certain additive type and concentration, %Dr Increases by decreasing the pipe diameter, which means that the additive will have a better media to work in within smaller pipes. Decreasing the pipe diameter, means increasing the velocity inside the pipe, this will increase the turbulence. Although, the flow inside the three pipes was turbulent but the degree of turbulence was different. For smaller pipe, the energy absorbed by the turbulence (eddies) from the main flow will be higher than that for larger pipes. That, whenever the degree of turbulence becomes higher, the number of collisions between eddies will be higher, which will produce smaller eddies. These collisions provide extra number of eddies absorbing energy from the main flow to complete their shape. The same behavior may also occur in large pipes but not in the same degree as in smaller pipes, which will lead to a lower amount of energy absorbed by the main flow.

It is clear from the figures that the powders work well whenever there is large number of small eddies (smaller pipes). Overcoming smaller eddies is easier by powders than larger once, because of the amount of energy absorbed by smaller eddies is lower. Large number of the experimental results in the present work supported this indication.

The results of the pipe diameter effect in the present investigation agree with those reported by; Toms (1948), Virk et. al. (1976) and Robert (2002).

4.2.4 Effect of pipe testing section length

Four testing sections lengths were investigated in the present work, which are (0.5, 1.0, 1.5 and 2.0 m) to show the effect of the testing section length on the performance of the drag reducing agents investigated. Figures 4.24 to 4.29, shows selected samples of the experimental data. The rest of the data can be seen in appendixes from A1 to C20.

Figures 4.24 shows the effect of testing section length on the %Dr for 300 ppm concentration of sand particles suspended in water flowing with particle size of 45 μm and pipe diameter of 0.0125 m I.D. This figure shows clearly that there is no noticeable effect for the testing section length on the %Dr, where all the experimental data point

interact and exchange positions in most of the Re range. This behavior changes only when reaching the maximum value of the Re where the difference in the %Dr values becomes more clear and distinguishable where, at $Re = 95749$ the value of the maximum %Dr reached was 29.6% with 300 ppm additive concentration and 1.0 m testing length. The second maximum %Dr appears with 1.5 m testing section length while these values are very close and mixed in the values of Re below 95749.

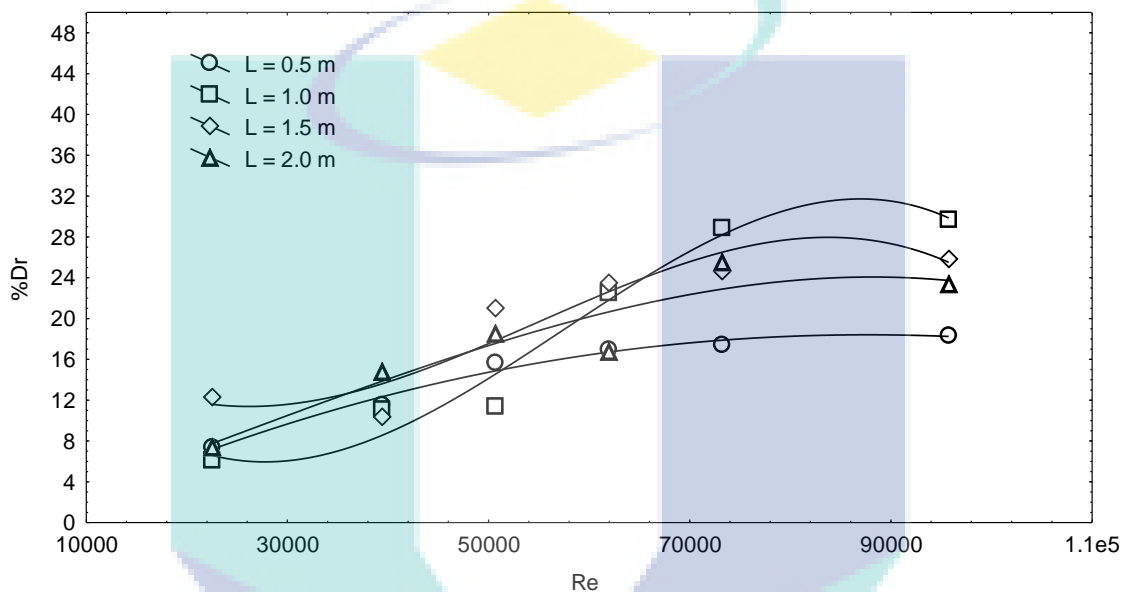


Figure 4.24: Effect of testing section length on the %Dr for 300 ppm concentration of Sand particles suspended in water flowing with particle size of $45 \mu\text{m}$ and pipe diameter of 0.0125 m I.D.

For the same powder mentioned above, but by changing the additive concentration, almost same behavior can be seen for the pipe diameter and particle size, as shown in figure 4.25. This figure represents the effect of testing section length on the %Dr for 500 ppm concentration of sand particles suspended in water flowing with particle size of $45 \mu\text{m}$ and pipe diameter of 0.0125 m I.D. More randomness in the relation between the %Dr and the Re with different testing section lengths tested can be observed. On the opposite of figure 4.24, it is very difficult even to distinguish the testing section length effect.

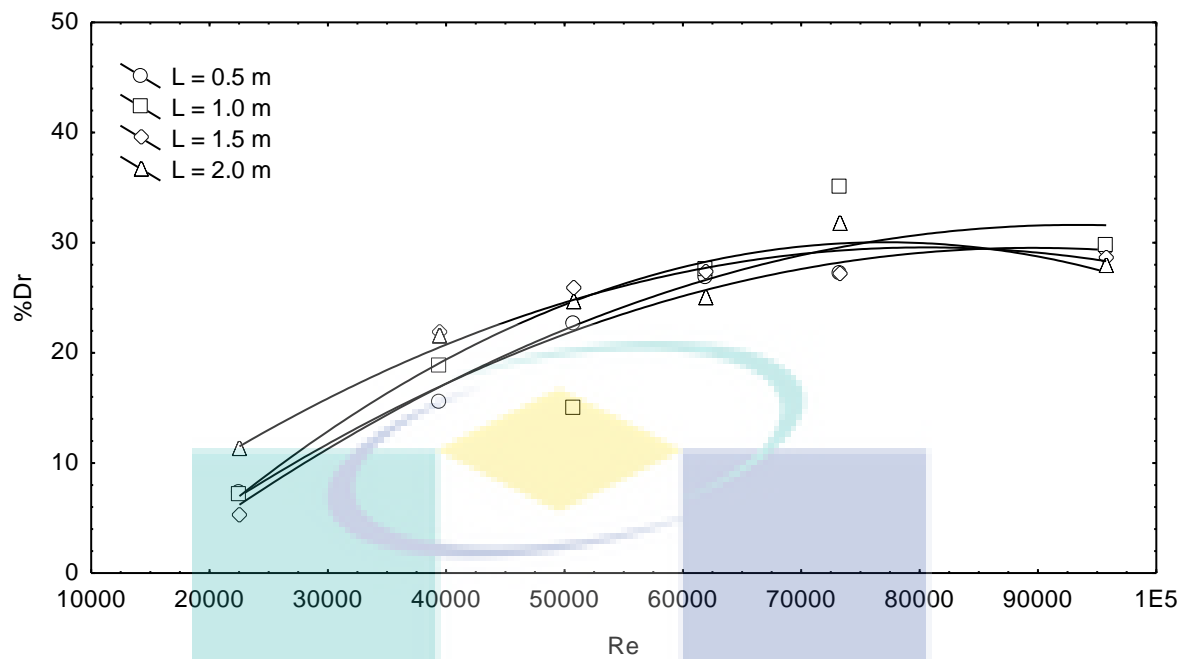


Figure 4.25: Effect of testing section length on the %Dr for 500 ppm concentration of Sand particles suspended in water flowing with particle size of 45 μm and pipe diameter of 0.0125 m I.D.

The same random and non-uniform behavior observed when using Aluminum and Coal powders as drag reducing agents. The aluminum powder effect can be seen from figures 4.26 and 4.27, while the coal powder effect and behavior can be seen in figures 4.28 and 4.29. In both cases no clear effect of section length (from 0.5 to 2 m).

The only behavior that can be highlighted is the one of the aluminum powder in figure 4.26. In this case, the %Dr reach its maximum value (20.3%) at $\text{Re} = 58951$ where the figure shows that the highest %Dr is achieved within the maximum testing section length 2.0 m which disagrees with the only distinguishable behavior observed in figure 4.24.

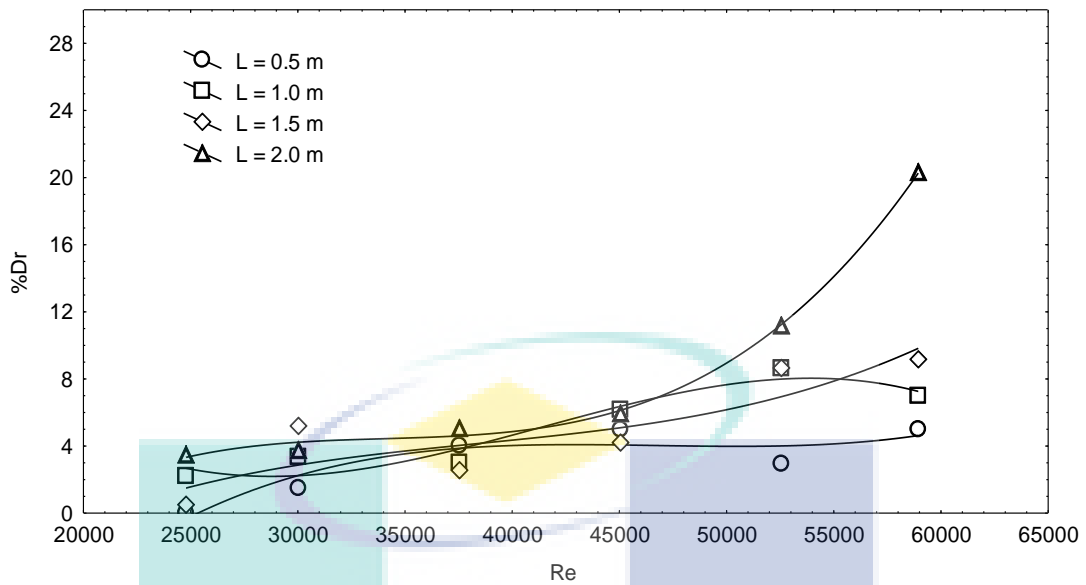


Figure 4.26: Effect of testing section length on the %Dr for 100 ppm concentration of Aluminum particles suspended in water flowing with particle size of 71 μm and pipe diameter of 0.0381 m I.D.

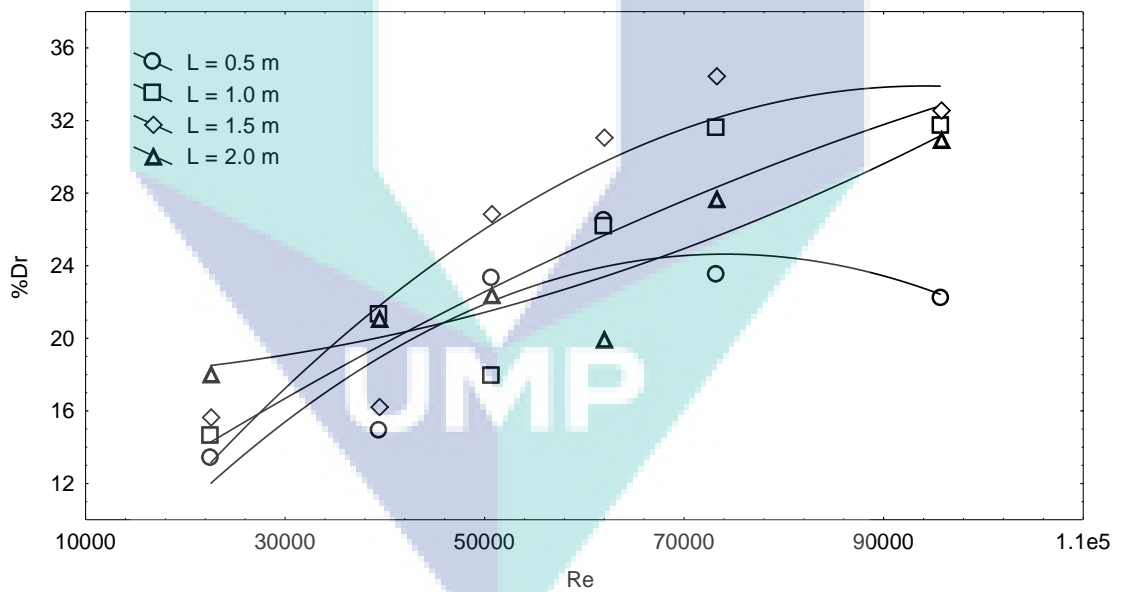


Figure 4.27: Effect of testing section length on the %Dr for 300 ppm concentration of Aluminum particles suspended in water flowing with particle size of 71 μm and pipe diameter of 0.0125 m I.D.

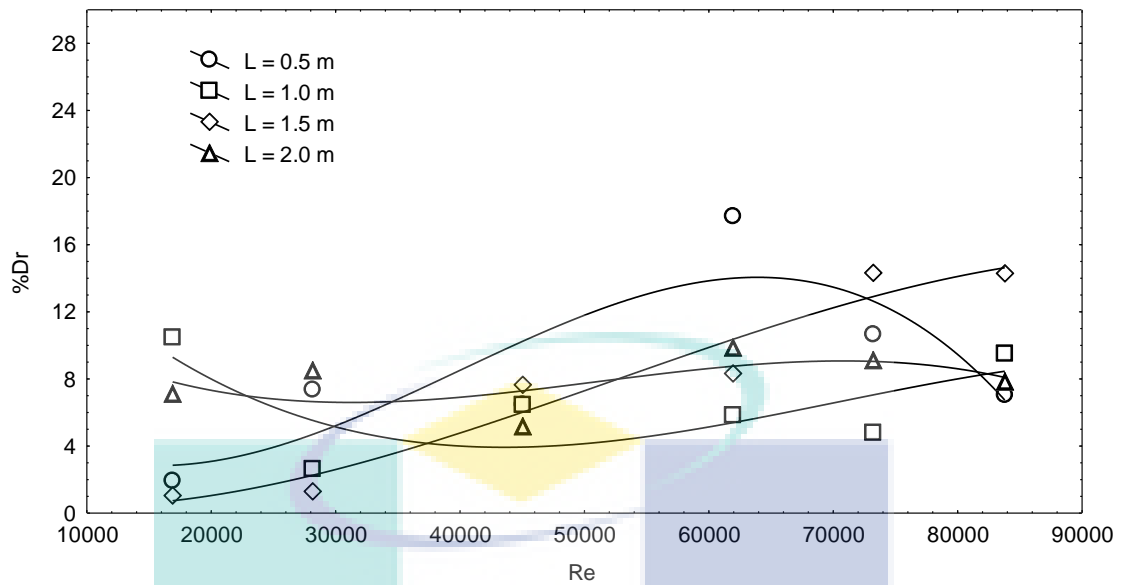


Figure 4.28: Effect of testing section length on the %Dr for 100 ppm concentration of Coal particles suspended in water flowing with particle size of 71 μm and pipe diameter of 0.0254 m I.D.

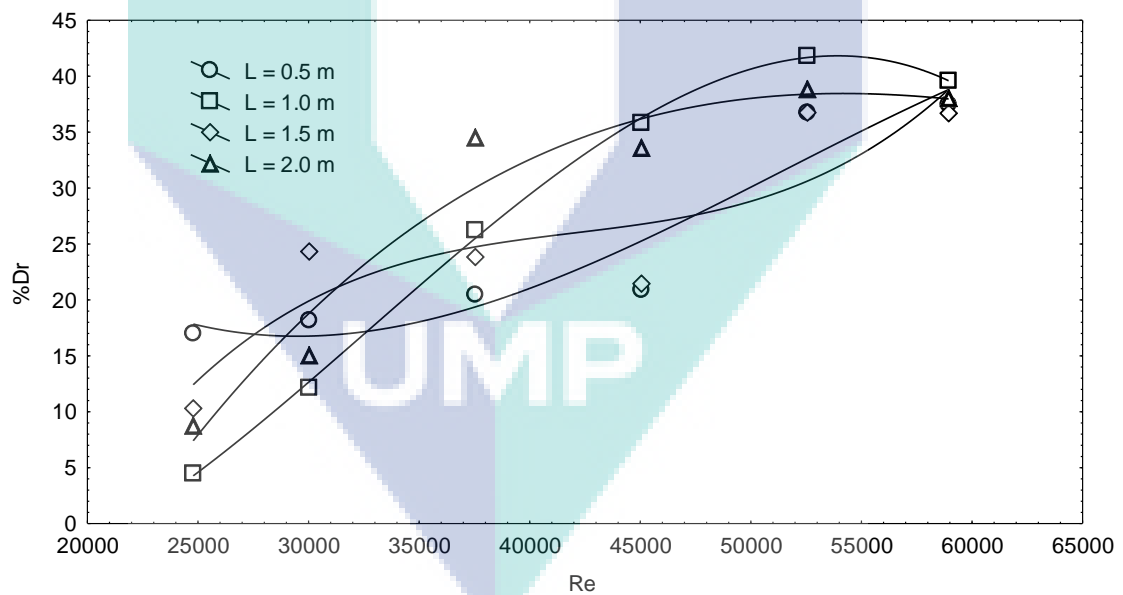


Figure 4.29: Effect of testing section length on the %Dr for 500 ppm concentration of Coal particles suspended in water flowing with particle size of 71 μm and pipe diameter of 0.0381 m I.D.

The non-uniform and undistinguishable effect of the testing section length on the powder performance as drag reducing agent plus the close values of the %Dr observed for all the powders investigated, shows and confirms the drag reduction performance stability of the powders investigated to length. One of the major problems facing the

drag reduction science when using the commercial polymers and surfactants (especially polymers) is the mechanical degradation of the polymer when exposed to high shear stress either in the pumping station or during its transportation through with high turbulent mode. This problem added huge limitation for the usage of the polymers in strategic pipelines and led to the re-injection of the polymer after certain distance to regain its drag reducing ability. It is believed, that the powders investigated in the present work can overcome the degradation problems facing other materials used commercially as drag reducing agent because of its solid nature and insolubility in the transported media which give a stable performance with the testing section length and that was proven in the present section.

4.2.5 Effect of particle size on the %Dr

One of the most important factors influencing the drag reduction operation in the present investigation with the introduction of the suspended powders as drag reducing agents is the particle size or diameter.

Figures 4.30, shows the effect of particle size on the %Dr for 300 ppm concentration of sand particles suspended in water flowing with pipe diameter of 0.0381 m I.D and pipe length of 1 m. This figure shows that the values of %Dr for the 45 μm are higher than those of the 71 μm for the Re range below 50,000.00. While the behavior changes to the opposite when the Re is higher than 50,000.00 where the particles with the size of 71 μm dominate and shows higher values of the %Dr.

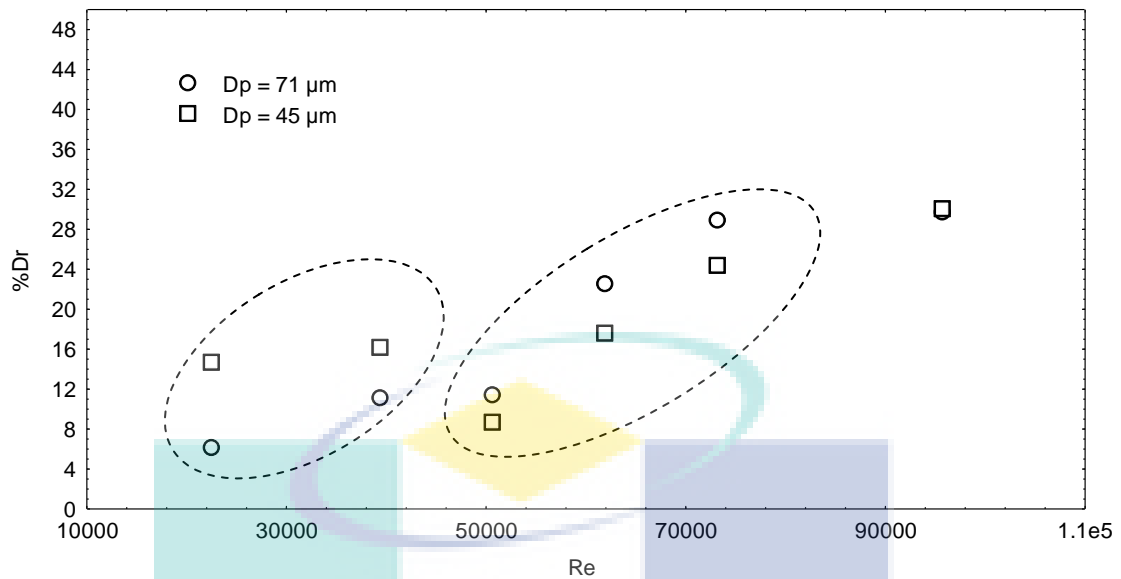


Figure 4.30: Effect of particle size on the %Dr for 300 ppm concentration of Sand particles suspended in water flowing with and pipe diameter of 0.0381 m I.D and pipe length of 1 m.

Figure 4.31, shows exactly the opposite performance for the same powder but with different addition concentration. This figure shows the effect of particle size on the %Dr for 500 ppm concentration of sand particles suspended in water flowing with and pipe diameter of 0.0381 m I.D and pipe length of 1.0 m. It is clear that the sand powder with the particle size 71 μm showed higher values of %Dr at the first range of Re ($Re < 50,000.00$) while the effect was reflected and the sand powders with the particle diameter of 45 μm dominated at $Re > 50,000.00$. To explain that, it is important to notice the relation between the degree of turbulence and the suspended solid properties like particle size. It is known that, for each drag reduction system, there is what is called “onset point”, where the interaction between all the properties performing became optimum. It is believed that, for the first range of Re ($Re < 50,000.00$), the degree of turbulence already reached the drag reduction onset point with the smaller particle size while for larger particle it needs more power “degrees of turbulence” to carry up the larger particles in a way to reach the optimum drag reduction onset point.

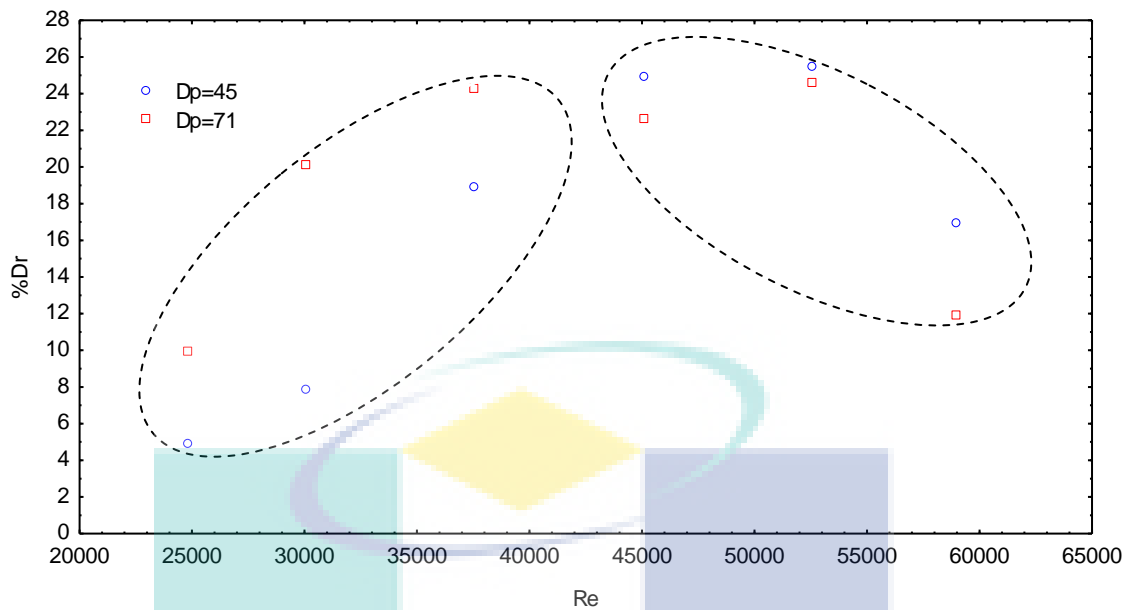


Figure 4.31: Effect of particle size on the %Dr for 500 ppm concentration of Sand particles suspended in water flowing with and pipe diameter of 0.0381 m I.D and pipe length of 1.0 m.

To complete the picture and to cover all the possible experimental work data with all the experimental variables like the pipe diameter and the testing section length for the sand powder, an additional figure (figure 4.32) is presented. This figure shows, the effect of particle size on the %Dr for 500 ppm concentration of sand particles suspended in water flowing with and pipe diameter of 0.0381 m I.D and pipe length of 2.0 m. From that figure, it can be seen that dominating particle size effect on the values of the %Dr is the 45 μm in most of the experimental data for the experimental conditions specified. This behavior highlight certain agreement with some of the experimental data presented in the previous two figures but it cannot give a conclusion regarding the final effect of the particle size in the sand powder.

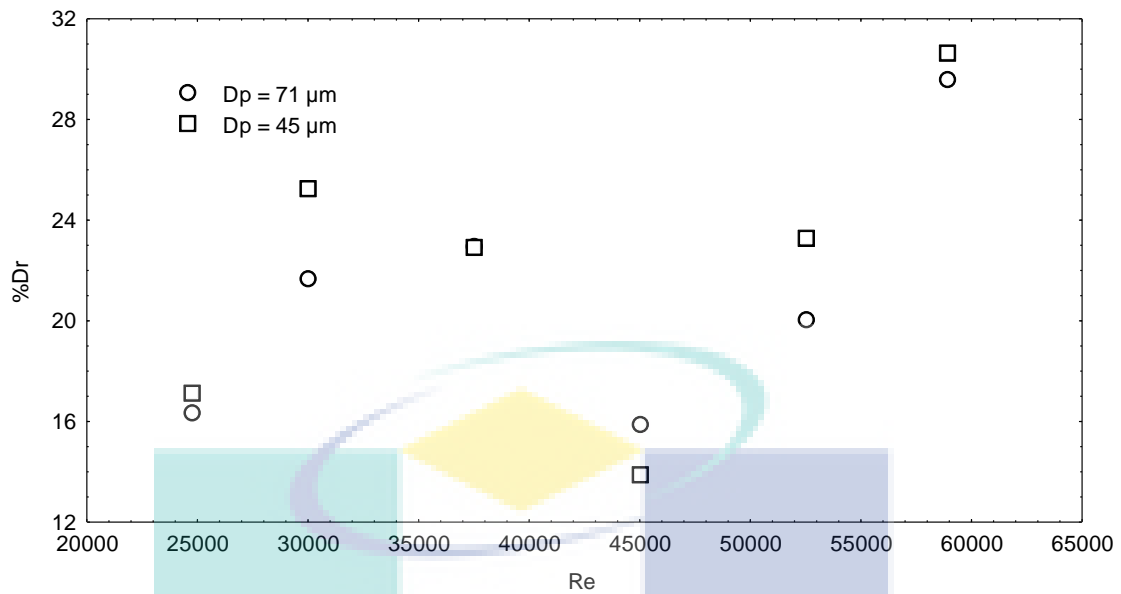


Figure 4.32: Effect of particle size on the %Dr for 500 ppm concentration of Sand particles suspended in water flowing with pipe diameter of 0.0381 m I.D and pipe length of 2.0 m.

The same argument can rise for the case of using the aluminum powder as drag reducing agent with different particle diameters. Figure 4.33, shows the effect of particle size on the %Dr for 300 ppm concentration of aluminum particles suspended in water flowing, with pipe diameter of 0.0125 m I.D and pipe length of 0.5 m. From this figure it can be noticed that the 71 μm system showed higher values when $Re < 70,000.00$ and the behavior change to the opposite when the range of $Re > 70,000.00$. Again, this behavior shows clearly the effect of the disturbed media drag reducing agent taking action in also the effect of the other experimental variables involved in each experiment and sometimes in each point.

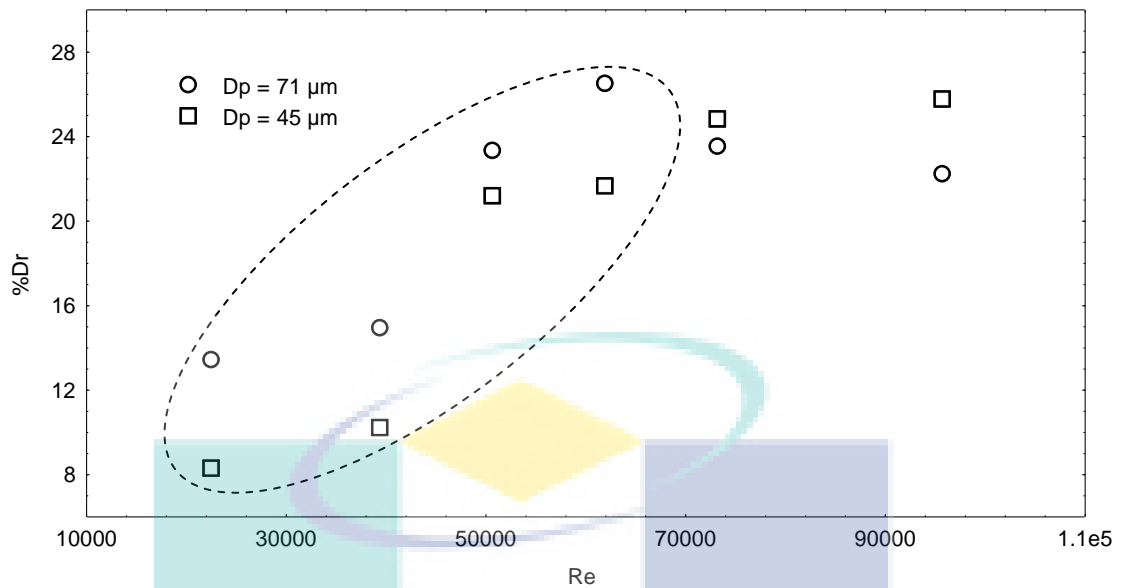


Figure 4.33: Effect of particle size on the %Dr for 300 ppm concentration of Aluminum particles suspended in water flowing with and pipe diameter of 0.0125 m I.D and pipe length of 0.5 m.

A more clear and distinguishable behavior can be seen in figure 4.34 for the aluminum powder also, where the 71 μm particle showed higher values of the %Dr in most of the Re range which suggest the possibility of having a uniform behavior by changing the particle size of the proposed powder drag reducing agent. The same clear behavior can be seen also in figure 4.35. This figure represents the effect of particle size on the %Dr for 300 ppm concentration of coal particles suspended in water flowing with pipe diameter of 0.0125 m I.D and pipe length of 0.5 m, but this time the domination is opposite to figure 4.34 where the higher values of the %Dr were shown by the 45 μm particle size.

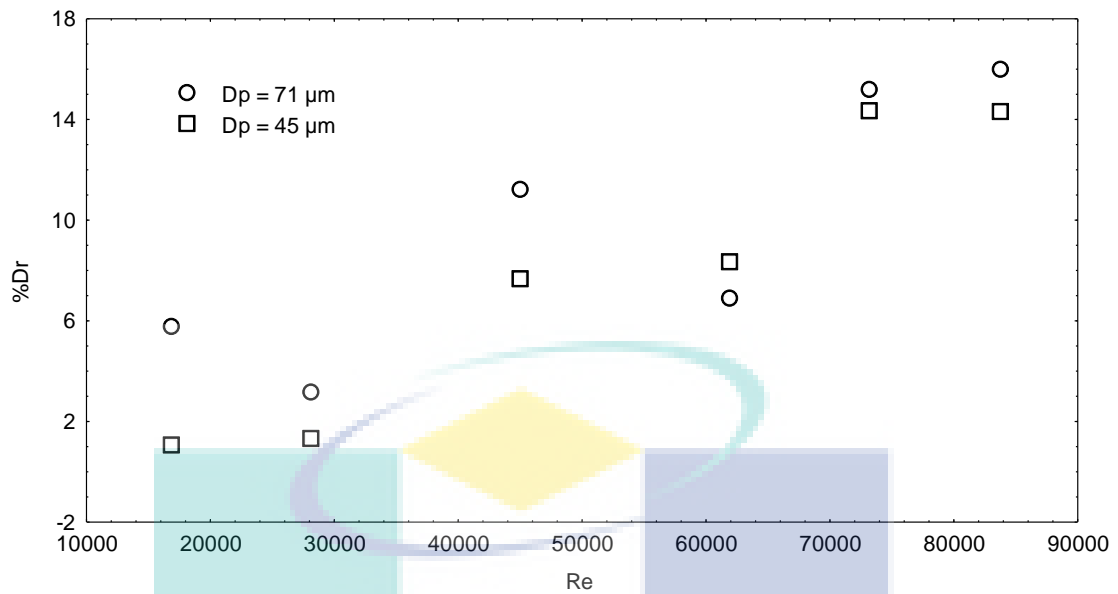


Figure 4.34: Effect of particle size on the %Dr for 100 ppm concentration of Aluminum particles suspended in water flowing with and pipe diameter of 0.0254 m I.D and pipe length of 1.5 m.

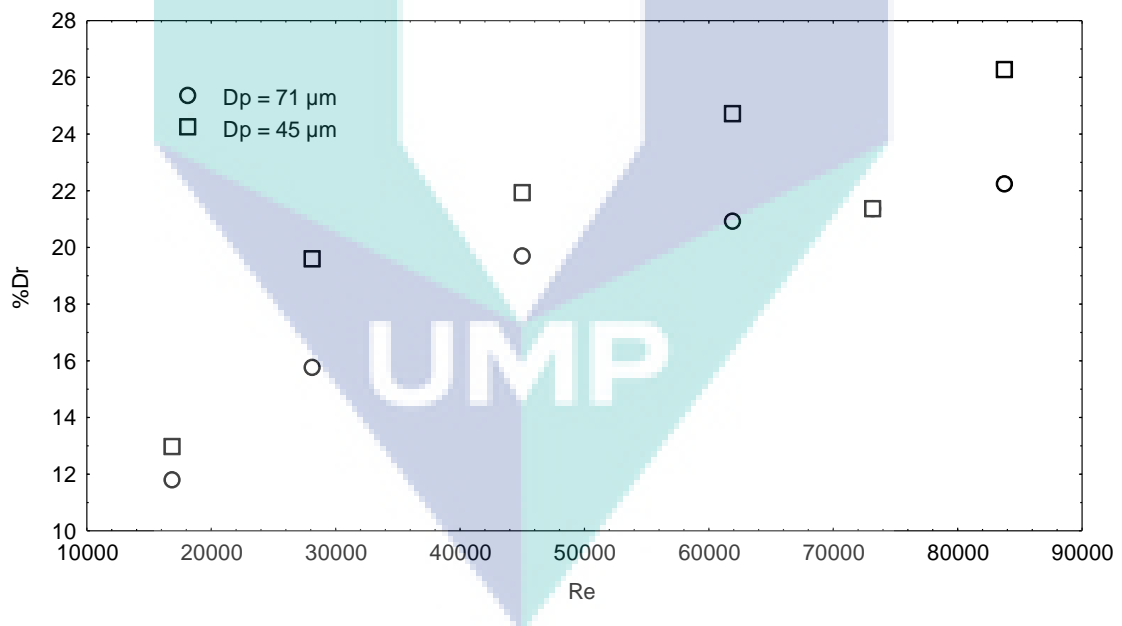


Figure 4.35: Effect of particle size on the %Dr for 300 ppm concentration of Coal particles suspended in water flowing with and pipe diameter of 0.0125 m I.D and pipe length of 0.5 m.

The general conclusion that can be drawn from the results shown above is the fact that the particle sizes of the proposed powders have a clear effect on the drag reduction process. The effect of the particle size was obvious but it is difficult to decide

that by increasing or decreasing the particle size the %Dr can increase. The effect of the particle size is so critical and depends on the experimental variables for each point and not for each curve. That also highlights the experimental variables interaction effect, especially the degree of turbulence represented by the Re. The degree of turbulence influence highly the interaction between the suspended solid and the turbulence structures inside the pipe which was clear in most of the figures when the same powder shows different behavior (dominating or nominating) with different Re values in the same experiment and sometimes reflect and exchange positions more than one time in the experiment.

This behavior also affects any drag reduction mechanism proposed if the effect on the degree of turbulence adopted, instead of the wall effect, “which mostly accepted in the case of suspended powders”. That, the interaction and the balance between the suspended solid presence and concentration with shape and number of the turbulent structures inside the pipe, will control the drag reduction performance of the drag reducing agent.

4.2.6 Effect of particle type on the %Dr

Three types of powders were select to be investigated in the present work, which are sand, aluminum and coal powders. The reason behind choosing these powders precisely is the difference in its physical properties especially the density ($\rho_{\text{sand}} = 1640$, $\rho_{\text{aluminum}} = 2700$ and $\rho_{\text{coal}} = 1170$) which will be highlighted in the present section.

Figures 4.36 shows the effect of particle type on the %Dr for 500 ppm concentration of sand, coal and aluminum particles suspended in water flowing with pipe diameter of 0.0254 m I.D and pipe length of 1.5 m. The results of this figure shows that the sand powder performance as drag reducing agent is higher compared with the coal and the aluminum powders when $Re < 70,000.00$ while this behavior changes by further increase in the value of Re and the aluminum particles perform with higher values of %Dr. The thing to be observed is that the difference between the sand %Dr values and those of the aluminum and coal is higher when $Re < 70,000.00$, while the difference between these point become lower for higher value of Re. The experimental

data showed that the difference in the %Dr was 31% at $Re = 16900$ and start to narrow down to 8.5% at $Re = 45058$ and the action was converted after this Re point. The purpose behind this behavior is what is called the "Drag reduction onset point" and its relation to the density of the suspended particles. It is believed that, when using the lower density particles (sand particles), the onset point will start earlier (lower Re) compared with the higher density particles (aluminum particles) because the degree of turbulence needed to have a maximum drag reduction performance will be lower for lower density particles. By increasing the Re the degree of turbulence will be enough for the aluminum particles to interfere within the turbulent structures inside the pipeline and this is why the aluminum powder %Dr was higher for higher Re .

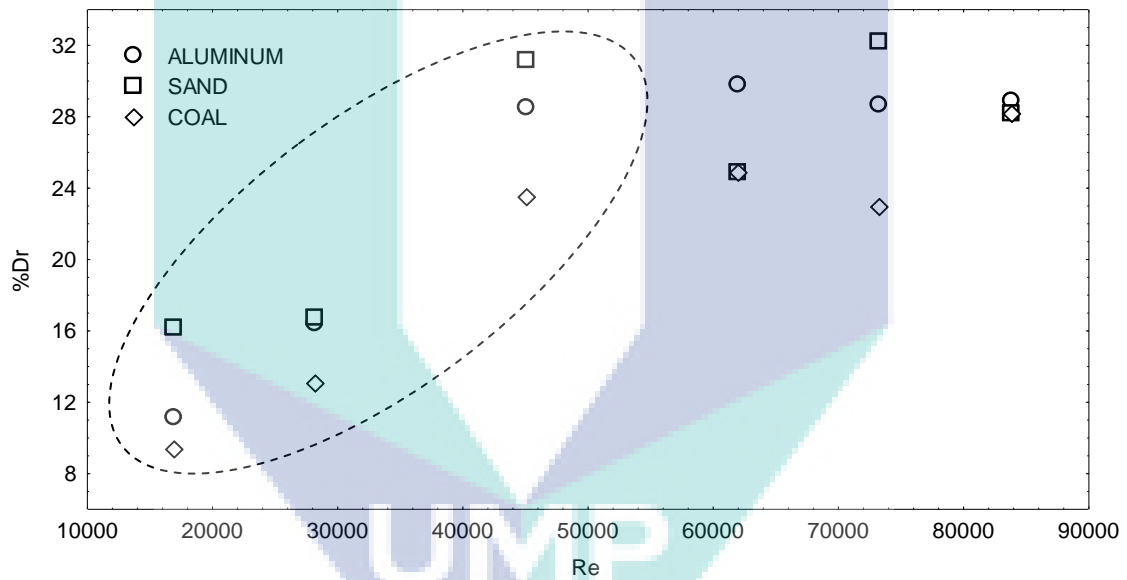


Figure 4.36: Effect of particle type on the %Dr for 500 ppm concentration of Sand, Coal and Aluminum particles suspended in water flowing with particle size of $71 \mu\text{m}$, pipe diameter of 0.0254 m I.D and pipe length of 2.0 m.

To investigate more on the effect of the particle type on the %Dr, figures 4.37 and 4.38 are presented to show the effect of particle type on the %Dr for different additive concentrations. At the same operating conditions of sand, coal and aluminum particles suspended in water flowing with the same pipe diameter (0.0125 m I.D) and pipe length (1.0 m). From these figures, it can be seen clearly that within the same operating conditions and with different concentrations of the powders, the aluminum powder gave the highest performance in the drag reduction in most of the points

presented. While coal showed also good drag reduction ability and higher values of the %Dr compared with sand.

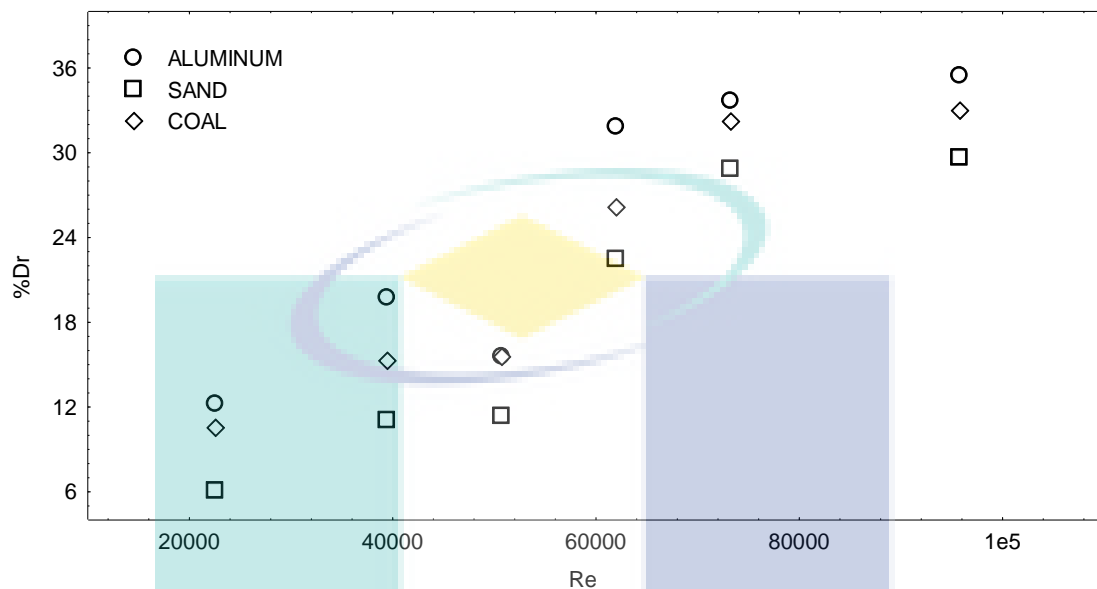


Figure 4.37: Effect of particle type on the %Dr for 300 ppm concentration of Sand, Coal and Aluminum particles suspended in water flowing with particle size of 71 μm with pipe diameter of 0.0125 m I.D and pipe length of 1.0 m.

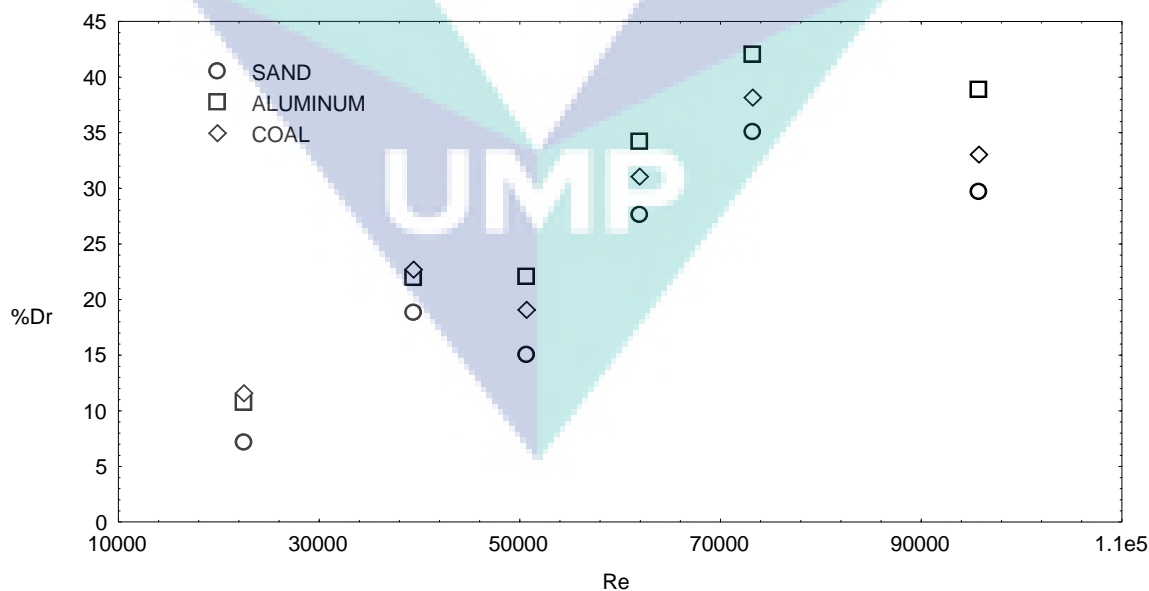


Figure 4.38: Effect of particle type on the %Dr for 500 ppm concentration of Sand, Coal and Aluminum particles suspended in water flowing with particle size of 45 μm with pipe diameter of 0.0125 m I.D and pipe length of 1.0 m.

The density of the powder controls in a way or another, the drag reduction ability and performance of the powders as drag reducing agent. Although that was not completely monitored from the experimental data where some of the results showed that other powders (sand or coal) dominated in some of the experiments but generally it can be concluded that the higher the density of the powder the better the drag reduction ability. This conclusion is limited, because the relation between the density, particle size and the ability of the powder to be suspended in the liquid is highly influencing the behavior.

From the drag reduction point of view, the drag reduction can occur when the suspended particles interact with the turbulence, and the turbulent structures inside the pipe reduces the elasticity of the eddy formed and preventing it from completing its shape. This is because the glob of liquid forming this eddy will have higher apparent density compared with the eddy in the additive-free liquid transportation. Therefore, as the density of the powder interacted with the turbulence is higher, as the density of the eddy formed is higher too and that will lead to breaking down the turbulent structures inside the pipe and increasing the flow. The experimental data did not conform the effect of density on the %Dr, where in certain cases by increasing the Re for very high values, e.g. more than 60000, the effect of the density is not there anymore and the relation changes to the opposite. This highlights also again, the relation between the parameters affecting the drag reduction performance, especially the degree of turbulence. Increasing Re means increasing the degree of turbulence in a way that overcomes the density effect “suspension – turbulence relation”, in another word, increasing Re means increasing the mobility of the transported liquid inside the pipe and that will terminate the balanced relation between the particles density and the chaotic behavior of the liquid structures inside the pipe.

4.3 EFFECT OF SURFACTANT ADDITIVE ON THE %Dr

In the present work, two different types of zwitterionic surfactant were chosen to act as drag reducing agent which are 3-(Decyldimethyle-ammonio) propanesulfonate inner salt (DAPI) and (3-(N-N,Dimethylpalmityl-ammino propanesulfonate)) (NNAP). The reason behind choosing these two surfactants is to examine the effect of the

Zwitterionic surfactants effect on the drag reduction performance of the powders chosen also to examine the effect of the chemical structure on the drag reduction performance in two-phase flow.

The following sections will show the effect of the addition of these two surfactants on the %Dr and the performance of the suspended solids. Graphical representation of the experimental data will be shown for selected samples of the experimental work and the rest of the experimental data can be seen in the experimental data tables in appendices A1- C20.

4.3.1 Effect of (DAPI) and (NNAP) additive on the %Dr-Re relation

Figures 4.39 to 4.41 show the effect of NNAP and DAPI on the flow behavior of additive-free water. Both surfactants drag reduction efficiencies were tested in the 0.0127 and 0.0254 m I.D pipes to ensure its ability to improve the flow in pipelines. Figure 4.39 shows the effect of adding 10, 20, and 30 ppm of DAPI to the water flowing in 0.0127 m I.D pipe and for 1 m testing section length. It can be noticed that the %Dr increases by increasing the Re reaching its maximum value within the Re range of 60,000 to 70,000 and after that it will start to show more stable values of start to decline. This is due to the relation between the effectiveness of the surfactant and the degree of turbulence. Increasing the Re will lead to the increase in the degree of turbulence inside the pipe and that will provide more suitable media to the surfactant molecules to act and interfere within the turbulent structures inside the pipe and suppressing the turbulent structures. Further increase in the Re will increase the degree of turbulence further more and that will bring the balance between the effectiveness of the additive and the degree of turbulence formed inside the pipe. This is why the %Dr value will start to decline and the additive will not be able anymore to perform within the same efficiency. The same behavior can be seen also in figures 4.40 and 4.41 for the NNAP surfactant flowing through 0.0127 m I.D pipe and 1 m testing section length and for the NNAP surfactant flowing through the 0.0254 m I.D pipe and with 1 m testing section length. Figures 4.39 to 4.41 show that the %Dr increases by increasing the addition concentration. Increasing the addition concentration means increasing the number of additive molecules involved in the drag reduction operation and increasing

the number of additive molecules interfering within the turbulent structures formed inside the pipeline and that will increase its drag reduction efficiency.

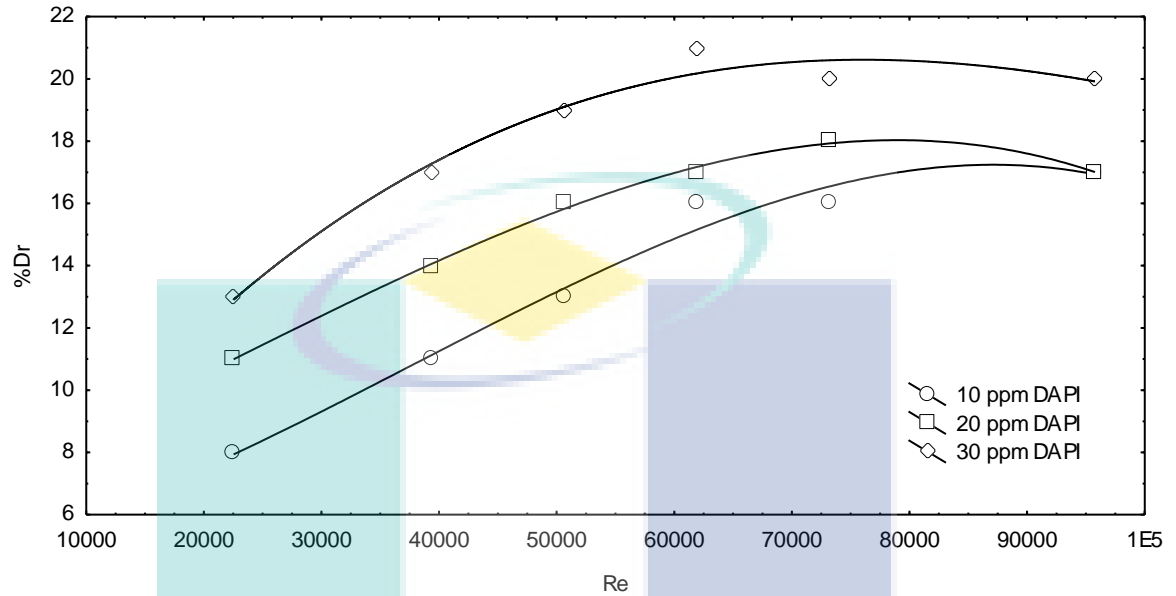


Figure 4.39: Effect of DAPI surfactant Additive on the %Dr for water flowing through 0.0127 m I.D pipe and for 1 m pipe length.

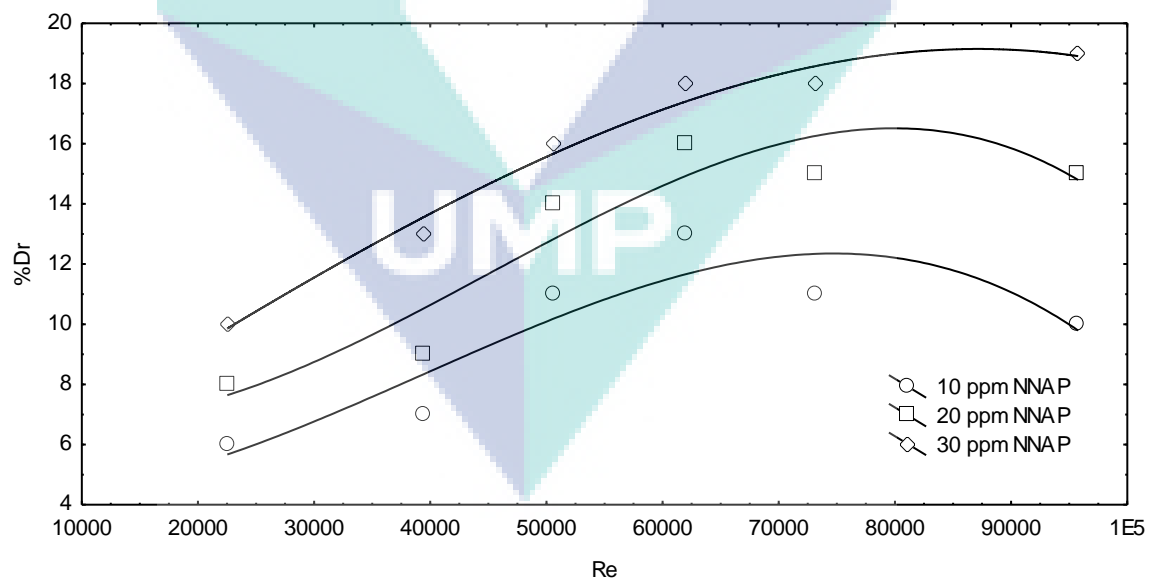


Figure 4.40: Effect of NNAP surfactant Additive on the %Dr for water flowing through 0.0127 m I.D pipe and for 1 m pipe length.

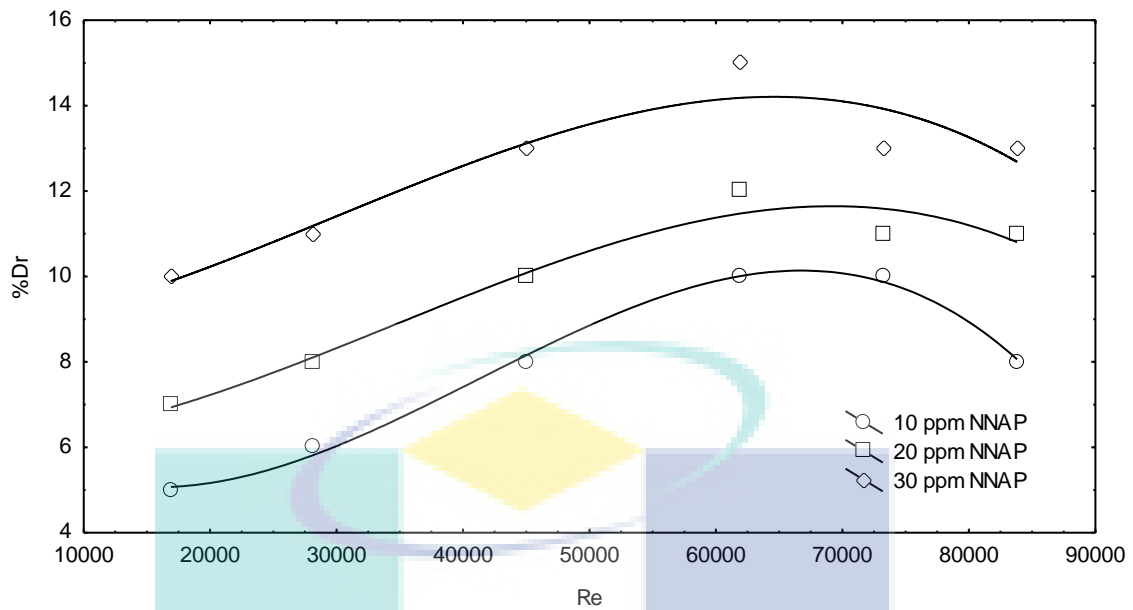


Figure 4.41: Effect of NNAP surfactant Addition on the %Dr for water flowing through 0.0254 m I.D pipe and for 1 m pipe length.

Figure 4.42, shows the effect 10 ppm of DAPI surfactant addition concentration on the Re-%Dr relation for aluminum particles ($D_p = 45 \mu\text{m}$) suspended in water and flowing in 0.0254 m I.D. and 1.5 m pipe length. This figure shows that the relation between the Re and %Dr, when adding the surfactant to the suspension flowing in a turbulent manner didn't change. The %Dr increases by increasing Re till reaching the maximum %Dr of 47.1, 51.08 and 52.4 for the 100,300 and 500 ppm additive concentrations and then by further increase in the Re, the value of the %Dr will be stable or start to decline. This indicates that the addition of the surfactant did not change %Dr-Re relation discussed in section 4.2.1.

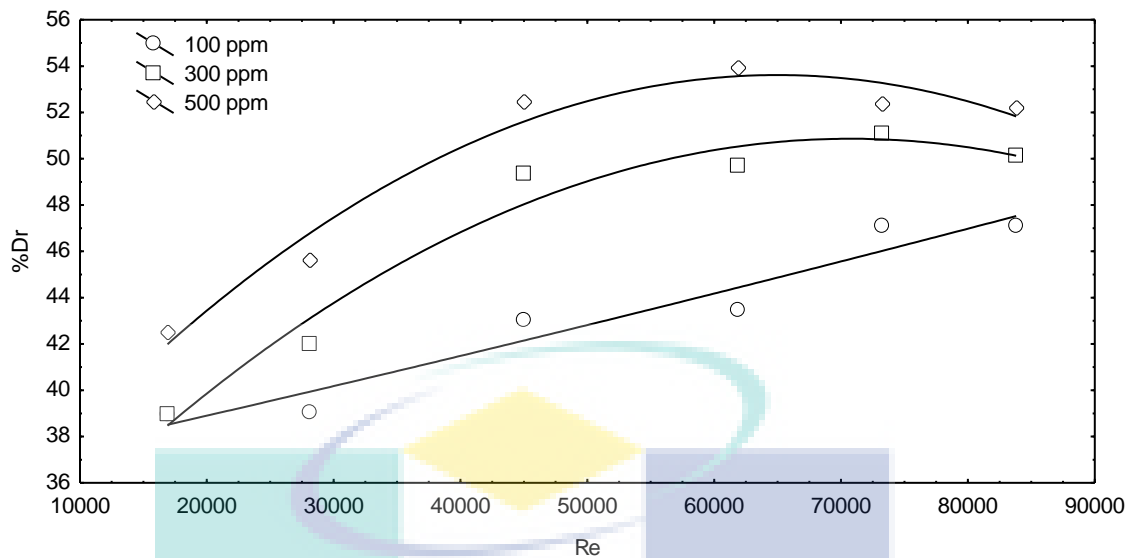


Figure 4.42: Effect of 10 ppm of DAPI surfactant additive on the Re-%Dr relation for Aluminum particles ($D_p = 45 \mu\text{m}$) suspended in water and flowing in 0.0254 m I.D. and 1.0 m pipe length.

The same behavior can be seen in figure 4.43 for the DAPI with aluminum powder but with different operating conditions that shows the effect of 10 ppm DAPI surfactant addition on the Re-%Dr relation for aluminum particles ($D_p = 45 \mu\text{m}$) suspended in water and flowing in 0.0381 m I.D. and 1.0 m pipe length. This figure shows more typical and uniform behavior of the %Dr with Re. Maximum %Dr values of 42.5, 44.45 and 53.07 for the 100, 300 and 500 ppm additive concentration. The value of the %Dr start to decline by further increase in the Re ($Re > 50000$) and that is due to the effect of the degree of turbulence on the drag reduction behavior.

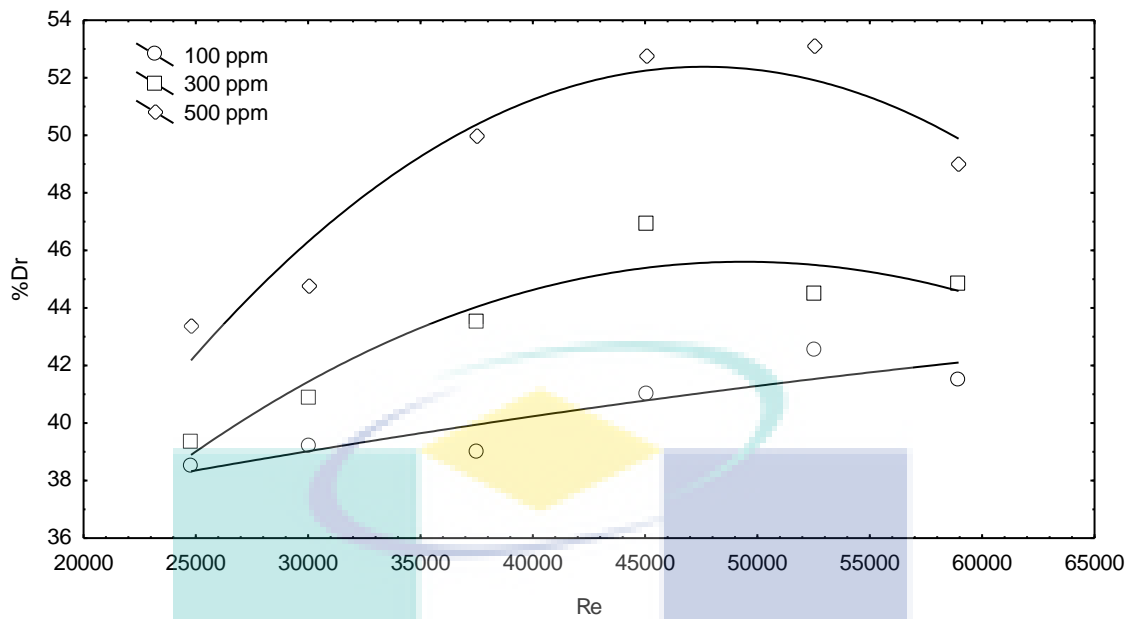


Figure 4.43: Effect of 10 ppm of DAPI surfactant additive on the Re-%Dr relation for Aluminum particles ($D_p = 45 \mu\text{m}$) suspended in water and flowing in 0.0381 m I.D and 1.0 m pipe length.

Figures 4.44 and 4.45, shows almost the same behavior when selecting different experimental data for comparison. Figure 4.44 and 4.45 shows the effect of 10 ppm of DAPI surfactant addition on the Re-%Dr relation for sand particles ($D_p=45 \mu\text{m}$) suspended in water and flowing in 0.0125 and 0.0254 m I.D respectively and 2.0 m pipe length. By the addition of DAPI surfactant, the %Dr-Re relation didn't change in behavior than that observed and discussed in section 4.2.1, but the values of %Dr became higher compared with the %Dr of the suspended solids without the addition of the surfactant. Maximum %Dr of 57.86 and 55.6 for the 500 ppm solid and 10 ppm surfactant for figures 4.44 and 4.45 respectively. The curves shape in figure 4.45 are not the same as demonstrated in 4.44 that, the general behavior still the same (%Dr increases by increasing Re) but there was no clear maximum value for the %Dr. That can be seen clearly in all the curves, where the value of the maximum %Dr was 40.39 at $Re = 61955$ and then declined to 38.38 at $Re = 73220$. Finally by increasing the value of Re to 83808 the %Dr reaches another maximum value of 43.01. That behavior means that the combined effect of the suspended solids and the surfactants is not stable and the addition of the soluble drag reducing agent (surfactant) to an existing insoluble drag reducing agent (suspended solids) will change curves shapes and that will be discussed

in details in section 4.3.2. The same behavior can be seen in the other two curves with a non-distinguishable maximum %Dr.

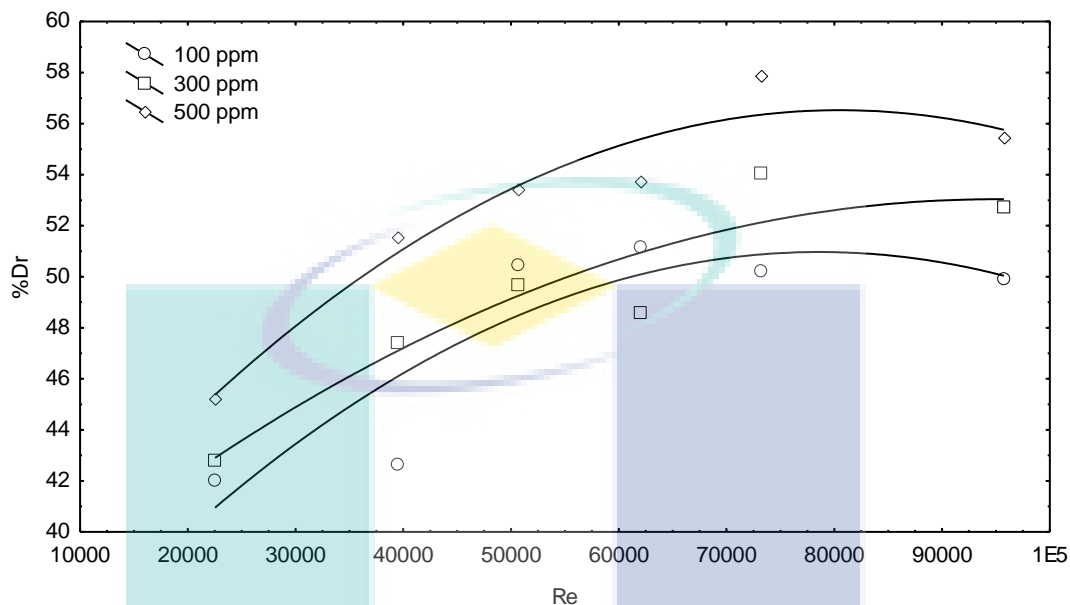


Figure 4.44: Effect of 10 ppm of DAPI surfactant additive on the Re-%Dr relation for Sand particles ($D_p = 45 \mu\text{m}$) suspended in water and flowing in 0.0125 m I.D. and 2.0 m pipe length.

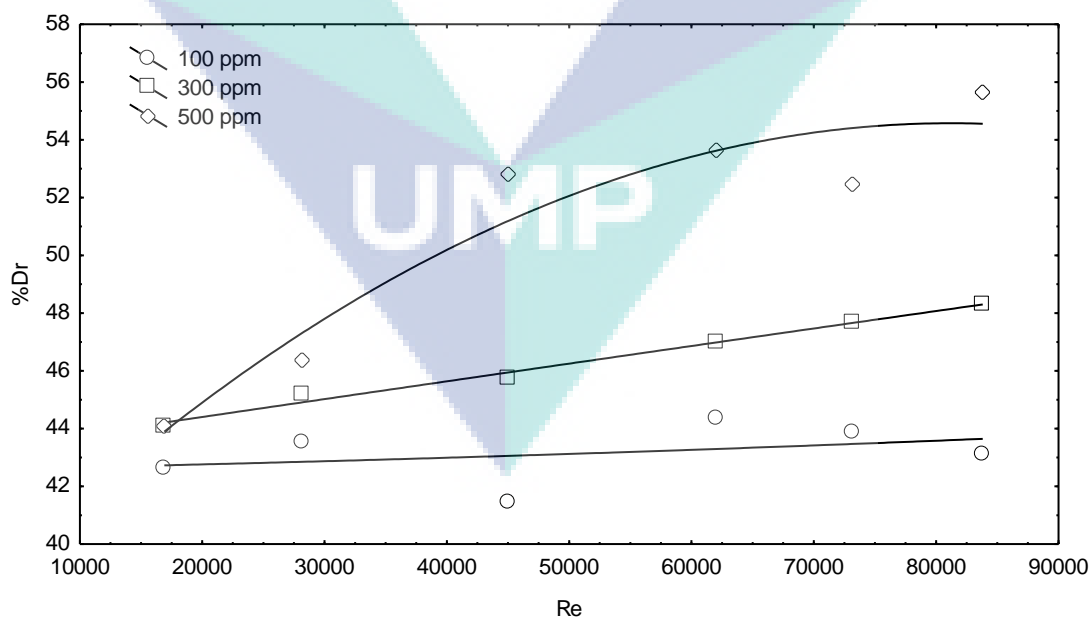


Figure 4.45: Effect of 10 ppm of DAPI surfactant additive on the Re-%Dr relation for Sand particles ($D_p = 45 \mu\text{m}$) suspended in water and flowing in 0.0254 m I.D. and 2.0 m pipe length.

Figure 4.46, shows the Effect of 20 ppm of NNAP surfactant addition on the Re-%Dr relation for coal particles ($D_p = 45 \mu\text{m}$) suspended in water and flowing in 0.0125 m I.D. and 0.5 m pipe length. The general shape of the curves differs from those observed in the previous sections. Although the %Dr increase with increasing Re and the addition concentration of the surfactant, but the shape and behavior is not distinguishable as in the previous results. In addition, the maximum value for the %Dr are not easy to classify in some cases and that is clearly shown within the 500 ppm curve where the values of the %Dr varies between 37% to 45% in all the Re range. Also, it can be seen that the differences in the %Dr values between the 100 and 300 ppm addition concentrations with the presence of 20 ppm NNAP became lower and much closer %Dr can be found. All that shows how effective the surfactant not in improving the flow in pipelines but in changing the flow behavior inside the pipe. In another word changing the way the suspended solid perform as drag reducing agent and that maybe due to the viscoelastic properties these surfactants can add to the whole flow system. More discussions on the surfactants effect can be found at the last paragraph of this section.

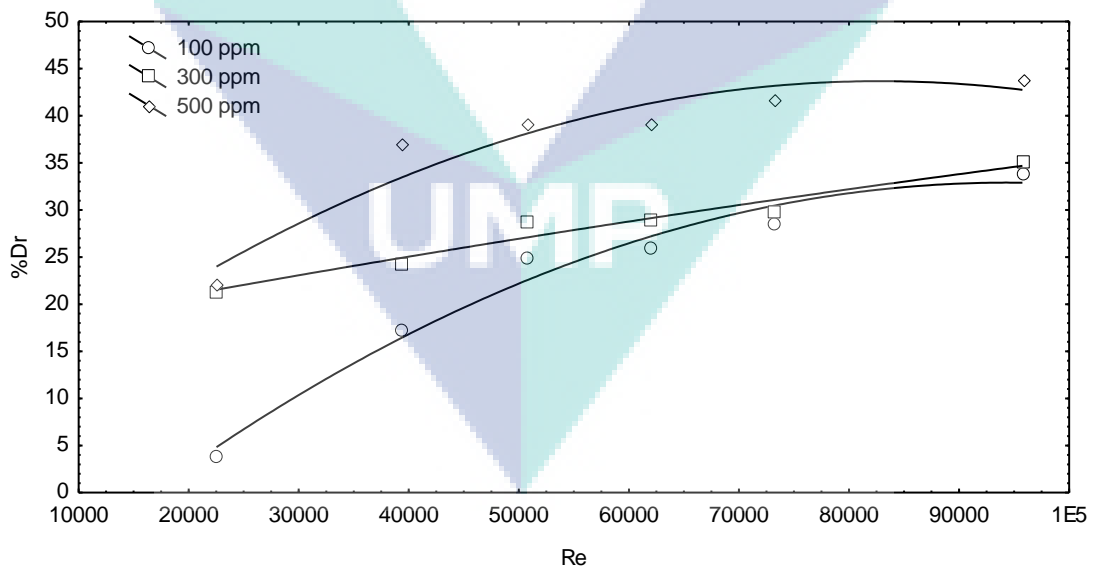


Figure 4.46: Effect of 20 ppm of NNAP surfactant additive on the Re-%Dr relation for Coal particles ($D_p = 45 \mu\text{m}$) suspended in water and flowing in 0.0125 m I.D. and 0.5 m pipe length.

To complete the comparison, figure 4.47 shows the experimental results for the same operating conditions mentioned in figure 4.46 but with different particle size (71 μm). It is very interesting to notice that by changing the particle size from 45 μm (figure 4.46) to 71 μm (figure 4.47), the relation between the %Dr and Re became smoother. In addition, the maximum %Dr for each curve became easier to find where maximum %Dr of 35.4, 42.3 and 47.19 were observed at $\text{Re} = 95749$, 61955 and 73220 for the 100, 300 and 500 ppm addition concentrations respectively. Again, the effect of the particle size dominates the drag reduction performance and values and it is believed that the interaction between the particle size effect and the other parameters controlling the drag reduction system led to that conclusion. Further discussions can be seen in section 4.5.

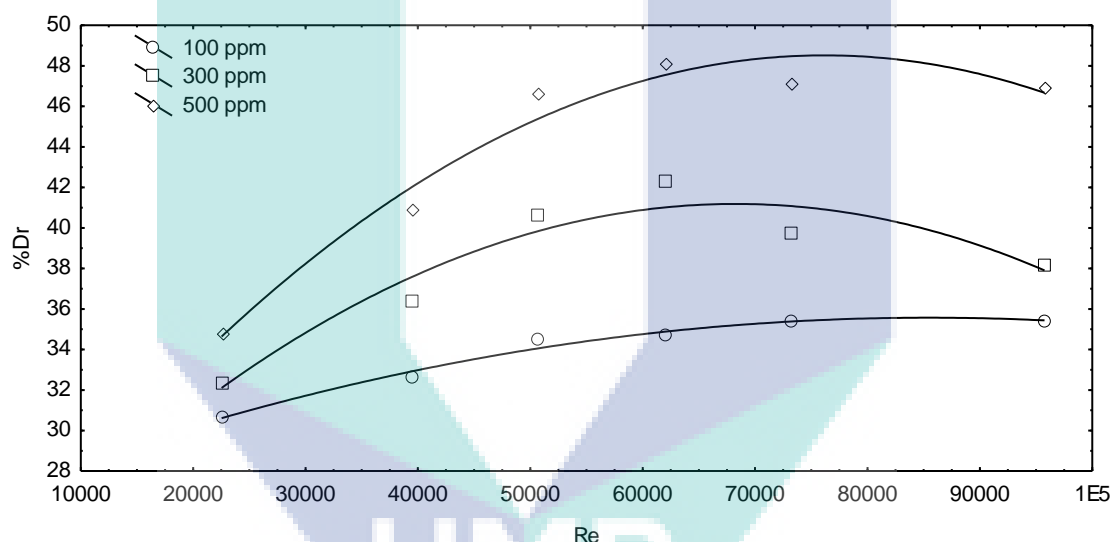


Figure 4.47: Effect of 20 ppm of NNAP surfactant additive on the Re-%Dr relation for Coal particles ($D_p = 71 \mu\text{m}$) suspended in water and flowing in 0.0125 m I.D. and 0.5 m pipe length.

The most sustainable clear effect of the NNAP surfactant on the drag reduction performance of the aluminum powder is shown in figure 4.48. This figure shows effect of 30 ppm of NNAP surfactant addition on the Re-%Dr relation for aluminum particles ($D_p = 71 \mu\text{m}$) suspended in water and flowing in 0.0125 m I.D. and 2.0 m pipe length. This figure highlights the normal relation between %Dr and Re to maximum %Dr of 45%, 41.5% and 39.5% at $\text{Re} = 95749$, 95749 and 73220 respectively for the three concentrations investigated. It can be notice that the values of the %Dr monitored for the coal powder are higher in value than the other powders. This fact will not be a final

conclusion because most of the data presented in the graphs or in the experimental data tables shows that the aluminum powder did show the higher and stable performance.

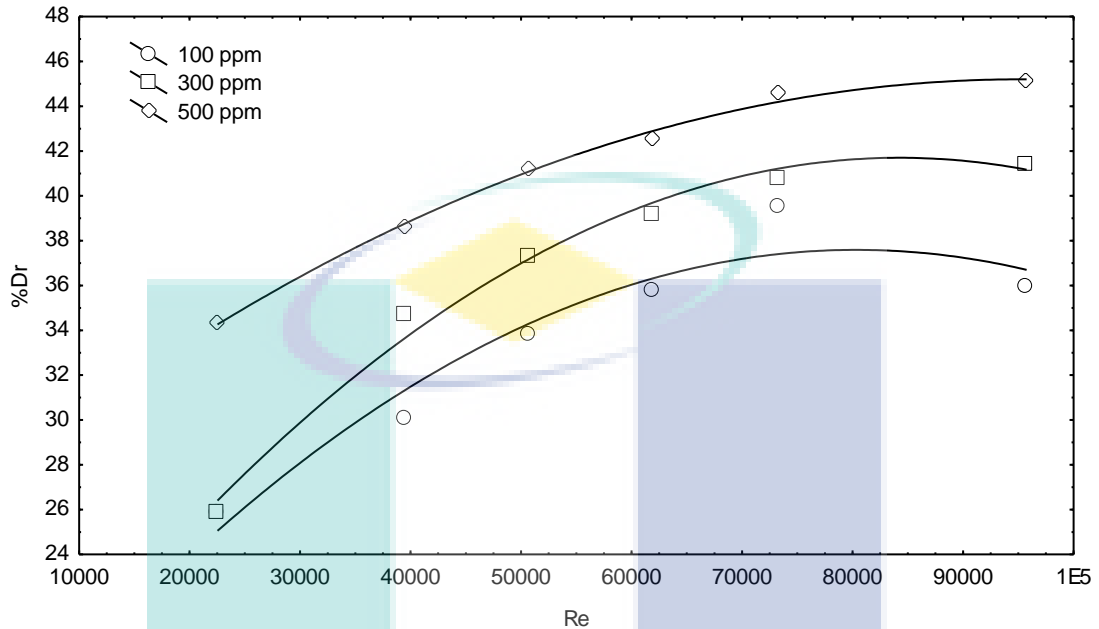


Figure 4.48: Effect of 30 ppm of NNAP surfactant additive on the Re-%Dr relation for Aluminum particles ($D_p = 71 \mu\text{m}$) suspended in water and flowing in 0.0125 m I.D. and 2.0 m pipe length.

Generally, the DAPI and NNAP surfactants can improve the performance of the suspended solid drag reduction ability when introduced in minute quantities to the main flow. Surfactants in general tend to form certain kind of aggregates when diluted in one-phase systems. These clusters are called micelles and it acts as one unit in the flow media. The micelles formed in the transported media investigated in the present work and interfered within the turbulence and the turbulent structures inside the pipe. This interference changes the properties of eddies, especially the eddy viscosity and the elasticity of the liquid glob that form the eddy. The viscoelastic properties of the micelles formed plus the effect of the added powder interfering within the turbulent structures suppresses eddies and prevent it from completing its shape, which means preventing eddies from absorbing more power from the main flow and that leads to improve of the flow inside the pipeline.

4.3.2 Effect of (DAPI) and (NNAP) additive on the %Dr for the suspended particles performance

Figures 4.49 to 4.56 show the effect of the two surfactants investigated on the drag reduction performance of each powder introduced as drag reducing agent before and after the addition of the surfactant. In addition, drag reduction performance comparison between the effects of the two surfactants in the same operating conditions and powders investigated are shown in figures 4.57 to 4.62.

Figure 4.49 shows the effect of DAPI surfactant additive on the sand particles ($D_p = 45 \mu\text{m}$ and 500 ppm additive concentration) performance as drag reducing agent for suspension in water and flowing in 0.0125 m I.D. and 0.5 m pipe length. Compared with the initial results for the surfactant-free drag reduction performance of sand, this figure shows that the addition of DAPI surfactant improves the performance of sand powder. The values of %Dr increased rapidly by the addition of DAPI surfactant with different additive concentrations (10, 20 and 30 ppm). The results showed that the maximum %Dr difference was 78% at $Re = 22533$ and the minimum %Dr difference was 35% at $Re = 95767$ which highlight clearly the effect of the degree of turbulence on the drag reduction performance. At low Re the maximum performance of the surfactant as drag reduction improver was observed which means that the surfactants performed better with lower degree of turbulence.

To investigate the effect of the suspended solid concentration on the drag reduction behavior of DAPI surfactant, additional experimental data are presented in figures 4.50 and 4.51 for the same experimental operation conditions but with different suspended solid concentrations. Figure 4.50 shows the effect of DAPI surfactant addition on sand particles ($D_p = 45 \mu\text{m}$ and 300 ppm additive concentration) performance as DRA for suspension in water and flowing in 0.0125 m I.D. and 0.5 m pipe length. From that figure, the general conclusion is that by the addition of DAPI surfactant, the drag reduction performance of the suspended sand particles become higher but the effect of the surfactant addition concentration is not as clear as that described in figure 4.49 where points are mixed and changes positions that make it difficult to decide the optimum operating condition. The same behavior can be seen in figure 4.51 where the highest value for the %Dr was achieved by the addition of the 10

ppm DAPI surfactant. These behaviors lead us to the conclusion that there are certain optimum conditions where the suspended solid size and concentration can act in ideal way as drag reducing agent with proposed concentration of the surfactant as shown in figure 4.49.

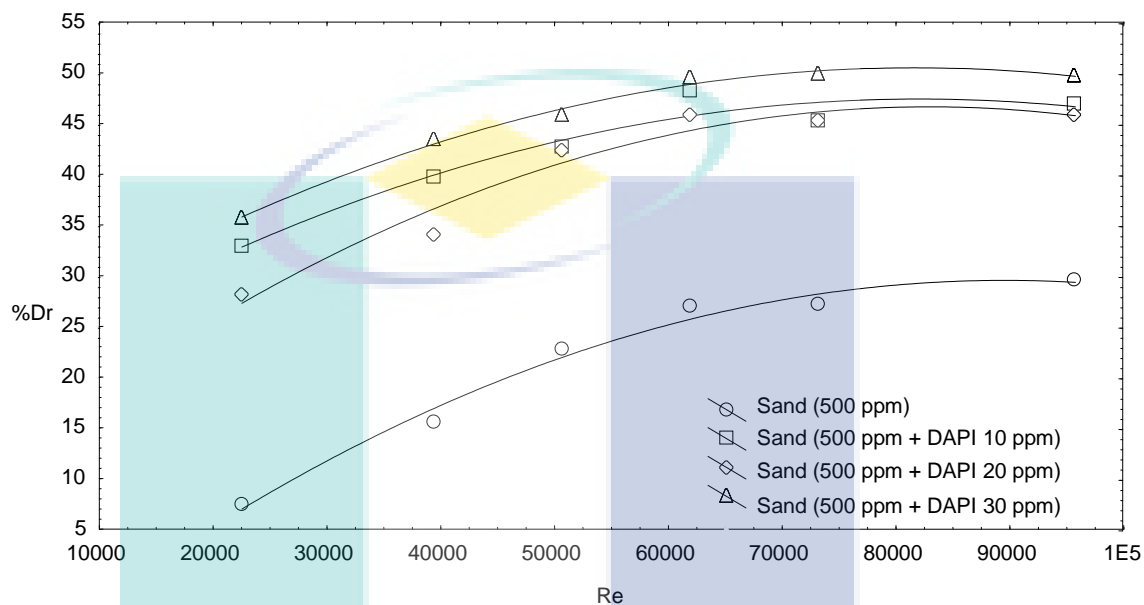


Figure 4.49: Effect of DAPI surfactant additive on the Sand particles ($D_p = 45 \mu\text{m}$ and 500 ppm additive concentration) performance as DRA for suspension in water and flowing in 0.0125 m I.D. and 0.5 m pipe length.

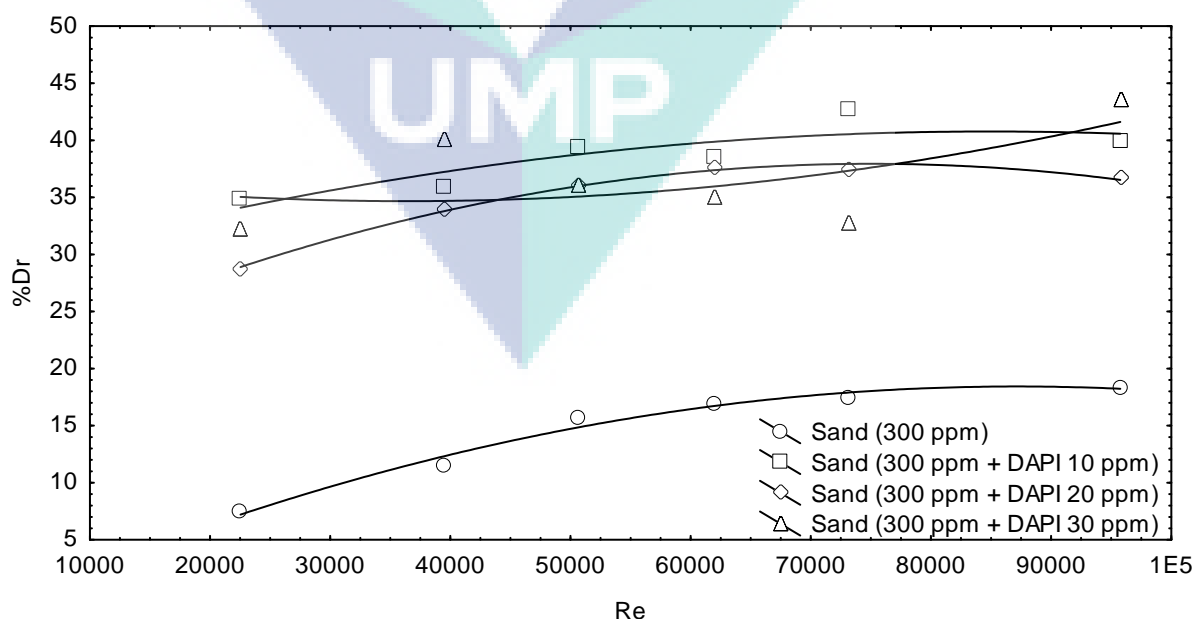


Figure 4.50: Effect of DAPI surfactant additive on the Sand particles ($D_p = 45 \mu\text{m}$ and 300 ppm additive concentration) performance as DRA for suspension in water and flowing in 0.0125 m I.D. and 0.5 m pipe length.

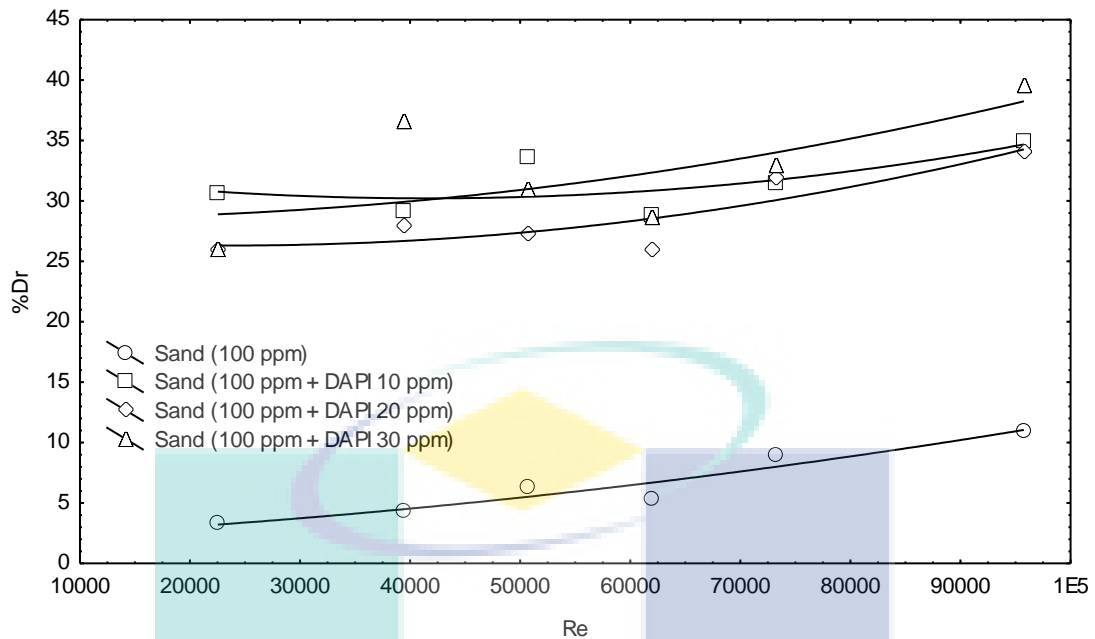


Figure 4.51: Effect of DAPI surfactant additive on the Sand particles ($D_p = 45 \mu\text{m}$ and 100 ppm additive concentration) performance as DRA for suspension in water and flowing in 0.0125 m I.D. and 0.5 m pipe length.

Figures 4.52 to 4.55 show the effect of the addition of NNAP surfactant on the drag reduction performance of aluminum powder in different operating conditions. The presentation of these figures highlights the effect of the testing section length on the drag reduction performance of the suspended solids. The first thing to observe is that NNAP improves the aluminum suspended solid performance in improving the flow in pipes. The difference in the drag reduction performance achieved between the aluminum surfactant-free curve and the 10 ppm NNAP curve is not so high as shown in figure (4.52), where the %Dr increased by 52% at $Re = 16900$ to 28% at $Re = 83808$. This percentage is rapidly increased to 78% at $Re = 16900$ to 49% at $Re = 83808$. From the results above, it can be noticed that at lower values of Re , the effect of the surfactant on the drag reduction performance of the suspended solid is higher. Moreover, by increasing the degree of turbulence the effect of the surfactant will be lower due to the increase in the degree of turbulence that will destruct the solid-surfactant micelle combination formed in the lower Re . Also, the behavior is different compared with that observed with DAPI and shown in figures 4.49 to 4.51 discussed before. Where all the surfactant curves showed high levels and differences compared with the suspension results (even the 10 ppm DAPI surfactant) while with NNAP surfactant the change was more gradual, that the 10 ppm surfactant curve was closer to the aluminum suspension

curve. This is due to the micelles nature of NNAP surfactant, which is different from those formed by DAPI, which will be discussed in the coming paragraphs.

From figures 4.52 to 4.55, it can be concluded that the testing section length have no effect on the drag reduction behavior. That can be concluded by observing the relations between the aluminum suspension %Dr and those achieved after the addition of NNAP surfactant with different concentrations for the four testing section investigated. The four figures show that the relation between the %Dr and Re didn't change by changing the testing section length and that highly support the conclusion observed in section 4.2.4.

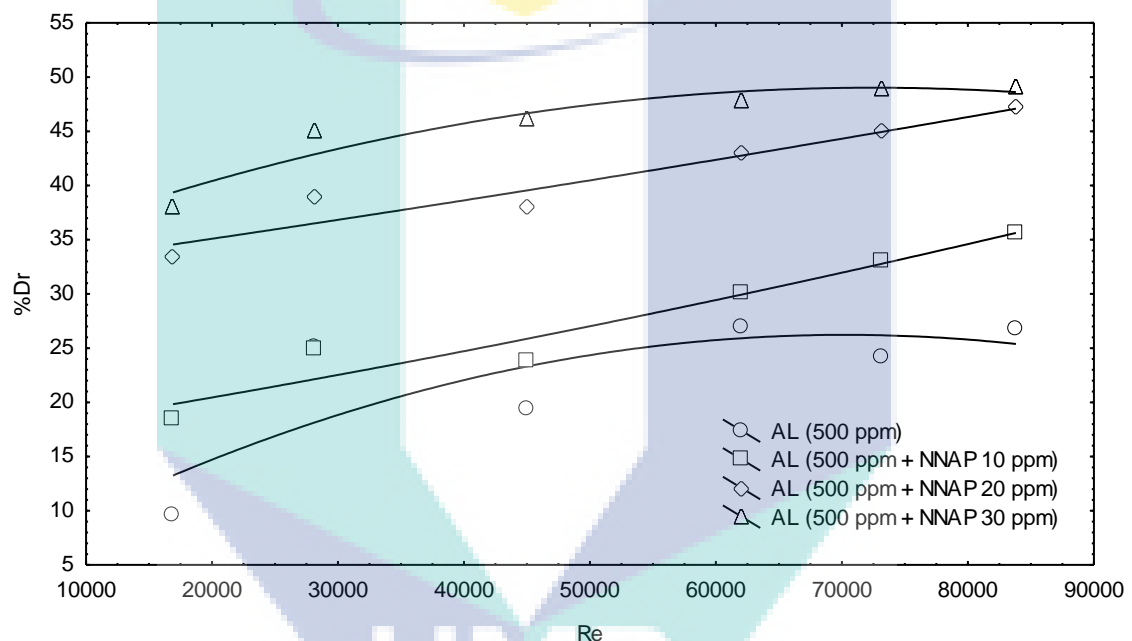


Figure 4.52: Effect of NNAP surfactant additive on the Aluminum particles ($D_p = 45 \mu\text{m}$ and 500 ppm addition concentration) performance as DRA for suspension in water and flowing in 0.0254 m I.D. and 0.5 m pipe length.

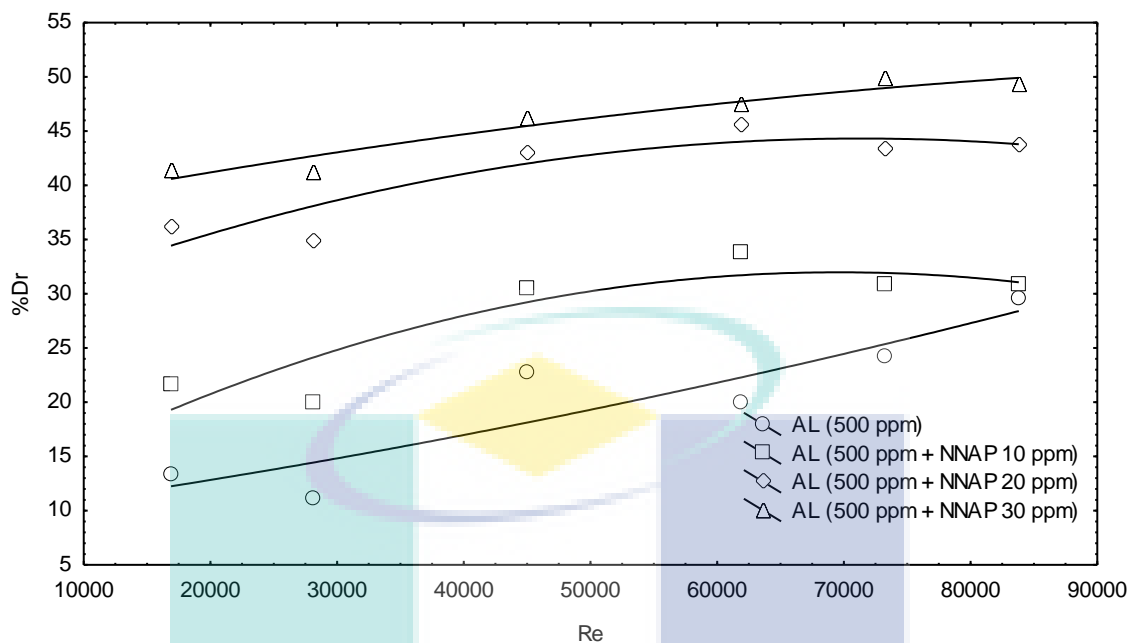


Figure 4.53: Effect of NNAP surfactant additive on the Aluminum particles ($D_p = 45 \mu\text{m}$ and 500 ppm addition concentration) performance as DRA for suspension in water and flowing in 0.0254 m I.D. and 1.0 m pipe length.

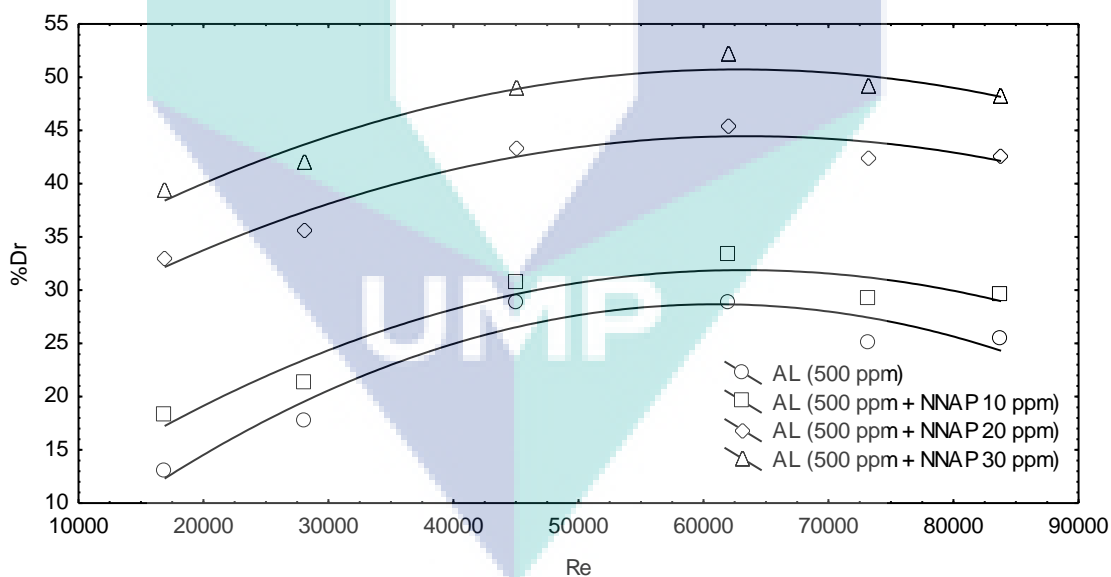


Figure 4.54: Effect of NNAP surfactant additive on the Aluminum particles ($D_p = 45 \mu\text{m}$ and 500 ppm addition concentration) performance as DRA for suspension in water and flowing in 0.0254 m I.D. and 1.5 m pipe length.

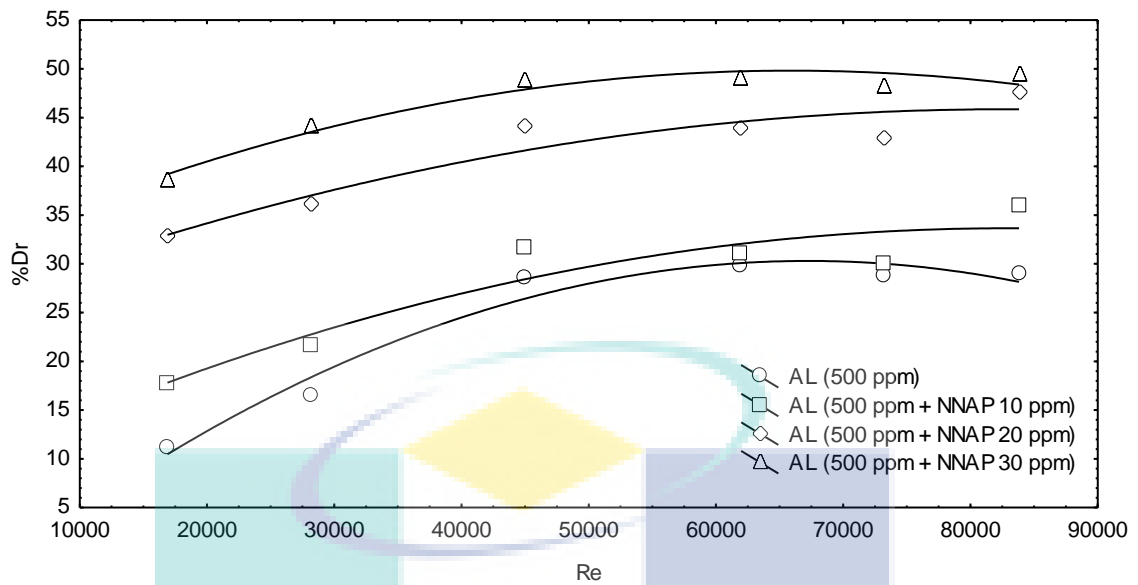


Figure 4.55: Effect of NNAP surfactant additive on the Aluminum particles ($D_p = 45 \mu\text{m}$ and 500 ppm addition concentration) performance as DRA for suspension in water and flowing in 0.0254 m I.D. and 2.0 m pipe length.

For the coal powder, figure 4.56 shows the Effect of DAPI surfactant addition on the Coal particles ($D_p = 71 \mu\text{m}$ and 100 ppm additive concentration) performance as DRA for suspension in water and flowing in 0.0125 m I.D. and 0.5 m pipe length. The maximum difference in the value of the %Dr between the coal-additive free solution drag reduction performance and the 30 ppm DAPI additive concentrations varies between 81% at $Re = 22533$ to 63% at $Re = 95767$. The coal experimental results show a uniform distribution for the effect of adding DAPI surfactant to coal suspension flow system with almost consistent clear differences in the %Dr values. This indicates a good combination between the coal powder physical properties and that of the surfactant that gave such uniform increase in the %Dr.

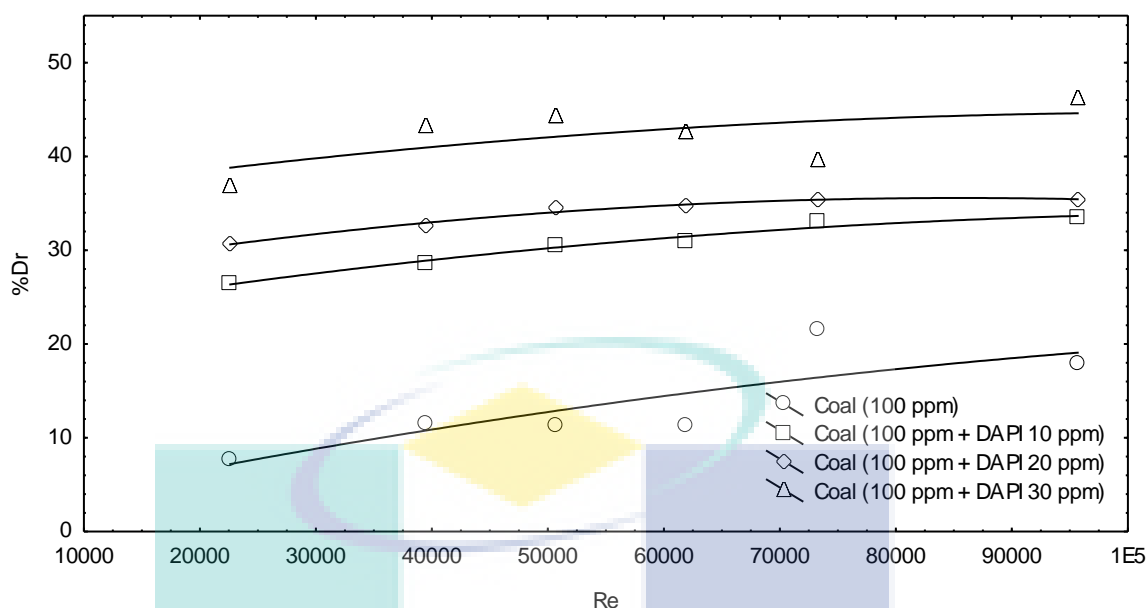


Figure 4.56: Effect of DAPI surfactant additive on the Coal particles ($D_p = 71 \mu\text{m}$ and 100 ppm addition concentration) performance as DRA for suspension in water and flowing in 0.0125 m I.D. and 0.5 m pipe length.

It is important to observe the overall behavior of all the proposed additives in the present investigation. Figure 4.57 shows the effect of DAPI surfactant and Aluminum powder with particle size of $71 \mu\text{m}$ on the %Dr for water flowing through 0.0127 m I.D. pipe and for 1 m testing section length. It is clear that %Dr for the DAPI surfactant alone with water is lower compared with the suspended solid-water solution values. That might be due to the concentration differences between the surfactant and suspended solid additive. Also it is important to note the high difference between the suspended solid physical properties (especially the density) and the surfactant physical properties. All that led to the differences in the %Dr values. What important is the differences between these results (DAPI +water and Aluminum Powder +water) and the results obtained when combining the two effects together. It is clear from the figure that the %Dr will be much higher compared with the results of the surfactant of the solid powder alone. This confirms the idea of combined effects of the two additives in the same time during the drag reduction process. It is believed that the surfactants micelles formed inside the main flow stream interact with the suspended solid particles and forming viscoelastic suspended solids globes that can improve the flow inside pipelines more efficiently than the suspended solids or the surfactants when acting individually as

flow improver. The same behavior can be seen for another two examples from the experimental data in figures 4.58, for the effect of DAPI surfactant and Coal powder with particle size of 71 μm on the %Dr for water flowing through 0.0127 m I.D. pipe and for 1 m testing section length. Also in figure 4.59 for the effect of NNAP surfactant and Sand powder with particle size of 45 μm on the %Dr for water flowing through 0.0254 m I.D. pipe and for 1 m testing section length.

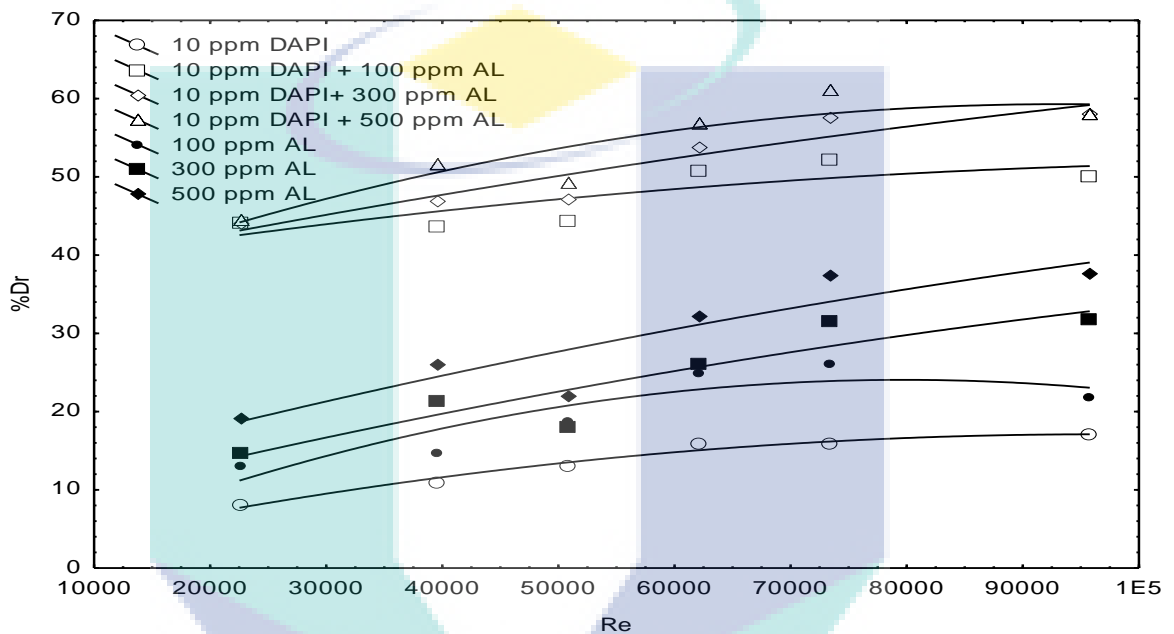


Figure 4.57: Effect of DAPI surfactant and Aluminum powder with particle size of 71 μm on the %Dr for water flowing through 0.0127 m I.D. pipe and for 1 m pipe length.

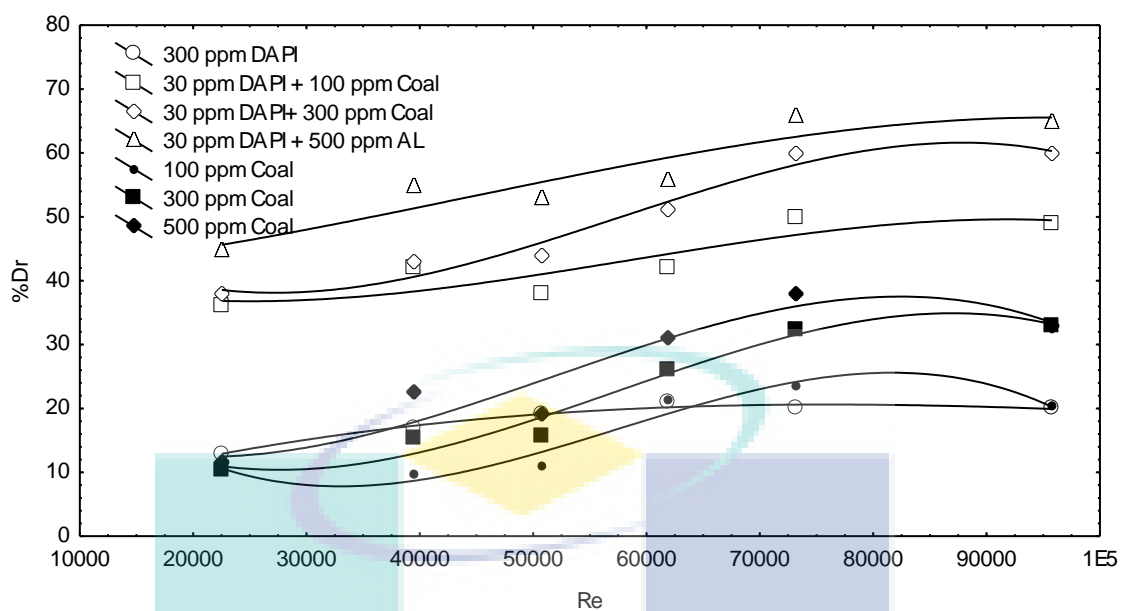


Figure 4.58: Effect of DAPI surfactant and Coal powder with particle size of 71 μm on the %Dr for water flowing through 0.0127 m I.D. pipe and for 1 m pipe length.

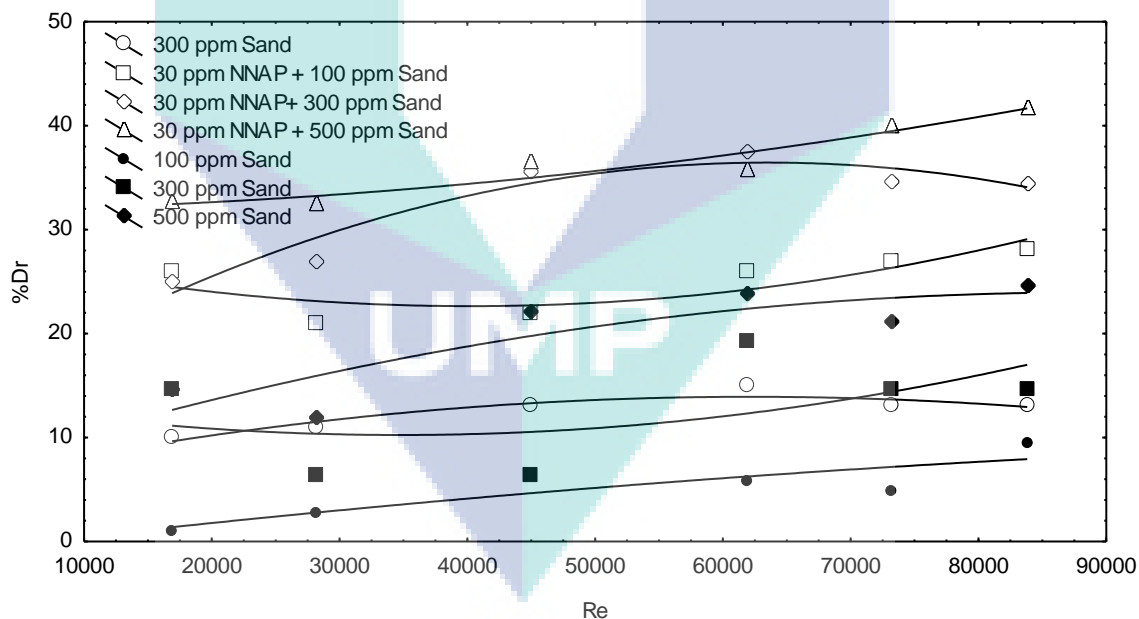


Figure 4.59: Effect of NNAP surfactant and Sand powder with particle size of 45 μm on the %Dr for water flowing through 0.0254 m I.D. pipe and for 1 m pipe length.

One of the objectives of the present work is to investigate the effect of the chemical structure on the Zwitterionic surfactant selected as drag reducing agent. The two Zwitterionic surfactants chosen carries a close value of the molecular number but

totally different structures where the 3-(Decyldimethyle-ammonio) propanesulfonate inner salt (DAPI) chain length and structure is different compared with (3-(N-N,Dimethylpalmityl-ammino propanesulfonate)) (NNAP). Figures 4.60 to 4.65 show a comparison for the surfactant investigated performances as drag reducing agents for the same operating conditions.

Figure 4.60 presents the effect of adding 20 ppm of DAPI and NNAP on the performance of sand powder ($D_p = 45 \mu\text{m}$) suspended in water and flowing 0.0254 m I.D. and 1.5 m pipe length. It can be seen clearly that DAPI surfactant showed higher values of the %Dr compared with NNAP for 20 ppm additive concentration. The figure shows also that the %Dr versus Re curves shape and zones are clearly appearing and the difference in the %Dr values are almost uniform where the average increase in the %Dr when adding 20 ppm of DAPI surfactant ranged from 65% at $Re = 16,900.00$ to 34% at $Re = 83,808.00$ compared with the sand-additive free results. In addition, by the addition of 20 ppm of NNAP, the %Dr increase ranged from 57% to 22% at $Re = 16,900.00$ and $83,808.00$ respectively compared with the sand-additive free results. Comparing the maximum and minimum values calculated above will show the high efficiency and performance that such surfactants provides with very low additive concentrations and highlight also the small differences in of the two surfactant effectiveness when compared with each other that the difference ranged from 8% at $Re = 16,900.00$ to 12% at $Re = 83,808.00$.

The logo for UMP (Universitas Muhammadiyah Purwokerto) is a large, stylized letter 'U' composed of four overlapping triangles in shades of blue and teal. The letters 'UMP' are printed in white, bold, sans-serif font across the center of the 'U'.

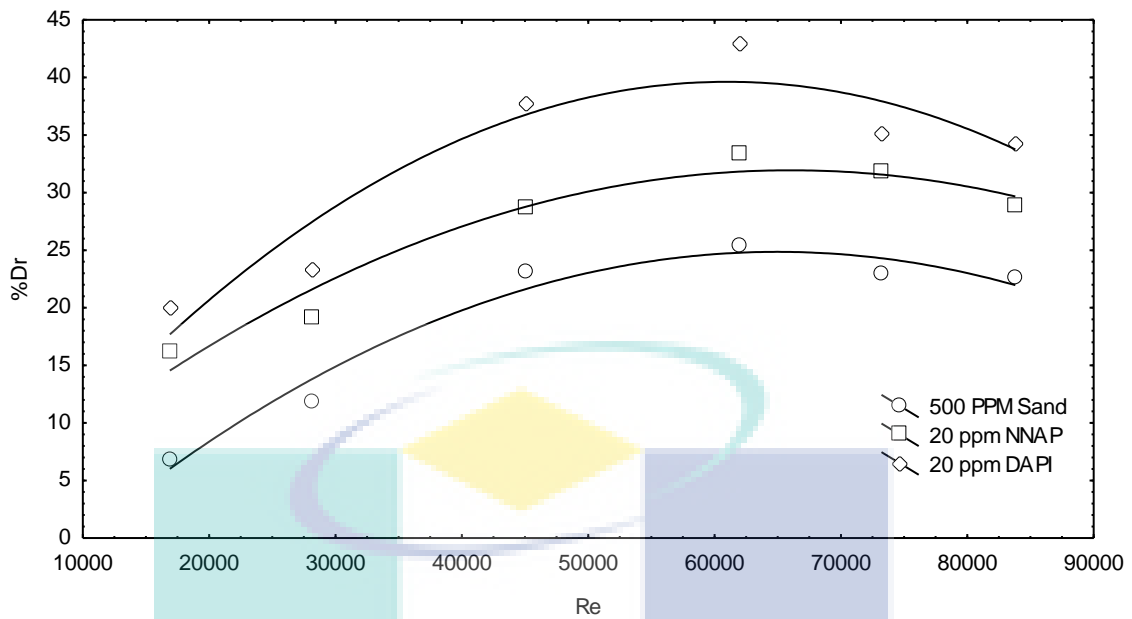


Figure 4.60: Effect of adding 20 ppm of DAPI and NNAP on the performance of the Aluminum powder ($D_p = 45 \mu\text{m}$) suspended in water and flowing in 0.0254 m I.D. and 1.5 m pipe length.

Another representation for the surfactant effect on the sand powder suspension is presented in figure 4.61. In this figure a non-uniform and unstable drag reduction performance appears where an intersection in the %Dr values happened. It is important to notice that the additive concentration is 10 ppm in this curve and that rise the question about the optimum concentration the additive can perform well with a clear distinguishable point. It is believed that if any intersection occurs in the low surfactant concentration system, it is due to the low presence of the surfactant molecules to cover the turbulence spectrum at that Re which lead to disorder and non-uniform behavior as shown in some points in the figure. However, that is not a reason to hide even in that figure, that these two surfactants showed good ability in improving the performance of sand as drag reduction.

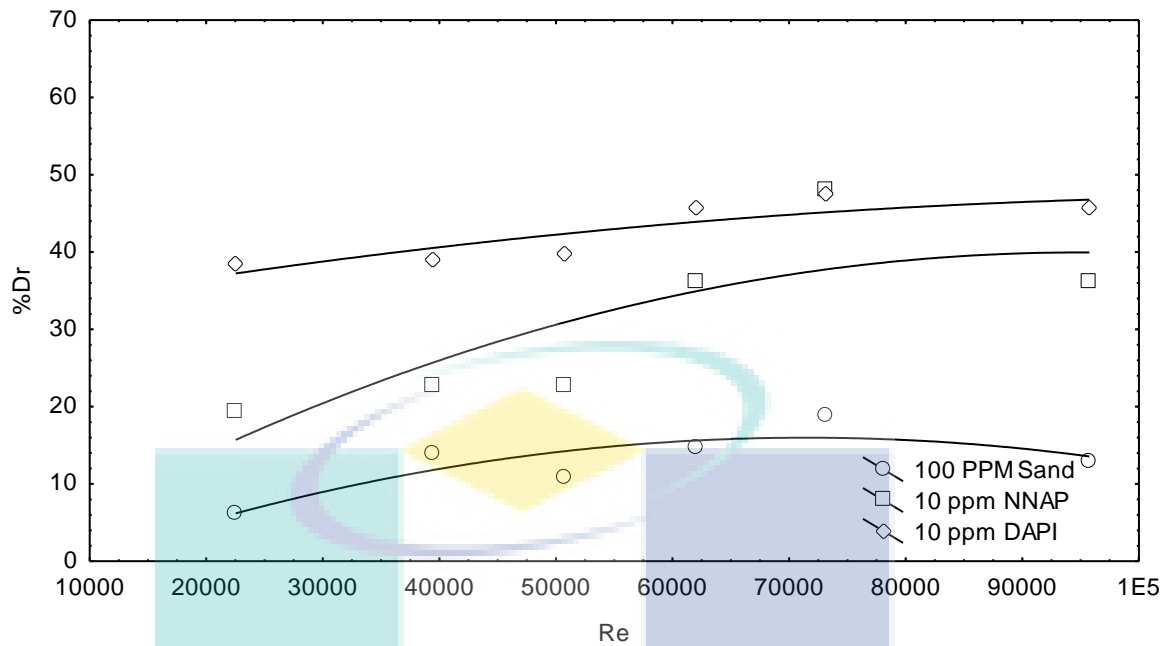


Figure 4.61: Effect of adding 10 ppm of DAPI and NNAP on the performance of the Sand powder ($D_p = 71 \mu\text{m}$) suspended in water and flowing in 0.0125 m I.D. and 1.0 m pipe length.

The effect of the two surfactants investigated on the aluminum powder suspension as drag reduction performance is shown in figures 4.62 and 4.63. Figure 4.62 shows the effect of adding 20 ppm of DAPI and NNAP on the performance of the Aluminum powder ($D_p = 45 \mu\text{m}$) suspended in water and flowing in 0.0254 m I.D. and 2.0 m pipe length. Again, the DAPI showed the highest values of the %Dr compared with NNAP surfactant and a uniform shape and behavior of the drag reduction curves and that can be seen also in figure 4.63 for the aluminum powder. It is worth to point that the consistence performance in the two curves occurs at additive concentration of 20 and 30 ppm respectively, which conform the conclusion mentioned above regarding the effect of additive concentration.

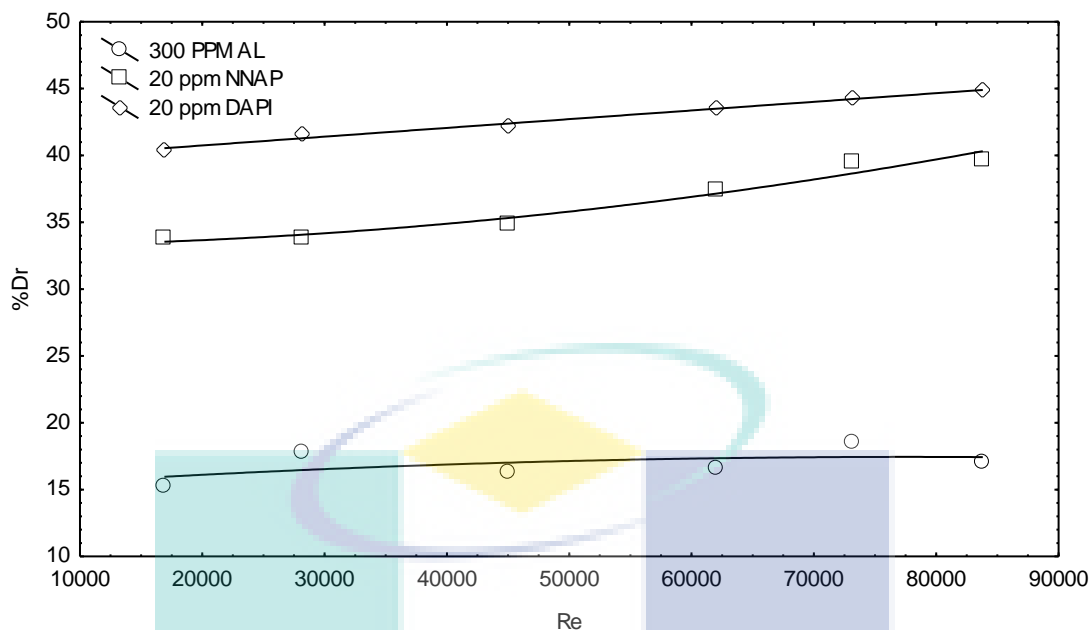


Figure 4.62: Effect of adding 20 ppm of DAPI and NNAP on the performance of the Aluminum powder ($D_p = 45 \mu\text{m}$) suspended in water and flowing in 0.0254 m I.D. and 2.0 m pipe length.

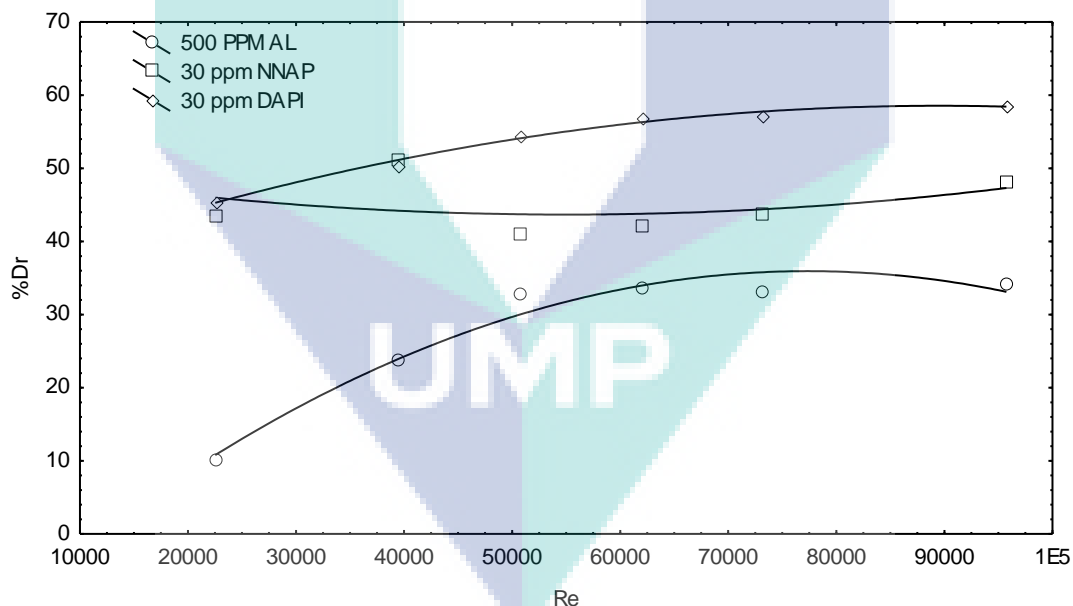


Figure 4.63: Effect of adding 30 ppm of DAPI and NNAP on the performance of the Aluminum powder ($D_p = 71 \mu\text{m}$) suspended in water and flowing in 0.0125 m I.D. and 0.5 m pipe length.

For the coal powder, the situation was different, that NNAP surfactant showed the highest values of the %Dr compared with DAPI surfactants results as shown in figures 4.64 and 4.65. In addition, a non-uniform and many intersections between the %Dr Values and point appears in the figures. It is believed that the intersections

between the point is due to all the properties effecting the drag reduction operation especially the turbulence and the way the surfactant interfere with the coal suspension to improve the action.

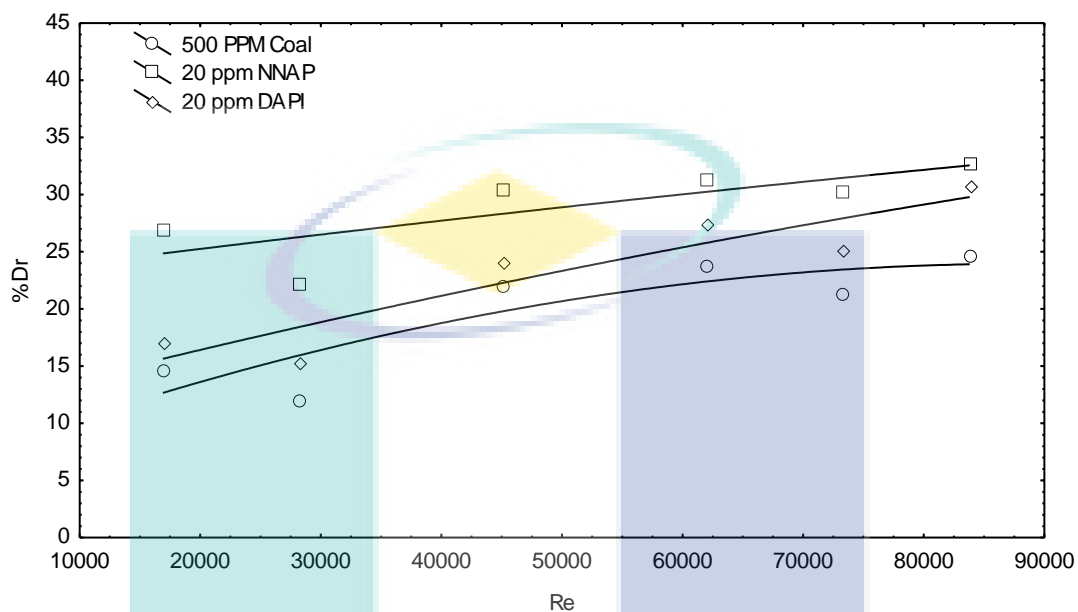


Figure 4.64: Effect of adding 20 ppm of DAPI and NNAP on the performance of the Coal powder ($D_p = 45 \mu\text{m}$) suspended in water and flowing in 0.0254 m I.D. and 1.0 m pipe length

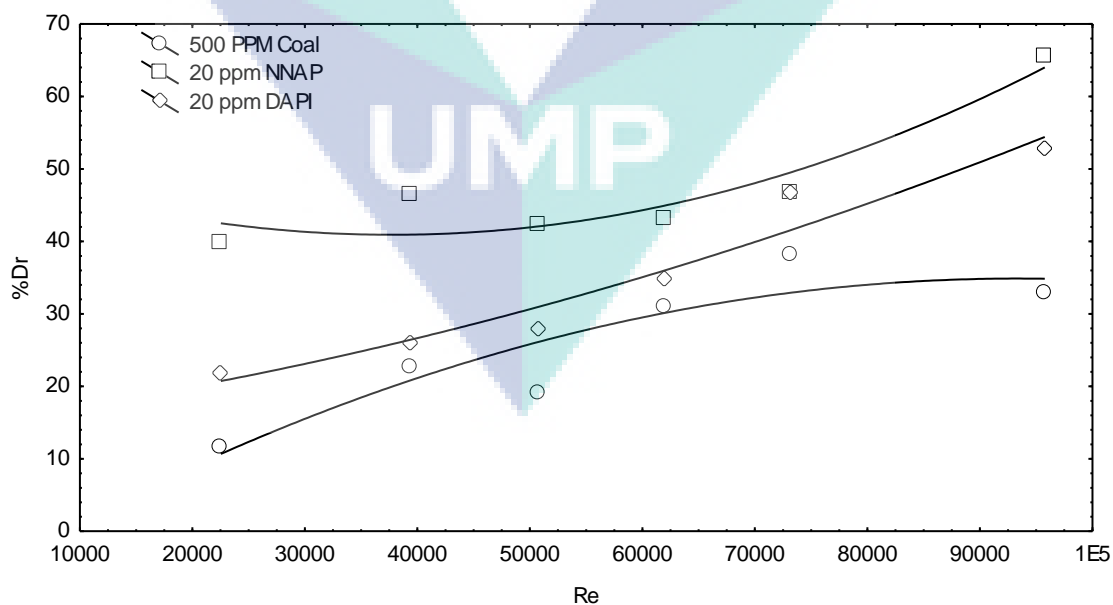


Figure 4.65: Effect of adding 20 ppm of DAPI and NNAP on the performance of the Coal powder ($D_p = 45 \mu\text{m}$) suspended in water and flowing in 0.0125 m I.D. and 1.0 m pipe length.

Generally, DAPI surfactant showed better performance compared with the NNAP surfactant in most of the experimental data. This may be due to the nature of the surfactant itself, that DAPI have less number of carbon molecules in its molecular structure ($C_{15}H_{33}NO_3S$) compared with the NNAP ($C_{21}H_{45}NO_3S$), which controls highly the shape and the length of the molecular micelles formed in the media. It is believed that the higher the hydrocarbon chain of the surfactant molecule the more effective the drag reduction abilities and the larger the micelle formed, but also the lower the ability to resist shearing and to regain the micelle shape after relaxing. The time needed for large micelles to regain its shape after shearing is higher comparing with the smaller one due to the difference in polarity. It is believed that DAPI surfactants formed smaller micelles compared with the NNAP surfactants but these micelles have higher abilities to resist high shearing forces and are faster in regaining its shape after the shearing effect is lost. This is why DAPI surfactant showed more stable and higher performance than NNAP.

4.4 NUMERICAL MODEL (CORRELATIONS)

In the present investigation, dimensional analysis is used to group the significant quantities into a dimensionless group to reduce the number of variables appearing and to make the results so compact and applicable to all similar situations.

The choice of the appropriate variables that influence the friction factor (f) in the case of drag reduction is a great task, since it is influenced by solvent physical and flow properties. Starting with the following relation:

$$\Delta P = f(d, \mu, \rho, v, l)$$

Therefore, by applying the dimensional analysis, the following non-dimensional relation was proposed:

$$f = F(Re) \tag{4.7}$$

or:

$$f=a(Re)^b \quad (4.8)$$

A detailed description for the dimensional analysis steps is shown in appendix D. The essential problem now is to find the values of the constants (a and b), that give the best fitting of the experimental data.

Least square method has been used to determine the coefficients. A computer program “STATISTICA 5.5” expressed this method. The coefficients for selected samples from the experimental work are tabulated in table 4.1. The STATISTICA 5.5 software correlation steps are shown graphically in details in appendix D1.

Table 4.1 shows, selected samples of the best results obtained in the experimental data from the statistical point of view. The table introduces the values of the constants (a and b) that showed the best variance (V) and (R) values.

The first observation from the table suggests that, the friction factor values vary oppositely with the Reynolds number due to the negative values that the b carries for all the cases. This conclusion supports the numerous effect of the degree of turbulence represented by Reynolds number on the percentage drag reduction (%Dr). The negative value for the b factor means that the friction factor decreases (the %Dr increases) by increasing the Re. This can be considered as an average behavior considering all the fluctuations the drag reducing agent showed when monitoring the relation between the %Dr and Re in the previous sections.

Figure 4.66 shows a comparison between the correlation equations introduced in the present work and the one suggested by Virk (Virk, 1975). The figure shows that for most of the cases investigated there is a good approach for Virk asymptote for maximum drag reduction. It is very interesting to reveal that one of the correlations predicted in the present work could approach and overcome Virk asymptote for maximum drag reduction as in case 5 which represents the effect of aluminum powder drag reduction combined with 10 ppm of NNAP surfactant. This case can be considered as the optimum drag reduction performance in the present investigation and it could

efficiently lower friction factor values compared with Virk results. The maximum drag reduction correlation in the present work is presented by the following equation:

$$f = 0.798 \text{ Re}^{-0.746} \quad (4.9)$$

Figures 4.67 to 4.75 show the relation between the observed values of friction factor taken from some of the experimental data and the predicted values from mathematical correlation. It can be noticed that most points lie at or close to the straight line, which means a good agreement between theoretical and experimental data.

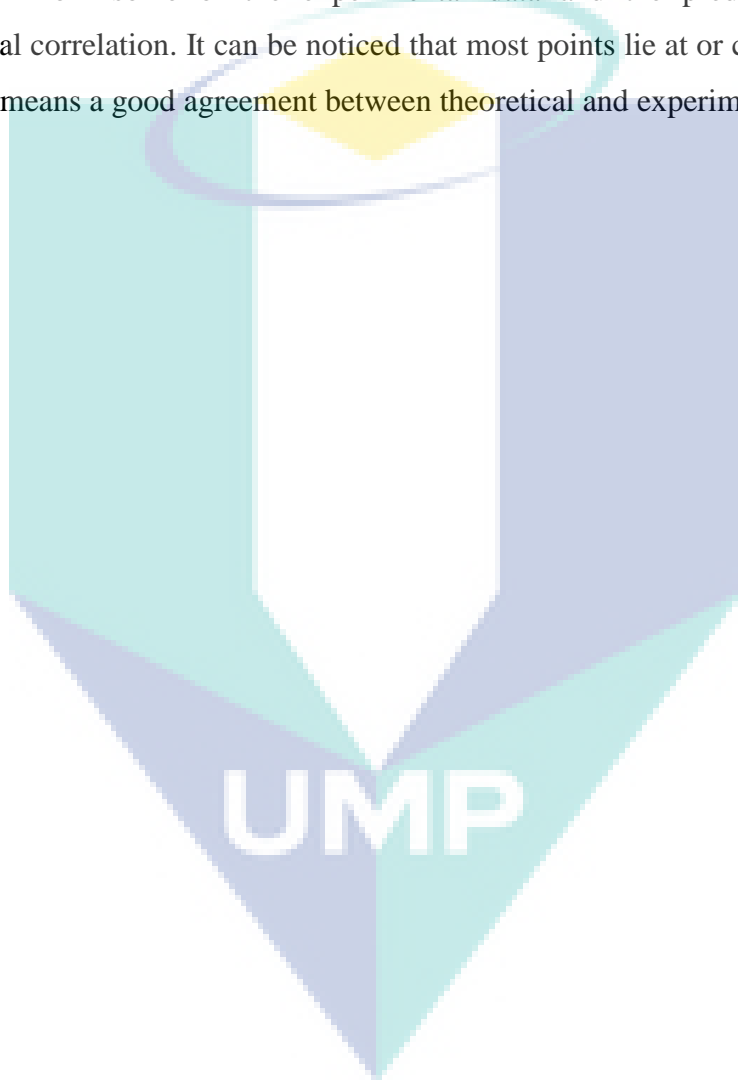


Table 4.1: Values of the correlations coefficients for selected samples of the experimental data.

Case No.	Powder	Surfactant	Particle size (μm)	Length (m)	Pip diameter (m)	Surfactant Concentration (ppm)	Powder concentration (ppm)	V	R	Av. Er. (%)	a	B
1	Aluminum	-	71	0.5	0.0125	-	100-500	0.887	0.941	11.21	0.430	-0.446
2	Aluminum	-	71	1.0	0.0254	-	100-500	0.911	0.952	5.74	0.100	-0.292
3	Aluminum	-	45	0.5	0.0125	-	100-500	0.882	0.944	9.93	0.513	-0.460
4	Aluminum	NNAP	45	1.0	0.0254	30	100-500	0.882	0.931	9.86	0.176	-0.359
5	Aluminum	NNAP	45	0.5	0.0381	10	100-500	0.973	0.986	2.11	0.798	-0.746
6	Aluminum	NNAP	45	1.0	0.0381	20	100-500	0.899	0.957	4.43	0.111	-0.304
7	Aluminum	NNAP	71	2.0	0.0254	10	100-500	0.922	0.971	4.99	0.117	-0.390
8	Aluminum	DAPI	45	0.5	0.0125	20	100-500	0.861	0.922	10.02	0.196	-0.420
9	Aluminum	DAPI	45	0.5	0.0254	20	100-500	0.962	0.988	2.43	0.671	-0.472
10	Aluminum	DAPI	71	2.0	0.0125	30	100-500	0.930	0.977	4.79	0.135	-0.391
11	Sand	-	45	0.5	0.0125	-	100-500	0.868	0.929	7.89	0.504	-0.420
12	Sand	-	45	1.0	0.0254	-	100-500	0.910	0.957	5.64	0.131	-0.292
13	Sand	-	71	0.5	0.0125	-	100-500	0.862	0.929	10.12	0.352	-0.420
14	Sand	NNAP	45	1.0	0.0254	10	100-500	0.889	0.933	8.45	0.130	-0.293
15	Sand	NNAP	45	1.5	0.0254	20	100-500	0.922	0.967	5.10	0.273	-0.371
16	Sand	DAPI	71	1.5	0.0381	30	100-500	0.921	0.970	4.87	0.202	-0.370
17	Sand	DAPI	71	0.5	0.0125	10	100-500	0.871	0.941	6.02	0.354	-0.430
18	Coal	-	45	0.5	0.0125	-	100-500	0.862	0.933	7.10	0.191	-0.341
19	Coal	-	71	2.0	0.0125	-	100-500	0.941	0.979	3.34	0.325	-0.395
20	Coal	NNAP	45	1.5	0.0254	20	100-500	0.920	0.962	6.24	0.293	-0.379
21	Coal	DAPI	71	1.5	0.0125	30	100-500	0.797	0.901	13.7	0.162	-0.403

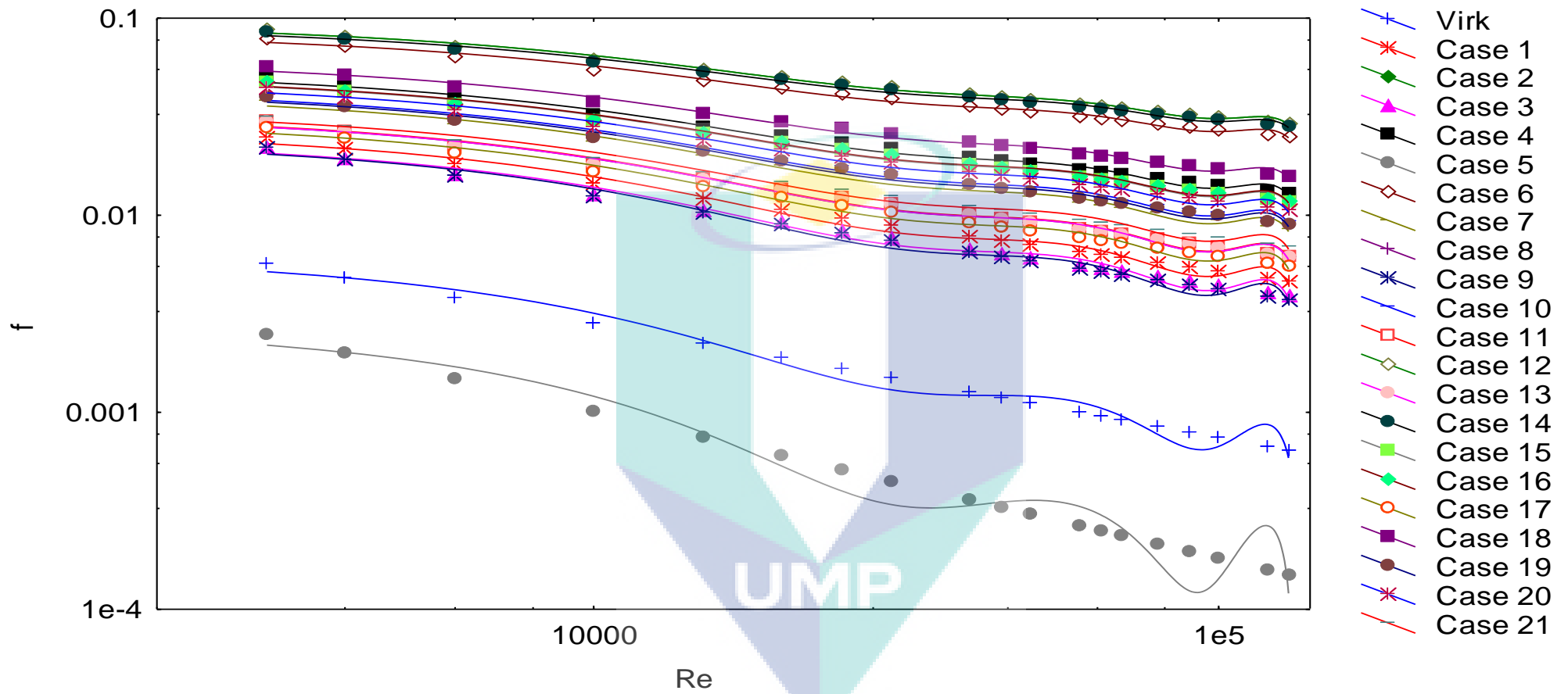


Figure 4.66: Friction factor versus Reynolds number correlations comparison with Virk correlation.

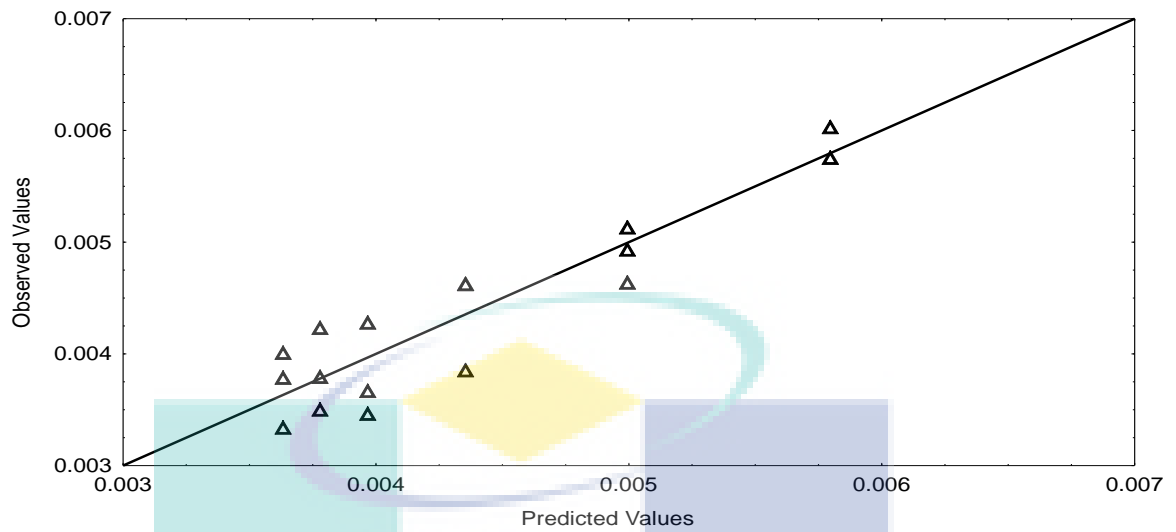


Figure 4.67: Predicted versus observed values for Aluminum-surfactant free solution flowing with 0.0254 m I.D. pipe, 1.0 m testing section length and 71- μm particle size.

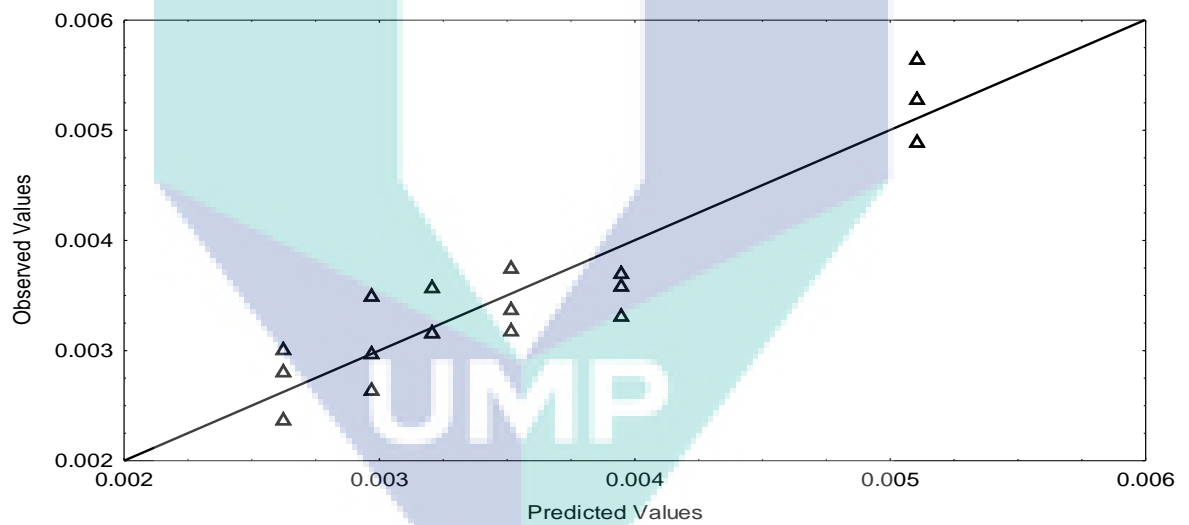


Figure 4.68: Predicted versus observed values for Aluminum-surfactant free solution flowing with 0.0125 m I.D. pipe, 0.5 m testing section length and 45- μm particle size.

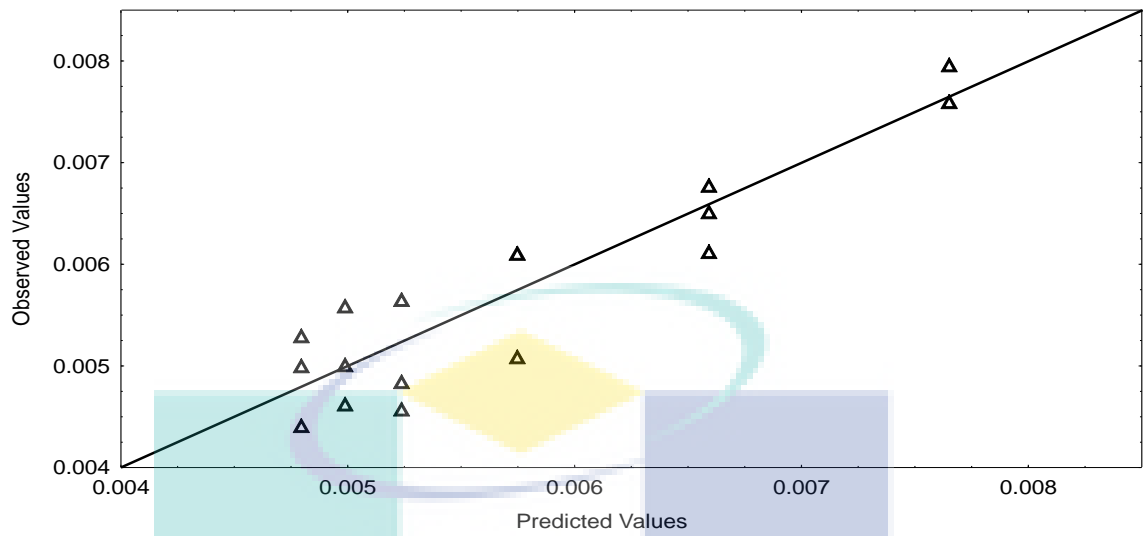


Figure 4.69: Predicted versus observed values for Sand-surfactant free solution flowing with 0.0254 m I.D. pipe, 1.0 m testing section length and 45- μ m particle size.

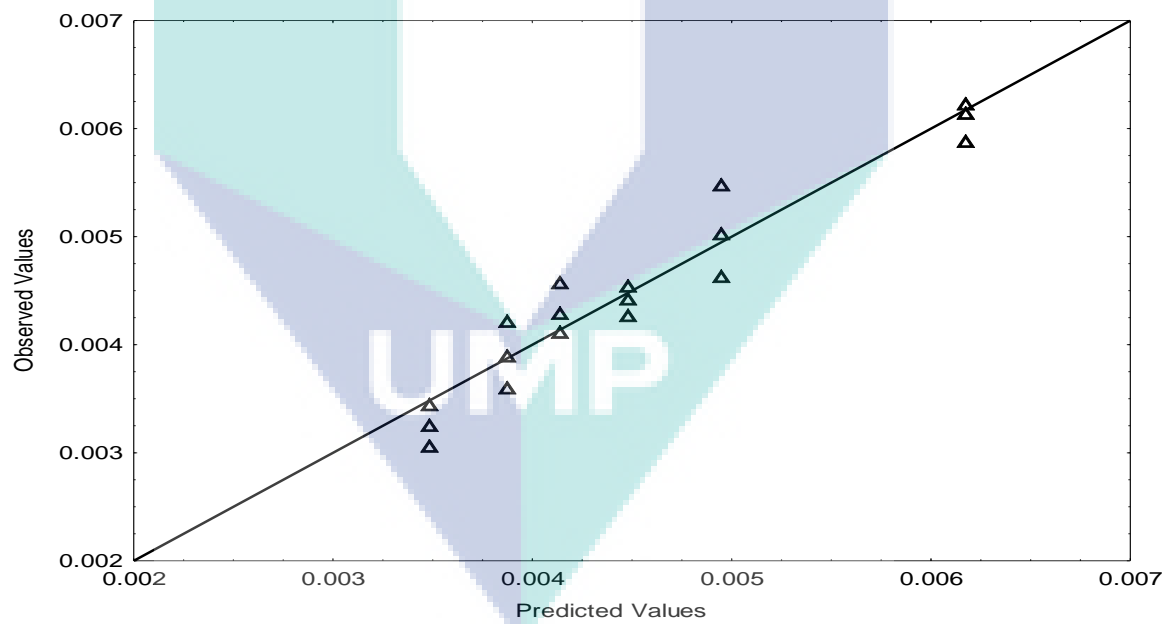


Figure 4.70: Predicted versus observed values for Coal-surfactant free solution flowing with 0.0125 m I.D. pipe, 2.0 m testing section length and 71- μ m particle size.

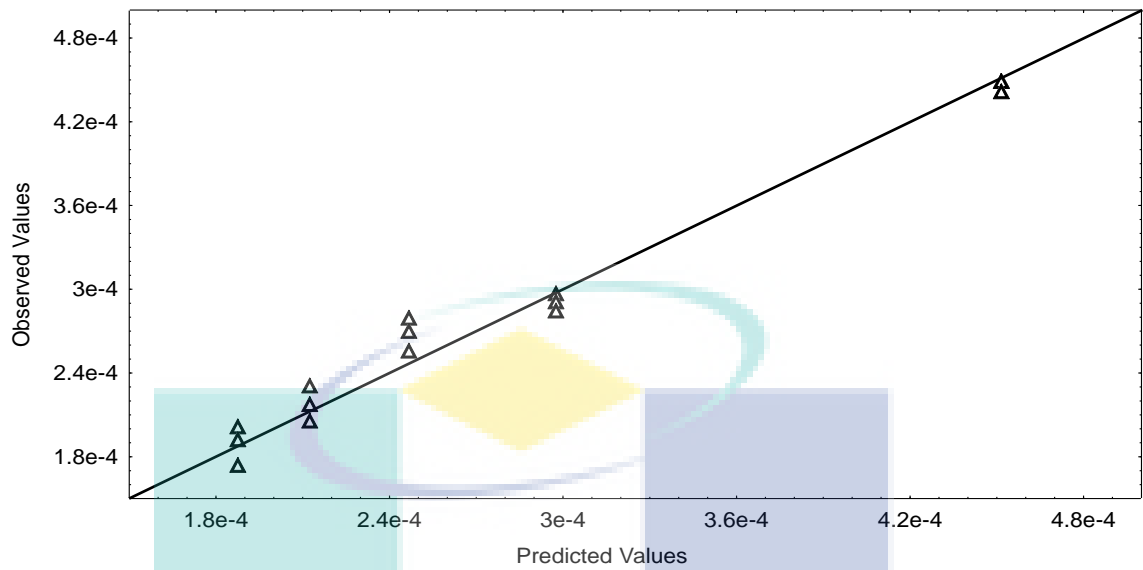


Figure 4.71: Predicted versus observed values for Aluminum-NNAP (10 ppm) solution flowing with 0.0381 m I.D. pipe, 0.5 m testing section length and 45- μ m particle size.

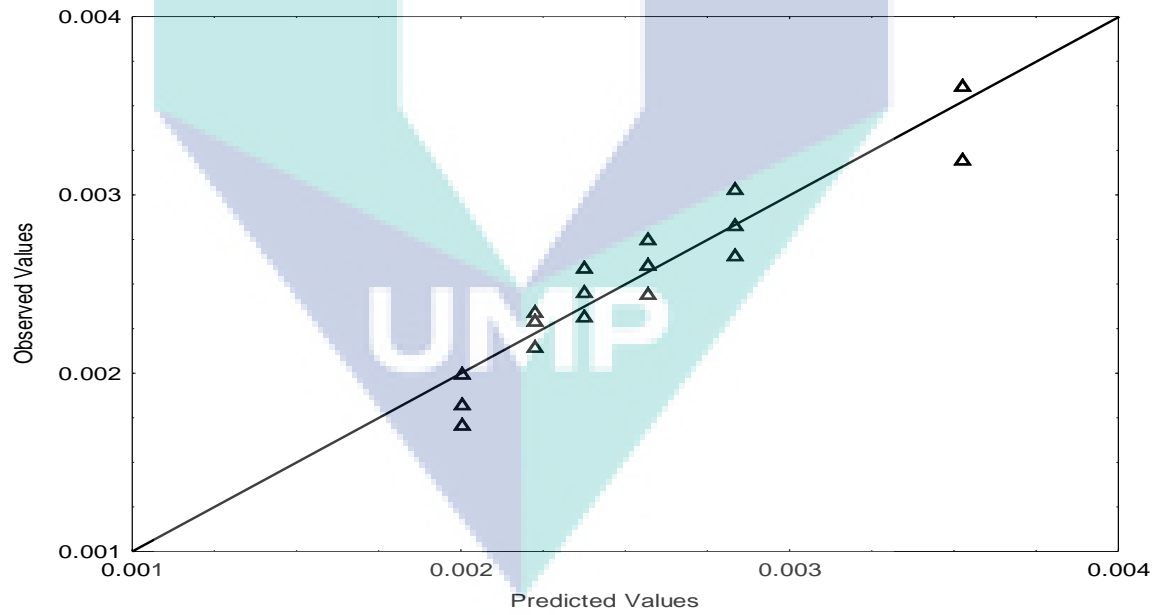


Figure 4.72: Predicted versus observed values for Aluminum-NNAP (10 ppm) solution flowing with 0.0254 m I.D. pipe, 2.0 m testing section length and 71- μ m particle size.

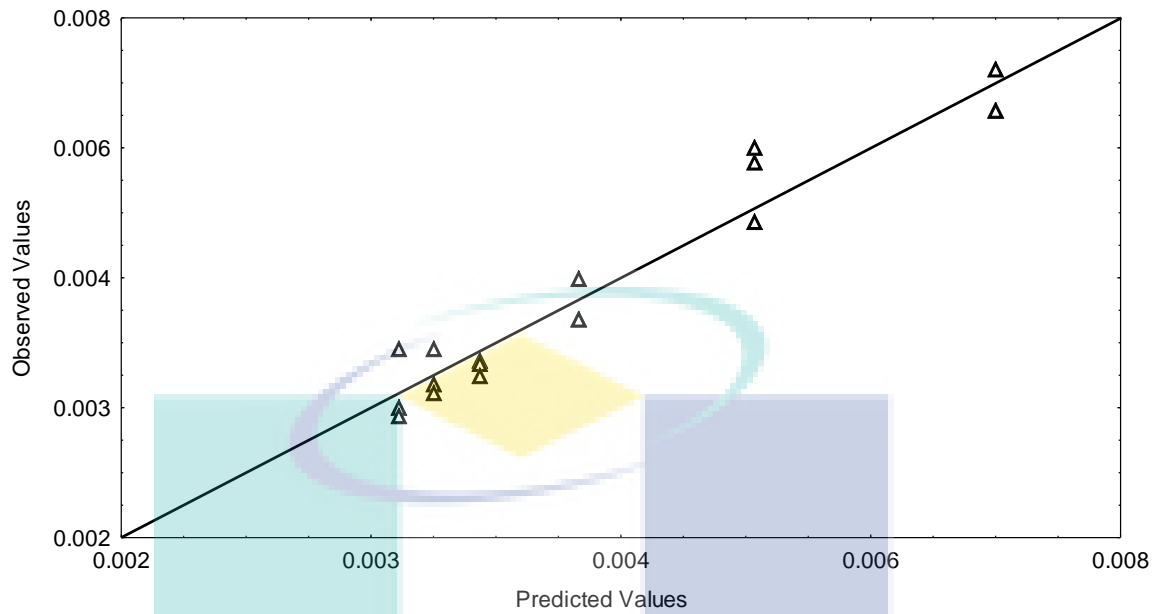


Figure 4.73: Predicted versus observed values for Aluminum-DAPI (20 ppm) solution flowing with 0.0254 m I.D. pipe, 0.5 m testing section length and 45- μ m particle size.

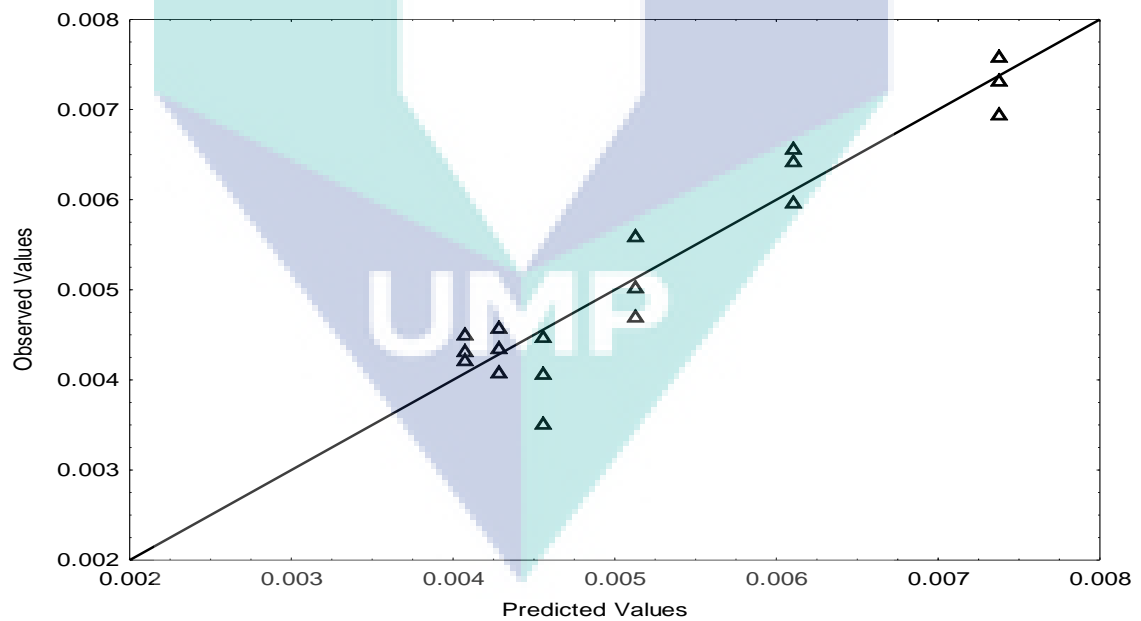


Figure 4.74: predicted versus observed values for Sand-NNAP (20 ppm) solution flowing with 0.0254 m I.D. pipe, 1.5 m testing section length and 45- μ m particle size.

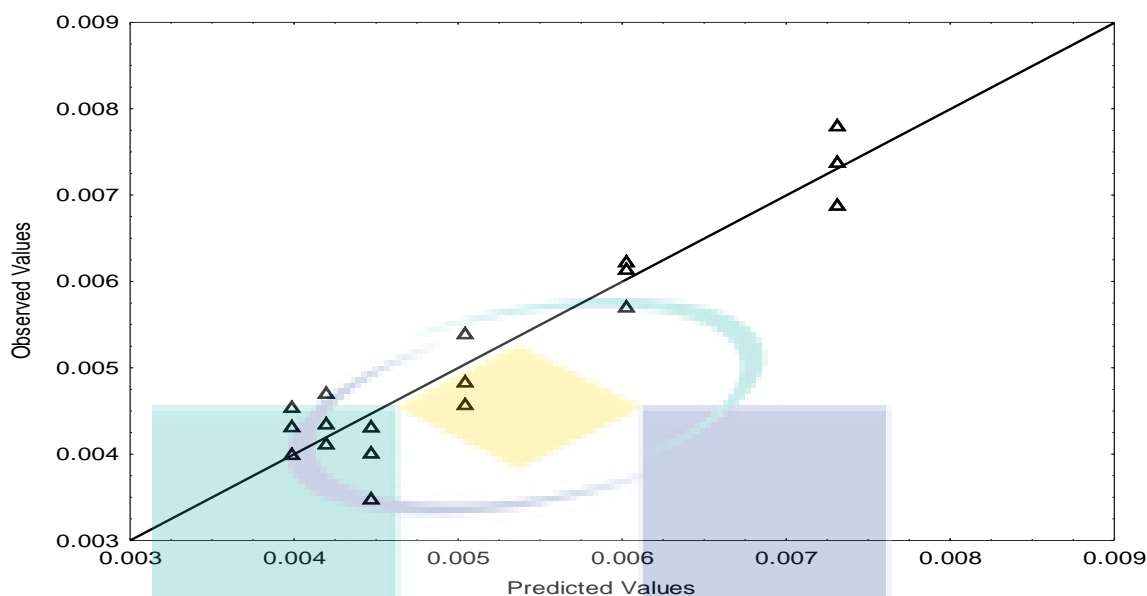


Figure 4.75: Predicted versus observed values for Coal-NNAP (20 ppm) solution flowing with 0.0254 m I.D. pipe, 1.5 m testing section length and 45- μm particle size.

4.5 MECHANISM

Drag reduction mechanism is the most complicated part of this phenomenon, which was under high argument and criticism. The unstable and sometimes “strange” behavior of the fluid in turbulent flow, and the highly chaotic movement of fluid molecular masses in different directions plus the absence of a clear and exact mapping of the turbulence inside the pipe, all these make it hard to give a clear idea about a certain mechanism that might control the drag reduction in pipe flow.

To have a clear understanding about the proposed mechanism controlling the drag reduction in the present work, it is reasonable to divide the action into two parts. The first part is about the drag reduction mechanism with the suspended solid and the second one is about the contribution that the investigated surfactants have on the drag reduction operation.

By introducing the powder to the main turbulent flow, the powder particles suspend, interfere and be part of the flow in general and the turbulent structures inside the media itself. When that interference occurs, the properties of the stretched globe of liquid forming the turbulent structure “eddy” are changed. The apparent viscoelastic

properties is different in a way that this globe of liquid cannot complete the stretching anymore for a complete eddy shape, and as it is known that, eddies are the main source of pumping power dissipation in turbulent flow. The suppressing action of the powder to eddy will lead to save the pumping power inside the pipe also to the redirection of the pumping power toward the main flow direction. That was proven experimentally in the present work where the %Dr was higher in smaller pipes where the degree of turbulence is higher and the number of eddies is higher too. The higher number of eddies provided a more suitable media for the drag reducing agent to interfere within the small turbulence structures formed, and that enabled suppressing larger number of smaller eddies which led to the improvement in the flow.

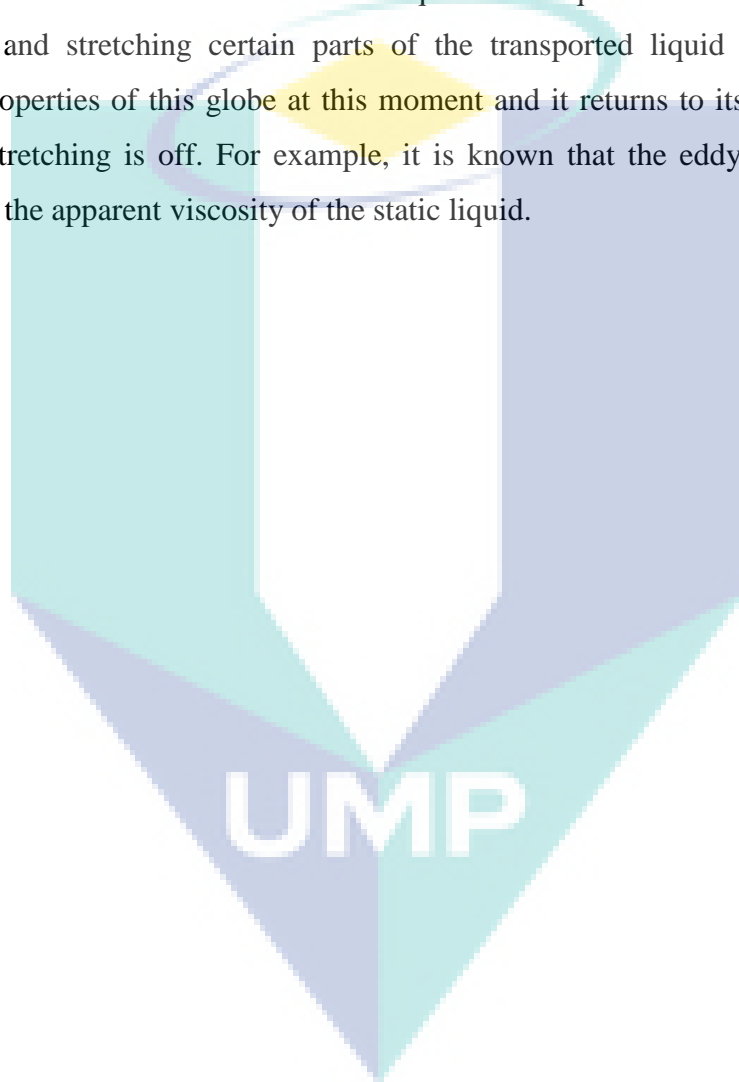
When the surfactant is introduced to the main flow of the suspended solid-liquid turbulent flow region, the drag reduction performance showed improvement compared with the drag reduction values recorded for the suspended solid effect alone. Such fact was approved experimentally in the present investigation.

To explain that, the surfactant molecules tends to form certain kind of aggregates called micelles and these micelles are formed due to the polarity attraction of the surfactant molecules itself. These micelles can act as a one big molecule in the same manner of the polymer molecule but with one more advantage which is the ability of these micelles to reform its structure after passing the high shearing areas in the system while the polymer molecules degrade to small parts called monomers and cannot regain its activity anymore. This is why the surfactants can be used more efficiently in many of the drag reduction application rather than the polymers.

The interference of the surfactants micelles with the turbulent structures carrying the suspended solid will change again the apparent physical properties of the liquid globe forming the eddy. This time the surfactant micelles will add its viscoelastic properties to the effect of the suspended solid, which will make it more difficult to the liquid globe to continue stretching and forming its shape. The viscoelastic property added to the main body of the eddy will act like a spring that can bend for a certain level of shear force but it return to its original shape by its elastic property it carries. This is why the addition of the surfactant to the turbulent structure will add the elastic part needed to suppress the turbulent eddies in the main flow. In the present work, the surfactants job was to improve the drag reduction performance of the suspended solid

and that was also proven experimentally where the surfactant micelles will increase the eddy viscosity

It is very important to mention that by assuming that the apparent physical properties of the liquid globe forming the eddy is changed, that does not mean changing the apparent physical properties of the transported liquid. As it is known the properties of the eddy itself differs than the static liquid. The liquid in the eddy is in dynamic movement and stretching certain parts of the transported liquid totally change the apparent properties of this globe at this moment and it returns to its normal properties when the stretching is off. For example, it is known that the eddy viscosity is much higher than the apparent viscosity of the static liquid.



CHAPTER 5

CONCLUSIONS AND RECOMMENDATIONS

5.1 CONCLUSIONS

In the present investigation, the effectiveness of the suspended solid powders tested (Aluminum, Sand and Coal) was proven and the powders can be introduced as drag reducing agents. In addition, the two Zwitterionic surfactants chosen to be investigated as drag reduction performance enhancers for the suspended solid performance, showed high abilities to improve the drag reduction action of the suspended solids.

The drag reducing agents chosen in the present work were tested with large number of experimental variables and the experimental results showed that:

1. The percentage drag reduction %Dr increases by increasing the solution flow rate for most of the suspended solids used until a certain value where the %Dr start to be more stable in the value or descend. It was concluded that, in a certain range of Reynolds Number (Re), the %Dr start to increase with any increase in the Re which means increasing the turbulence spectrum under the suspended solids effect reaching a maximum point where the suspended solid shows its maximum performance “ which might be considered as optimum performance for this point only”. After that and by a further increase in the value of Re the %Dr start to be more stable or decline in most cases due to the strong action of these turbulent structures on the suspended solid drag reduction abilities.
2. The %Dr increases by increasing the addition concentration. Increasing the addition concentration means increasing the number of suspended solid powders (in the case of suspended solids) or the number of surfactant micelles (in the case of

surfactants), involved in the drag reduction operation and that will lead to the increase in the area of turbulence that is under the new drag reducers effect.

3. The relation between the degree of turbulence and the investigated pipe geometry was so clear when investigating the effect of the pipe diameter and length on the %Dr. The experimental results showed that the values of the %Dr were higher in smaller pipe diameters compared with the larger ones. The experimental work proved that by decreasing the pipe diameter, larger numbers of smaller eddies with smaller space to form itself and to absorb more energy from the main flow will form. It will be much easier for the additives to overcome these small eddies than the larger ones due to the smaller force that these eddies absorb from the main flow. On the other hand, the larger number of eddies in the smaller pipes will balance the drag reduction efficiency of the proposed drag reducing agents, which led to the opposite behavior in some cases. Finally, the consistencies of the suspended solid drag reducing agents were proven from the effect of the testing section length on the %Dr.

4. The %Dr was higher for larger particle sizes investigated. Generally, the %Dr for the powders with the size of 71 μm was higher than that of the 45 μm . This can be considered as general conclusion for most of the powders investigated, but it cannot be so general without limitations. The particle size effect depends on the particle type, particle density and the ability to be suspended in the transported liquid. It is believed that the effect of the larger particles on suppressing the eddies is higher than that of the smaller ones in most of the cases where larger particles have more abilities to change the stretching properties of the liquid globe forming the turbulent eddies.

5. The aluminum powder showed the higher performance as drag reducing agent in most cases compared with the sand and the coal. The purpose behind that is the wide difference in the apparent physical properties of the aluminum powder (especially the density) compared with the other two powders. The higher the density (within certain limits), the better the effect of the suspended solids on suppressing the turbulent eddies inside the main flow, which will lead to a better performance.

6. The two Zwitterionic surfactants chosen (DAPI and NNAP) as Drag reduction performance enhancers showed high abilities to improve the performance of the investigated suspended powders with very small addition concentrations (10,20 and 30 ppm).
7. The addition of the DAPI and NNAP surfactants to all the investigated suspension improved the drag reduction performance and did not change the relation between the %Dr and Re as discussed above for all the addition concentrations.
8. Almost the same behavior for most of the variables investigated were observed with the addition of the surfactants investigated. The relation between the %Dr, pipe diameter, testing section length, addition concentration and particle size were the same which lead us to the conclusion that these additives improve the performance more than changing it in most cases.
9. A numerical model (correlation) is introduced in the present work. The dimensionless relation ($f=aRe^b$) was tested with the experimental data and compared with Virk asymptote for the maximum drag reduction performance. All the experimental data showed good approach to Virk drag reduction asymptote and effect of aluminum powder drag reduction combined with 10 ppm of NNAP surfactant showed the maximum performance with the following suggested correlation: $f = 0.798 Re^{-0.746}$

The graphical presentation of the data extracted from the correlation mentioned above showed higher performance compared with Virk asymptote.

5.2 RECOMMENDATIONS:

1. The usage of wider range of suspended solids with different physical properties to achieve a more unified conclusion regarding the effect of the suspended solid physical properties on the %Dr.

2. Investigating a wider range of the suspended solid particle size to highlight more the effect of the particle size combined with the physical properties of the suspended solid its self on the suspension abilities of the solid in following media.
3. Introducing new visualization techniques in the experimental work to have a clearer vision regarding the real mechanism controlling the drag reduction operation.
4. Building up an advanced mathematical model by the aid of advanced visualization techniques such as the particle image velocimeter (PIV), to compare and validate the experimental data.
5. Carrying out a field test for the new drag reducing agent to transfer the experimental work for commercial application.
6. It is recommended to expand the dimensionless equation to be tested by including the investigated parameters in dimensionless forms such as the effect of pipe diameter to the pipe length (D/L) and the additive concentration plus Reynolds number (Re).

The logo for UMP (Universitas Muhammadiyah Purwokerto) is a large, stylized downward-pointing triangle. It is composed of four smaller triangles meeting at a central point. The top-left triangle is light blue, the top-right is light purple, the bottom-left is light green, and the bottom-right is light blue. The letters 'UMP' are written in a bold, white, sans-serif font across the center of the triangle.

UMP

REFERENCES

- Al-Sarkhi, A. and Hanratty, T. J. 2001. Effect of drag-reducing polymers on annular gas-liquid flow in a horizontal pipe. *International Journal of Multiphase Flow*. **27**: 1151-1162.
- Al-Sarkhi, A., Abu-Nada, E. and Batayneh, M. 2006. Effect of drag reducing polymer on air-water annular flow in an inclined pipe. *International Journal of Multiphase Flow*. **32**: 926-934.
- Al-Wahaibi, T., Smith, M. and Angeli, P. 2007. Effect of drag-reducing polymers on horizontal oil-water flows. *Journal of Petroleum Science and Engineering*. **57**:334-346.
- Andrej Krope and Lucija C. Lipus. 2010. Drag reducing surfactants for district heating. *Applied Thermal Engineering*. **30**. 833-838.
- Antonello A. Barresi. 1997. Experimental investigation of interaction between turbulent liquid flow and solid particles and its effects on fast reactions”, *Chemical Engineering Science*, **52** (5): pp 807-814
- Attwood, A. T. and Florence A. T.,. 1983. *Surfactant systems, their chemistry, pharmacy and biology*. London: Chapman and Hall.
- Backtiyarov, S. I. and Oliver, D. R. 1983. “Drag reduction in exceptionally dilute polymer solutions” *J, Non-Newtonian fluid Mech.*, **12**,: pp 113-118.
- Bandyopadhyay, R., . 1986. Aspects of the Equilibrium Puff in Transitional Pipe Flow. *J.Fluid Mech.* **163**: 439–458.
- Billington, E. W. and Tate, A. 1981. *Physics of deformation and flow*. London: McGraw-Hill Inc.
- Bottural,L. 1999. Friction factor correlations. MICROSOFT. Feb., <http://www.cryosoft.com>
- Cheng, L., Mewes, D. and Luke, A. 2007.Boiling phenomena with surfactants and polymeric additives: A state-of-the-art review. *International Journal of Heat and Mass Transfer*. **50**:2744-2771.
- Cho, S.H., Tae, C.S. and Zaheeruddin, M. 2007. Effect of fluid velocity temperature and concentration of non-ionic surfactants on drag reduction. *Energy Conversion and Management*. **48**:913-918.
- ConocoPhilips . 2006. *Sustainable Development Report*. USA: ConocoPhilips

- Coulson, J.M. and Richardson, J.F. 1999. *Chemical Engineering*, 6thed.Vol.1: Butterworth-Heinemann
- Cowie, J. M. G. 1973. *Polymers: chemistry and physics*.1st ed. London:Billings and Sons Ltd.
- Cruz,D.O.A .Pinho,F.T.and Resende,P.R. 2004. Modelling the new stress for improved drag reduction predictions of viscoelastic pipe flow. *J. Non-Newtonian Fluid Mech.* **121**: 127-141.
- Danov K.D., et. al. 2004. Mixed Solutions of Anionic and Zwitterionic Surfactant (Betaine): Surface Tension Isotherms, Adsorption and Relaxation Kinetics. *Langmuir*. **20**: 5445-5453.
- Davidson, A. and Milwidsky, B.M., 1972. *Synthetic detergents*. 5th edition. London: Leonard Hill.
- Davidson, P.A . 2004. *Turbulence an Introduction for Scientists and Engineers*. Oxford New York: Oxford.
- Dawn Y. 2005. *Fluid flow*. part 1. Geology, University of California, Davis.
- Dean, R. C., .1959. On the necessity of unsteady flow fluid mechanics. *ASME J.***81**: 24-28.
- Dodge, D.W. and Metzner, A.B. 1959. Turbulent Flow in Non-Newtonian Systems. *ALChE J.*, **5**: 189–204.
- Dong, S., Feng, X. and Salcudean, M. G. 2003. Concentration of pulp fibers in 3D turbulent channel flow. *International Journal of Multiphase Flow.*, **29**: 1-21
- Duangprasert, T., Sirivat, A., Siemanond, K and Wilkes, J.O. 2008. Vertical two-phase flow regimes and pressure gradients under the influence of SDS surfactant. *Experimental Thermal and Fluid Science*. **32**: 808-817.
- Finnemore, E. J. and Franzini, J. B. 2002. *Fluid Mechanics with Engineering Application*.10th ed. New York: McGraw-Hill.
- Fichman, M. and Hetsroni,G. 2004. Electrokinetic aspects of turbulent drag reduction in surfactant solutions. *Physics of fluids* 21 October, 16(12).
- Frank, M. White. 1999. *Fluid Mechanics*. 4th edition. New York: McGraw-Hill.
- Friedmann, M., Gillis, J. and Liron, N. 1968. Laminar flow in a pipe at low and moderate Reynolds numbers. *Applied Scientific Research*. **19**: 426-438.

- Ge, W., Kesselman, E., Talmon, Y., Hart, D.J. and Zakin, J.L. 2008. Effects of chemical structures of para-halobenzoates on micelle nanostructure, drag reduction and rheological behaviors of dilute CTAC solutions. *J. Non-Newtonian Fluid Mech.*, **154**: 1-12.
- Hall, C.D. and Osterhout, R. S. 1961. Reduction of friction loss in fracturing operations. *J. Pet. Tech.* **13**: 217-222
- Hamilton, J.M., Kim, J. and Walefe, F. 1995. Regeneration mechanism of near-wall turbulence structure. *J. Fluid Mech.* **287**: 317-348.
- Hayder A. Abdul Bari, Emma Suali and Zulkafli Bin Hassan. 2008. "Investigating the Behavior of Copper Powder as Drag reducing Agent in Aqueous Media". Engineering Postgraduate Conference (EPC), UKM.
- Hayder, A.A.B. 2006. Studying the effect of polycrylamide on increasing the percentage drag reduction established by using two types of suspended solids in water. Working Paper. Proceedings of the 11th APCCChE Congress 2006. Kuala Lumpur: 27-30 August.
- Hershy, H. C., Mcmillan, M. L. and Boxter, R. A.,. 1971. Effect of aging, concentration, temperature, method of preparation and other variables on the drag reduction. *Chem. Eng. Progr. Symp.* ,**111**: 67-74.
- Heywood, Karen J. 1993. Fluid Flows in the Environment: An Introduction. *Physics Education* **28**:43.
- Hiemenz, P.C. ; Rajagopalan, R. , .1997. *Principle of colloid and surface chemistry*. 3rded. New York: Dekker.
- Holland, F. A. 1973. *Fluid flow for chemical engineering*. 1sted London, Edward Arnold,
- Holland, F. A. and Bragg, R., .1995. *Fluid Flow for Chemical Engineers*. 2nd ed. London: Edward Arnold. A division of Hodder Headline PLC, 56.
- Hoyer, K.W. and Gyr, A. 1998. Heterogeneous Drag Reduction Concepts and Consequences. *Journal of Fluid Engineering*. **120**: 818-823.
- Hoyt, J. W. 1972. The effect of additives on fluid friction. *ASME J. Basi Eng.*:**94**: 258-293.
- Hunt, J.C.R. and Caruthers, D.J. 1990. Rapid Distortion Theory and the 'Problems' of Turbulence. *J. Fluid Mech.* **212**: 497-532.
- Inaba, H., Haruki, N. and Horibe, A. 2000. Flow drag and heat transfer reduction of flowing water containing fibrous material in a straight pipe. *Int. J. Therm. Sci.*, **39**: 18-29.

- Inaba, H., K. Ozaki, Haruki, N. and Asano, H., 1995. Flow resistance and heat transfer characteristics of water solution flow with surfactant in circular tubes. *Trans. Jap. Soc. Mech. Eng.*, **61**:3304-3310.
- Indartono Y.S. et.al. 2005. Temperature and diameter effect on hydrodynamic characteristic of surfactant drag-reducing flow. *Korea-Australia Rheology Journal*, **17**:157-164.
- Jamal Saleh. 2002. *Fluid flow handbook*. New York: McGraw-Hill Companies, In. *Journal of Heat and Mass Transfer*. **49**: 1462-1471.
- Kang, K.H., Kim, H.U., Lim, K.H. and Jeong, N.H. 2001. Mixed micellization of anionic ammonium dodecyl sulfate and cationic octadecyl trimethyl ammonium chloride. *Bull. Korean Chem. Soc.*, **22** (9):1009 - 1014.
- Kawaguchi, Y., Segawa, T., Feng, Z. and Li, P. 2002. Experimental study on drag-reducing channel flow with surfactant additives-spatial structure of turbulence investigated by PIV system. *International Journal of Heat and Fluid Flow.*, **23**: 700-709.
- Kazi, M.S.N., Duffy, G.G and Chen, X. D. 1999. Heat transfer in the drag reducing regime of wood pulp fibre suspensions. *Chemical Engineering Journal* .**73**: 247-253.
- Kerekes, R. J. and Garner, R. G., .1982. Measurement of Turbulence in Pulp Suspension by Laser Anemometry. *Trans. Tech. Sect. CPPA*, **8**(3): 53-69.
- Lee, W.K. R.C. 1974. Turbulent drag reduction in polymeric solutions containing suspended fibers. *AICHE J.*, **20**(2): 128-134.
- Lester, C.B. 1985. The basic of drag reduction. *Oil & Gas J.* **83**, **5**:51-56.
- Li, F.C., Kawaguchi, Y., Yu, B., Wei, J.J. and Hishida. K. 2008. Experimental study of drag reduction mechanism for a dilute surfactant solution flow. *International Journal of Heat and Mass Transfer* .**51**:835-843.
- Li, Y.H., Plano and Tex. 1991. *Drag Reduction for Gas Pipelines*. U.S. Patent 5,020,561.
- Lu, B., Li, X., Scriven, L.E., Davis, H.T., Talmon, Y. and Zakin, J.L. 1998. Effect of Chemical Structure on Viscoelasticity and Extensional Viscosity of Drag-Reducing Cationic Surfactant Solutions .*Langmuir*.**14**:8-16.
- Luetgen, C.O., Lindsay, J. D. and Stratton, R.A. 1991. Turbulent dispersion in pulp flow: preliminary results and implications for the mechanisms of fiber-turbulence interactions. *ipst technical paper series*. **408**.

- Luettgen, C.O., Lindsay, J.D. and Stratton, R.A. 1991. Turbulent dispersion in pulp flow: Preliminary results and implications for the mechanisms of fiber-turbulence interactions. Technical Paper. IPST Georgia: IPST Technical Paper Series No.408.
- Manhart M. 2003. Rheology of suspensions of rigid-rod like particles in turbulent channel flow, *J. Non-Newtonian Fluid Mech.* **112**: pp 269–293 McGraw-Hill.
- Min, T. and Choi, H. 2005. Combined effects of polymers and active blowing/suction on drag reduction. *J. Non-Newtonian Fluid Mech.* **131**:53-58.
- Moghaddam, M. D. and Toll. S. 2006. Fibre suspension rheology: effect of concentration, aspect ratio and fibre size. *Rheol Acta.***45**:315-320.
- Molerus, O. and Heucke, U. 1999. Pneumatic transport of coarse grained particles in horizontal pipes. *Powder Technology.***102**:135-150.
- Mowla, D. and Naderi, A. 2006. Experimental study of drag reduction by a polymeric additive in slug two-phase flow of crude oil and air in horizontal pipes. *Chemical Engineering Science.* **61**:1549-1554.
- Mysels, K.J., Agoston, G. A., Harte, H. W., Hottel, H.C., Klemm, W.A., Pomeroy, H.H. and Thompson, J.M., .1954. Flow of gasoline thickened by napalm. *Ind. Eng. Chem.* **46**: 1017-1019.
- Myska, J. and Mik, V. 2003. Application of a Drag Reducing Surfactant in the Heating Circuit. *Energy and Buildings.***35**: 813-819.
- Myska, J. and Mik, V. 2004. Degradation of surfactant solutions by age and by a flow singularity. *Chemical Engineering and Processing.* **43**: 1495-1501.
- Nelson. J. 2004. Optimising production using drag reducing agents in water injection wells (technical paper online).
http://www.liquidpower.com/EN/whatsnew/csapi%20news/documents/oe_techpaper.pdf
- Nicole Marheineke and Raimund Wegener. 2010. Modeling and application of a stochastic drag for fibers in turbulent flows, *International Journal of Multiphase Flow.* 1st October 2010 (In press).
- Oldroyd, J. G. 1948. *A suggested method of detecting wall effects in turbulent flow through pipes.* In Proc. First Int. Congr. on Rheol., Vol.2, North Holland, Amsterdam, 130-134.
- Paul J. Krochak , James A. Olson ,D. Mark Martinez. 2009. Fiber suspension flow in a tapered channel: The effect of flow/fiber coupling. *International Journal of Multiphase Flow.*, **35**: 676–688.

- Perry, R.H., Chilton, C.H. and Kirkpatrick, S.D. 1963. *Chemical Engineers' Handbook: Prepared by a staff of specialists*. University of Michigan: McGraw-Hill.
- Peyser, P., .1973. The drag reduction of chrysotil asbestos dispersion. *J. App. Polymer Sci.*, **17**: 421-429.
- Qi, Y.,and Zakin,J.L . 2002. Chemical and Rheological Characterization of Drag-Reducing Cationic Surfactant Systems. *Ind. Eng. Chem. Res.*, **41**: 6326-6336
- Radin, I.; Zakin, J. L., and Patterson, G. K., . 1975. Drag Reduction in Solid-Fluid Systems. *AIChE J.*, **21**(2): 358.
- Ragsdale, R. 2007. Chemical additive enables Alyeska Pipeline Service Co. to achieve huge cost savings. *Petroleum News*.-12 (41).
- Ram, A., Elata, C. and Finkelstin, E., . 1967. Reduction of friction in oil pipelines by polymer additives. *Ind. Eng. Chem.*, **6**: 381-391.
- Rashidi, M. and Banerjee, S. 1990. The effect of boundary conditions and shear rate on streak formation and break down in turbulent channel flows. *Phys. Of Fluids A2*. 1827-1831.
- Ray, A. 1971. Solvophobic Interactions and Micelle Formation in Structure Forming Nonaqueous Solvents .*Nature*.**231**: 313-315.
- Roberto,B. 2002. A simple model for drag reduction. <http://www.arxiv:Cond mat/0210523>.v1.(Oct. 2002).
- Rose, G. D., Faster, K. L., Slocum, V. L. and Lenhart, J. G., . 1984. *Drag reduction and heat transfer of viscoelastic surfactant*. 3rd Int. Conf. on the drag reduction, Bristol, paper D6.
- Rosen, M. J. 2004. *Surfactants and Interfacial Phenomena*. USA: John Wiley & Sons, Incorporated.
- Rosen, M. J. 2004. *Surfactants and Interfacial Phenomena*. USA: John Wiley & Sons, Incorporated.
- Rozenblit, R., Gurevich, M., Lengel, Y. and Hetsroni, G. 2006. Flow patterns and heat transfer in vertical upward air-water flow with surfactant. *International Journal of Multiphase Flow* .**32**: 889-901.
- Seely, T. L., 1968. Turbulent Tube Flow of Dilute Fiber Suspensions. *Ph.D. Dissertation, Institute of Paper Chemistry, Appleton, WI*.
- Sellin, R. H. J and M. Ollis .1980. "Polymer Drag Reduction in Large Pipes and Sewers: *Results of Recent Field* "Trials *J. Rheol.* , **24**(5): 667-684

- Shanliang, Z., Jianzhong, L. and Weifeng, Z. 2007. Numerical Research on the Fiber Suspensions in a turbulent T-shaped Branching Channel Flow. *Chin. J. Chem. Eng.* **15**(1): 30-38.
- Sharma, R., Ed.,. 1995. Surfactant Adsorption and surface Solubilization. *American Chemical Society*. Washington.
- Skelland, A. H. P. 1967. *Non-Newtonian Flow and Heat Transfer*. John Wiley: New York .
- Solomons, T.W.G. and Fryhle, C.B. 2004 .*Organic Chemistry*. 8th ed. Singapore: John Wiley & Sons (Asia) Pte. Ltd.
- Suksamranchit, S. and Sirivat, A. 2007. Influence of Ionic Strength on Complex Formation between Poly (ethylene oxide) and Cationic Surfactant and Turbulent Wall Shear Stress in Aqueous Solution. *Chemical Engineering Journal*. **128**: 11-20.
- Toms, B. A. 1948. Some observations on the flow of linear polymer solutions through straight pipe at large Reynolds numbers. Proceeding of the international congress on rheology, Scheveningen. The Netherlands. **2**: 135-141.
- Toms. B.A. 1949. *Proceedings of International Congress on Rheology*. Vol. II, pp. 135, North Holland, Amsterdam.
- Tullis, J. P and Rama, k. L. V., 1974, "Drag reduction in developed pipe flow with polymer injection", Int. Conf. on drag reduction, University of Cambridge, BHRA, paper G3.
- Varade, D., Abreu, C.R., Shrestha, L.K. and Aramaki, K. 2007. Wormlike Micelles in Mixed Surfactant Systems: Effect of Cosolvents. *Phys. Chem.B.*, **111**: 10438-10447.
- Vaseleski, R. C. and Metzner, A. B .1974. Drag reduction in the turbulent flow of fiber suspensions. *AICHE J.*, **20**: 301-306
- Versteeg, H.K. and Malalasekera, W.,. 1995. *An introduction to computational fluid dynamic*. New York: Longman group Ltd. 41.
- Virk, P. S., Merrill, E. W., Mickely, H. S, Smith, K. A. and Mollo, E.L. 1967. The Toms phenomena: turbulent pipe flow of dilute polymer solution. *J. Fluid Mech.* **30**: 20-31.
- Virk, P.S. 1975. Drag reduction fundamentals. *AICHE J.* **21**: 625-656.

- Warholic, M.D., Massah, H. and Hanratty, T. J. 1999. Influence of drag-reducing polymers on turbulence: effects of Reynolds number, concentration and mixing. *Experiments in Fluids*. **27**: 461- 472.
- White, A., 1967. Flow characteristics of complex soap system. *Nature*, **214**: 585-586.
- Wilkins, R.J. and Thomas, D.K. 2007. Effect of eliminating slugs. *International Journal of Multiphase Flow*. **33**:134-146.
- Wilmarth, T., Ishii, M., 1993. Two-phase flow regimes in narrow rectangular vertical and horizontal channels. *Int. J. Heat Mass Transfer*. **37**:1749-1758.
- Xu, J. L., Cheng, P. and Zhao, T. S. 1999. Gas-liquid two-phase flow regimes in rectangular channels with mini/micro gaps. *International Journal of Multiphase flow*, **25**: 411- 432
- Yunus A, et. al. 2006. *Fluid Mechanics Fundamental and Applications*. New York:
- Zakin, J. L., 1983. Variables affecting drag reduction by non-ionic surfactant additives. *Chem. Eng. Common.* , **23**: 77-88.
- Zhang, Y., Schmidt, J., Talmon, Y. and Zakin, J. L. 2005. Co-solvent effects on drag reduction, rheological properties and micelle microstructures of cationic surfactants. *Journal of Colloid and Interface Science*, **286**: 696-709.
- Zhou, T., Leong, K.C. and Yeo, K.H. 2006. Experimental study of heat transfer enhancement in a drag-reducing two-dimensional channel flow. *International Journal of Heat and Mass Transfer*. 49:1462-1471.

APPENDIX A1

EXPERIMENTAL DATA FOR COAL POWDER ($D_p=45$, $D=0.0127$ m, $L=0.5$ m)

Conc. =100 ppm

ΔP_b	ΔP_a	%Dr	$Q(m^3/s)$	$v(m/s)$	Re	f
1619	1496	7.574154	0.0002	1.579118	22533.48	762.2191
3552	3238	8.84907	0.00035	2.763457	39433.59	538.5029
6098	5442	10.75172	0.00045	3.553016	50700.34	547.4975
8600	7755	9.826344	0.00055	4.342575	61967.08	522.2719
11762	10204	13.24488	0.00065	5.132134	73233.82	492.0188
19242	16327	15.14939	0.00085	6.711252	95767.3	460.3525

Conc. =300 ppm

ΔP_b	ΔP_a	%Dr	$Q(m^3/s)$	$v(m/s)$	Re	f
1619	1429	11.77533	0.0002	1.579118	22533.48	727.5728
3553	2993	15.74284	0.00035	2.763457	39433.59	497.7758
6098	4898	19.67655	0.00045	3.553016	50700.34	492.7477
8600	6803	20.9003	0.00055	4.342575	61967.08	458.1332
11761	9252	21.34202	0.00065	5.132134	73233.82	446.0971
19242	14966	22.22027	0.00085	6.711252	95767.3	421.9898

Conc. =500 ppm

ΔP_b	ΔP_a	%Dr	$Q(m^3/s)$	$v(m/s)$	Re	f
1619	1429	11.77533	0.0002	1.579118	22533.48	727.5728
3553	2857	19.57271	0.00035	2.763457	39433.59	475.1496
6098	4490	26.37017	0.00045	3.553016	50700.34	451.6854
8600	5986	30.39227	0.00055	4.342575	61967.08	403.1572
11761	8163	30.5959	0.00065	5.132134	73233.82	393.615
19242	12925	32.8266	0.00085	6.711252	95767.3	364.4458

APPENDIX A2

EXPERIMENTAL DATA FOR COAL POWDER ($D_p = 45$, $D = 0.0127$ m, $L = 1$ m)

Conc. =100 ppm

ΔP_b	ΔP_a	%Dr	$Q(m^3/s)$	$v(m/s)$	Re	f
2739	2449	10.57174	0.0002	1.579118	22533.48	623.6338
7391	6667	9.795608	0.00035	2.763457	39433.59	554.3412
11767	10476	10.96988	0.00045	3.553016	50700.34	526.9663
16772	13197	21.31269	0.00055	4.342575	61967.08	444.3892
23095	17687	23.41699	0.00065	5.132134	73233.82	426.4163
40626	32381	20.29472	0.00085	6.711252	95767.3	456.5163

Conc. =300 ppm

ΔP_b	ΔP_a	%Dr	$Q(m^3/s)$	$v(m/s)$	Re	f
2739	2449	10.57174	0.0002	1.579118	22533.48	623.6338
7391	6259	15.31833	0.00035	2.763457	39433.59	520.4019
11767	9932	15.59482	0.00045	3.553016	50700.34	499.5914
16772	12381	26.17994	0.00055	4.342575	61967.08	416.9012
23095	15646	32.25349	0.00065	5.132134	73233.82	377.2144
40626	27211	33.02077	0.00085	6.711252	95767.3	383.6271

Conc. =500 ppm

ΔP_b	ΔP_a	%Dr	$Q(m^3/s)$	$v(m/s)$	Re	f
2739	2422	11.56539	0.0002	1.579118	22533.48	616.7046
7391	5714	22.68195	0.00035	2.763457	39433.59	475.1496
11767	9524	19.06352	0.00045	3.553016	50700.34	479.0603
16772	11565	31.0472	0.00055	4.342575	61967.08	389.4132
23095	14286	38.14449	0.00065	5.132134	73233.82	344.4132
40626	27211	33.02077	0.00085	6.711252	95767.3	383.6271

APPENDIX A3

EXPERIMENTAL DATA FOR COAL POWDER ($D_p = 45$, $D = 0.0127$ m, $L = 1.5$ m)

Conc. =100 ppm

ΔP_b	ΔP_a	%Dr	$Q(m^3/s)$	$v(m/s)$	Re	f
4072	3674	9.787395	0.0002	1.579118	22533.48	623.6338
11157	9932	10.9828	0.00035	2.763457	39433.59	550.5702
17364	13605	21.64936	0.00045	3.553016	50700.34	456.2479
25586	19184	25.02357	0.00055	4.342575	61967.08	430.6452
34500	25850	25.07168	0.00065	5.132134	73233.82	415.4826
52010	37007	28.84705	0.00085	6.711252	95767.3	347.8219

Conc. =300 ppm

ΔP_b	ΔP_a	%Dr	$Q(m^3/s)$	$v(m/s)$	Re	f
4072	3401	16.46981	0.0002	1.579118	22533.48	577.4387
11157	9524	14.64104	0.00035	2.763457	39433.59	527.944
17364	13061	24.78338	0.00045	3.553016	50700.34	437.998
25586	18640	27.15056	0.00055	4.342575	61967.08	418.4283
34500	24762	28.22655	0.00065	5.132134	73233.82	397.9885
52010	36735	29.37023	0.00085	6.711252	95767.3	345.2644

Conc. =500 ppm

ΔP_b	ΔP_a	%Dr	$Q(m^3/s)$	$v(m/s)$	Re	F
4072	3674	9.787395	0.0002	1.579118	22533.48	623.6338
11157	8299	25.61576	0.00035	2.763457	39433.59	460.0655
17364	12245	29.48442	0.00045	3.553016	50700.34	410.6231
25586	17687	30.87279	0.00055	4.342575	61967.08	397.0488
34500	23946	30.59271	0.00065	5.132134	73233.82	384.868
52010	35374	31.98615	0.00085	6.711252	95767.3	332.4768

APPENDIX A4

EXPERIMENTAL DATA FOR COAL POWDER ($D_p = 45$, $D = 0.0127$ m, $L = 2$ m)

Conc. =100 ppm

ΔP_b	ΔP_a	%Dr	$Q(m^3/s)$	$v(m/s)$	Re	f
5477	4898	10.57174	0.0002	1.579118	22533.48	623.6338
14924	13197	11.57071	0.00035	2.763457	39433.59	548.6846
23677	18095	23.57427	0.00045	3.553016	50700.34	455.1073
34329	25850	24.69893	0.00055	4.342575	61967.08	435.2266
46048	35374	23.1794	0.00065	5.132134	73233.82	426.4163
63395	48980	22.73851	0.00085	6.711252	95767.3	345.2644

Conc. =300 ppm

ΔP_b	ΔP_a	%Dr	$Q(m^3/s)$	$v(m/s)$	Re	f
5477	4830	11.8138	0.0002	1.579118	22533.48	614.9723
14924	12109	18.86385	0.00035	2.763457	39433.59	503.4323
23677	18367	22.42501	0.00045	3.553016	50700.34	461.951
34329	27211	20.73572	0.00055	4.342575	61967.08	458.1332
46048	32653	29.08868	0.00065	5.132134	73233.82	393.615
63395	46259	27.03081	0.00085	6.711252	95767.3	326.0831

Conc. =500 ppm

ΔP_b	ΔP_a	%Dr	$Q(m^3/s)$	$v(m/s)$	Re	f
5477	4626	15.53998	0.0002	1.579118	22533.48	588.9875
14924	11157	25.24534	0.00035	2.763457	39433.59	463.8365
23677	17007	28.17131	0.00045	3.553016	50700.34	427.7324
34329	24490	28.66215	0.00055	4.342575	61967.08	412.3199
46048	29932	34.99796	0.00065	5.132134	73233.82	360.8138
63395	43537	31.32312	0.00085	6.711252	95767.3	306.9017

APPENDIX A5

EXPERIMENTAL DATA FOR COAL POWDER ($D_p = 71$, $D = 0.0127$ m, $L = 0.5$ m)

Conc. =100 ppm

ΔP_b	ΔP_a	%Dr	$Q(m^3/s)$	$v(m/s)$	Re	f
1619	1497	7.574154	0.0002	1.579118	22533.48	762.2191
3553	3143	11.52998	0.00035	2.763457	39433.59	522.6646
6098	5410	11.28721	0.00045	3.553016	50700.34	544.2125
8600	7619	11.40834	0.00055	4.342575	61967.08	513.1092
11762	9238	21.45769	0.00065	5.132134	73233.82	445.441
19242	15810	17.83632	0.00085	6.711252	95767.3	445.7747

Conc. =300 ppm

ΔP_b	ΔP_a	%Dr	$Q(m^3/s)$	$v(m/s)$	Re	f
1619	1410	12.95166	0.0002	1.579118	22533.48	717.8718
3553	2857	19.57271	0.00035	2.763457	39433.59	475.1496
6098	4762	21.90775	0.00045	3.553016	50700.34	479.0603
8600	6476	24.69709	0.00055	4.342575	61967.08	436.1428
11762	9252	21.34202	0.00065	5.132134	73233.82	446.0971
19242	14191	26.25067	0.00085	6.711252	95767.3	400.1231

Conc. =500 ppm

ΔP_b	ΔP_a	%Dr	$Q(m^3/s)$	$v(m/s)$	Re	f
1619	1429	11.77533	0.0002	1.579118	22533.48	727.5728
3553	2857	19.57271	0.00035	2.763457	39433.59	475.1496
6098	4467	26.74947	0.00045	3.553016	50700.34	449.3586
8600	5620	34.66365	0.00055	4.342575	61967.08	378.418
11762	8163	30.5959	0.00065	5.132134	73233.82	393.615
19242	12571	34.66503	0.00085	6.711252	95767.3	354.4715

APPENDIX A6

EXPERIMENTAL DATA FOR COAL POWDER ($D_p = 71$, $D = 0.0127$ m, $L = 1$ m)

Conc. =100 ppm

ΔP_b	ΔP_a	%Dr	$Q(m^3/s)$	$v(m/s)$	Re	f
2739	2449	10.57174	0.0002	1.579118	22533.48	623.6338
7391	6591	10.82652	0.00035	2.763457	39433.59	548.0059
11767	10286	12.58861	0.00045	3.553016	50700.34	517.3851
16772	13197	21.31269	0.00055	4.342575	61967.08	444.3892
23095	17687	23.41699	0.00065	5.132134	73233.82	426.4163
40626	33333	17.95045	0.00085	6.711252	95767.3	469.9432

Conc. =300 ppm

ΔP_b	ΔP_a	%Dr	$Q(m^3/s)$	$v(m/s)$	Re	f
2739	2449	10.57174	0.0002	1.579118	22533.48	623.6338
7391	6000	18.81605	0.00035	2.763457	39433.59	498.9071
11767	9429	19.87289	0.00045	3.553016	50700.34	474.2697
16772	12191	27.31564	0.00055	4.342575	61967.08	410.4874
23095	15646	32.25349	0.00065	5.132134	73233.82	377.2144
40626	27211	33.02077	0.00085	6.711252	95767.3	383.6271

Conc. =500 ppm

ΔP_b	ΔP_a	%Dr	$Q(m^3/s)$	$v(m/s)$	Re	f
2739	2422	11.56539	0.0002	1.579118	22533.48	616.7046
7391	5714	22.68195	0.00035	2.763457	39433.59	475.1496
11767	9522	19.06352	0.00045	3.553016	50700.34	479.0603
16772	11565	31.0472	0.00055	4.342575	61967.08	389.4132
23095	14286	38.14449	0.00065	5.132134	73233.82	344.4132
40626	27211	33.02077	0.00085	6.711252	95767.3	383.6271

APPENDIX A7

EXPERIMENTAL DATA FOR COAL POWDER ($D_p = 71$, $D = 0.0127$ m, $L = 1.5$ m)

Conc. =100 ppm

ΔP_b	ΔP_a	%Dr	$Q(m^3/s)$	$v(m/s)$	Re	f
4072	3674	9.787395	0.0002	1.579118	22533.48	623.6338
11157	9932	10.9828	0.00035	2.763457	39433.59	550.5702
17365	13333	23.21637	0.00045	3.553016	50700.34	447.1229
25586	18857	26.29976	0.00055	4.342575	61967.08	423.3151
34500	25238	26.84629	0.00065	5.132134	73233.82	405.6422
52010	37007	28.84705	0.00085	6.711252	95767.3	347.8219

Conc. =300 ppm

ΔP_b	ΔP_a	%Dr	$Q(m^3/s)$	$v(m/s)$	Re	f
4072	3401	16.46981	0.0002	1.579118	22533.48	577.4387
11157	9524	14.64104	0.00035	2.763457	39433.59	527.944
17365	12191	29.79782	0.00045	3.553016	50700.34	408.7981
25586	18640	27.15056	0.00055	4.342575	61967.08	418.4283
34500	24762	28.22655	0.00065	5.132134	73233.82	397.9885
52010	36735	29.37023	0.00085	6.711252	95767.3	345.2644

Conc. =500 ppm

ΔP_b	ΔP_a	%Dr	$Q(m^3/s)$	$v(m/s)$	Re	f
4072	3674	9.787395	0.0002	1.579118	22533.48	623.6338
11157	8191	26.59129	0.00035	2.763457	39433.59	454.0318
17365	12245	29.48442	0.00045	3.553016	50700.34	410.6231
25586	17143	32.99979	0.00055	4.342575	61967.08	384.8319
34500	23946	30.59271	0.00065	5.132134	73233.82	384.868
52010	35374	31.98615	0.00085	6.711252	95767.3	332.4768

APPENDIX A8

EXPERIMENTAL DATA FOR COAL POWDER ($D_p = 71$, $D = 0.0127$ m, $L = 2$ m)

Conc. =100 ppm

ΔP_b	ΔP_a	%Dr	$Q(m^3/s)$	$v(m/s)$	Re	f
5477	4898	10.57174	0.0002	1.579118	22533.48	623.6338
14924	13197	11.57071	0.00035	2.763457	39433.59	548.6846
23677	18095	23.57427	0.00045	3.553016	50700.34	455.1073
34329	25524	25.65011	0.00055	4.342575	61967.08	429.729
46048	35048	23.88852	0.00065	5.132134	73233.82	422.4802
63395	48980	22.73851	0.00085	6.711252	95767.3	345.2644

Conc. =300 ppm

ΔP_b	ΔP_a	%Dr	$Q(m^3/s)$	$v(m/s)$	Re	f
5477	4830	11.8138	0.0002	1.579118	22533.48	614.9723
14924	12109	18.86385	0.00035	2.763457	39433.59	503.4323
23677	17619	25.58547	0.00045	3.553016	50700.34	443.1308
34329	27211	20.73572	0.00055	4.342575	61967.08	458.1332
46048	32381	29.67961	0.00065	5.132134	73233.82	390.3349
63395	46259	27.03081	0.00085	6.711252	95767.3	326.0831

Conc. =500 ppm

ΔP_b	ΔP_a	%Dr	$Q(m^3/s)$	$v(m/s)$	Re	f
5477	4626	15.53998	0.0002	1.579118	22533.48	588.9875
14924	11157	25.24534	0.00035	2.763457	39433.59	463.8365
23677	17007	28.17131	0.00045	3.553016	50700.34	427.7324
34329	24490	28.66215	0.00055	4.342575	61967.08	412.3199
46048	29932	34.99796	0.00065	5.132134	73233.82	360.8138
63395	43537	31.32312	0.00085	6.711252	95767.3	306.9017

APPENDIX A9

**EXPERIMENTAL DATA FOR COAL POWDER (NNAP 20 ppm, D_p =45,
D=0.0254 m, L=0.5 m)**

Conc. =100 ppm

ΔP_b	ΔP_a	%Dr	Q(m ³ /s)	v(m/s)	Re	f
148	136	8.351203	0.0003	0.592169	16900.11	981.5811
367	321	12.60363	0.0005	0.986763	28161.54	836.7224
716	651	9.193351	0.0008	1.57882	45058.46	662.8358
1215	935	23.08091	0.0011	2.170878	61955.39	503.7084
1623	1330	18.03195	0.0013	2.565583	73220	513.3377
2044	1306	36.09121	0.001488	2.936606	83808.74	384.7579

Conc. =300 ppm

ΔP_b	ΔP_a	%Dr	Q(m ³ /s)	v(m/s)	Re	f
148	1295	-775.573	0.0003	0.592169	16900.11	9377.605
367	1272	-246.564	0.0005	0.986763	28161.54	3317.963
716	122	83.02183	0.0008	1.57882	45058.46	123.9308
1215	120	90.16729	0.0011	2.170878	61955.39	64.38998
1623	121	92.57291	0.0013	2.565583	73220	46.51333
2044	1348	34.05992	0.001488	2.936606	83808.74	396.9871

Conc. =500 ppm

ΔP_b	ΔP_a	%Dr	Q(m ³ /s)	v(m/s)	Re	f
148	129	13.04651	0.0003	0.592169	16900.11	931.2932
367	256	30.13563	0.0005	0.986763	28161.54	668.8731
716	531	25.87702	0.0008	1.57882	45058.46	541.0547
1215	848	30.18906	0.0011	2.170878	61955.39	457.1604
1623	1147	29.33789	0.0013	2.565583	73220	442.5325
2044	1339	34.47774	0.001488	2.936606	83808.74	394.4716

APPENDIX A10

**EXPERIMENTAL DATA FOR COAL POWDER (NNAP 20 ppm, $D_p = 45$,
 $D=0.0254$ m, $L=1$ m)
 Conc. =100 ppm**

ΔP_b	ΔP_a	%Dr	Q(m ³ /s)	v(m/s)	Re	f
246	195	20.76888	0.0003	0.592169	16900.11	705.1089
534	464	13.05884	0.0005	0.986763	28161.54	605.569
1283	1122	12.56641	0.0008	1.57882	45058.46	571.3942
2230	1927	13.60639	0.0011	2.170878	61955.39	519.1894
3046	2613	14.22354	0.0013	2.565583	73220	504.0884
3978	3303	16.97524	0.001488	2.936606	83808.74	486.3943

Conc. =300 ppm

ΔP_b	ΔP_a	%Dr	Q(m ³ /s)	v(m/s)	Re	f
246	184	25.03372	0.0003	0.592169	16900.11	667.1545
534	451	15.6496	0.0005	0.986763	28161.54	587.5237
1283	1062	17.2089	0.0008	1.57882	45058.46	541.0547
2230	1607	27.93186	0.0011	2.170878	61955.39	433.0993
3046	2261	25.77186	0.0013	2.565583	73220	436.2216
3978	3301	17.02002	0.001488	2.936606	83808.74	486.132

Conc. =500 ppm

ΔP_b	ΔP_a	%Dr	Q(m ³ /s)	v(m/s)	Re	f
246	180	26.95593	0.0003	0.592169	16900.11	650.048
534	416	22.11398	0.0005	0.986763	28161.54	542.4975
1283	893	30.39141	0.0008	1.57882	45058.46	454.9046
2230	1532	31.32246	0.0011	2.170878	61955.39	412.7232
3046	2124	30.269	0.0013	2.565583	73220	409.7929
3978	2679	32.66593	0.001488	2.936606	83808.74	394.4716

APPENDIX A11

**EXPERIMENTAL DATA FOR COAL POWDER (NNAP 20 ppm, D_p =45,
D=0.0254 m, L=1.5 m)**

Conc. =100 ppm

ΔP_b	ΔP_a	%Dr	Q(m ³ /s)	v(m/s)	Re	f
344	324	5.756122	0.0003	0.592169	16900.11	781.8264
851	718	15.63811	0.0005	0.986763	28161.54	624.2816
1949	1593	18.27086	0.0008	1.57882	45058.46	541.0547
2945	2411	18.14349	0.0011	2.170878	61955.39	433.0993
4669	3670	21.39827	0.0013	2.565583	73220	472.0347
6067	4643	23.47422	0.001488	2.936606	83808.74	455.8338

Conc. =300 ppm

ΔP_b	ΔP_a	%Dr	Q(m ³ /s)	v(m/s)	Re	f
344	306	10.85039	0.0003	0.592169	16900.11	739.5655
851	708	16.81128	0.0005	0.986763	28161.54	615.6
1949	1429	26.70323	0.0008	1.57882	45058.46	485.2316
2945	2243	23.83859	0.0011	2.170878	61955.39	402.9667
4669	3395	27.2934	0.0013	2.565583	73220	436.6321
6067	4414	27.23952	0.001488	2.936606	83808.74	433.4054

Conc. =500 ppm

ΔP_b	ΔP_a	%Dr	Q(m ³ /s)	v(m/s)	Re	f
344	286	16.84364	0.0003	0.592169	16900.11	689.8468
851	658	22.6947	0.0005	0.986763	28161.54	572.0625
1949	1351	30.66522	0.0008	1.57882	45058.46	459.0029
2945	1947	33.89235	0.0011	2.170878	61955.39	349.7727
4669	3214	31.1533	0.0013	2.565583	73220	413.4518
6067	4087	32.63683	0.001488	2.936606	83808.74	401.2557

APPENDIX A12

**EXPERIMENTAL DATA FOR COAL POWDER (NNAP 20 ppm, Dp =45,
D=0.0254 m, L=2 m)**

Conc. =100 ppm

ΔP_b	ΔP_a	%Dr	Q(m ³ /s)	v(m/s)	Re	f
442	366	17.07504	0.0003	0.592169	16900.11	662.8997
1093	870	20.44568	0.0005	0.986763	28161.54	567.0881
2615	2408	7.93763	0.0008	1.57882	45058.46	613.3704
4660	4000	14.16429	0.0011	2.170878	61955.39	538.968
6492	5043	22.32	0.0013	2.565583	73220	486.4831
8356	6814	18.45254	0.001488	2.936606	83808.74	501.7585

Conc. =300 ppm

ΔP_b	ΔP_a	%Dr	Q(m ³ /s)	v(m/s)	Re	f
442	367	16.87092	0.0003	0.592169	16900.11	664.5313
1093	866	20.76532	0.0005	0.986763	28161.54	564.8096
2615	2018	22.85804	0.0008	1.57882	45058.46	513.9624
4660	3604	22.67053	0.0011	2.170878	61955.39	485.5568
6492	4867	25.02313	0.0013	2.565583	73220	469.5544
8356	6250	25.20404	0.001488	2.936606	83808.74	460.2168

Conc. =500 ppm

ΔP_b	ΔP_a	%Dr	Q(m ³ /s)	v(m/s)	Re	F
442	367	16.87092	0.0003	0.592169	16900.11	664.5313
1093	856	21.69992	0.0005	0.986763	28161.54	558.1475
2615	1835	29.84297	0.0008	1.57882	45058.46	467.4249
4660	3125	32.94085	0.0011	2.170878	61955.39	421.0687
6492	4386	32.43711	0.0013	2.565583	73220	423.1232
8356	5405	35.3116	0.001488	2.936606	83808.74	398.0254

APPENDIX A13

**EXPERIMENTAL DATA FOR COAL POWDER (DAPI 30 ppm, $D_p = 71$,
 $D=0.0127$ m, $L=0.5$ m)**

Conc. =100 ppm

ΔP_b	ΔP_a	%Dr	$Q(m^3/s)$	$v(m/s)$	Re	f
1134	714	36.98238	0.0002	1.579118	22533.48	363.7864
2487	1409	43.36106	0.00035	2.762935	39426.16	234.3171
4269	2378	44.29784	0.00045	3.552345	50690.77	239.2854
6020	3448	42.72091	0.00055	4.341756	61955.39	232.3138
8233	4965	39.70211	0.00065	5.131166	73220	239.4697
13469	7246	46.19979	0.00085	6.709986	95749.24	204.4003

Conc. =300 ppm

ΔP_b	ΔP_a	%Dr	$Q(m^3/s)$	$v(m/s)$	Re	f
1134	657	42.04219	0.0002	1.579118	22533.48	334.5773
2487	1079	56.60398	0.00035	2.762935	39426.16	179.5307
4269	2113	50.50491	0.00045	3.552345	50690.77	212.621
6020	2778	53.85851	0.00055	4.341756	61955.39	187.1417
8233	4015	51.23982	0.00065	5.131166	73220	193.6483
13469	6061	55.00346	0.00085	6.709986	95749.24	170.9529

Conc. =500 ppm

ΔP_b	ΔP_a	%Dr	$Q(m^3/s)$	$v(m/s)$	Re	f
1134	578	49.05336	0.0002	1.579118	22533.48	294.1034
2487	909	63.44214	0.00035	2.762935	39426.16	151.241
4269	1517	64.45456	0.00045	3.552345	50690.77	152.6961
6020	1986	67.01374	0.00055	4.341756	61955.39	133.7864
8233	3623	55.99378	0.00065	5.131166	73220	174.7683
13469	5263	60.92406	0.00085	6.709986	95749.24	148.4591

APPENDIX A14

**EXPERIMENTAL DATA FOR COAL POWDER (DAPI 30 ppm, $D_p = 71$,
 $D=0.0127$ m, $L=1$ m)
 Conc. =100 ppm**

ΔP_b	ΔP_a	%Dr	$Q(m^3/s)$	$v(m/s)$	Re	f
1917	1221	36.32091	0.0002	1.579118	22533.48	310.8492
5173	2979	42.42273	0.00035	2.762935	39426.16	247.7778
8237	5073	38.4179	0.00045	3.552345	50690.77	255.248
11740	6767	42.36144	0.00055	4.341756	61955.39	227.947
16167	8029	50.33499	0.00065	5.131166	73220	193.6483
28438	14389	49.40418	0.00085	6.709986	95749.24	202.9297

Conc. =300 ppm

ΔP_b	ΔP_a	%Dr	$Q(m^3/s)$	$v(m/s)$	Re	f
1917	1181	38.41457	0.0002	1.579118	22533.48	300.629
5173	2920	43.56347	0.00035	2.762935	39426.16	242.8688
8237	4546	44.81604	0.00045	3.552345	50690.77	228.7287
11740	5714	51.32744	0.00055	4.341756	61955.39	192.4886
16167	6338	60.79581	0.00065	5.131166	73220	152.8607
28438	11189	60.65556	0.00085	6.709986	95749.24	157.8027

Conc. =500 ppm

ΔP_b	ΔP_a	%Dr	$Q(m^3/s)$	$v(m/s)$	Re	f
1917	1064	44.50374	0.0002	1.579118	22533.48	270.9048
5173	2318	55.17794	0.00035	2.762935	39426.16	192.8871
8237	3796	53.91938	0.00045	3.552345	50690.77	190.9968
11740	5108	56.49233	0.00055	4.341756	61955.39	172.0626
16167	5421	66.45863	0.00065	5.131166	73220	130.7808
28438	9722	65.81269	0.00085	6.709986	95749.24	137.1185

APPENDIX A15

**EXPERIMENTAL DATA FOR COAL POWDER (DAPI 30 ppm, $D_p = 71$,
 $D=0.0127$ m, $L=1.5$ m)**

Conc. =100 ppm

ΔP_b	ΔP_a	%Dr	$Q(m^3/s)$	$v(m/s)$	Re	f
2850	1786	37.35236	0.0002	1.579118	22533.48	303.1553
7810	4930	36.88246	0.00035	2.762935	39426.16	273.3699
12155	6224	48.79813	0.00045	3.552345	50690.77	208.7883
17910	9241	48.40213	0.00055	4.341756	61955.39	207.5337
24150	12837	46.84536	0.00065	5.131166	73220	206.4001
36407	18116	50.2407	0.00085	6.709986	95749.24	170.3335

Conc. =300 ppm

ΔP_b	ΔP_a	%Dr	$Q(m^3/s)$	$v(m/s)$	Re	f
2850	1679	41.10207	0.0002	1.579118	22533.48	285.0103
7810	4336	44.48683	0.00035	2.762935	39426.16	240.4344
12155	5517	54.61066	0.00045	3.552345	50690.77	185.0862
17910	8511	52.48212	0.00055	4.341756	61955.39	191.1234
24150	12029	50.19067	0.00065	5.131166	73220	193.4102
36407	15790	56.63084	0.00085	6.709986	95749.24	148.4591

Conc. =500 ppm

ΔP_b	ΔP_a	%Dr	$Q(m^3/s)$	$v(m/s)$	Re	f
2850	1439	49.52132	0.0002	1.579118	22533.48	244.2691
7810	4225	45.89925	0.00035	2.762935	39426.16	234.3171
12155	4861	60.00853	0.00045	3.552345	50690.77	163.0751
17910	7299	59.24561	0.00055	4.341756	61955.39	163.9197
24150	10949	54.66304	0.00065	5.131166	73220	176.0439
36407	12950	64.43105	0.00085	6.709986	95749.24	121.7578

APPENDIX A16

**EXPERIMENTAL DATA FOR COAL POWDER (DAPI 30 ppm, $D_p = 71$,
 $D=0.0127$ m, $L=2$ m)
 Conc. =100 ppm**

ΔP_b	ΔP_a	%Dr	$Q(m^3/s)$	$v(m/s)$	Re	f
3834	2409	37.17175	0.0002	1.579118	22533.48	306.6958
10447	6970	33.28437	0.00035	2.762935	39426.16	289.8786
16574	9143	44.83556	0.00045	3.552345	50690.77	230.0357
24031	11972	50.18073	0.00055	4.341756	61955.39	201.6386
32233	16084	50.10174	0.00065	5.131166	73220	193.9561
44376	22069	50.26846	0.00085	6.709986	95749.24	155.6261

Conc. =300 ppm

ΔP_b	ΔP_a	%Dr	$Q(m^3/s)$	$v(m/s)$	Re	f
3834	2246	41.40721	0.0002	1.579118	22533.48	286.0205
10447	6767	35.22542	0.00035	2.762935	39426.16	281.4448
16574	8686	47.59127	0.00045	3.552345	50690.77	218.5444
24031	10699	55.4762	0.00055	4.341756	61955.39	180.2056
32233	13793	57.20869	0.00065	5.131166	73220	166.3312
44376	20567	53.65224	0.00085	6.709986	95749.24	145.0372

Conc. =500 ppm

ΔP_b	ΔP_a	%Dr	$Q(m^3/s)$	$v(m/s)$	Re	f
3834	2181	43.12676	0.0002	1.579118	22533.48	277.6265
10447	5912	43.40499	0.00035	2.762935	39426.16	245.9046
16574	7194	56.59273	0.00045	3.552345	50690.77	181.0083
24031	10421	56.62793	0.00055	4.341756	61955.39	175.5442
32233	12500	61.22037	0.00065	5.131166	73220	150.7376
44376	18248	58.87846	0.00085	6.709986	95749.24	128.6826

APPENDIX B1

**EXPERIMENTAL DATA FOR ALUMINUM POWDER ($D_p = 71$, $D = 0.0127$ m,
 $L = 0.5$ m)**

Conc. =100 ppm

ΔP_b	ΔP_a	%Dr	$Q(m^3/s)$	$v(m/s)$	Re	F
1134	1000	11.77533	0.0002	1.579118	22533.48	0.005093
2487	2225	10.55283	0.00035	2.762935	39426.16	0.0037
4269	3704	13.23084	0.00045	3.552345	50690.77	0.003727
6020	5135	14.7006	0.00055	4.341756	61955.39	0.00346
8233	6522	20.7888	0.00065	5.131166	73220	0.003146
13469	10909	19.00623	0.00085	6.709986	95749.24	0.003077

Conc. =300 ppm

ΔP_b	ΔP_a	%Dr	$Q(m^3/s)$	$v(m/s)$	Re	F
1134	981	13.42439	0.0002	1.579118	22533.48	0.004998
2487	2115	14.93267	0.00035	2.762935	39426.16	0.003519
4269	3273	23.32761	0.00045	3.552345	50690.77	0.003294
6020	4425	26.50028	0.00055	4.341756	61955.39	0.002981
8233	6296	23.52696	0.00065	5.131166	73220	0.003037
13469	10476	22.22027	0.00085	6.709986	95749.24	0.002955

Conc. =500 ppm

ΔP_b	ΔP_a	%Dr	$Q(m^3/s)$	$v(m/s)$	Re	f
1134	1019	10.06223	0.0002	1.579118	22533.48	0.005192
2487	1892	23.92013	0.00035	2.762935	39426.16	0.003147
4269	2870	32.77276	0.00045	3.552345	50690.77	0.002888
6020	4000	33.55625	0.00055	4.341756	61955.39	0.002695
8233	5505	33.14284	0.00065	5.131166	73220	0.002655
13469	8879	34.08218	0.00085	6.709986	95749.24	0.002504

APPENDIX B2

**EXPERIMENTAL DATA FOR ALUMINUM POWDER ($D_p = 71$, $D = 0.0127$ m,
 $L = 1$ m)**

Conc. =100 ppm

ΔP_b	ΔP_a	%Dr	Q(m ³ /s)	v(m/s)	Re	f
1917	1667	13.05586	0.0002	1.579118	22533.48	0.004244
5173	4414	14.67152	0.00035	2.762935	39426.16	0.003672
8237	6696	18.71163	0.00045	3.552345	50690.77	0.003369
11740	8818	24.88938	0.00055	4.341756	61955.39	0.00297
16167	11927	26.22738	0.00065	5.131166	73220	0.002876
28438	22243	21.78454	0.00085	6.709986	95749.24	0.003137

Conc. =300 ppm

ΔP_b	ΔP_a	%Dr	Q(m ³ /s)	v(m/s)	Re	f
1917	1636	14.63666	0.0002	1.579118	22533.48	0.004167
5173	4071	21.31349	0.00035	2.762935	39426.16	0.003386
8237	6759	17.93941	0.00045	3.552345	50690.77	0.003401
11740	8667	26.17994	0.00055	4.341756	61955.39	0.002919
16167	11058	31.60208	0.00065	5.131166	73220	0.002667
28438	19418	31.72021	0.00085	6.709986	95749.24	0.002739

Conc. =500 ppm

ΔP_b	ΔP_a	%Dr	Q(m ³ /s)	v(m/s)	Re	f
1917	1548	19.25535	0.0002	1.579118	22533.48	0.003942
5173	3818	26.19641	0.00035	2.762935	39426.16	0.003176
8237	6422	22.03367	0.00045	3.552345	50690.77	0.003232
11740	7944	32.33604	0.00055	4.341756	61955.39	0.002676
16167	10096	37.54973	0.00065	5.131166	73220	0.002435
28438	17699	37.76267	0.00085	6.709986	95749.24	0.002496

APPENDIX B3

**EXPERIMENTAL DATA FOR ALUMINUM POWDER ($D_p = 71$, $D = 0.0127$ m,
 $L = 1.5$ m)**

Conc. = 100 ppm

ΔP_b	ΔP_a	%Dr	$Q(m^3/s)$	$v(m/s)$	Re	f
2850	2596	8.919966	0.0002	1.579118	22533.48	0.004407
7810	7087	9.254306	0.00035	2.762935	39426.16	0.00393
12155	9009	25.88453	0.00045	3.552345	50690.77	0.003022
17910	12261	31.54326	0.00055	4.341756	61955.39	0.002753
24150	17273	28.47751	0.00065	5.131166	73220	0.002777
36407	24954	31.45816	0.00085	6.709986	95749.24	0.002346

Conc. = 300 ppm

ΔP_b	ΔP_a	%Dr	$Q(m^3/s)$	$v(m/s)$	Re	f
2850	2404	15.66664	0.0002	1.579118	22533.48	0.004081
7810	6542	16.23653	0.00035	2.762935	39426.16	0.003628
12155	8889	26.87273	0.00045	3.552345	50690.77	0.002982
17910	12342	31.08837	0.00055	4.341756	61955.39	0.002772
24150	15826	34.46772	0.00065	5.131166	73220	0.002545
36407	24546	32.58067	0.00085	6.709986	95749.24	0.002308

Conc. = 500 ppm

ΔP_b	ΔP_a	%Dr	$Q(m^3/s)$	$v(m/s)$	Re	f
2850	2523	11.47361	0.0002	1.579118	22533.48	0.004284
7810	5398	30.8819	0.00035	2.762935	39426.16	0.002994
12155	8333	31.44319	0.00045	3.552345	50690.77	0.002796
17910	12381	30.87279	0.00055	4.341756	61955.39	0.00278
24150	16923	29.92533	0.00065	5.131166	73220	0.002721
36407	25243	30.66549	0.00085	6.709986	95749.24	0.002373

APPENDIX B4

EXPERIMENTAL DATA FOR ALUMINUM POWDER ($D_p = 71$, $D = 0.0127$ m,
 $L = 2$ m)

Conc. =100 ppm

ΔP_b	ΔP_a	%Dr	$Q(m^3/s)$	$v(m/s)$	Re	f
3834	3273	14.63666	0.0002	1.579118	22533.48	0.004167
10447	8899	14.81582	0.00035	2.762935	39426.16	0.003701
16574	12430	25.00279	0.00045	3.552345	50690.77	0.003127
24031	18269	23.97489	0.00055	4.341756	61955.39	0.003077
32233	24299	24.6153	0.00065	5.131166	73220	0.00293
44376	33333	24.88466	0.00085	6.709986	95749.24	0.002351

Conc. =300 ppm

ΔP_b	ΔP_a	%Dr	$Q(m^3/s)$	$v(m/s)$	Re	f
3834	3142	18.05707	0.0002	1.579118	22533.48	0.004
10447	8241	21.11763	0.00035	2.762935	39426.16	0.003427
16574	12857	22.42501	0.00045	3.552345	50690.77	0.003235
24031	19231	19.97356	0.00055	4.341756	61955.39	0.003239
32233	23301	27.71176	0.00065	5.131166	73220	0.00281
44376	30631	30.97509	0.00085	6.709986	95749.24	0.00216

Conc. =500 ppm

ΔP_b	ΔP_a	%Dr	$Q(m^3/s)$	$v(m/s)$	Re	f
3834	3091	19.37907	0.0002	1.579118	22533.48	0.003936
10447	7523	27.98863	0.00035	2.762935	39426.16	0.003129
16574	11682	29.5139	0.00045	3.552345	50690.77	0.002939
24031	17308	27.97621	0.00055	4.341756	61955.39	0.002915
32233	20561	36.21295	0.00065	5.131166	73220	0.002479
44376	29630	33.23081	0.00085	6.709986	95749.24	0.002089

APPENDIX B5

EXPERIMENTAL DATA FOR ALUMINUM POWDER ($D_p = 71$, $D = 0.0381$ m,
 $L = 0.5$ m)

Conc. =100 ppm

ΔP_b	ΔP_a	Dr%	Q(m ³ /s)	v(m/s)	Re	f
77	77	0.021992	0.00066	0.57901	24786.83	0.008779
157	155	1.491127	0.0008	0.701698	30038.98	0.011994
256	246	4.020861	0.001	0.877122	37548.72	0.012174
316	300	4.992116	0.0012	1.052547	45058.46	0.010317
378	367	2.945307	0.0014	1.227971	52568.21	0.009264
439	417	4.998121	0.00157	1.377082	58951.49	0.008371

Conc. =300 ppm

ΔP_b	ΔP_a	Dr%	Q(m ³ /s)	v(m/s)	Re	f
77	77	0.021992	0.00066	0.57901	24786.83	0.008779
157	154	2.020744	0.0008	0.701698	30038.98	0.011929
256	238	7.274391	0.001	0.877122	37548.72	0.011762
316	283	10.27033	0.0012	1.052547	45058.46	0.009744
378	350	7.356884	0.0014	1.227971	52568.21	0.008843
439	400	8.798196	0.00157	1.377082	58951.49	0.008036

Conc. =500 ppm

ΔP_b	ΔP_a	Dr%	Q(m ³ /s)	v(m/s)	Re	f
77	76	1.855461	0.00066	0.57901	24786.83	0.008618
157	150	4.668832	0.0008	0.701698	30038.98	0.011607
256	221	13.78145	0.001	0.877122	37548.72	0.010936
316	267	15.54855	0.0012	1.052547	45058.46	0.009171
378	317	16.18004	0.0014	1.227971	52568.21	0.008001
439	375	14.49831	0.00157	1.377082	58951.49	0.007534

APPENDIX B6

**EXPERIMENTAL DATA FOR ALUMINUM POWDER ($D_p = 71$, $I.D = 0.0381$ m,
 $L = 1$ m)**

Conc. = 100 ppm

ΔP_b	ΔP_a	Dr%	Q(m ³ /s)	v(m/s)	Re	f
130	127	2.213564	0.00066	0.57901	24786.83	0.007198
190	183	3.352337	0.0008	0.701698	30038.98	0.007093
325	315	3.006519	0.001	0.877122	37548.72	0.0078
444	417	6.161765	0.0012	1.052547	45058.46	0.007165
547	500	8.634811	0.0014	1.227971	52568.21	0.006317
627	583	6.990434	0.00157	1.377082	58951.49	0.00586

Conc. = 300 ppm

ΔP_b	ΔP_a	Dr%	Q(m ³ /s)	v(m/s)	Re	f
130	125	3.500228	0.00066	0.57901	24786.83	0.007103
190	178	5.988182	0.0008	0.701698	30038.98	0.0069
325	292	10.19122	0.001	0.877122	37548.72	0.007222
444	375	15.54559	0.0012	1.052547	45058.46	0.006448
547	483	11.68032	0.0014	1.227971	52568.21	0.006106
627	550	12.30527	0.00157	1.377082	58951.49	0.005525

Conc. = 500 ppm

ΔP_b	ΔP_a	Dr%	Q(m ³ /s)	v(m/s)	Re	f
130	117	9.933546	0.00066	0.57901	24786.83	0.006629
190	167	12.13849	0.0008	0.701698	30038.98	0.006448
325	258	20.45508	0.001	0.877122	37548.72	0.006397
444	333	24.92941	0.0012	1.052547	45058.46	0.005732
547	408	25.3851	0.0014	1.227971	52568.21	0.005159
627	508	18.94881	0.00157	1.377082	58951.49	0.005107

APPENDIX B7

**EXPERIMENTAL DATA FOR ALUMINUM POWDER ($D_p = 71$, I.D=0.0381 m,
L=1.5 m)**

Conc. =100 ppm

ΔP_b	ΔP_a	Dr%	Q(m ³ /s)	v(m/s)	Re	f
194	193	0.498013	0.00066	0.57901	24786.83	0.007324
264	250	5.197225	0.0008	0.701698	30038.98	0.006448
393	383	2.557933	0.001	0.877122	37548.72	0.006328
531	508	4.200685	0.0012	1.052547	45058.46	0.005827
675	617	8.648503	0.0014	1.227971	52568.21	0.005194
899	817	9.168103	0.00157	1.377082	58951.49	0.005469

Conc. =300 ppm

ΔP_b	ΔP_a	Dr%	Q(m ³ /s)	v(m/s)	Re	f
194	192	1.355789	0.00066	0.57901	24786.83	0.007261
264	225	14.6775	0.0008	0.701698	30038.98	0.005803
393	342	13.14946	0.001	0.877122	37548.72	0.00564
531	483	8.912127	0.0012	1.052547	45058.46	0.005541
675	592	12.35194	0.0014	1.227971	52568.21	0.004983
899	750	16.58295	0.00157	1.377082	58951.49	0.005023

Conc. =500 ppm

ΔP_b	ΔP_a	Dr%	Q(m ³ /s)	v(m/s)	Re	f
194	183	5.644667	0.00066	0.57901	24786.83	0.006945
264	208	20.99769	0.0008	0.701698	30038.98	0.005374
393	308	21.62269	0.001	0.877122	37548.72	0.00509
531	417	21.47597	0.0012	1.052547	45058.46	0.004776
675	517	23.46226	0.0014	1.227971	52568.21	0.004351
899	667	25.85151	0.00157	1.377082	58951.49	0.004465

APPENDIX B8

EXPERIMENTAL DATA FOR ALUMINUM POWDER ($D_p = 71$, $I.D = 0.0381$ m,
 $L = 2$ m)

Conc. = 100 ppm

ΔP_b	ΔP_a	Dr%	Q(m ³ /s)	v(m/s)	Re	f
259	250	3.500228	0.00066	0.57901	24786.83	0.007103
338	325	3.765938	0.0008	0.701698	30038.98	0.006287
483	458	5.079757	0.001	0.877122	37548.72	0.005674
638	600	5.963936	0.0012	1.052547	45058.46	0.005159
845	750	11.19097	0.0014	1.227971	52568.21	0.004738
1046	833	20.33279	0.00157	1.377082	58951.49	0.004186

Conc. = 300 ppm

ΔP_b	ΔP_a	Dr%	Q(m ³ /s)	v(m/s)	Re	f
259	242	6.716887	0.00066	0.57901	24786.83	0.006866
338	283	16.10364	0.0008	0.701698	30038.98	0.005481
483	417	13.70887	0.001	0.877122	37548.72	0.005159
638	567	11.18816	0.0012	1.052547	45058.46	0.004872
845	683	19.08511	0.0014	1.227971	52568.21	0.004316
1046	750	28.29951	0.00157	1.377082	58951.49	0.003767

Conc. = 500 ppm

ΔP_b	ΔP_a	Dr%	Q(m ³ /s)	v(m/s)	Re	f
259	208	19.58352	0.00066	0.57901	24786.83	0.005919
338	250	25.9738	0.0008	0.701698	30038.98	0.004836
483	350	27.51545	0.001	0.877122	37548.72	0.004333
638	517	19.0245	0.0012	1.052547	45058.46	0.004442
845	642	24.01894	0.0014	1.227971	52568.21	0.004053
1046	675	35.46956	0.00157	1.377082	58951.49	0.00339

APPENDIX B9

**EXPERIMENTAL DATA FOR ALUMINUM POWDER +10 ppm of NNAP (D_p
=45, $D=0.0127$ m, $L=1.5$ m)**

Conc. =100 ppm

ΔP_b	ΔP_a	Dr%	Q(m ³ /s)	v(m/s)	Re	f
1134	846	25.34836	0.0002	1.579118	22533.48	0.004309
2487	1817	26.94009	0.00035	2.762935	39426.16	0.003023
4269	3030	29.00705	0.00045	3.552345	50690.77	0.00305
6020	4419	26.60284	0.00055	4.341756	61955.39	0.002977
8233	5769	29.92855	0.00065	5.131166	73220	0.002783
13469	9091	32.50519	0.00085	6.709986	95749.24	0.002564

Conc. =300 ppm

ΔP_b	ΔP_a	Dr%	Q(m ³ /s)	v(m/s)	Re	f
1134	784	30.86873	0.0002	1.579118	22533.48	0.003991
2487	1705	31.41859	0.00035	2.762935	39426.16	0.002837
4269	2769	35.12336	0.00045	3.552345	50690.77	0.002787
6020	3846	36.11178	0.00055	4.341756	61955.39	0.002591
8233	5075	38.36502	0.00065	5.131166	73220	0.002448
13469	8333	38.12976	0.00085	6.709986	95749.24	0.002351

Conc. =500 ppm

ΔP_b	ΔP_a	Dr%	Q(m ³ /s)	v(m/s)	Re	f
1134	796	29.82128	0.0002	1.579118	22533.48	0.004051
2487	1628	34.53593	0.00035	2.762935	39426.16	0.002708
4269	2539	40.52975	0.00045	3.552345	50690.77	0.002555
6020	3333	44.63021	0.00055	4.341756	61955.39	0.002246
8233	4444	46.01903	0.00065	5.131166	73220	0.002144
13469	7090	47.36412	0.00085	6.709986	95749.24	0.002

APPENDIX B10

**EXPERIMENTAL DATA FOR ALUMINUM POWDER +10 ppm of NNAP (D_p
=45, $D=0.0127$ m, $L=1$ m)**

Conc. =100 ppm

ΔP_b	ΔP_a	Dr%	Q(m ³ /s)	v(m/s)	Re	f
1917	1374	28.32086	0.0002	1.579118	22533.48	0.003499
5173	3712	28.24651	0.00035	2.762935	39426.16	0.003088
8237	5969	27.53362	0.00045	3.552345	50690.77	0.003004
11740	7461	36.44486	0.00055	4.341756	61955.39	0.002513
16167	9849	39.0817	0.00065	5.131166	73220	0.002375
28438	17630	38.00701	0.00085	6.709986	95749.24	0.002486

Conc. =300 ppm

ΔP_b	ΔP_a	Dr%	Q(m ³ /s)	v(m/s)	Re	f
1917	1395	27.20956	0.0002	1.579118	22533.48	0.003553
5173	3539	31.60326	0.00035	2.762935	39426.16	0.002943
8237	5615	31.82658	0.00045	3.552345	50690.77	0.002826
11740	6791	42.15593	0.00055	4.341756	61955.39	0.002288
16167	8712	46.11073	0.00065	5.131166	73220	0.002101
28438	15267	46.31436	0.00085	6.709986	95749.24	0.002153

Conc. =500 ppm

ΔP_b	ΔP_a	Dr%	Q(m ³ /s)	v(m/s)	Re	f
1917	1380	28.01834	0.0002	1.579118	22533.48	0.003514
5173	3231	37.55081	0.00035	2.762935	39426.16	0.002687
8237	5303	35.61871	0.00045	3.552345	50690.77	0.002669
11740	6296	46.37004	0.00055	4.341756	61955.39	0.002121
16167	7836	51.53113	0.00065	5.131166	73220	0.00189
28438	15504	45.48203	0.00085	6.709986	95749.24	0.002187

APPENDIX B11

**EXPERIMENTAL DATA FOR ALUMINUM POWDER +10 ppm of NNAP (Dp
=45, D=0.0127 m, L=1.5 m)**

Conc. =100 ppm

ΔP_b	ΔP_a	Dr%	Q(m ³ /s)	v(m/s)	Re	f
2850	2000	29.83464	0.0002	1.579118	22533.48	0.003395
7810	5448	30.24771	0.00035	2.762935	39426.16	0.003021
12155	7752	36.22622	0.00045	3.552345	50690.77	0.002601
17910	10846	39.44211	0.00055	4.341756	61955.39	0.002436
24150	14504	39.94295	0.00065	5.131166	73220	0.002332
36407	20606	43.40106	0.00085	6.709986	95749.24	0.001937

Conc. =300 ppm

ΔP_b	ΔP_a	Dr%	Q(m ³ /s)	v(m/s)	Re	f
2850	1923	32.53331	0.0002	1.579118	22533.48	0.003265
7810	5303	32.10082	0.00035	2.762935	39426.16	0.002941
12155	7111	41.49819	0.00045	3.552345	50690.77	0.002386
17910	10224	42.91648	0.00055	4.341756	61955.39	0.002296
24150	14109	41.57975	0.00065	5.131166	73220	0.002268
36407	20769	42.95288	0.00085	6.709986	95749.24	0.001953

Conc. =500 ppm

ΔP_b	ΔP_a	Dr%	Q(m ³ /s)	v(m/s)	Re	f
2850	2015	29.31102	0.0002	1.579118	22533.48	0.003421
7810	4621	40.83072	0.00035	2.762935	39426.16	0.002563
12155	6870	43.47988	0.00045	3.552345	50690.77	0.002305
17910	9849	45.01245	0.00055	4.341756	61955.39	0.002212
24150	13643	43.50569	0.00065	5.131166	73220	0.002194
36407	20000	45.06573	0.00085	6.709986	95749.24	0.00188

APPENDIX B12

**EXPERIMENTAL DATA FOR ALUMINUM POWDER +10 ppm of NNAP (D_p
=45, $D=0.0127$ m, $L=2$ m)**

Conc. =100 ppm

ΔP_b	ΔP_a	Dr%	Q(m ³ /s)	v(m/s)	Re	F
3834	2687	29.92562	0.0002	1.579118	22533.48	0.003421
10447	7519	28.02267	0.00035	2.762935	39426.16	0.003127
16574	10231	38.27153	0.00045	3.552345	50690.77	0.002574
24031	14615	39.17991	0.00055	4.341756	61955.39	0.002462
32233	19403	39.80476	0.00065	5.131166	73220	0.00234
44376	27273	38.54199	0.00085	6.709986	95749.24	0.001923

Conc. =300 ppm

ΔP_b	ΔP_a	Dr%	Q(m ³ /s)	v(m/s)	Re	f
3834	2689	29.85189	0.0002	1.579118	22533.48	0.003424
10447	6899	33.95894	0.00035	2.762935	39426.16	0.002869
16574	10385	37.34328	0.00045	3.552345	50690.77	0.002613
24031	15152	36.94887	0.00055	4.341756	61955.39	0.002552
32233	17778	44.84675	0.00065	5.131166	73220	0.002144
44376	25373	42.82265	0.00085	6.709986	95749.24	0.001789

Conc. =500 ppm

ΔP_b	ΔP_a	Dr%	Q(m ³ /s)	v(m/s)	Re	f
3834	2615	31.78229	0.0002	1.579118	22533.48	0.00333
10447	6260	40.08214	0.00035	2.762935	39426.16	0.002603
16574	9470	42.86354	0.00045	3.552345	50690.77	0.002383
24031	13954	41.93431	0.00055	4.341756	61955.39	0.00235
32233	16923	47.49835	0.00065	5.131166	73220	0.002041
44376	24242	45.37066	0.00085	6.709986	95749.24	0.00171

APPENDIX B13

**EXPERIMENTAL DATA FOR ALUMINUM POWDER +30 ppm of NNAP (D_p
=45, $D=0.0127$ m, $L=0.5$ m)**

Conc. =100 ppm

ΔP_b	ΔP_a	Dr%	Q(m ³ /s)	v(m/s)	Re	f
1134	629	44.51279	0.0002	1.579118	22533.48	320.3151
2487	1313	47.21959	0.00035	2.762935	39426.16	218.3542
4269	2547	40.33946	0.00045	3.552345	50690.77	256.2898
6020	3608	40.07447	0.00055	4.341756	61955.39	243.0473
8233	4214	48.81993	0.00065	5.131166	73220	203.2588
13469	6211	53.88554	0.00085	6.709986	95749.24	175.2002

Conc. =300 ppm

ΔP_b	ΔP_a	Dr%	Q(m ³ /s)	v(m/s)	Re	f
1134	522	53.99327	0.0002	1.579118	22533.48	265.5864
2487	1139	54.18699	0.00035	2.762935	39426.16	189.5299
4269	2264	46.95621	0.00045	3.552345	50690.77	227.8656
6020	3082	48.80906	0.00055	4.341756	61955.39	207.6213
8233	3926	52.31129	0.00065	5.131166	73220	189.393
13469	5839	56.6524	0.00085	6.709986	95749.24	164.6882

Conc. =500 ppm

ΔP_b	ΔP_a	Dr%	Q(m ³ /s)	v(m/s)	Re	f
1134	491	56.70963	0.0002	1.579118	22533.48	249.9054
2487	949	61.82249	0.00035	2.762935	39426.16	157.9416
4269	1950	54.3234	0.00045	3.552345	50690.77	196.2176
6020	2671	55.63539	0.00055	4.341756	61955.39	179.935
8233	3476	57.78623	0.00065	5.131166	73220	167.6497
13469	5276	60.82817	0.00085	6.709986	95749.24	148.8234

APPENDIX B14

**EXPERIMENTAL DATA FOR ALUMINUM POWDER +30 ppm of NNAP (D_p
=45, $D=0.0127$ m, $L=1$ m)**

Conc. =100 ppm

ΔP_b	ΔP_a	Dr%	Q(m ³ /s)	v(m/s)	Re	f
1917	1063	44.57311	0.0002	1.579118	22533.48	270.5661
5173	3044	41.17105	0.00035	2.762935	39426.16	253.1643
8237	4494	45.44472	0.00045	3.552345	50690.77	226.1229
11740	5849	50.1795	0.00055	4.341756	61955.39	197.0284
16167	7826	51.59134	0.00065	5.131166	73220	188.7497
28438	12805	54.97281	0.00085	6.709986	95749.24	180.5951

Conc. =300 ppm

ΔP_b	ΔP_a	Dr%	Q(m ³ /s)	v(m/s)	Re	f
1917	949	50.47486	0.0002	1.579118	22533.48	241.7568
5173	2767	46.50952	0.00035	2.762935	39426.16	230.1907
8237	3899	52.6598	0.00045	3.552345	50690.77	196.2176
11740	5276	55.05999	0.00055	4.341756	61955.39	177.7272
16167	7391	54.28071	0.00065	5.131166	73220	178.2636
28438	12375	56.48443	0.00085	6.709986	95749.24	174.5323

Conc. =500 ppm

ΔP_b	ΔP_a	Dr%	Q(m ³ /s)	v(m/s)	Re	f
1917	823	57.07821	0.0002	1.579118	22533.48	209.5226
5173	2642	48.94091	0.00035	2.762935	39426.16	219.7275
8237	3727	54.75601	0.00045	3.552345	50690.77	187.5291
11740	5122	56.37276	0.00055	4.341756	61955.39	172.5355
16167	6994	56.73909	0.00065	5.131166	73220	168.6782
28438	11899	58.15918	0.00085	6.709986	95749.24	167.8152

APPENDIX B15

**EXPERIMENTAL DATA FOR ALUMINUM POWDER +30 ppm of NNAP (D_p
=45, $D=0.0127$ m, $L=1.5$ m)**

Conc. =100 ppm

ΔP_b	ΔP_a	Dr%	Q(m ³ /s)	v(m/s)	Re	f
2850	1524	46.52031	0.0002	1.579118	22533.48	258.7911
7810	4417	43.44314	0.00035	2.762935	39426.16	244.9548
12155	6139	49.49359	0.00045	3.552345	50690.77	205.9523
17910	8742	51.18957	0.00055	4.341756	61955.39	196.3222
24150	11250	53.41627	0.00065	5.131166	73220	180.8852
36407	15528	57.34917	0.00085	6.709986	95749.24	146.0002

Conc. =300 ppm

ΔP_b	ΔP_a	Dr%	Q(m ³ /s)	v(m/s)	Re	f
2850	1447	49.25147	0.0002	1.579118	22533.48	245.5749
7810	4162	46.71692	0.00035	2.762935	39426.16	230.7756
12155	5610	53.84956	0.00045	3.552345	50690.77	188.1898
17910	8221	54.10006	0.00055	4.341756	61955.39	184.6158
24150	11392	52.82661	0.00065	5.131166	73220	183.1748
36407	14465	60.26767	0.00085	6.709986	95749.24	136.0097

Conc. =500 ppm

ΔP_b	ΔP_a	Dr%	Q(m ³ /s)	v(m/s)	Re	f
2850	1227	56.95377	0.0002	1.579118	22533.48	208.3031
7810	3603	53.87435	0.00035	2.762935	39426.16	199.7759
12155	5500	54.7525	0.00045	3.552345	50690.77	184.5078
17910	7888	55.95742	0.00055	4.341756	61955.39	177.1453
24150	10696	55.70942	0.00065	5.131166	73220	171.9808
36407	14465	60.2677	0.00085	6.709986	95749.24	136.0097

APPENDIX B16

**EXPERIMENTAL DATA FOR ALUMINUM POWDER +30 ppm of NNAP (D_p
=45, $D=0.0127$ m, $L=2$ m)**

Conc. =100 ppm

ΔP_b	ΔP_a	Dr%	Q(m ³ /s)	v(m/s)	Re	f
3834	2147	43.99304	0.0002	1.579118	22533.48	273.3978
10447	5696	45.47457	0.00035	2.762935	39426.16	236.9124
16574	8491	48.77123	0.00045	3.552345	50690.77	213.624
24031	11950	50.27288	0.00055	4.341756	61955.39	201.2656
32233	14724	54.32093	0.00065	5.131166	73220	177.556
44376	21739	51.01173	0.00085	6.709986	95749.24	153.3002

Conc. =300 ppm

ΔP_b	ΔP_a	Dr%	Q(m ³ /s)	v(m/s)	Re	f
3834	2174	43.2973	0.0002	1.579118	22533.48	276.794
10447	5317	49.10959	0.00035	2.762935	39426.16	221.1182
16574	8050	51.42754	0.00045	3.552345	50690.77	202.5472
24031	11180	53.47531	0.00055	4.341756	61955.39	188.304
32233	14329	55.5453	0.00065	5.131166	73220	172.7968
44376	19632	55.76029	0.00085	6.709986	95749.24	138.4404

Conc. =500 ppm

ΔP_b	ΔP_a	Dr%	Q(m ³ /s)	v(m/s)	Re	f
3834	1950	49.14588	0.0002	1.579118	22533.48	248.2442
10447	4938	52.73705	0.00035	2.762935	39426.16	205.3569
16574	7453	55.02899	0.00045	3.552345	50690.77	187.5291
24031	10760	55.22572	0.00055	4.341756	61955.39	181.2195
32233	13837	57.07412	0.00065	5.131166	73220	166.8542
44376	18634	58.01006	0.00085	6.709986	95749.24	131.4002

APPENDIX B17

**EXPERIMENTAL DATA FOR ALUMINUM POWDER +10 ppm of NNAP (D_p
=71, $D=0.0381$ m, $L=0.5$ m)**

Conc. =100 ppm

ΔP_b	ΔP_a	Dr%	Q(m ³ /s)	v(m/s)	Re	f
93	85	8.019845	0.00066	0.57901	24786.83	969.2157
189	171	9.371607	0.0008	0.701698	30038.98	1324.114
307	271	11.69906	0.001	0.877122	37548.72	1344.047
379	331	12.59276	0.0012	1.052547	45058.46	1139.023
453	405	10.70976	0.0014	1.227971	52568.21	1022.796
526	460	12.59821	0.00157	1.377082	58951.49	924.194

Conc. =300 ppm

ΔP_B	ΔP_A	Dr%	Q(m ³ /s)	v(m/s)	Re	f
93	85	8.019845	0.00066	0.57901	24786.83	969.2157
189	170	9.858857	0.0008	0.701698	30038.98	1316.995
307	262	14.69231	0.001	0.877122	37548.72	1298.486
379	313	17.44872	0.0012	1.052547	45058.46	1075.744
453	386	14.7684	0.0014	1.227971	52568.21	976.3054
526	442	16.09428	0.00157	1.377082	58951.49	887.2263

Conc. =500 ppm

ΔP_b	ΔP_a	Dr%	Q(m ³ /s)	v(m/s)	Re	f
93	84	9.706644	0.00066	0.57901	24786.83	951.4416
189	166	12.2951	0.0008	0.701698	30038.98	1281.401
307	244	20.67882	0.001	0.877122	37548.72	1207.364
379	294	22.30468	0.0012	1.052547	45058.46	1012.465
453	350	22.8857	0.0014	1.227971	52568.21	883.3239
526	414	21.33839	0.00157	1.377082	58951.49	831.7746

APPENDIX B18

**EXPERIMENTAL DATA FOR ALUMINUM POWDER +10 ppm of NNAP (D_p
=71, $D=0.0381$ m, $L=1$ m)**

Conc. =100 ppm

ΔP_b	ΔP_a	Dr%	Q(m ³ /s)	v(m/s)	Re	f
155	140	10.03661	0.00066	0.57901	24786.83	794.6105
228	202	11.08417	0.0008	0.701698	30038.98	783.0783
390	348	10.76602	0.001	0.877122	37548.72	861.1014
533	460	13.66885	0.0012	1.052547	45058.46	790.9882
657	552	15.94399	0.0014	1.227971	52568.21	697.361
753	644	14.43123	0.00157	1.377082	58951.49	646.9358

Conc. =300 ppm

ΔP_b	ΔP_a	Dr%	Q(m ³ /s)	v(m/s)	Re	f
155	138	11.22033	0.00066	0.57901	24786.83	784.1551
228	197	13.50914	0.0008	0.701698	30038.98	761.7216
390	322	17.37594	0.001	0.877122	37548.72	797.3161
533	414	22.30196	0.0012	1.052547	45058.46	711.8893
657	534	18.74586	0.0014	1.227971	52568.21	674.1156
753	607	19.32087	0.00157	1.377082	58951.49	609.9681

Conc. =500 ppm

ΔP_b	ΔP_a	Dr%	Q(m ³ /s)	v(m/s)	Re	f
155	129	17.13898	0.00066	0.57901	24786.83	731.8781
228	184	19.16742	0.0008	0.701698	30038.98	711.8893
390	285	26.81869	0.001	0.877122	37548.72	706.1942
533	368	30.93508	0.0012	1.052547	45058.46	632.7905
657	451	31.35426	0.0014	1.227971	52568.21	569.5115
753	561	25.43293	0.00157	1.377082	58951.49	563.7584

APPENDIX B19

**EXPERIMENTAL DATA FOR ALUMINUM POWDER +10 ppm of NNAP (D_p
=71, $D=0.0381$ m, $L=1.5$ m)**

Conc. =100 ppm

ΔP_b	ΔP_a	Dr%	Q(m ³ /s)	v(m/s)	Re	f
233	213	8.458104	0.00066	0.57901	24786.83	808.5511
316	276	12.78133	0.0008	0.701698	30038.98	711.8893
472	423	10.35323	0.001	0.877122	37548.72	698.6007
637	561	11.86466	0.0012	1.052547	45058.46	643.337
810	681	15.95664	0.0014	1.227971	52568.21	573.3857
1079	902	16.43464	0.00157	1.377082	58951.49	603.8068

Conc. =300 ppm

ΔP_b	ΔP_a	Dr%	Q(m ³ /s)	v(m/s)	Re	f
233	212	9.247258	0.00066	0.57901	24786.83	801.5808
316	248	21.50319	0.0008	0.701698	30038.98	640.7004
472	377	20.09744	0.001	0.877122	37548.72	622.6659
637	534	16.19919	0.0012	1.052547	45058.46	611.6975
810	653	19.3638	0.0014	1.227971	52568.21	550.1403
1079	828	23.25631	0.00157	1.377082	58951.49	554.5164

Conc. =500 ppm

ΔP_b	ΔP_a	Dr%	Q(m ³ /s)	v(m/s)	Re	f
233	202	13.19303	0.00066	0.57901	24786.83	766.7295
316	230	27.31777	0.0008	0.701698	30038.98	593.2411
472	340	27.89281	0.001	0.877122	37548.72	561.918
637	460	27.75792	0.0012	1.052547	45058.46	527.3254
810	570	29.58529	0.0014	1.227971	52568.21	480.4042
1079	736	31.78338	0.00157	1.377082	58951.49	492.9035

APPENDIX B20

**EXPERIMENTAL DATA FOR ALUMINUM POWDER +10 ppm of NNAP (D_p
=71, $D=0.0381$ m, $L=2$ m)**

Conc. =100 ppm

ΔP_b	ΔP_a	Dr%	Q(m ³ /s)	v(m/s)	Re	f
311	276	11.22033	0.00066	0.57901	24786.83	784.1551
405	359	11.46468	0.0008	0.701698	30038.98	694.0921
579	506	12.6734	0.001	0.877122	37548.72	626.4626
766	662	13.48686	0.0012	1.052547	45058.46	569.5115
1013	828	18.29574	0.0014	1.227971	52568.21	523.0207
1255	920	26.70619	0.00157	1.377082	58951.49	462.097

Conc. =300 ppm

ΔP_b	ΔP_a	Dr%	Q(m ³ /s)	v(m/s)	Re	f
311	267	14.17966	0.00066	0.57901	24786.83	758.0166
405	313	22.81536	0.0008	0.701698	30038.98	605.1059
579	460	20.61218	0.001	0.877122	37548.72	569.5115
766	626	18.29314	0.0012	1.052547	45058.46	537.872
1013	754	25.55834	0.0014	1.227971	52568.21	476.53
1255	828	34.03557	0.00157	1.377082	58951.49	415.8873

Conc. =500 ppm

ΔP_b	ΔP_a	Dr%	Q(m ³ /s)	v(m/s)	Re	f
311	230	26.01695	0.00066	0.57901	24786.83	653.4626
405	276	31.89591	0.0008	0.701698	30038.98	533.917
579	386	33.31423	0.001	0.877122	37548.72	478.3896
766	570	25.50257	0.0012	1.052547	45058.46	490.4127
1013	708	30.09746	0.0014	1.227971	52568.21	447.4733
1255	745	40.63202	0.00157	1.377082	58951.49	374.2986

APPENDIX C1

**EXPERIMENTAL DATA FOR SAND POWDER (NNAP 10 ppm, $D_p = 45$,
 $D=0.0254$ m, $L=0.5$ m)**

Conc. =100 ppm

ΔP_b	ΔP_a	%Dr	Q(m ³ /s)	v(m/s)	Re	f
148	138	6.605512	0.0003	0.592169	16900.11	1000.278
367	322	12.18943	0.0005	0.986763	28161.54	840.6879
716	657	8.30309	0.0008	1.57882	45058.46	669.3342
1215	990	18.51146	0.0011	2.170878	61955.39	533.6317
1623	1450	10.65483	0.0013	2.565583	73220	559.5381
2044	1776	13.12688	0.001488	2.936606	83808.74	523.0128

Conc. =300 ppm

ΔP_b	ΔP_a	%Dr	Q(m ³ /s)	v(m/s)	Re	f
148	135	8.698837	0.0003	0.592169	16900.11	977.8579
367	330	10.03315	0.0005	0.986763	28161.54	861.3319
716	576	19.5399	0.0008	1.57882	45058.46	587.312
1215	990	18.51961	0.0011	2.170878	61955.39	533.5783
1623	1290	20.51361	0.0013	2.565583	73220	497.7959
2044	1449	29.12982	0.001488	2.936606	83808.74	426.6683

Conc. =500 ppm

ΔP_b	ΔP_a	%Dr	Q(m ³ /s)	v(m/s)	Re	f
148	128	13.45861	0.0003	0.592169	16900.11	926.8795
367	294	19.86146	0.0005	0.986763	28161.54	767.2368
716	594	17.07033	0.0008	1.57882	45058.46	605.3384
1215	950	21.81175	0.0011	2.170878	61955.39	512.0196
1623	1168	28.0171	0.0013	2.565583	73220	450.8041
2044	1500	26.61507	0.001488	2.936606	83808.74	441.8082

APPENDIX C2

**EXPERIMENTAL DATA FOR SAND POWDER (NNAP 10 ppm, $D_p = 45$,
 $D=0.0254$ m, $L=1$ m)**

Conc. =100 ppm

ΔP_b	ΔP_a	%Dr	$Q(m^3/s)$	$v(m/s)$	Re	f
246	211	13.99504	0.0003	0.592169	16900.11	765.392
534	520	2.625899	0.0005	0.986763	28161.54	678.2373
1283	1200	6.446061	0.0008	1.57882	45058.46	611.3918
2230	1963	11.99156	0.0011	2.170878	61955.39	528.8938
3046	2900	4.788129	0.0013	2.565583	73220	559.5381
3978	3600	9.503013	0.001488	2.936606	83808.74	530.1698

Conc. =300 ppm

ΔP_b	ΔP_a	%Dr	$Q(m^3/s)$	$v(m/s)$	Re	f
246	202	17.90436	0.0003	0.592169	16900.11	730.6015
534	500	6.371056	0.0005	0.986763	28161.54	652.1513
1283	1200	6.446061	0.0008	1.57882	45058.46	611.3918
2230	1682	24.56419	0.0011	2.170878	61955.39	453.3376
3046	2476	18.70251	0.0013	2.565583	73220	477.7665
3978	3223	18.98637	0.001488	2.936606	83808.74	474.6123

Conc. =500 ppm

ΔP_b	ΔP_a	%Dr	$Q(m^3/s)$	$v(m/s)$	Re	f
246	208	15.38459	0.0003	0.592169	16900.11	753.0259
534	465	12.86019	0.0005	0.986763	28161.54	606.9527
1283	1000	22.03838	0.0008	1.57882	45058.46	509.4932
2230	1589	28.75507	0.0011	2.170878	61955.39	428.1521
3046	2400	21.20397	0.0013	2.565583	73220	463.066
3978	3000	24.58584	0.001488	2.936606	83808.74	441.8082

APPENDIX C3

**EXPERIMENTAL DATA FOR SAND POWDER (NNAP 10 ppm, $D_p = 45$,
 $D=0.0254$ m, $L=1.5$ m)**

Conc. =100 ppm

ΔP_b	ΔP_a	%Dr	Q(m ³ /s)	v(m/s)	Re	f
344	340	1.043928	0.0003	0.592169	16900.11	820.9177
851	840	1.296587	0.0005	0.986763	28161.54	730.4094
1949	1682	13.68792	0.0008	1.57882	45058.46	571.3942
2945	2571	12.68638	0.0011	2.170878	61955.39	461.9726
4669	3792	18.79062	0.0013	2.565583	73220	487.6946
6067	5098	15.97169	0.001488	2.936606	83808.74	500.5234

Conc. =300 ppm

ΔP_b	ΔP_a	%Dr	Q(m ³ /s)	v(m/s)	Re	f
344	340	1.043928	0.0003	0.592169	16900.11	820.9177
851	748	12.14649	0.0005	0.986763	28161.54	650.1196
1949	1600	17.90762	0.0008	1.57882	45058.46	543.4594
2945	2400	18.50729	0.0011	2.170878	61955.39	431.1744
4669	3491	25.23566	0.0013	2.565583	73220	448.9896
6067	4707	22.41678	0.001488	2.936606	83808.74	462.1326

Conc. =500 ppm

ΔP_b	ΔP_a	%Dr	Q(m ³ /s)	v(m/s)	Re	f
344	320	6.864874	0.0003	0.592169	16900.11	772.6284
851	743	12.74451	0.0005	0.986763	28161.54	645.6943
1949	1500	23.03839	0.0008	1.57882	45058.46	509.4932
2945	2056	30.18538	0.0011	2.170878	61955.39	369.3862
4669	3600	22.8917	0.0013	2.565583	73220	463.066
6067	4700	22.53236	0.001488	2.936606	83808.74	461.4441

APPENDIX C4

**EXPERIMENTAL DATA FOR SAND POWDER (NNAP 10 ppm, $D_p = 45$,
 $D=0.0254$ m, $L=2$ m)**

Conc. =100 ppm

ΔP_b	ΔP_a	%Dr	$Q(m^3/s)$	$v(m/s)$	Re	f
442	410	7.124039	0.0003	0.592169	16900.11	742.4476
1093	1000	8.512534	0.0005	0.986763	28161.54	652.1513
2615	2318	11.37921	0.0008	1.57882	45058.46	590.4407
4660	4000	14.16429	0.0011	2.170878	61955.39	538.968
6492	5592	13.85251	0.0013	2.565583	73220	539.5121
8356	7549	9.658209	0.001488	3.37E-07	28.38323	1.25E+20

Conc. =300 ppm

ΔP_b	ΔP_a	%Dr	$Q(m^3/s)$	$v(m/s)$	Re	f
442	400	9.389307	0.0003	0.592169	16900.11	724.3392
1093	907	17.06276	0.0005	0.986763	28161.54	591.2026
2615	2300	12.05816	0.0008	1.57882	45058.46	585.9172
4660	4000	14.16429	0.0011	2.170878	61955.39	538.968
6492	5189	20.07182	0.0013	2.565583	73220	500.5627
8356	6724	19.52788	0.001488	2.936606	83808.74	495.142

Conc. =500 ppm

ΔP_b	ΔP_a	%Dr	$Q(m^3/s)$	$v(m/s)$	Re	f
442	400	9.389307	0.0003	0.592169	16900.11	724.3392
1093	888	18.77281	0.0005	0.986763	28161.54	579.0128
2615	2000	23.52884	0.0008	1.57882	45058.46	509.4932
4660	3500	24.89375	0.0011	2.170878	61955.39	471.597
6492	4717	27.33802	0.0013	2.565583	73220	455.057
8356	5764	31.0239	0.001488	2.936606	83808.74	424.4075

APPENDIX C5

**EXPERIMENTAL DATA FOR SAND POWDER (NNAP 20 ppm, $D_p = 45$,
 $D=0.0127$ m, $L=0.5$ m)**

Conc. =100 ppm

ΔP_b	ΔP_a	%Dr	Q(m ³ /s)	v(m/s)	Re	f
1134	1058	6.685444	0.0002	1.579118	22533.48	538.6837
248	2059	17.2072	0.00035	2.763457	39433.59	342.3872
4269	3204	24.94046	0.00045	3.553016	50700.34	322.3192
6020	4348	27.77854	0.00055	4.342575	61967.08	292.8069
8233	5769	29.92855	0.00065	5.132134	73233.82	278.1799
13469	8818	34.53265	0.00085	6.711252	95767.3	248.6328

Conc. =300 ppm

ΔP_b	ΔP_a	%Dr	Q(m ³ /s)	v(m/s)	Re	f
1134	877	22.60994	0.0002	1.579118	22533.48	446.7552
248	1852	25.53029	0.00035	2.763457	39433.59	307.9673
4269	3010	29.48953	0.00045	3.553016	50700.34	302.7847
6020	4000	33.55625	0.00055	4.342575	61967.08	269.3823
8233	5900	28.34027	0.00065	5.132134	73233.82	284.4853
13469	8654	35.75014	0.00085	6.711252	95767.3	244.009

Conc. =500 ppm

ΔP_b	ΔP_a	%Dr	Q(m ³ /s)	v(m/s)	Re	f
1134	900	20.5978	0.0002	1.579118	22533.48	458.3709
248	1455	41.50742	0.00035	2.763457	39433.59	241.8943
4269	2432	43.01377	0.00045	3.553016	50700.34	244.7092
6020	3558	40.9034	0.00055	4.342575	61967.08	239.5949
8233	4667	43.31999	0.00065	5.132134	73233.82	225.0166
13469	7500	44.31678	0.00085	6.711252	95767.3	211.4745

APPENDIX C6

**EXPERIMENTAL DATA FOR SAND POWDER (NNAP 20 ppm, $D_p = 45$,
 $D=0.0127$ m, $L=1$ m)
 Conc. =100 ppm**

ΔP_b	ΔP_a	%Dr	Q(m ³ /s)	v(m/s)	Re	f
1917	1739	9.275679	0.0002	1.579118	22533.48	442.8704
5173	3750	27.51433	0.00035	2.763457	39433.59	311.8169
8237	5814	29.41586	0.00045	3.553016	50700.34	292.4496
11740	7977	32.05727	0.00055	4.342575	61967.08	268.5962
16167	1072	33.68318	0.00065	5.132134	73233.82	258.4777
28438	18031	36.59496	0.00085	6.711252	95767.3	254.2091

Conc. =300 ppm

ΔP_b	ΔP_a	%Dr	Q(m ³ /s)	v(m/s)	Re	f
1917	1364	28.86388	0.0002	1.579118	22533.48	347.2507
5173	3700	28.4808	0.00035	2.763457	39426.16	307.6594
8237	5577	32.29353	0.00045	3.553016	50690.77	280.5267
11740	7752	33.97133	0.00055	4.342575	61955.39	261.0294
16167	9728	39.82927	0.00065	5.132134	73220	234.5226
28438	16569	41.73591	0.00085	6.711252	95749.24	233.5975

Conc. =500 ppm

ΔP_b	ΔP_a	%Dr	Q(m ³ /s)	v(m/s)	Re	f
1917	1165	39.22351	0.0002	1.579118	22533.48	296.6802
5173	2818	45.52592	0.00035	2.763457	39433.59	234.3351
8237	4700	42.93978	0.00045	3.553016	50700.34	236.4163
11740	6058	48.4024	0.00055	4.342575	61967.08	203.9794
16167	8400	48.04137	0.00065	5.132134	73233.82	202.5149
28438	14200	50.06699	0.00085	6.711252	95767.3	200.1958

APPENDIX C7

**EXPERIMENTAL DATA FOR SAND POWDER (NNAP 20 ppm, $D_p = 45$,
 $D=0.0127$ m, $L=1.5$ m)**

Conc. =100 ppm

ΔP_b	ΔP_a	%Dr	$Q(m^3/s)$	$v(m/s)$	Re	f
2850	2115	25.78664	0.0002	1.579118	22533.48	359.1225
7810	5524	29.274	0.00035	2.763457	39433.59	306.2075
12155	8558	29.59743	0.00045	3.553016	50700.34	286.9755
17910	12745	28.83964	0.00055	4.342575	61967.08	286.1087
24150	16505	31.6571	0.00065	5.132134	73233.82	265.2762
36407	24155	33.65427	0.00085	6.711252	95767.3	227.0257

Conc. =300 ppm

ΔP_b	ΔP_a	%Dr	$Q(m^3/s)$	$v(m/s)$	Re	f
2850	2035	28.61083	0.0002	1.579118	22533.48	345.4561
7810	5253	32.74245	0.00035	2.763457	39433.59	291.1909
12155	7810	35.75247	0.00045	3.553016	50700.34	261.8863
17910	10577	40.94532	0.00055	4.342575	61967.08	237.4363
24150	14216	41.13603	0.00065	5.132134	73233.82	228.4832
36407	24272	33.3322	0.00085	6.711252	95767.3	228.1278

Conc. =500 ppm

ΔP_b	ΔP_a	%Dr	$Q(m^3/s)$	$v(m/s)$	Re	f
2850	1923	32.53331	0.0002	1.579118	22533.48	326.475
7810	4942	36.72519	0.00035	2.763457	39433.59	273.9477
12155	7393	39.17917	0.00045	3.553016	50700.34	247.9184
17910	10721	40.13951	0.00055	4.342575	61967.08	240.6762
24150	13450	44.30536	0.00065	5.132134	73233.82	216.1814
36407	24272	33.3322	0.00085	6.711252	95767.3	228.1278

APPENDIX C8

**EXPERIMENTAL DATA FOR SAND POWDER (NNAP 20 ppm, $D_p = 45$,
 $D=0.0127$ m, $L=2$ m)**

Conc. =100 ppm

ΔP_b	ΔP_a	%Dr	$Q(m^3/s)$	$v(m/s)$	Re	f
3834	2981	22.25187	0.0002	1.579118	22533.48	379.5272
10447	7655	26.72411	0.00035	2.763457	39433.59	318.2627
16574	11770	28.98183	0.00045	3.553016	50700.34	296.0341
24031	16667	30.64375	0.00055	4.342575	61967.08	280.6066
32233	21930	31.96556	0.00065	5.132134	73233.82	264.3522
44376	24272	45.30436	0.00085	6.711252	95767.3	171.0958

Conc. =300 ppm

ΔP_b	ΔP_a	%Dr	$Q(m^3/s)$	$v(m/s)$	Re	f
3834	2800	26.96692	0.0002	1.579118	22533.48	356.5107
10447	7308	30.04899	0.00035	2.763457	39433.59	303.8216
16574	11900	28.20004	0.00045	3.553016	50700.34	299.2929
24031	17600	26.75981	0.00055	4.342575	61967.08	296.3206
32233	19091	40.77293	0.00065	5.132134	73233.82	230.1306
44376	22523	49.24639	0.00085	6.711252	95767.3	158.7646

Conc. =500 ppm

ΔP_b	ΔP_a	%Dr	$Q(m^3/s)$	$v(m/s)$	Re	f
3834	2381	37.89704	0.0002	1.579118	22533.48	303.1553
10447	6323	39.47512	0.00035	2.763457	39433.59	262.8807
16574	9747	41.19288	0.00045	3.553016	50700.34	245.1332
24031	13645	43.21711	0.00055	4.342575	61967.08	229.7364
32233	17476	45.78382	0.00065	5.132134	73233.82	210.6605
44376	22727	48.78499	0.00085	6.711252	95767.3	160.2079

APPENDIX C9

**EXPERIMENTAL DATA FOR SAND POWDER (NNAP 30 ppm, $D_p = 45$,
 $D=0.0254$ m, $L=0.5$ m)**

Conc. =100 ppm

ΔP_b	ΔP_a	%Dr	Q(m ³ /s)	v(m/s)	Re	f
148	117	21.09776	0.0003	0.592169	16900.11	845.0624
367	271	26.10955	0.0005	0.986763	28161.54	707.4183
716	529	26.09503	0.0008	1.57882	45058.46	539.4634
1215	824	32.16371	0.0011	2.170878	61955.39	444.2293
1623	1186	26.89466	0.0013	2.565583	73220	457.8336
2044	1453	28.91489	0.001488	2.936606	83808.74	427.9623

Conc. =300 ppm

ΔP_b	ΔP_a	%Dr	Q(m ³ /s)	v(m/s)	Re	f
148	107	27.33914	0.0003	0.592169	16900.11	778.2156
367	246	32.99893	0.0005	0.986763	28161.54	641.4603
716	481	32.80747	0.0008	1.57882	45058.46	490.4665
1215	791	34.87776	0.0011	2.170878	61955.39	426.4562
1623	996	38.63832	0.0013	2.565583	73220	384.2871
2044	1243	39.25089	0.001488	2.936606	83808.74	365.7352

Conc. =500 ppm

ΔP_b	ΔP_a	%Dr	Q(m ³ /s)	v(m/s)	Re	f
148	108	27.03764	0.0003	0.592169	16900.11	781.4447
367	236	35.78124	0.0005	0.986763	28161.54	614.8227
716	448	37.44143	0.0008	1.57882	45058.46	456.6412
1215	745	38.68122	0.0011	2.170878	61955.39	401.549
1623	984	39.39276	0.0013	2.565583	73220	379.5623
2044	1245	39.09965	0.001488	2.936606	83808.74	366.6458

APPENDIX C10

**EXPERIMENTAL DATA FOR SAND POWDER (NNAP 30 ppm, $D_p = 45$,
 $D=0.0254$ m, $L=1$ m)**

Conc. =100 ppm

ΔP_b	ΔP_a	%Dr	Q(m ³ /s)	v(m/s)	Re	f
246	182	25.8848	0.0003	0.592169	16900.11	659.5804
534	424	20.65344	0.0005	0.986763	28161.54	552.6706
1283	1008	21.37205	0.0008	1.57882	45058.46	513.8478
2230	1653	25.88034	0.0011	2.170878	61955.39	445.4281
3046	2231	26.73923	0.0013	2.565583	73220	430.5366
3978	2869	27.88264	0.001488	2.936606	83808.74	422.4942

Conc. =300 ppm

ΔP_b	ΔP_a	%Dr	Q(m ³ /s)	v(m/s)	Re	F
246	185	24.63707	0.0003	0.592169	16900.11	670.6844
534	390	26.96165	0.0005	0.986763	28161.54	508.7321
1283	828	35.46224	0.0008	1.57882	45058.46	421.7659
2230	1393	37.51469	0.0011	2.170878	61955.39	375.5105
3046	1992	34.6091	0.0013	2.565583	73220	384.2871
3978	2609	34.40407	0.001488	2.936606	83808.74	384.2888

Conc. =500 ppm

ΔP_b	ΔP_a	%Dr	Q(m ³ /s)	v(m/s)	Re	f
246	165.5629	32.62255	0.0003	0.592169	16900.11	599.6185
534	361	32.46437	0.0005	0.986763	28161.54	470.4042
1283	813	36.59553	0.0008	1.57882	45058.46	414.3596
2230	1431	35.83159	0.0011	2.170878	61955.39	385.6252
3046	1826	40.05834	0.0013	2.565583	73220	352.2632
3978	2318	41.73299	0.001488	2.936606	83808.74	341.3529

APPENDIX C11

**EXPERIMENTAL DATA FOR SAND POWDER (NNAP 30 ppm, $D_p = 45$,
 $D=0.0254$ m, $L=1.5$ m)**

Conc. =100 ppm

ΔP_b	ΔP_a	%Dr	Q(m ³ /s)	v(m/s)	Re	f
344	269	21.60343	0.0003	0.592169	16900.11	650.3606
851	664	21.989	0.0005	0.986763	28161.54	577.2847
1949	1407	27.7954	0.0008	1.57882	45058.46	478.0013
2945	2049	30.41948	0.0011	2.170878	61955.39	368.1475
4669	3154	32.45469	0.0013	2.565583	73220	405.6364
6067	4209	30.62931	0.001488	2.936606	83808.74	413.2138

Conc. =300 ppm

ΔP_b	ΔP_a	%Dr	Q(m ³ /s)	v(m/s)	Re	f
344	265	22.90139	0.0003	0.592169	16900.11	639.5931
851	653	23.32362	0.0005	0.986763	28161.54	567.4085
1949	1282	34.22085	0.0008	1.57882	45058.46	435.4643
2945	1901	35.45688	0.0011	2.170878	61955.39	341.4949
4669	2893	38.04429	0.0013	2.565583	73220	372.0686
6067	3851	36.50193	0.001488	2.936606	83808.74	378.2329

Conc. =500 ppm

ΔP_b	ΔP_a	%Dr	Q(m ³ /s)	v(m/s)	Re	f
344	253	26.50321	0.0003	0.592169	16900.11	609.7131
851	581	31.74038	0.0005	0.986763	28161.54	505.1241
1949	1158	40.53739	0.0008	1.57882	45058.46	393.6482
2945	1639	44.33558	0.0011	2.170878	61955.39	294.518
4669	2732	41.48791	0.0013	2.565583	73220	351.3884
6067	3607	40.555	0.001488	2.936606	83808.74	354.0903

APPENDIX C12

**EXPERIMENTAL DATA FOR SAND POWDER (NNAP 30 ppm, $D_p = 45$,
 $D=0.0254$ m, $L=2$ m)**

Conc. =100 ppm

ΔP_b	ΔP_a	%Dr	Q(m ³ /s)	v(m/s)	Re	f
442	349	21.04462	0.0003	0.592169	16900.11	631.1669
1093	811	25.78004	0.0005	0.986763	28161.54	529.0631
2615	1967	24.78246	0.0008	1.57882	45058.46	501.1408
4660.	3486	25.2054	0.0011	2.170878	61955.39	469.6402
6492	4882	24.79363	0.0013	2.565583	73220	470.9916
8356	5975	28.49382	0.001488	2.936606	83808.74	439.9749

Conc. =300 ppm

ΔP_b	ΔP_a	%Dr	Q(m ³ /s)	v(m/s)	Re	f
442	339	23.21128	0.0003	0.592169	16900.11	613.8467
1093	769	29.62503	0.0005	0.986763	28161.54	501.6548
2615	1736	33.64073	0.0008	1.57882	45058.46	442.1222
4660.	3058	34.38179	0.0011	2.170878	61955.39	412.021
6492	4262	34.34216	0.0013	2.565583	73220	411.1925
8356	5311	36.43895	0.001488	2.936606	83808.74	391.0888

Conc. =500 ppm

ΔP_b	ΔP_a	%Dr	Q(m ³ /s)	v(m/s)	Re	f
442	315	28.56418	0.0003	0.592169	16900.11	571.0558
1093	712	34.86819	0.0005	0.986763	28161.54	464.2799
2615	1557	40.45278	0.0008	1.57882	45058.46	396.7365
4660	2739	41.23281	0.0011	2.170878	61955.39	369.003
6492	3956	39.05691	0.0013	2.565583	73220	381.6656
8356	4979	40.41151	0.001488	2.936606	83808.74	366.6458

APPENDIX C13

**EXPERIMENTAL DATA FOR SAND POWDER (NNAP 10 ppm, $D_p = 71$,
 $D=0.0127$ m, $L=0.5$ m)**

Conc. =100 ppm

ΔP_b	ΔP_a	%Dr	$Q(m^3/s)$	$v(m/s)$	Re	f
1134	833	26.47944	0.0002	1.579118	22533.48	424.4175
2487	1639	34.07599	0.00035	2.762935	39426.16	272.7297
4269	3200	25.03144	0.00045	3.552345	50690.77	322.05
6020	4643	22.87779	0.00055	4.341756	61955.39	312.7939
8233	5645	31.43547	0.00065	5.131166	73220	272.3002
13469	8333	38.12976	0.00085	6.709986	95749.24	235.0603

Conc. =300 ppm

ΔP_b	ΔP_a	%Dr	$Q(m^3/s)$	$v(m/s)$	Re	f
1134	818	27.81618	0.0002	1.579118	22533.48	416.7008
2487	1546	37.85164	0.00035	2.762935	39426.16	257.1097
4269	2655	37.80264	0.00045	3.552345	50690.77	267.1875
6020	4167	30.78776	0.00055	4.341756	61955.39	280.7125
8233	5042	38.76109	0.00065	5.131166	73220	243.2069
13469	7273	46.00415	0.00085	6.709986	95749.24	205.1435

Conc. =500 ppm

ΔP_b	ΔP_a	%Dr	$Q(m^3/s)$	$v(m/s)$	Re	f
1134	781	31.10073	0.0002	1.579118	22533.48	397.7398
2487	1301	47.68957	0.00035	2.762935	39426.16	216.4099
4269	2000	53.14465	0.00045	3.552345	50690.77	201.2813
6020	3390	43.69174	0.00055	4.341756	61955.39	228.3763
8233	4464	45.77805	0.00065	5.131166	73220	215.3395
13469	5887	56.29167	0.00085	6.709986	95749.24	166.0587

APPENDIX C14

**EXPERIMENTAL DATA FOR SAND POWDER (NNAP 10 ppm, $D_p = 71$,
 $D=0.0127$ m, $L=1$ m)**

Conc. =100 ppm

ΔP_b	ΔP_a	%Dr	$Q(m^3/s)$	$v(m/s)$	Re	f
1917	1546	19.37907	0.0002	1.579118	22533.48	393.5507
5173	4000	22.68195	0.00035	2.762935	39426.16	332.7302
8237	6372	22.64478	0.00045	3.552345	50690.77	320.625
11740	7500	36.11726	0.00055	4.341756	61955.39	252.6412
16167	8403	48.02058	0.00065	5.131166	73220	202.6724
28438	18181	36.06528	0.00085	6.709986	95749.24	256.4294

Conc. =300 ppm

ΔP_b	ΔP_a	%Dr	$Q(m^3/s)$	$v(m/s)$	Re	f
1917	1416	26.13595	0.0002	1.579118	22533.48	360.5671
5173	3333	35.56829	0.00035	2.762935	39426.16	277.2752
8237	5882	28.58546	0.00045	3.552345	50690.77	296.0018
11740	7546	35.73009	0.00055	4.341756	61955.39	254.1724
16167	9000	44.33004	0.00065	5.131166	73220	217.0622
28438	16191	43.06766	0.00085	6.709986	95749.24	228.3443

Conc. =500 ppm

ΔP_b	ΔP_a	%Dr	$Q(m^3/s)$	$v(m/s)$	Re	f
1917	1250	34.79189	0.0002	1.579118	22533.48	318.3131
5173	3051	41.02861	0.00035	2.762935	39426.16	253.7773
8237	5536	32.79382	0.00045	3.552345	50690.77	278.5589
11740	6452	45.0471	0.00055	4.341756	61955.39	217.3258
16167	7333	54.63929	0.00065	5.131166	73220	176.8655
28438	14000	50.77027	0.00085	6.709986	95749.24	197.4506

APPENDIX C15

**EXPERIMENTAL DATA FOR SAND POWDER (NNAP 10 ppm, $D_p = 71$,
 $D=0.0127$ m, $L=1.5$ m)**

Conc. =100 ppm

ΔP_b	ΔP_a	%Dr	$Q(m^3/s)$	$v(m/s)$	Re	f
2850	2143	24.82283	0.0002	1.579118	22533.48	363.7864
7810	5645	27.72023	0.00035	2.762935	39426.16	313.0526
12155	7500	38.29887	0.00045	3.552345	50690.77	251.6016
17910	12000	32.99979	0.00055	4.341756	61955.39	269.484
24150	15455	36.00619	0.00065	5.131166	73220	248.4887
36407	18182	50.05976	0.00085	6.709986	95749.24	170.9529

Conc. =300 ppm

ΔP_b	ΔP_a	%Dr	$Q(m^3/s)$	$v(m/s)$	Re	f
2850	1750	38.60531	0.0002	1.579118	22533.48	297.0922
7810	5630	27.91113	0.00035	2.762935	39426.16	312.2259
12155	8000	34.18546	0.00045	3.552345	50690.77	268.375
17910	11000	38.58314	0.00055	4.341756	61955.39	247.027
24150	13333	44.78966	0.00065	5.131166	73220	214.3824
36407	15447	57.5711	0.00085	6.709986	95749.24	145.2405

Conc. =500 ppm

ΔP_b	ΔP_a	%Dr	$Q(m^3/s)$	$v(m/s)$	Re	f
2850	1695	40.53783	0.0002	1.579118	22533.48	287.7407
7810	5804	25.69197	0.00035	2.762935	39426.16	321.8373
12155	6452	46.92376	0.00045	3.552345	50690.77	216.4315
17910	8333	53.47207	0.00055	4.341756	61955.39	187.1417
24150	13000	46.16991	0.00065	5.131166	73220	209.0228
36407	15455	57.5508	0.00085	6.709986	95749.24	145.31

APPENDIX C16

**EXPERIMENTAL DATA FOR SAND POWDER (NNAP 10 ppm, $D_p = 71$,
 $D=0.0127$ m, $L=2$ m)**

Conc. =100 ppm

ΔP_b	ΔP_a	%Dr	$Q(m^3/s)$	$v(m/s)$	Re	f
3834	2833	26.09748	0.0002	1.579118	22533.48	360.7549
10447	7983	23.58293	0.00035	2.762935	39426.16	332.0312
16574	9091	45.149	0.00045	3.552345	50690.77	228.7287
24031	17000	29.25663	0.00055	4.341756	61955.39	286.3267
32233	19469	39.59987	0.00065	5.131166	73220	234.7772
44376.2	25000	43.66349	0.00085	6.709986	95749.24	176.2952

Conc. =300 ppm

ΔP_b	ΔP_a	%Dr	$Q(m^3/s)$	$v(m/s)$	Re	f
3834	3000	21.75027	0.0002	1.579118	22533.48	381.9757
10447	9000	13.84981	0.00035	2.762935	39426.16	374.3215
16574	12381	25.29816	0.00045	3.552345	50690.77	311.5067
24031	13821	42.48506	0.00055	4.341756	61955.39	232.786
32233	17500	45.70852	0.00065	5.131166	73220	211.0327
44376.2	25424	42.70864	0.00085	6.709986	95749.24	179.2833

Conc. =500 ppm

ΔP_b	ΔP_a	%Dr	$Q(m^3/s)$	$v(m/s)$	Re	f
3834	2419	36.89538	0.0002	1.579118	22533.48	308.0449
10447	6833	34.58967	0.00035	2.762935	39426.16	284.2071
16574	12000	27.59668	0.00045	3.552345	50690.77	301.9219
24031	12500	47.98282	0.00055	4.341756	61955.39	210.5344
32233	16129	49.96177	0.00065	5.131166	73220	194.5002
44376.2	20000	54.9308	0.00085	6.709986	95749.24	141.0362

APPENDIX C17

**EXPERIMENTAL DATA FOR SAND POWDER (DAPI 10 ppm, $D_p = 45$,
 $D=0.0127$ m, $L=0.5$ m)**

Conc. =100 ppm

ΔP_b	ΔP_a	%Dr	$Q(m^3/s)$	$v(m/s)$	Re	f
1134	786	30.68062	0.0002	1.579118	22533.48	400.165
2487	1763	29.10483	0.00035	2.763457	39433.59	293.1849
4269	2837	33.53851	0.00045	3.553016	50700.34	285.3976
6020	4286	28.81027	0.00055	4.342575	61967.08	288.6239
8233	5639	31.50911	0.00065	5.132134	73233.82	271.9051
13469	8759	34.96851	0.00085	6.711252	95767.3	246.9775

Conc. =300 ppm

ΔP_b	ΔP_a	%Dr	$Q(m^3/s)$	$v(m/s)$	Re	f
1134	739	34.76345	0.0002	1.579118	22533.48	376.5958
2487	1594	35.89129	0.00035	2.763457	39433.59	265.1197
4269	2590	39.32401	0.00045	3.553016	50700.34	260.5537
6020	3704	38.47801	0.00055	4.342575	61967.08	249.4281
8233	4722	42.64522	0.00065	5.132134	73233.82	227.6954
13469	8088	39.94947	0.00085	6.711252	95767.3	228.0607

Conc. =500 ppm

ΔP_b	ΔP_a	%Dr	$Q(m^3/s)$	$v(m/s)$	Re	f
1134	761	32.87253	0.0002	1.579118	22533.48	387.5116
2487	1500	39.67953	0.00035	2.763457	39433.59	249.4535
4269	2444	42.73235	0.00045	3.553016	50700.34	245.9176
6020	3121	48.16445	0.00055	4.342575	61967.08	210.1564
8233	4511	45.20729	0.00065	5.132134	73233.82	217.5241
13469	7141	46.96837	0.00085	6.711252	95767.3	201.4042

APPENDIX C18

**EXPERIMENTAL DATA FOR SAND POWDER (DAPI 10 ppm, $D_p = 45$,
 $D=0.0127$ m, $L=1$ m)
 Conc. =100 ppm**

ΔP_b	ΔP_a	%Dr	$Q(m^3/s)$	$v(m/s)$	Re	f
1917	1268	33.87347	0.0002	1.579118	22533.48	322.7964
5173	3551	31.36622	0.00035	2.763457	39433.59	295.2469
8237	5540	32.74703	0.00045	3.553016	50700.34	278.6477
11740	7029	40.12922	0.00055	4.342575	61967.08	236.6856
16167	9353	42.14953	0.00065	5.132134	73233.82	225.4791
28438	17630	38.00701	0.00085	6.711252	95767.3	248.5478

Conc. =300 ppm

ΔP_b	ΔP_a	%Dr	$Q(m^3/s)$	$v(m/s)$	Re	f
1917	1324	30.95612	0.0002	1.579118	22533.48	337.0374
5173	3262	36.93918	0.00035	2.763457	39426.16	271.2733
8237	5290	35.77867	0.00045	3.553016	50690.77	266.0867
11740	6500	44.63496	0.00055	4.342575	61955.39	218.8731
16167	8519	47.30827	0.00065	5.132134	73220	205.3723
28438	14184	50.12185	0.00085	6.711252	95749.24	199.9758

Conc. =500 ppm

ΔP_b	ΔP_a	%Dr	$Q(m^3/s)$	$v(m/s)$	Re	f
1917	1338	30.1832	0.0002	1.579118	22533.48	340.8104
5173	3044	41.17105	0.00035	2.763457	39433.59	253.0688
8237	5036	38.86094	0.00045	3.553016	50700.34	253.3161
11740	6296	46.37004	0.00055	4.342575	61967.08	212.0139
16167	7292	54.89703	0.00065	5.132134	73233.82	175.7942
28438	14706	48.2881	0.00085	6.711252	95767.3	207.3279

APPENDIX C19

**EXPERIMENTAL DATA FOR SAND POWDER (DAPI 10 ppm, $D_p = 45$,
 $D=0.0127$ m, $L=1.5$ m)**

Conc. =100 ppm

ΔP_b	ΔP_a	%Dr	Q(m ³ /s)	v(m/s)	Re	f
2850	1929	32.34055	0.0002	1.579118	22533.48	327.4078
7810	5407	30.7644	0.00035	2.763457	39433.59	299.7549
12155	7092	41.65378	0.00045	3.553016	50700.34	237.8313
17910	10602	40.80808	0.00055	4.342575	61967.08	237.9881
24150	14286	40.84606	0.00065	5.132134	73233.82	229.6088
36407	20148	44.65881	0.00085	6.711252	95767.3	189.3697

Conc. =300 ppm

ΔP_b	ΔP_a	%Dr	Q(m ³ /s)	v(m/s)	Re	f
2850	1838	35.50978	0.0002	1.579118	22533.48	312.0717
7810	4965	36.43481	0.00035	2.763457	39433.59	275.2048
12155	6957	42.76997	0.00045	3.553016	50700.34	233.2815
17910	9786	45.36292	0.00055	4.342575	61967.08	219.6749
24150	13482	44.17621	0.00065	5.132134	73233.82	216.6827
36407	19149	47.40336	0.00085	6.711252	95767.3	179.9783

Conc. =500 ppm

ΔP_b	ΔP_a	%Dr	Q(m ³ /s)	v(m/s)	Re	f
2850	2030	28.77952	0.0002	1.579118	22533.48	344.6398
7810	4453	42.99018	0.00035	2.763457	39433.59	246.8235
12155	6338	47.8582	0.00045	3.553016	50700.34	212.5408
17910	9155	48.88481	0.00055	4.342575	61967.08	205.5147
24150	12754	47.19011	0.00065	5.132134	73233.82	204.9841
36407	18705	48.62263	0.00085	6.711252	95767.3	175.8061

APPENDIX C20

**EXPERIMENTAL DATA FOR SAND POWDER (DAPI 10 ppm, $D_p = 45$,
 $D=0.0127$ m, $L=2$ m)
 Conc. =100 ppm**

ΔP_b	ΔP_a	%Dr	$Q(m^3/s)$	$v(m/s)$	Re	f
3834	2667	30.44469	0.0002	1.579118	22533.48	339.534
10447	6736	35.52031	0.00035	2.763457	39433.59	280.0578
16574	9779	40.99484	0.00045	3.553016	50700.34	245.9587
24031	13475	43.92474	0.00055	4.342575	61967.08	226.8734
32233	18841	41.54955	0.00065	5.132134	73233.82	227.113
44376	25714	42.05388	0.00085	6.711252	95767.3	181.2638

Conc. =300 ppm

ΔP_b	ΔP_a	%Dr	$Q(m^3/s)$	$v(m/s)$	Re	f
3834	2518	34.32943	0.0002	1.579118	22533.48	320.5706
10447	6692	35.94514	0.00035	2.763457	39433.59	278.2126
16574	10150	38.75659	0.00045	3.553016	50700.34	255.2887
24031	14493	39.69022	0.00055	4.342575	61967.08	244.0057
32233	17266	46.43389	0.00065	5.132134	73233.82	208.1346
44376	25185	43.24619	0.00085	6.711252	95767.3	177.5341

Conc. =500 ppm

ΔP_b	ΔP_a	%Dr	$Q(m^3/s)$	$v(m/s)$	Re	f
3834	2500	34.79189	0.0002	1.579118	22533.48	318.3131
10447	5816	44.33164	0.00035	2.763457	39433.59	241.7871
16574	9058	45.34773	0.00045	3.553016	50700.34	227.814
24031	12857	46.49661	0.00055	4.342575	61967.08	216.4679
32233	15942	50.54192	0.00065	5.132134	73233.82	192.1726
44376	22857	48.49234	0.00085	6.711252	95767.3	161.1234

APPENDIX D1

CORRELATION EQUATION PARAMETERS ESTIMATION STEPS

1. **Step 1:** Starting the STATISTICA 5.5 software and inserting in the values for the variables investigated which is friction factor VAR1 and Reynolds number VAR2

The screenshot displays the STATISTICA 5.5 software interface. The main window shows a data table with 10 variables (VAR1 to VAR10) and 24 rows of data. The 'Basic Statistics and Tables' dialog box is open, showing a list of statistical tests. The 'Descriptive statistics' option is selected. The dialog box also includes buttons for 'OK', 'Cancel', and 'Open Data'.

NUMÉ VALU	1 VAR1	2 VAR2	3 VAR3	4 VAR4	5 VAR5	6 VAR6	7 VAR7	8 VAR8	9 VAR9	10 VAR10
1	.00044964000	22533.48								
2	.00029753762	39426.16								
3	.00028008477	50690.77								
4	.00023142710	61955.39								
5	.00020213198	73220.00								
6	.00013561171	95749.24								
7	.00044964000	22533.48								
8	.00029173031	39426.16								
9	.00027059037	50690.77								
10	.00021815371	61955.39								
11	.00019294416	73220.00								
12	.00013018724	95749.24								
13	.00044223653	22533.48								
14	.00028519735	39426.16								
15	.00025644006	50690.77								
16	.00020630354	61955.39								
17	.00017456853	73220.00								
18	.00012031522	95749.24								
19										
20										
21										
22										
23										
24										

Basic Statistics and Tables dialog box options:

- Descriptive statistics (selected)
- Correlation matrices
- t-test for independent samples
- t-test for dependent samples
- Breakdown & one-way ANOVA
- Frequency tables
- Tables and banners
- Probability calculator
- Other significance tests

Buttons: OK, Cancel, Open Data, Select Cases, Print, Help.

Auto Task Buttons: Customize...

Status bar: Ready | Output: OFF | Set OFF | Weight: OFF

Step 2: Selecting the nonlinear estimation mode.

The screenshot shows the STATISTICA software interface with the 'STATISTICA Module Switcher' dialog box open. The dialog box lists various statistical modules, and 'Nonlinear Estimation' is highlighted. The background shows a data table with columns labeled VAR1 through VAR10 and rows numbered 1 through 39. The status bar at the bottom indicates 'Ready' and 'Output: OFF | Set: OFF | Weight: OFF'.

NUM	1	2	3	4	5	6	7	8	9	10
VALU	VAR1	VAR2	VAR3	VAR4	VAR5	VAR6	VAR7	VAR8	VAR9	VAR10
1	.00044964000	22533.48								
2	.00029753762	39426.16								
3	.00028008477	50690.77								
4	.00023142710	61955.39								
5	.00020213198	73220.00								
6	.00013561171	95749.24								
7	.00044964000	22533.48								
8	.00029173031	39426.16								
9	.00027059037	50690.77								
10	.00021815371	61955.39								
11	.00019294416	73220.00								
12	.00013018724	95749.24								
13	.00044223653	22533.48								
14	.00028519735	39426.16								
15	.00025644006	50690.77								
16	.00020630354	61955.39								
17	.00017456853	73220.00								
18	.00012031522	95749.24								
19										
20										
21										
22										
23										
24										
25										
26										
27										
28										
29										
30										
31										
32										
33										
34										
35										
36										
37										
38										
39										

STATISTICA Module Switcher

- Basic Statistics
- Nonparametrics/Distrib.
- ANOVA/MANOVA
- Multiple Regression
- Nonlinear Estimation**
- Time Series/Forecasting
- Cluster Analysis
- Data Management/MFM
- Factor Analysis

General nonlinear model fitting procedure. fit any user defined function or choose predefined analyses (stepwise logit, probit, exponential, piecewise models); least-squares, maximum likelihood estimation, or user-defined loss functions; see also Generalized Linear Model.

Switch To Customize list...

End & Switch To Cancel

Ready Output: OFF Set: OFF Weight: OFF

UMP

Step 4: Typing the equation derived from the dimensional analysis, which is $f=aRe^b$

The screenshot shows the STATISTICA software interface. The main window displays a data table with 10 variables (VAR1 to VAR10) and 24 rows of data. A 'Model Estimation' dialog box is open, showing the following details:

- Model is: $v1=a*v2**b$
- Number of parameters to be estimated: 2
- Loss function: $(OBS-PRED)**2$
- Dependent variable: VAR1
- Independent variables: VAR2
- Missing data are casewise deleted
- Number of valid cases: 18
- Estimation method: Quasi-Newton
- Asymptotic standard errors
- Eta for finite diff. approx., 1.E- 0
- Maximum number of iterations: 50
- Convergence criterion: .0001
- Start values: .1 for all parameters
- Initial step size: .50 for all parameters

Buttons for 'OK', 'Cancel', 'Means & standard deviations', 'Matrix plot for all variables', and 'Box & whisker plot for all vars.' are visible in the dialog box.

UMP

Step 5: Starting the iteration analysis

STATISTICA: Nonlinear Estimation

File Edit View Analysis Graphs Options Window Help

61955.3879150968

Data: NEW.STA.10v*110c

NUMÉ VALU	1 VAR1	2 VAR2	3 VAR3	4 VAR4	5 VAR5	6 VAR6	7 VAR7	8 VAR8	9 VAR9	10 VAR10
1	.00044964000	22533.48								
2	.00029753762	39426.16								
3	.00028008477	50690.77								
4	.00023142710	61955.39								
5	.00020213198	73220.00								
6	.00013561171	95749.24								
7	.00044964000	22533.48								
8	.00029173031	39426.16								
9	.00027059037	50690.77								
10	.00021815371	61955.39								
11	.00019294416	73220.00								
12	.00013018724	95749.24								
13	.00044223653	22533.48								
14	.00028519735	39426.16								
15	.00025644006	50690.77								
16	.00020630354	61955.39								
17	.00017456853	73220.00								
18	.00012031522	95749.24								
19										
20										
21										
22										
23										
24										

Model Estimation

Model is: $v1=a*v2**b$
 Number of parameters to be estimated: 2
 Loss function: $(OBS-PRED)**2$

Parameter Estimation

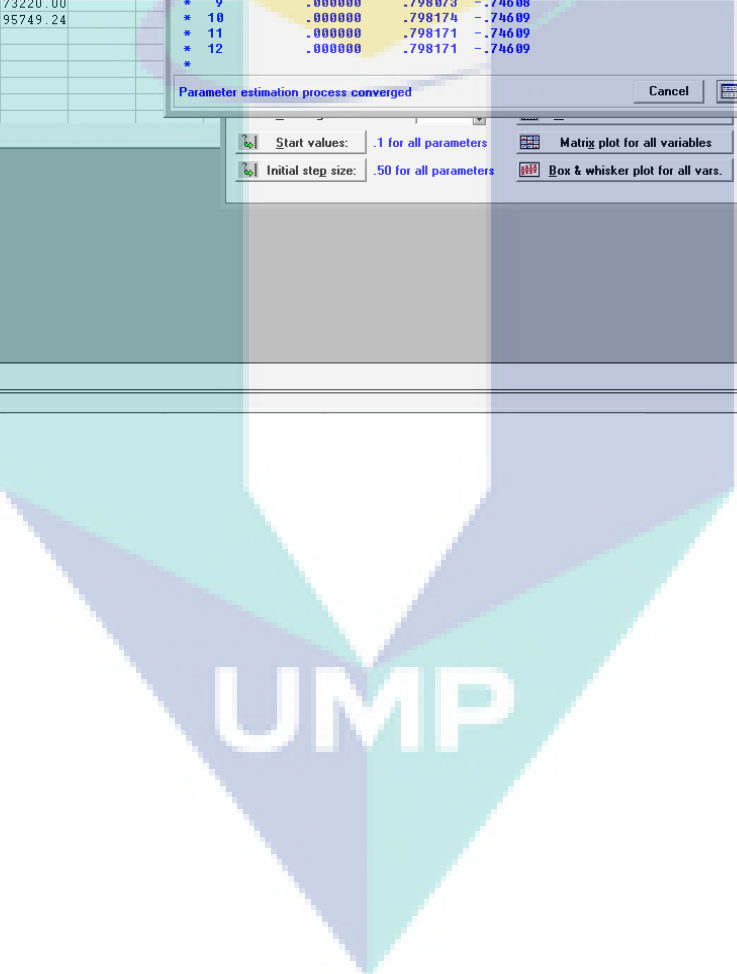
Iteration	Loss	Parameters
* 6	.000000	.818323 -.74860
* 7	.000000	.804270 -.74683
* 8	.000000	.796385 -.74587
* 9	.000000	.798073 -.74608
* 10	.000000	.798174 -.74609
* 11	.000000	.798171 -.74609
* 12	.000000	.798171 -.74609

Parameter estimation process converged

Start values: .1 for all parameters Matrig plot for all variables
 Initial step size: .50 for all parameters Box & whisker plot for all vars.

Customize...

For help, Press F1 [Output:OFF] [Set:OFF] [Weight:OFF]



Step 6: Revealing the iteration results. It can be noticed that all the statistical parameter appears in the final window.

The screenshot shows the STATISTICA software interface. The main window displays a data table with columns labeled VAR1 through VAR10. A 'Results' dialog box is open, showing the following information:

Model is: $v1=a*v2**b$

Dependent variable: VAR1 Independent variables: 1

Loss function: (OBS-PRED)**2

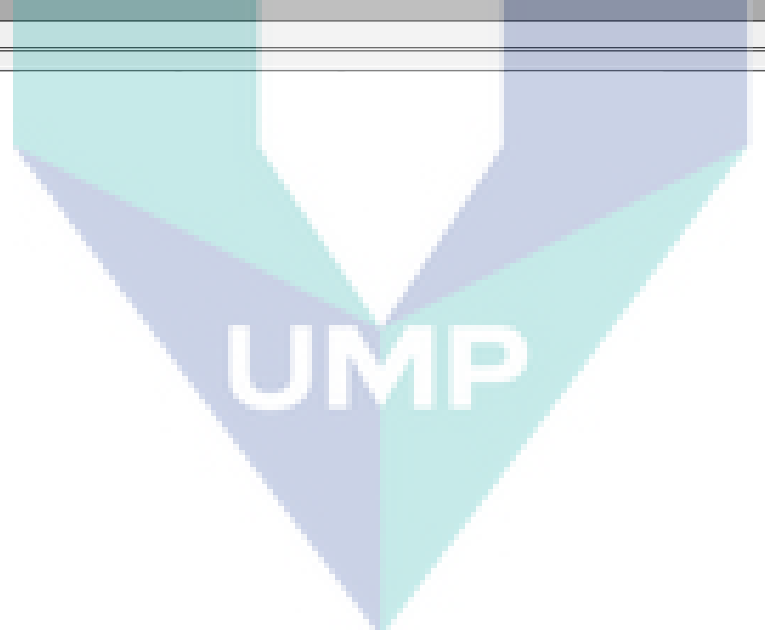
Final value: .000000005

Proportion of variance accounted for: .973085262 R = .986450841

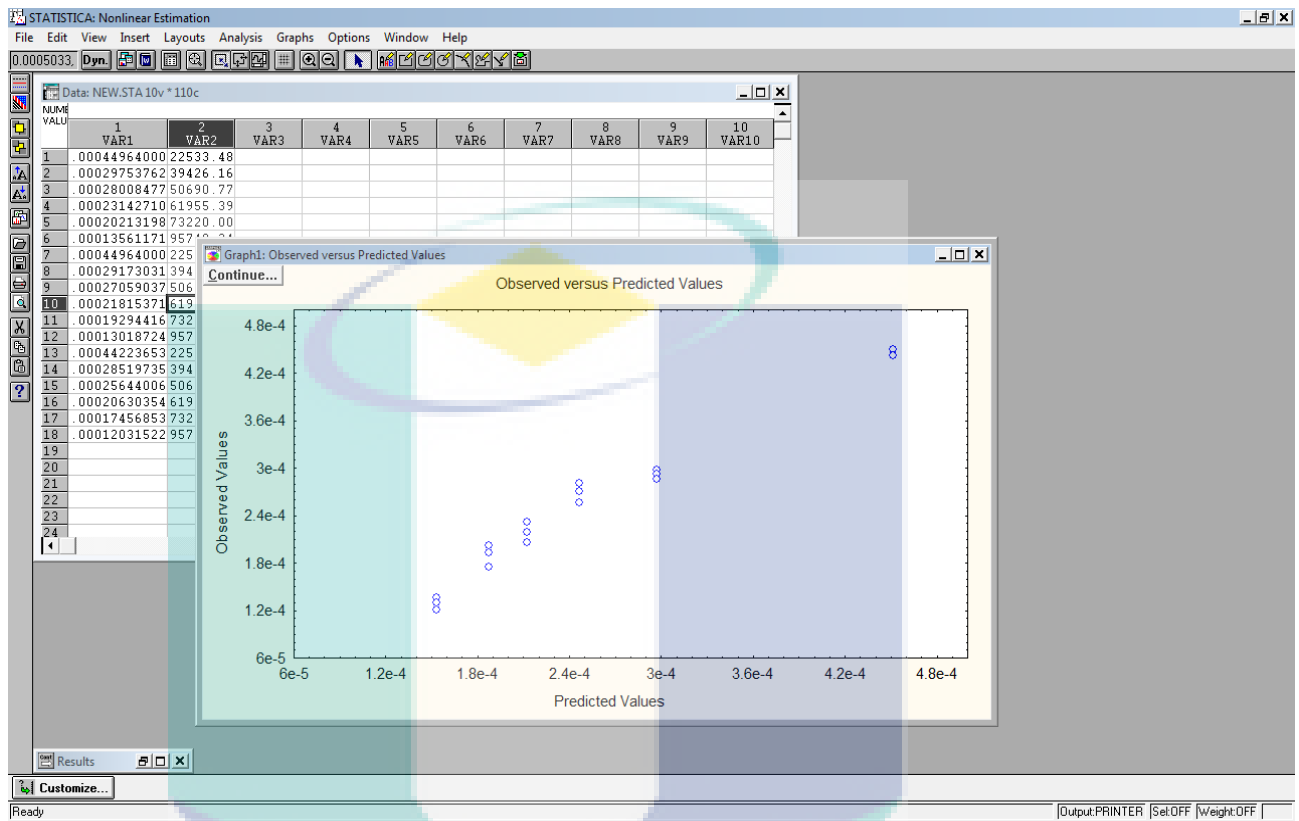
The dialog box contains several sections of options:

- Parameters & standard errors** (highlighted)
- Cov./covs. of parameters**
- Scale MS-error to 1** (checkbox)
- Residual values**
- Predicted values**
- Observed values**
- Means & standard deviations**
- Difference (previous model)**
- Save predicted and residual values**
- Fitted 2D function & observed vals**
- Fitted 3D function & observed vals**
- Distribution of residuals**
- Normal probability plot of residuals**
- Half-normal probability plot**
- Predicted vs. observed values**
- Predicted vs. residual values**
- Matrix plot for all variables**
- Box & whisker plot for all vars.**

Buttons for 'OK' and 'Cancel' are visible at the bottom right of the dialog box.



Step 7: Showing the observed versus the predicted values.



UMP

APPENDIX D2

CORRELATION EQUATION DERIVATIVE

Dimensional analysis depends upon the fundamental principle that any equation or relation between variables must be *dimensionally consistent*, that is, each term in the relationship must have the same dimensions. Thus, in the simple application of the principle, an equation may consist of a number of terms, each representing, and therefore having, the dimensions of length.

It is not permissible to add, say, lengths and velocities in an algebraic equation because they are quantities of different characters. The corollary of this principle is that if the whole equation is divided through by any one of the terms, each remaining term in the equation must be dimensionless. The use of these *dimensionless groups*, or *dimensionless numbers* as they are called, is of considerable value in developing relationships in chemical engineering. (Coulson and Richardson, 1999).

It is found, as a result of experiment, that the pressure difference (ΔP) between two ends of a pipe in which a fluid is flowing is a function of the pipe diameter (d), the pipe length (l), the fluid velocity (u), the fluid density (ρ) and the fluid viscosity (μ).

$$\Delta P = f(d, \mu, \rho, u, l)$$

The form of the function is unknown, though since any function can be expanded as a power series, the function may be regarded as the sum of a number of terms each consisting of products of powers of the variables. The simplest form of relation will be where the function consists simply of a single term, or:

$$\Delta P = \text{const } d^{n_1} L^{n_2} V^{n_3} \rho^{n_4} \mu^{n_5} \text{-----(1)}$$

Each of the variables in equation (1) may be expressed in terms of mass, length, and time. Thus, dimensionally:

$$\Delta P \equiv ML^{-1}T^{-2} \text{----- (2)}$$

$$D \equiv L \text{----- (3)}$$

$$L \equiv L \text{----- (4)}$$

$$V \equiv LT^{-1} \text{----- (5)}$$

$$\rho \equiv ML^{-3} \text{----- (6)}$$

$$\mu \equiv ML^{-1}T^{-1} \text{----- (7)}$$

substituting equations (2) to (7) into (1):

$$ML^{-1}T^{-1} \equiv L^{n_1} L^{n_2} (LT^{-1})^{n_3} (ML^{-3})^{n_4} (ML^{-1}T^{-1})^{n_5} \text{----- (8)}$$

The conditions of dimensional consistency must be met for each of the fundamentals of M, L, and T and the indices of each of these variables may be equated. Thus:

$$-1 = n_1 + n_2 + (2-n_5) - 3(1-n_5) - n_5 \text{ -----(9)}$$

$$0 = n_1 + n_2 + n_5 \text{ -----(10)}$$

$$n_1 = -n_2 - n_5 \text{ -----(11)}$$

Substituting equations (9) to (11) in (8):

$$\Delta P = \text{const } d^{-n_2-n_5} L^{n_2} V^{2-n_5} \rho^{1-n_5} \mu^{n_5} \text{ -----(12)}$$

Rearranging:

$$\frac{\Delta p}{\rho V^2} = \text{const} \left(\frac{L}{D}\right)^{n_2} \left(\frac{\mu}{D.V.\rho}\right)^{n_5} \text{ -----(13)}$$

$$f = \text{const} \left(\frac{\mu}{D.V.\rho}\right)^{n_5} \text{ -----(14)}$$

Where;

$$\frac{\mu}{D.V.\rho} = Re \text{ -----(15)}$$



UMP

APPENDIX E

SAMPLE OF CALCULATIONS

Sample of calculations for Aluminum powder with particle size diameter (71 μ m) was added to surfactant (3-(Decyldimethyle-ammonio) Propanesulfonate inner salt) (8 gm) for Reynolds Number (Re) and friction factors (f) was calculated as below:

$$\Delta p_b = 0.033 \text{ bar}$$

$$\Delta p_a = 0.031 \text{ bar}$$

$$\%Dr = \frac{\Delta p_b - \Delta p_a}{\Delta p_b}$$

$$\%Dr = 6.0606$$

$$\text{Concentration} = 100 \text{ ppm}$$

$$Q = 0.00045 \text{ m}^3/\text{s}$$

$$D = 0.0127 \text{ m}$$

$$L = 0.5 \text{ m}$$

$$\rho = 1000 \text{ kg/m}^3$$

$$\mu \text{ of water at } 25 \text{ }^\circ\text{C} = 0.890 \text{ kg/m.s}$$

$$A = (3.141/4) * D^2$$

$$A = 0.000127 \text{ m}^2$$

$$v = Q/A$$

$$v = 3.5523 \text{ m/s}$$

$$Re = \frac{\rho * D * v}{\mu}$$

$$Re = 50690.77$$

$$f_a = \frac{(\Delta p_a * D)}{(2 * \rho * L * v^2)}$$

$$f_a = 3.12 * 10^8$$

$$f_b = 3.321 * 10^8$$